AD_____

AD NUMBER

102 197

NEW LIMITATION CHANGE

TO Approved for Public Release;
Distribution Unlimited.
** St'mt: A
** Code: 1

FROM

N/A

AUTHORITY

ONR - 28 Jul 77

DISCLAIMER NOTICE

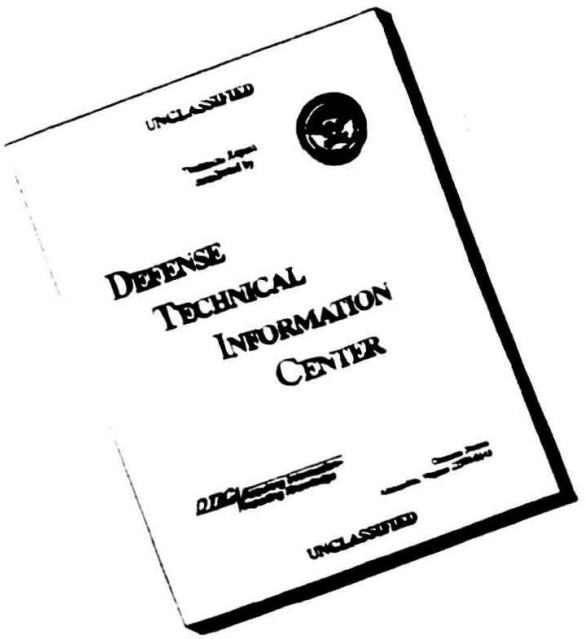

THIS DOCUMENT IS BEST QUALITY AVAILABLE. THE COPY FURNISHED TO DTIC CONTAINED A SIGNIFICANT NUMBER OF PAGES WHICH DO NOT REPRODUCE LEGIBLY.

Contract No. Nonr-1675(00)

DUCTED PROPELLER ASSAULT TRANSPORT

Duct and Propeller Analysis

Report No. D181-945-006

15 May 1956

BELL Aircraft CORP.

BELL Aircraft CORPORATION

BUFFALO 5, NEW YORK

TECHNICAL DATA

NOTICE: This document contains information affecting the national defense of the United States within the meaning of the Espionage Laws, Title 18 U.S.C.; Sect. 793 and 794. Its transmission or the revelation of its contents in any manner to an unauthorized person is prohibited by law.

BY R. E. Macey DATE May 15, 1956
R. E. Macey, Aerodynamicist

CHECKED ..... DATE .....

APPROVED J. A. O'Malley, Jr. DATE .....
J. A. O'Malley, Jr., Project Aerodynamicist

APPROVED P. C. Emmons DATE .....
P. C. Emmons, Chief Aerodynamicist

CONTRACT NO. Nonr 1675 (00) NO. OF PAGES 278

REPORT NO. D181-945-006 MODEL

DUCTED PROPELLER ASSAULT TRANSPORT STUDY

DUCT AND PROPELLER ANALYSIS

REVISIONS

DATE	PAGE NO.

Form E9-1 C

BELL Aircraft CORPORATION

FOREWORD

Contract Nonr 1675 (00) was awarded to Bell Aircraft Corporation by the Office of Naval Research under sponsorship of the Army Transportation Corps. This is one of a series of five study contracts let to investigate the application of various schemes to the design of Vertical Take-off and Landing (VTOL) or Short Take-off (STOL) Assault Transport Aircraft.

The particular field of investigation at Bell Aircraft is the application of ducted propeller propulsion systems to the design of aircraft capable of performing the Assault Transport mission. The results of the investigation are presented in the following listed reports:

TITLE	REPORT NUMBER
Summary Report	D181-945-001
Design Report	D181-945-002
Survey of the State of the Art	D181-945-003
Performance	D181-945-004
Stability and Control	D181-945-005
Duct and Propeller Analysis	D181-945-006
Preliminary Structural Analysis	D181-945-007
Standard Aircraft Characteristics Chart	D181-945-008

This document has been reviewed in accordance with [illegible] security classification assigned hereto is correct.

Date: 7/30/52

By direction of
Chief of Naval Research (Code 461)

FOREWORD

Contract Nonr 1675 (00) was awarded to Bell Aircraft Corporation by the Office of Naval Research under sponsorship of the Army Transportation Corps. This is one of a series of five study contracts let to investigate the application of various schemes to the design of Vertical Take-off and Landing (VTOL) or Short Take-off (STO) Assault Transport Aircraft.

The particular field of investigation at Bell Aircraft is the application of ducted propeller propulsion systems to the design of aircraft capable of performing the Assault Transport mission. The results of the investigation are presented in the following listed reports:

TITLE	REPORT NUMBER
Summary Report	D181-945-001
Design Report	D181-945-002
Survey of the State of the Art	D181-945-003
Performance	D181-945-004
Stability and Control	D181-945-005
Duct and Propeller Analysis	D181-945-006
Preliminary Structural Analysis	D181-945-007
Standard Aircraft Characteristics Chart	D181-945-008

This document has been reviewed in accordance with OPNAVINST 5510.17, paragraph 5. The security classification assigned hereto is correct.

Date: 7/30/56

By direction of
Chief of Naval Research (Code 461)

ABSTRACT

This report contains the results of the ducted propeller studies conducted under Contract No. Nonr 1675 (00). An extensive compressible momentum analysis has been made, for both the static and the in-flight cases, and curves covering the complete results are contained in Appendices A and B. A survey of the available turboprop power plants was completed, and is presented in table form. Shroud and hub design are discussed, including the use of variable inlet area in order to increase static thrust. A useful design procedure has been developed and is presented in detail. Three basic types of ducted propeller are discussed. These are configurations which use inlet guide vanes, variable-pitch configurations and contra-rotating configurations. All of the designs covered by this report belong to one of these three categories. Several propeller designs are included, and their operating characteristics are presented graphically. The forthcoming wind tunnel tests at the University of Wichita are covered in the last section of the report, and model specifications and photographs are included.

TABLE OF CONTENTS

TABLE OF CONTENTS (Cont'd)

SUMMARY AND CONCLUSIONS

Bell Aircraft Corporation has conducted a systematic analysis of the effects of various design parameters on ducted propeller performance. A preliminary design procedure has been established, and the detail design of several different ducted propeller configurations has been completed. Wind tunnel tests now underway at the University of Wichita will provide experimental data which will be compared to the theoretical results of this report.

A generalized compressible momentum study has been completed which shows the effects of duct geometry, horsepower input and altitude on ducted propeller performance. Preliminary analyses show that high subsonic speeds may be attained with this type of aircraft. Detailed analyses have shown that, for a given power input, there is an optimum static pressure ratio at which the best values of thrust/horsepower ratio may be obtained. The parameter HP/A_{in} is critical in determining the static thrust obtainable, lower values of HP/A_{in} resulting in higher values of static thrust/horsepower. Under forward flight conditions, it has been shown that low disk power loadings are desirable. However, low power loadings result in a greater range of fan velocities over which the propeller must operate, thereby increasing the off-design problems. A complete summary of the momentum studies carried out under this contract is presented in Appendices A and B. Judicious use of the momentum data presented in this report should enable the design of a practical ducted propeller system.

In the design of a ducted propeller system, it is essential that the duct design and engine selection be carried out simultaneously, since the

internal geometry of the duct and the power available are critical factors in determining the amount of thrust available from the system. All of the ducted propeller configurations presented in this report have been designed in conjunction with a specific turboprop engine. A turboprop power plant is the most logical installation for ducted propeller applications, due to the low weight/power ratios available and the reduced frontal area. A survey of foreign and domestic power plants available has been made, and is presented in table form. For the particular engines used, the variation of the important characteristics with speed and altitude are presented.

Duct design is covered in Section B, Part II. In order to resolve the conflicting requirements of a large inlet area under static conditions and a low drag configuration for high speed flight, retractable inlet flaps have been utilized in all designs. It is expected that good results will be obtained from the resultant split-flap arrangement, and this assumption is supported by the experimental results of Krüger (Reference 6). The effects of shroud length and hub-tip ratio are also discussed in this section. Krüger (Reference 6) has shown the desirability of small shroud length/diameter ratios. A large hub-tip ratio has the advantages of less twist, less sensitivity of the system to off-design operation, and large volume to permit engine installation in the hub or the use of multi-bladed variable pitch mechanisms. Disadvantages are the weight and the adverse effects of drag. These factors must be compromised in the selection of hub size.

Due to the over-all size limitations imposed upon the designs, it was necessary that high power loadings be employed. These high power loadings resulted in solidities and pressure ratios which were much higher than

those obtained on present day propellers. As a consequence, low speed cascade data, such as that used in the design of axial-flow fans and compressors, was used in the design of the ducted propeller configurations presented in this report. A modified NACA 65 - series compressor blade section has been used for rotor design. In some instances, solidities lower than those covered by the available NACA data have been used. In these cases, the available data has been extrapolated to cover the lower solidity range. These extrapolations have been checked by experimental tests, and found to be in fairly good agreement at the design point. At off-design points, however, agreement was poor. Nevertheless, it is felt that the data thus obtained is valid within the scope of this study, since the low-solidity data was used with variable pitch configurations where the blade angle of attack variation over the speed range is not as great as for a fixed pitch configuration. Further cascade tests in the low-solidity range are desirable. The C-factor of Reference 16 was used to check blade limit loading, and the data of that report has been replotted in carpet form. A linear variation in blade thickness has been assumed, the variation being from 10% at a relative inlet Mach number of .4 to 4% at a relative inlet Mach number of 1.0. In the configuration which employed exit stators, the exit stators have been designed to remove all of the residual whirl in the air stream under static conditions at 6000 feet on a 95° day.

The design of a ducted propeller system which will perform satisfactorily at a given point in the flight regime is relatively straightforward, but operation at other than the design point presents several problems.

At other points in the flight regime the forward velocity, altitude, horsepower input, rotational velocity, or a combination of these parameters may be different than at the design point. Under these conditions, a fixed pitch configuration will operate inefficiently and, over a large range of operating conditions, may overspeed or suffer a drastic reduction in thrust. With a direct-drive constant-speed engine such as a turboprop, trying to alleviate these conditions by varying engine RPM is unsatisfactory. The most practical means of solving the off-design problem is to incorporate into the design some means of varying the effective angle of attack of the blades, such as the use of variable pitch or variable inlet guide vanes. Both types of configuration have been included in this report. A simplified expression which indicates power absorption at off-design conditions, called the power factor, has been developed. This factor indicates the inlet guide vane turning or pitch change necessary to absorb the full power input.

Three specific engines were used in the ducted propeller systems designed under this study. They are the Wright Aeronautical T-49, the Rolls-Royce RB-109 and the Allison 550-B1. The T-49 configurations were fixed pitch rotor configurations, employing variable inlet guide vanes and exit stators. This configuration was also used with the RB-109 engine and, in addition, a variable pitch configuration employing exit stators was also designed for this power plant. In addition to the inlet guide vane configuration, a contra-rotating propeller was designed for use with the Allison 550-B1.

The most satisfactory T-49 configuration has a design flight speed of 200 knots at sea level standard conditions. The fan diameter is 11.6 feet and the inlet diameter under static conditions is 15.5 feet. This design has 17 fixed-pitch rotor blades, 19 exit stators, and 21 symmetrical variable-pitch inlet guide vanes. The fan rotates at 1235 RPM, the power available at the design point is 9383 HP, and the design will put out a static fan thrust of 17,370 pounds at 6000 feet on a 95° day. The inlet guide vane settings range from +18° to -15° at sea level. While this is not an optimum design, it is nevertheless an acceptable configuration which will operate satisfactorily over the required speed range.

The best RB-109 design was a variable pitch configuration having a design point of 200 knots at sea level. This configuration has 10 variable-pitch rotor blades and 15 exit stators. The fan and inlet diameters are the same as for the T-49 design, but the hub is somewhat smaller, the hub-tip ratio being .3 as compared to .4 for the T-49. The fan rotates at 1143 RPM and is designed for a static thrust of 11,317 pounds at 6000 feet on a 95° day. The required pitch change ranges from approximately 10° under static conditions to -16° at a forward speed of 400 knots.

In addition to a fixed pitch, inlet guide vane configuration, a contra-rotating fan was designed for use with the Allison 550-B1. The contra-rotating configuration has a hub tip ratio of .5, thereby permitting the installation of two 550-B1's in the hub. The fan diameter of this design is 11.8 feet and the static inlet diameter is 15 feet. The contra-rotating propellers turn at 996 RPM and are designed for a total static thrust of 22,550 pounds at the high altitude and temperature conditions. Assuming

that the maximum forward flight speed is 400 knots at sea level, the maximum pitch change required for the front rotor is 10.25° and for the rear rotor it is 11.75°. Several designs having high pre-whirl inlet vanes were also attempted, but proved to be unsatisfactory. Since a lack of time prevented any concerted effort to overcome the difficulties which were encountered in these high pre-whirl designs, it is felt that the potentialities of this concept have not been fully exploited.

As a result of the studies contained in this report, it appears that both inlet guide vanes and variable pitch are feasible means of obtaining satisfactory off-design operation. A variable pitch configuration is somewhat more desirable, since the range of the variation in blade effective angle of attack is smaller. Although the incorporation of variable pitch into a fan having 10 or 12 blades might necessitate an extensive development program, the large volume of the hub should be adequate to house a practical variable pitch mechanism. With the inlet guide vane designs, the high speed end of the flight regime has been limited due to the prohibitive vane angles required, but it is felt that a further study of the concept would result in modifications which would enable these configurations to attain forward speeds competitive to the variable pitch designs.

On April 23, 1956, wind tunnel tests were begun at the University of Wichita to check the theoretical methods of this report. Two models will be tested. They are 1/10 scale models of the 200 knot T-49 configuration and the RB-109 variable pitch configuration. A slight modification has been made to the T-49 design, in that the number of inlet stators has been

changed from 21 to 18. Model specifications are included as part of this report. Both force tests and pressure tests will be conducted, at angles of yaw from 0° to 90°. The inlet sections of the models are interchangeable, so that both high speed and static configurations may be tested. The results of these tests will be published by the University of Wichita in a future report.

INTRODUCTION

Bell Aircraft Corporation, under Contract No. Nonr-1675(00), has conducted a study for the Office of Naval Research, Department of the Navy, to investigate and evaluate the application of a ducted propeller propulsion system to the design of an assault transport aircraft. The aerodynamic portion of this program was conducted in four phases:

1. A general review of the state of the art. This phase included a survey of the available literature on ducted propeller theory, design and experimental results, and visits to various private and government agencies to discuss particular design aspects.
2. A systematic analysis of the effects of various parameters on ducted propeller performance, and the establishment of a satisfactory design procedure. The detail design of several different ducted propeller configurations was included in this portion of the program.
3. An examination of the effect of various aerodynamic parameters on the performance of ducted propeller aircraft, and detailed performance analyses of several assault transport configurations.
4. A preliminary stability and control analysis of the final configuration chosen, including hovering, transitional and forward flight.

This report covers phase 2 above, and is one of four aerodynamic reports to be submitted under this contract.

The studies included in this report are presented in two parts. Part I covers the extensive momentum analyses which were conducted to determine the effects of various design parameters on the performance of a ducted propeller. The general design procedures used are contained in Part II, which also covers the detailed design of all ducted propeller configurations investigated under this contract. Throughout this report, the terms "propeller" and "fan" are used interchangeably.

PART I

PART I

MOMENTUM ANALYSIS

In order to conduct a detailed investigation of the influence of various parameters on ducted propeller design, it is necessary to utilize a general type of approach to the problem so that the results may be applied to any configuration which is to be designed or studied in detail. A momentum approach is ideally suited to this type of situation. Through the use of a generalized momentum analysis, it is possible to calculate the forces and velocities produced by the flow through a duct without regard to the mechanism which is producing the flow. In the case of a ducted propeller study, it therefore becomes possible to determine the thrust which will be generated by a particular system, as well as the velocity of the flow through the duct, without first establishing a detail design of the propeller itself.

The general momentum studies conducted at Bell Aircraft Corporation during the course of this study are outlined in the following sections. Preliminary studies were conducted without regard for pressure losses, since only general trends which would indicate the effects of various parameters were desired. More refined momentum analyses for both the static and forward flight cases are presented in Sections B and C, respectively. Originally, these calculations were performed as required on desk calculators. Subsequently, however, as the need for information grew, and in order to make the study completely general, solutions were obtained by the use of IBM equipment, covering a complete range of variables.

A. Preliminary Momentum Studies

The momentum studies conducted during this part of the program were based on the one-dimensional compressible channel flow equations and the general approach of Reference 1 was followed. The following assumptions are made throughout:

1. The total temperature is constant through the duct except for energy addition at the propeller.
2. The mass flow is constant.
3. The total pressure at the inlet is equal to free stream total pressure.
4. The static pressure at the exit is equal to free stream static pressure.

From the momentum theorem, it may be found that the thrust from a ducted propeller system is given by

$$F_e = W/g\,(V_e - V_o) \tag{1-1}$$

where F_e = thrust

W/g = mass flow

$(V_e - V_o)$ = change in velocity through the duct

The classical derivation of this equation may be found in various texts, such as Küchemann and Weber (Reference 2). The exit velocity may be obtained from the relationship

$$\frac{V}{\sqrt{T_t}} = \frac{\sqrt{\gamma g R}\, M}{\sqrt{1 + \frac{\gamma - 1}{2} M^2}} \tag{1-2}$$

It is also known that

$$\frac{P_t}{P} = \left(1 + \frac{\gamma - 1}{2} M^2\right)^{\frac{\gamma}{\gamma - 1}} \tag{1-3}$$

and

$$T_{t_2} - T_{t_1} = \frac{T_{t_1}}{\eta}\left[(R_F)^{\frac{\gamma - 1}{\gamma}} - 1\right] \tag{1-4}$$

where R_F is the total pressure ratio across the propeller or fan, η is the adiabatic efficiency, and the subscripts 1 and 2 refer to stations immediately in front of and behind the propeller.

Using Equations (1-2), (1-3) and (1-4), and recalling that $\frac{\gamma}{\gamma - 1} = \frac{C_p}{R}$, Equation (1-1) may now be written as

$$F_e = W\left\{\sqrt{\frac{2C_pJT_{t_1}}{g}\left[1 - \left(\frac{P_o}{P_{t_2}}\right)^{\frac{\gamma - 1}{\gamma}}\right]\left[1 + \frac{1}{\eta}\left\{\left(\frac{P_{t_2}}{P_o}\right)^{\frac{\gamma - 1}{\gamma}} - 1\right\}\right]} - \frac{V_o}{g}\right\} \tag{1-5}$$

The horsepower absorbed by the propeller is

$$HP = \frac{WC_pJ}{550}\,\frac{T_{t_1}}{\eta}\left[\left(\frac{P_{t_2}}{P_{t_1}}\right)^{\frac{\gamma - 1}{\gamma}} - 1\right] \tag{1-6}$$

Under static conditions and considering no inlet losses, $P_o = P_{t_1}$. Setting $V_o = 0$ and dividing (1-5) by (1-6), the static thrust/horsepower ratio becomes

$$\frac{F_e}{HP} = \frac{1100}{\sqrt{2gJC_p}}\left(\frac{\eta}{\sqrt{T_{t_1}}}\right)\sqrt{\left[1 - \left(\frac{P_{t_1}}{P_{t_2}}\right)^{\frac{\gamma - 1}{\gamma}}\right]\left[\frac{1}{\left(\frac{P_{t_2}}{P_{t_1}}\right)^{\frac{\gamma - 1}{\gamma}}} + \frac{1}{\eta}\right]} \tag{1-7}$$

It can be seen from the above expression that the static propeller performance improves with decreasing ambient temperature and is nearly proportional to the efficiency, as would be expected. Equation (1-7) is plotted in Figure 1, for $\eta = .9$ and $T_{t_1} = 519°R$. Since no inlet losses are included, this curve represents an ideal condition and is presented here merely to indicate the general operating characteristics. As is well known, more thrust per unit of power input is obtained by handling a large quantity of air at low energy levels, and this trend is substantiated by Figure 1 which shows that a higher thrust-horsepower ratio may be obtained by the use of low-pressure ratio configurations.

At forward speeds the pressure and temperature entering the propeller are increased by ram, so that neglecting inlet losses

$$P_{t_1} = P_{t_0} = \left(\frac{P_{t_0}}{P_0}\right) P_0$$

and

$$T_{t_1} = T_{t_0} = \left(\frac{T_{t_0}}{T_0}\right) T_0$$

where $\frac{P_{t_0}}{P_0}$ is given by Equation (1-3) and $\frac{T_{t_0}}{T_0}$ is obtained from the relationship

$$\frac{T_T}{T} = 1 + \frac{\gamma - 1}{2} M^2 \qquad (1\text{-}8)$$

Equations (1-5) and (1-6) are valid at forward speeds. Due to the cumbersome nature of the algebra, it is usually more convenient to solve (1-5) and (1-6) separately and find the quotient. Figure 2 was obtained in this manner. From

CONFIDENTIAL

Figure 1

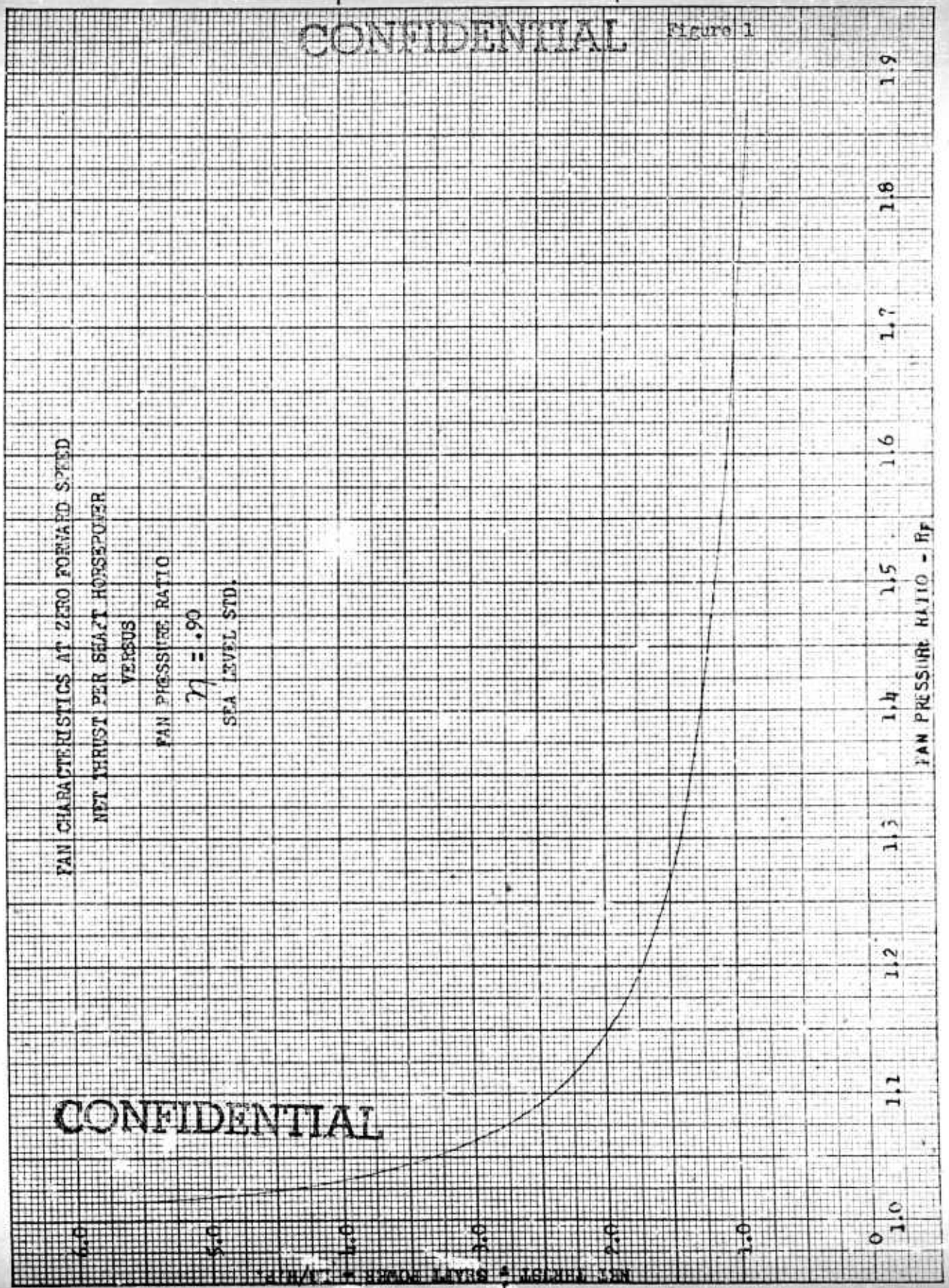

CONFIDENTIAL

CONFIDENTIAL

Figure 2

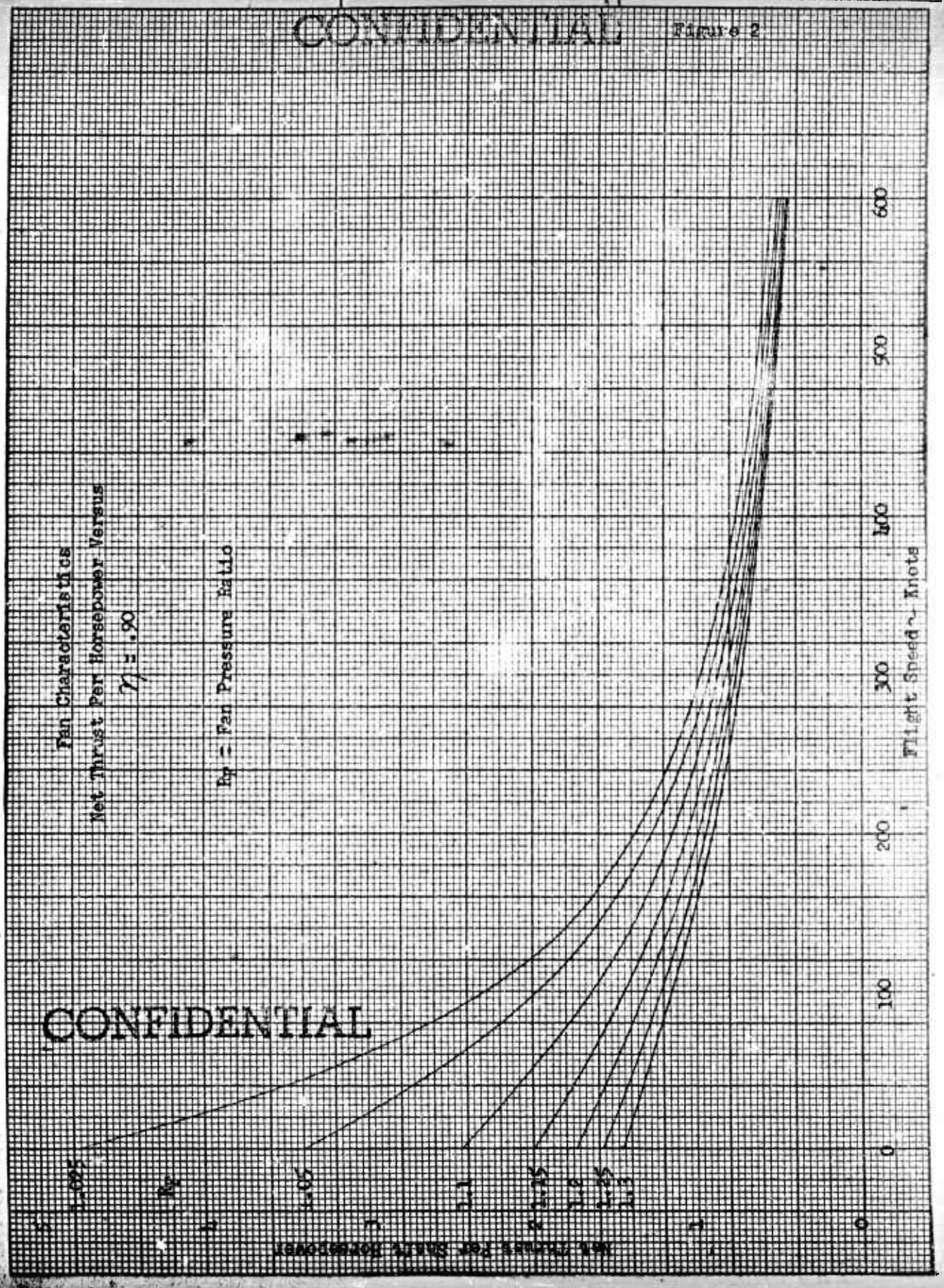

CONFIDENTIAL

this plot it may be seen that the net thrust per horsepower at constant pressure ratio decreases with increasing forward speed. The drop-off is more severe for a low pressure ratio fan, since more air is handled per unit of power.

As the forward speed increases, the density of the air passing through the fan is increased due to ram. Thus, in order to develop the same pressure ratio more power must be provided to handle the increased airflow. With the assumption that the horsepower available from a turbo-prop engine increases in approximately the same relationship, the variation at constant pressure ratio of propeller or fan thrust as a percentage of static thrust is approximately

$$\frac{F_e}{F_{e_{static}}} = \frac{F_e/HP}{(F_e/HP)_{static}} \times \frac{\rho_{t_1}}{\rho_0} \tag{1-9}$$

Since inlet losses are being disregarded for the present,

$$\rho_{t_1} = \rho_{t_0} = \left(\frac{\rho_{t_0}}{\rho_0}\right)\rho_0$$

From consideration of isentropic channel flow

$$\frac{\rho_{t_0}}{\rho_0} = \left(1 + \frac{\gamma-1}{2} M_0^2\right)^{\frac{1}{\gamma-1}} \tag{1-10}$$

and Equation (1-9) becomes

$$\frac{F_e}{F_{e_{static}}} = \frac{F_e/HP}{(F_e/HP)_{static}} \times \left(1 + \frac{\gamma-1}{2} M_0^2\right)^{\frac{1}{\gamma-1}} \tag{1-11}$$

This expression is plotted in Figure 3, for various values of fan pressure ratio.

Figure 3

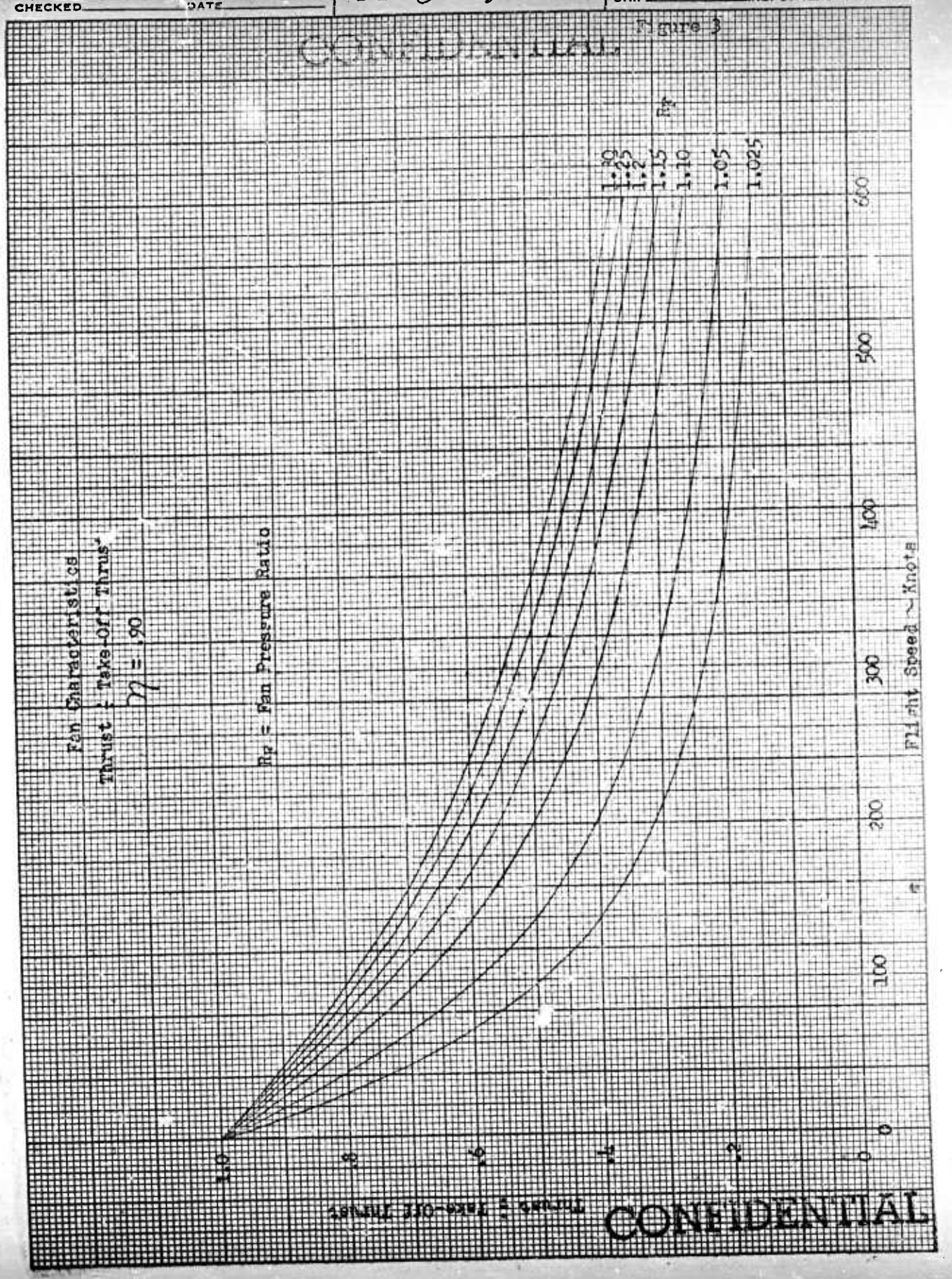

A turboprop engine also produces a small amount of residual thrust which decreases almost linearly with speed. Figure 4 shows the variation of thrust divided by static thrust for a typical fan plus turboprop engine combination.

Figures 3 and 4 are generalized curves which are intended only to show general trends. Both curves apply only at constant altitude and disregard inlet losses. Some important implications may be drawn from an inspection of these graphs. For a vertical take-off airplane propelled by ducted fans, the available thrust at take-off altitude is at least 15% of the take-off thrust, even for pressure ratios as low as 1.025. Considering a static thrust-weight ratio of 1.0, which is the minimum allowable, this means that the airplane is inherently capable of maximum speeds (at take-off altitude) such that the drag is about 15% of the airplane weight, which is a nominal value for this type aircraft. The realization of this subsonic speed capability requires a fan capable of absorbing maximum power with good efficiency at high forward speeds. This will necessarily require some satisfactory means of varying the effective pitch of the propeller blades, such as the use of a variable pitch mechanism, inlet guide vanes, variable duct geometry, or a combination of these methods.

Up to this point a simplified analysis has been presented, without regard for the effects of inlet losses or duct geometry. A more refined method is presented in the following sections, along with the results of a generalized study which was accomplished through the use of IBM equipment.

CONFIDENTIAL

Figure 4

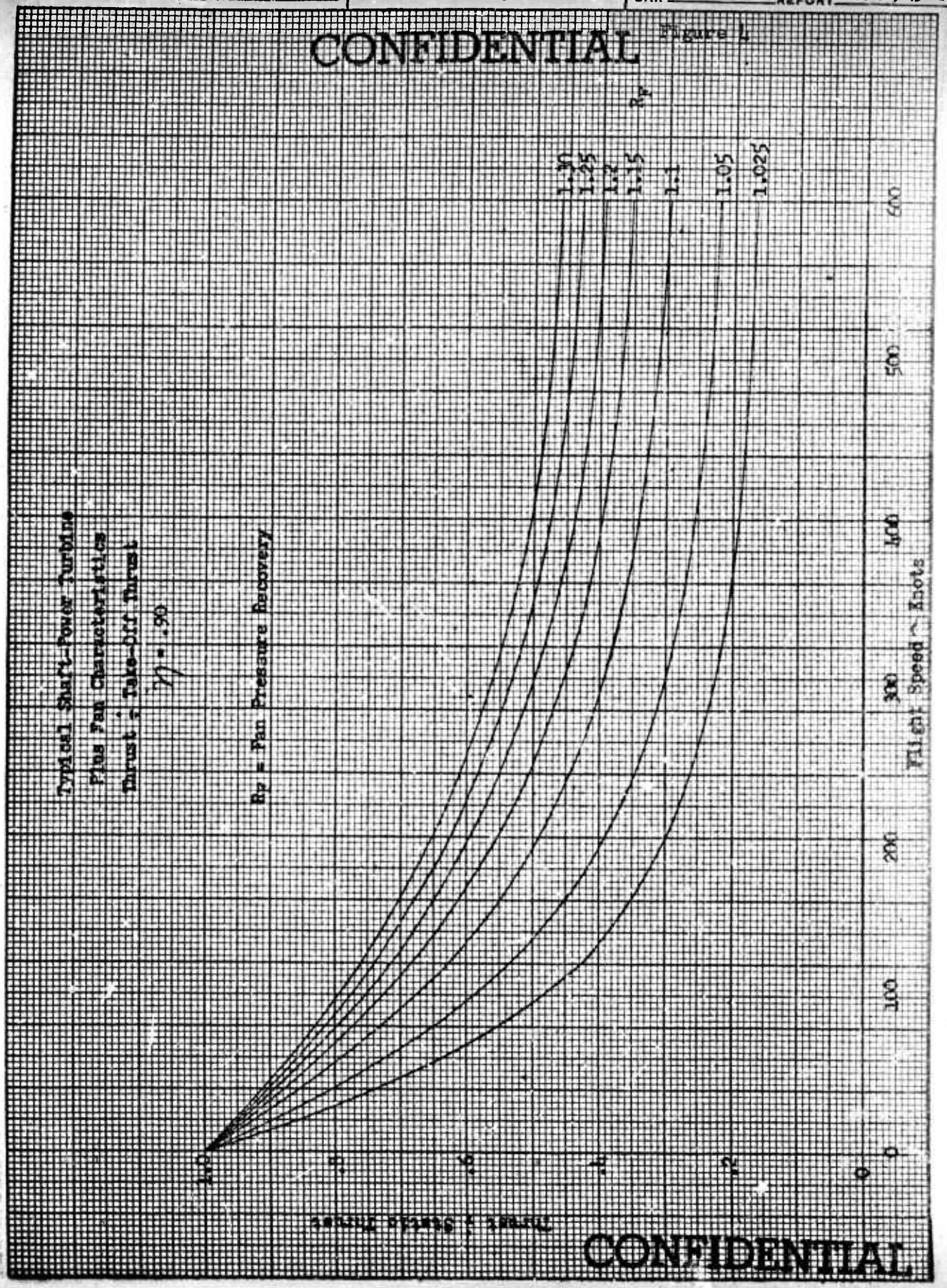

CONFIDENTIAL

B. Static Momentum Analysis

In order to determine the optimum design for a ducted propeller, it is necessary to consider such items as power absorption, inlet losses and duct geometry in the generalized momentum studies. Consequently, these parameters have been included in the following analysis. The general assumptions which were made in Part A are still applicable.

1. Method of Analysis

In considering the flow through a propeller-duct conbination, the horsepower input must be known in crder to determine the parameters necessary for detail design of the propeller itself. Then the power absorbed by the prcpeller or fan may be written

$$HP = \frac{WC_p J}{550} \Delta T_t$$

or, using (1-4)

$$\frac{HP}{W} = \frac{C_p J}{550}\left(\frac{T_{t_1}}{\eta}\right)\left[\left(R_F\right)^{\frac{\gamma-}{\gamma}} - 1\right] \qquad (1\text{-}12)$$

where η is the adiabatic fan efficiency and $R_F = \frac{P_{t_2}}{P_{t_1}}$ (see Figure 5). The weight flow may then be obtained by dividing the horsepower available by Equation (1-12).

Also,

$$W = \rho g A V = \sqrt{\frac{\gamma g}{RT}}\ PAM$$

and, using (1-3) and (1-8)

$$\frac{W\sqrt{T_t}}{AP_t} = \frac{\sqrt{\frac{\gamma g}{R}}\ M}{\left(1+\frac{\gamma-1}{2}M^2\right)^{\frac{\gamma+1}{2(\gamma-1)}}} \qquad (1\text{-}13)$$

Figure 5

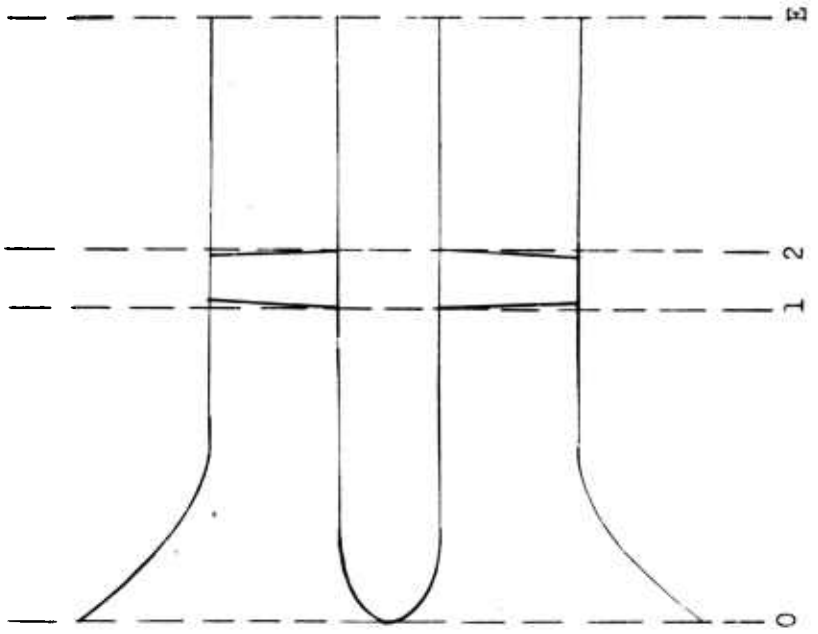

REFERENCE STATIONS FOR DUCTED PROPELLER MOMENTUM ANALYSIS

From the isentropic channel flow equations,

$$\frac{m}{m^*} = \frac{M}{\left[\frac{2}{\gamma+1}\left(1 + \frac{\gamma-1}{2} M^2\right)\right]^{\frac{\gamma+1}{\gamma-1}}}$$

Using (1-13), with $\gamma = 1.4$, $R = 53.3$ and $g = 32.2$, the mass flow ratio is

$$\frac{m}{m^*} = 1.879 \left(\frac{W\sqrt{T_{t_o}}}{A_o P_{t_o}}\right) \qquad (1\text{-}14)$$

where m* is the critical mass flow for the duct. The static inlet pressure recovery, $\frac{P_{t_1}}{P_{t_o}}$ may then be determined from Figure 6. The values obtained from Figure 6 are probably somewhat conservative, since they are based on experimental data obtained from tests on ducts which employed a slight amount of diffusion just behind the inlet (Reference 3).

Assuming that the static pressure at the exit is ambient, the exit pressure ratio may be determined from

$$\frac{P_{t_e}}{P_e} = \frac{P_{t_o}}{P_o}\left(R_F\right)\left(\frac{P_{t_1}}{P_{t_o}}\right)\left(\frac{P_{t_e}}{P_{t_2}}\right) \qquad (1\text{-}15)$$

For the static case $\frac{P_{t_o}}{P_o} = 1$, and if no expansion or contraction losses behind the fan are considered (i.e., $A_f = A_e$)

$$\frac{P_{t_e}}{P_e} = R_F\left(\frac{P_{t_1}}{P_{t_o}}\right) = R_F\left(\frac{P_{t_1}}{P_o}\right) \qquad (1\text{-}16)$$

CONFIDENTIAL

Figure 6

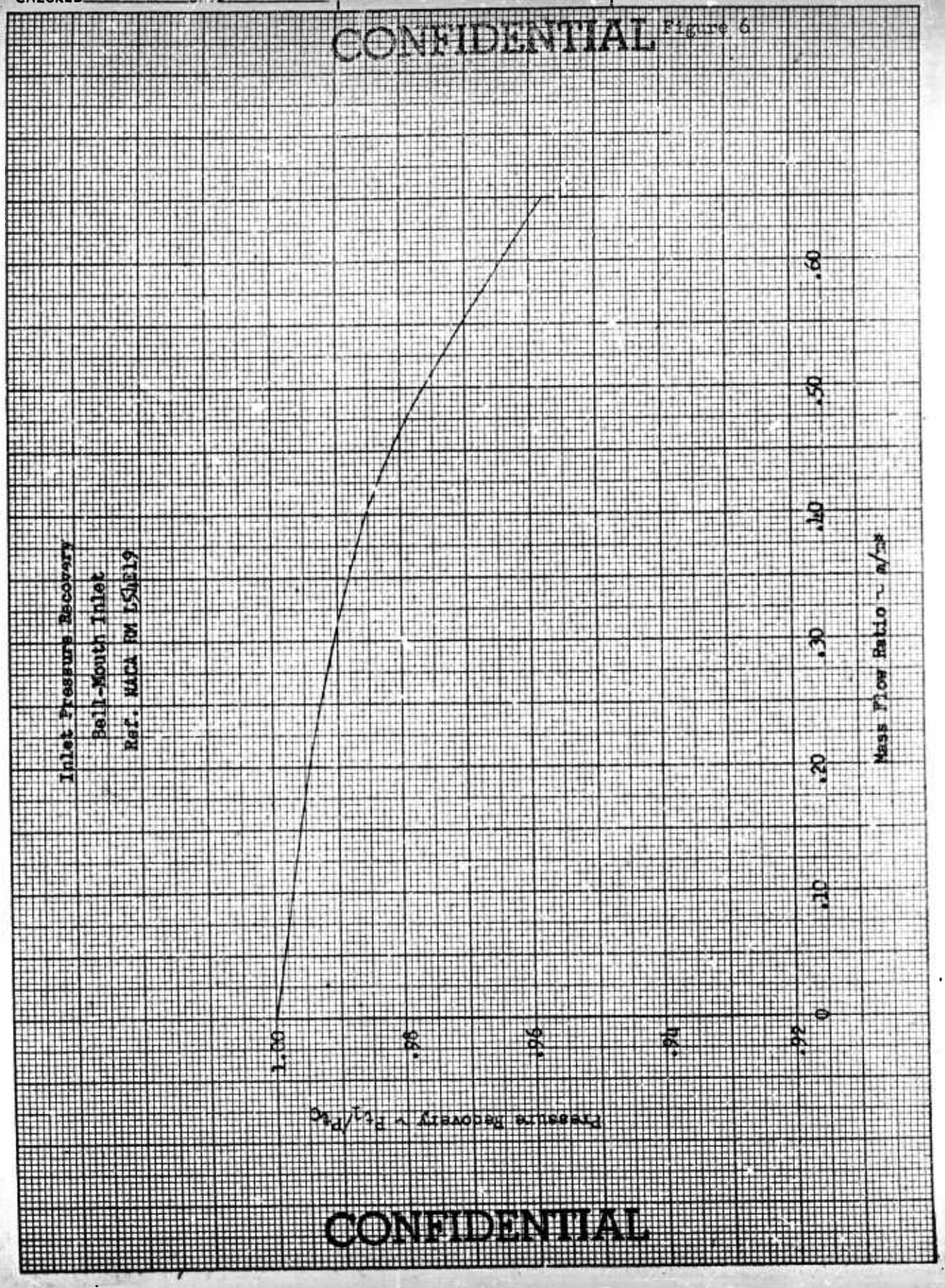

CONFIDENTIAL

Using (1-16), the axial Mach number at the duct exit, M_e, can now be determined from the relationship given in (1-3).

The net thrust of the system may be expressed as

$$F_e = \rho A V (V_e - V_o) \tag{1-17}$$

Since under static conditions $V_o = 0$, this may be written as

$$F_e = \rho_e A_e V_e^2 = \gamma P_e A_e M_e^2$$

or, using (1-8)

$$\frac{F_e}{W\sqrt{T_{t_e}}} = \frac{\sqrt{\frac{\gamma R}{g}}\, M_e}{\sqrt{1 + \frac{\gamma - 1}{2} M_e^2}} \tag{1-18}$$

Also, under static conditions, $T_{t_o} = T_o = T_e$.

Therefore, from (1-3) and (1-8)

$$\sqrt{\frac{T_{t_e}}{T_{t_o}}} = \left(\frac{P_{t_e}}{P_e}\right)^{\frac{\gamma - 1}{2\gamma}}$$

and

$$\sqrt{T_{t_e}} = \sqrt{T_{t_o}} \sqrt{\frac{T_{t_e}}{T_{t_o}}} = \sqrt{T_{t_o}} \left(\frac{P_{t_e}}{P_e}\right)^{\frac{\gamma - 1}{\gamma}} \tag{1-19}$$

The assumption that $T_{t_o} = T_o = T_e$ is not strictly valid. The correct

expression for $\sqrt{\frac{T_{t_e}}{T_{t_o}}}$ is

$$\sqrt{\frac{T_{t_e}}{T_{t_o}}} = \sqrt{\left(\frac{P_{t_1}}{P_{t_o}}\right)^{\frac{\gamma-1}{\gamma}} \left[1 + \frac{1}{r}\left(R_F^{\frac{\gamma-1}{\gamma}} - 1\right)\right]}$$

so that the assumption $T_e = T_{t_o}$ is valid only for a fan efficiency of 100%. The use of Equation (1-19), however, results in only a very small error, and this Equation was used for simplicity.

The static thrust may then be obtained from

$$F_e = W\sqrt{T_{t_e}}\left(\frac{F_e}{W\sqrt{T_{t_e}}}\right) \tag{1-20}$$

Using Equation (1-13) and the relationship $P_{t_e} = P_o\left(\frac{P_{t_e}}{P_e}\right)$, the area at the exit is

$$A_e = \frac{W\sqrt{T_{t_e}}}{P_{t_e}} \Bigg/ \left(\frac{W\sqrt{T_t}}{A\,P_t}\right)_e \tag{1-21}$$

Now

$$\left(\frac{W\sqrt{T_t}}{AP_t}\right)_1 = \left(\frac{W\sqrt{T_t}}{AP_t}\right)_e \left(\frac{P_{t_2}}{P_{t_1}}\right)\left(\frac{T_{t_2}}{T_{t_1}}\right)^{1/2}\left(\frac{P_{t_e}}{P_{t_2}}\right)\left(\frac{T_{t_2}}{T_{t_e}}\right)^{1/2}\left(\frac{A_1}{A_e}\right)$$

$$= \left(\frac{W\sqrt{T_t}}{A\,P_t}\right)_e \left(\frac{A_1}{A_e}\right)\left(\frac{P_{t_e}}{P_{t_2}}\right)^{\frac{\gamma+1}{2\gamma}} R_F^{\frac{\gamma+1}{2\gamma}} \tag{1-22}$$

If no diffusion losses are considered, the fan area equals the exit area, and (1-22) becomes

$$\left(\frac{W\sqrt{T_t}}{A P_t}\right)_1 = \left(\frac{W\sqrt{T_t}}{A P_t}\right)_e R_F^{\frac{\gamma+1}{2\gamma}} \qquad (1\text{-}23)$$

Then the Mach number at the fan ($M_f = M_1$) may be calculated from (1-13), and $\left(\frac{V}{\sqrt{T_t}}\right)_1$ can be obtained from (1-2).

The velocity at the fan is then

$$V_f = V_1 = \left(\frac{V}{\sqrt{T_t}}\right)_1 \sqrt{T_{t_0}} \left(\frac{P_{t_1}}{P_{t_0}}\right)^{\frac{\gamma-1}{2\gamma}} \qquad (1\text{-}24)$$

Since the Mach number and total temperature at the exit have previously been determined, the exit velocity, V_e, may also be obtained from the relationship given in (1-2).

The procedure outlined above may be used to determine the flow conditions in a duct of any given geometry, provided the power input, adiabatic fan efficiency and pressure recovery factors are known. In the momentum studies undertaken as a part of this contract, the pressure recovery factors used were supported by experimental data and a wide range of power input and efficiencies were assumed.

In Reference 4, Platt has shown that the thrust of a ducted propeller may be theoretically expressed by

$$\frac{F_{e\ ducted}}{F_{e\ unducted}} = 1.26 \left(\frac{A_e}{A_2}\right)^{1/3}$$

for equal operating conditions. This equation would indicate that the thrust available from a ducted propeller system is 26% greater than for an unducted propeller and can be substantially increased by increasing the size of the exit area, assuming 100% diffuser efficiency. It might also be pointed out that increasing the ratio of shroud exit area to area at the propeller plane decreases the exit velocity while increasing the mass flow. This increases the theoretical propeller efficiency but, at the same time, increases the velocity of the flow through the propeller, resulting in higher tip Mach numbers. Platt tested three ducted propellers to check the effects of diffusion behind the propeller. The ducts which were tested had length-diameter ratios ranging from .671 to .836 and ratios of exit area to propeller area ranging from 1.1 to 1.3. In the range tested, it was found that variations in the ratio of exit area to propeller area had little effect on the static thrust of the ducted propellers.

For the Assault Transport application, the use of a short duct is necessary in order to allow rotation to the vertical position while on

the ground. Various methods of short-length diffusion were discussed in some of the conferences held during the study (Reference 5), and, as yet, it has not been shown that any practical means is available. Kruger (Reference 6) has shown that diffuser losses will offset any gain obtainable unless a diffuser efficiency of about .95 can be attained. This is not considered a practical minimum for short-length diffusers. Consequently, in the studies conducted under this contract, the exit area of the duct has been considered to be equal to the disk area of the propeller.

The effect of fan pressure ratio on the thrust/horsepower ratio for several different values of inlet diameter is shown in Figure 7. The horsepower available from a T-49 turboprop engine at 6000 feet and a temperature of 95°F has been used in this example. Gearing losses and inlet losses to the engine have been included. A tendency toward establishing an optimum pressure ratio is evident, especially for the smaller inlet conditions. It can be seen from this curve that, for a given horsepower input, as the inlet area is decreased the maximum static $\frac{F_e}{HP}$ is decreased and the optimum pressure ratio is increased.

The variation of fan or exit area required with pressure ratio is shown in Figure 8. As would be expected, this curve shows that the fan area required increases rapidly with decreasing pressure ratio. Figure 9 shows the variation of fan and exit velocity with pressure ratio. Both fan and exit velocity increase with increasing pressure ratio, which is the logical trend. It may also be noted from this curve that the exit velocity is less than the fan velocity at all values of R_F. This would be true of any subsonic compressible analysis in which the exit area was considered to be

Figure 7

MOMENTUM ANALYSIS

POUNDS OF THRUST PER HORSEPOWER

STATIC CONDITIONS AT 6,000 FT. & 95°F.
6095 HP
T 49 TURBOPROP

Inlet
○ dia. = 12.5'
□ dia. = 14.0'
◇ dia. = 15.5'
△ dia. = 17.0'

T/HP ~ LB. THRUST PER HORSEPOWER

3.2
3.0
2.8
2.6
2.4
2.2
2.0
1.8
1.6

1.04 1.05 1.06 1.07 1.08 1.09 1.10

R_p = FAN PRESSURE RATIO

Figure 5

MOMENTUM ANALYSIS

FLOW AREA AT FAN OR EXIT

STATIC CONDITIONS AT 6,000 FT. & 95°F.
6095 HP
T 49 TURBOPROP

Inlet
○ dia. = 12.5'
□ dia. = 14.0'
◇ dia. = 15.5'
△ dia. = 17.0'

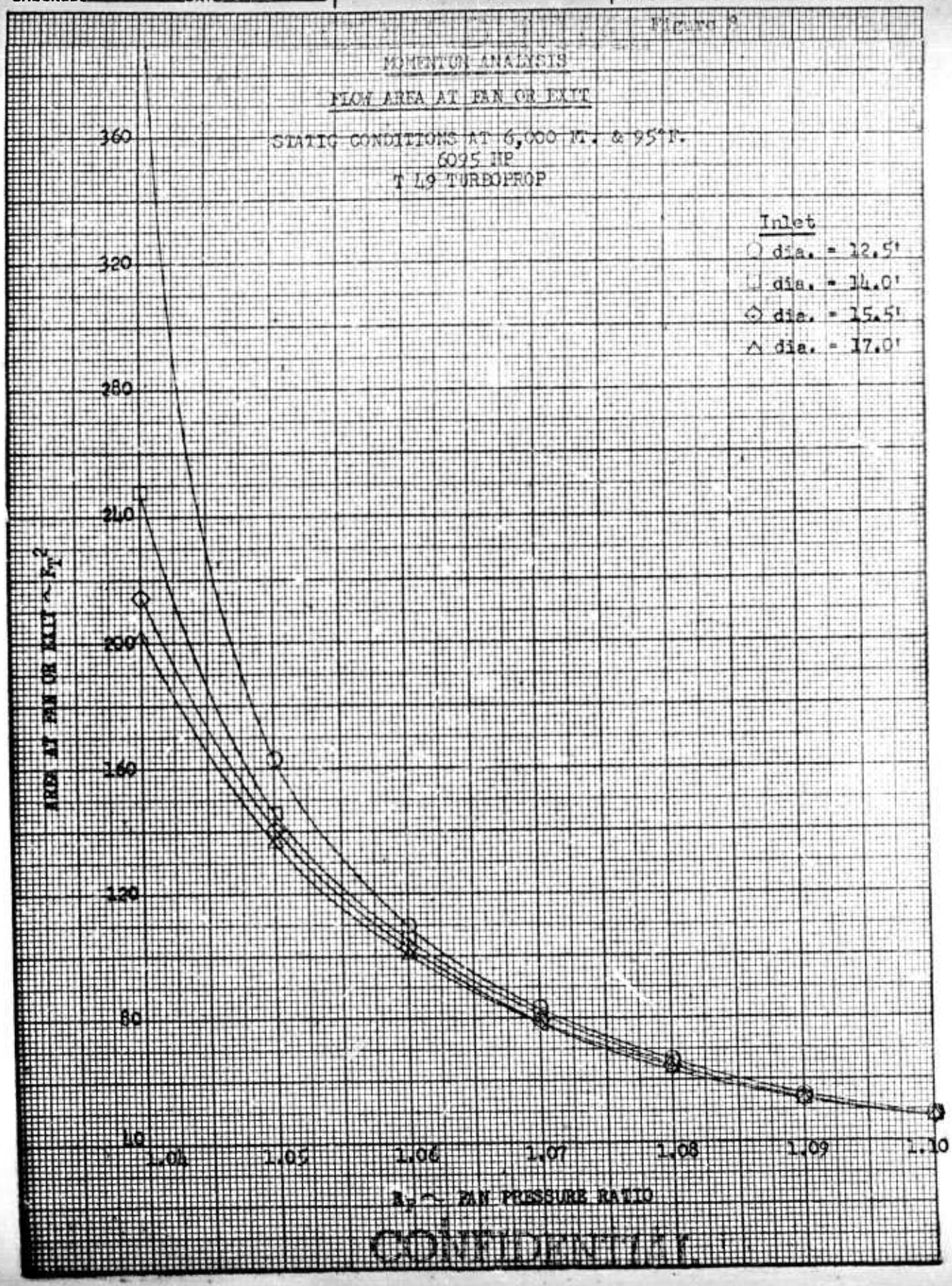

Figure 9

MOMENTUM ANALYSIS

FLOW VELOCITY AT FAN & EXIT

STATIC CONDITIONS AT 6,000 FT. & 95°F.
6095 HP
T 49 TURBOPROP

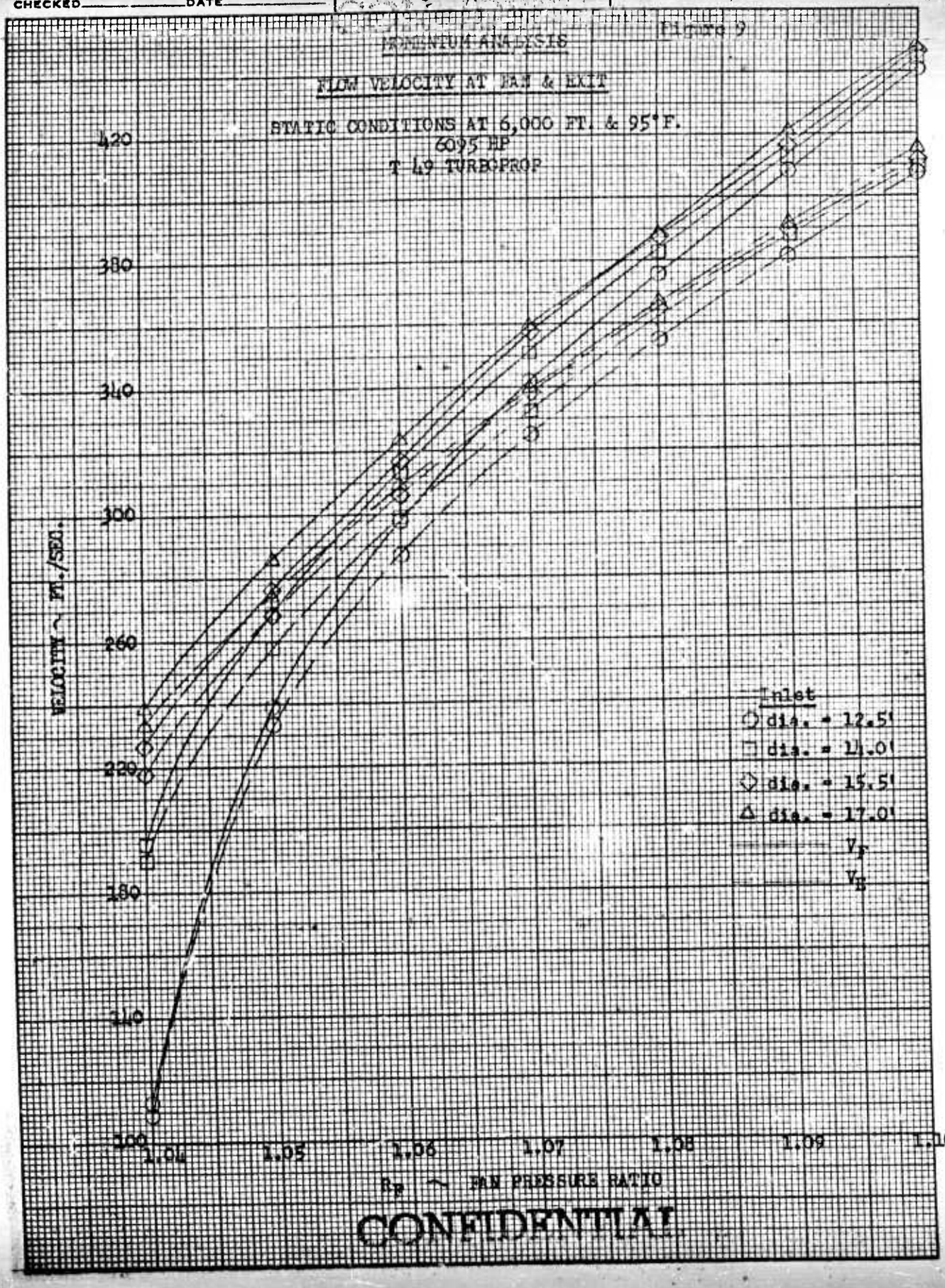

CONFIDENTIAL

FIGURE 10

MOMENTUM ANALYSIS

CONFIDENTIAL

THRUST

STATIC CONDITIONS AT 6,000 FT. & 95°F.
6095 HP
T 49 TURBOPROP

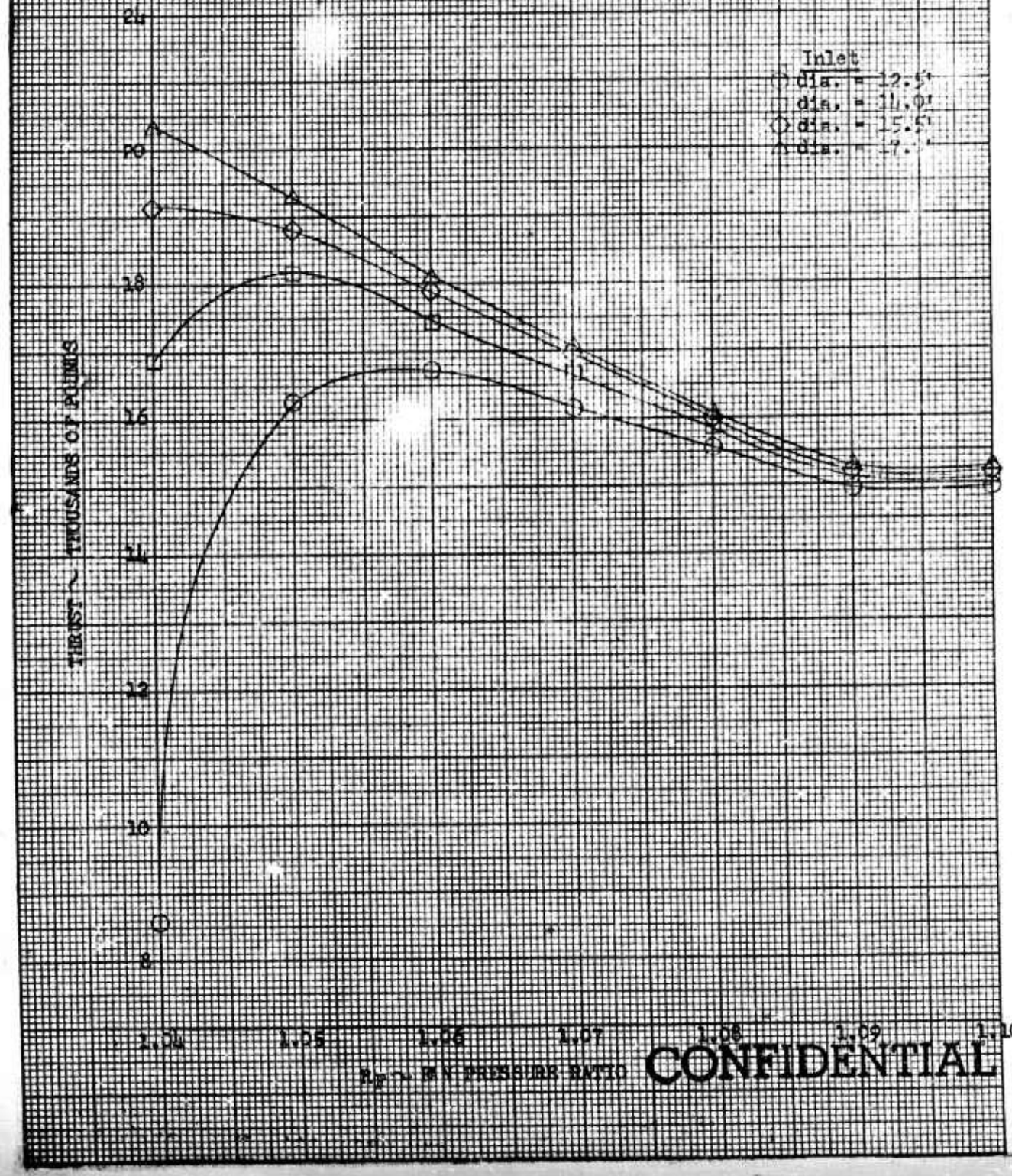

CONFIDENTIAL

equal to the fan area. Figure 10 shows the variation of thrust resulting from this analysis.

Figures 7 through 10 show the results of a typical static momentum analysis for a given set of input conditions. Desk calculators were used in the solution of the momentum equations. In order to obtain an optimum combination of shroud, propeller and engine, it is necessary to conduct a completely generalized study over a wide range of variables, so that the effects of the various parameters become known under all conditions. Such an analysis is presented in the following section for the static case.

2. Generalized IBM Analysis

The procedure outlined in Section B-1 may be adapted for solution on IBM equipment. As mentioned previously, the exit area has been considered equal to the fan area in this analysis.

For a given combination of altitude and atmospheric conditions, and for given values of R_F and η, $\frac{HP}{W}$ may be determined from Equation (1-12). Then for a predetermined value of $\frac{HP}{A_{in}}$,

$$\frac{W}{A_{in}} = \frac{HP}{A_{in}} \Big/ \frac{HP}{W} \qquad (1\text{-}25)$$

where A_{in} is the inlet area and is equal to A_o. Then the mass flow ratio, $\frac{m}{m^*}$, may be determined from Equation (1-14). In order to calculate the static inlet pressure recovery on IBM equipment, it is necessary to put the curve of Figure 6 into algebraic form. In this case a fourth degree polynomial approximation was used. The polynomial coefficients were calculated to

six decimal places, the final equation being

$$\frac{P_{t_1}}{P_{t_0}} = 1.000000 - .041714\left(\frac{m}{m^*}\right) + .126200\left(\frac{m}{m^*}\right)^2 - .340242\left(\frac{m}{m^*}\right)^3 + 133175\left(\frac{m}{m^*}\right)^4 \qquad (1\text{-}26)$$

Then the exit pressure ratio, $\frac{P_{t_e}}{P_e}$, may be obtained from (1-16).

Rearranging equation (1-3), the Mach number at the exit is

$$M_e = \sqrt{\frac{2}{\gamma - 1}\left[\left(\frac{P_{t_e}}{P_e}\right)^{\frac{\gamma-1}{\gamma}} - 1\right]} \qquad (1\text{-}27)$$

From Equation (1-13)

$$\left(\frac{W\sqrt{T_t}}{A P_t}\right)_e = \frac{\sqrt{\frac{\gamma g}{R}}\, M_e}{\left(1 + \frac{\gamma - 1}{2} M_e^2\right)^{\frac{\gamma+1}{2(\gamma-1)}}} \qquad (1\text{-}28)$$

Also,

$$\frac{W\sqrt{T_{t_e}}}{A_{in}\, P_{t_e}} = \frac{W}{A_{in}} \frac{\sqrt{T_{t_e}}}{P_0\left(\frac{P_{t_e}}{P_e}\right)} \qquad (1\text{-}29)$$

where $\sqrt{T_{t_e}}$ is given by (1-19) and $\frac{W}{A_{in}}$ by (1-25). Then the area ratio, $\frac{A_e}{A_{in}}$, between the exit (or fan) and inlet may be obtained by dividing (1-29) by (1-28). Using (1-23), the Mach number at the fan (Reference Station 1) can be determined from the relationship given by Equation (1-13).

Referring again to Equation (1-2), the velocity entering the fan, $V_f = V_1$, is given by

$$V_f = \frac{\sqrt{\gamma g R}\, M \sqrt{T_{t_0}} \left(\frac{P_{t_1}}{P_{t_0}}\right)^{\frac{\gamma-1}{2\gamma}}}{\sqrt{1 + \frac{\gamma-1}{2} M_1^2}} \tag{1-30}$$

and the velocity at the exit is

$$V_e = \frac{\sqrt{\gamma g R}\; M_e \sqrt{T_{te}}}{\sqrt{1 + \frac{\gamma-1}{2} M_e^2}} \tag{1-31}$$

Finally, since $V_o = 0$, using (1-25)

$$\frac{F_e}{A_{in}} = \frac{W}{A_{in}} \frac{V_e}{g} \tag{1-32}$$

The thrust-horsepower ratio for a given set of input values can now be determined by dividing Equation (1-32) by the input value of $\frac{HP}{A_{in}}$. The method outlined above was coded for IBM calculation, and a complete step by step summary of the procedure is given in Appendix A. These calculations give completely general results over a large range of variables. The parameter $\frac{HP}{A_{in}}$ was varied from values of 4 to 44, the fan efficiency ranged from 60% to 100%, and the fan pressure ratio covered a bracket from 1.01 to 1.10. The two operating conditions investigated were sea level on a standard day, and 6000 feet on a 95 degree day. A complete set of the carpet plots obtained from these calculations is presented in Appendix A.

Results of the static momentum analysis for a fan efficiency of 90% at sea level standard conditions are presented in Figures 11 through 13. From Figure 11 it may be seen that, for a given exit area to inlet area ratio, a reduction in the value of $\frac{HP}{A_{in}}$ results in a rather rapid reduction in pressure ratio. From Figure 12 it is evident that this reduction in pressure ratio results in a desirable increase in the thrust-horsepower ratio. This carpet plot illustrates the desirability of maintaining a low pressure ratio in ducted fan design, in order to achieve desirable values of static thrust/HP. It may also be seen that for a given value of $\frac{HP}{A_{in}}$ there is a peak value of $\frac{F_e}{HP}$. Theoretically, for any given value of $\frac{HP}{A_{in}}$, the optimum static pressure ratio for which a fan should be designed is the pressure ratio corresponding to the peak value of $\frac{F_e}{HP}$. In actual practice, it is usually more desirable to choose a pressure ratio which falls a little below this peak. Figures 11 and 12 show that lower pressure ratios may be obtained by decreasing the values of $\frac{HP}{A_{in}}$, by increasing $\frac{A_e}{A_{in}}$ for a constant inlet area, or by a combination of both. Figure 13 shows the variation in fan velocity. This plot demonstrates that the effect of the parameter $\frac{HP}{A_{in}}$ on fan velocity is slight at the higher pressure ratios, but can be appreciable at the lower pressure ratios. As would be expected, it also shows that the fan velocity increases rapidly with increasing R_F.

Figures 11, 12 and 13 may be used in the following manner: If the horsepower input to the fan is known, and also the geometry of the shroud (exit area and inlet area), then the fan pressure ratio may be determined from Figure 11. The static thrust-horsepower ratio may then be determined from Figure 12, and the velocity at the fan from Figure 13. Conversely, if

Figure 11

STATIC MOMENTUM DATA

$\frac{A_e}{A_{in}}$ vs R_p & $\frac{HP}{A_{in}}$

CONFIDENTIAL

Sea Level Standard

$\eta = .9$

Bell-Mouth Pressure Recovery

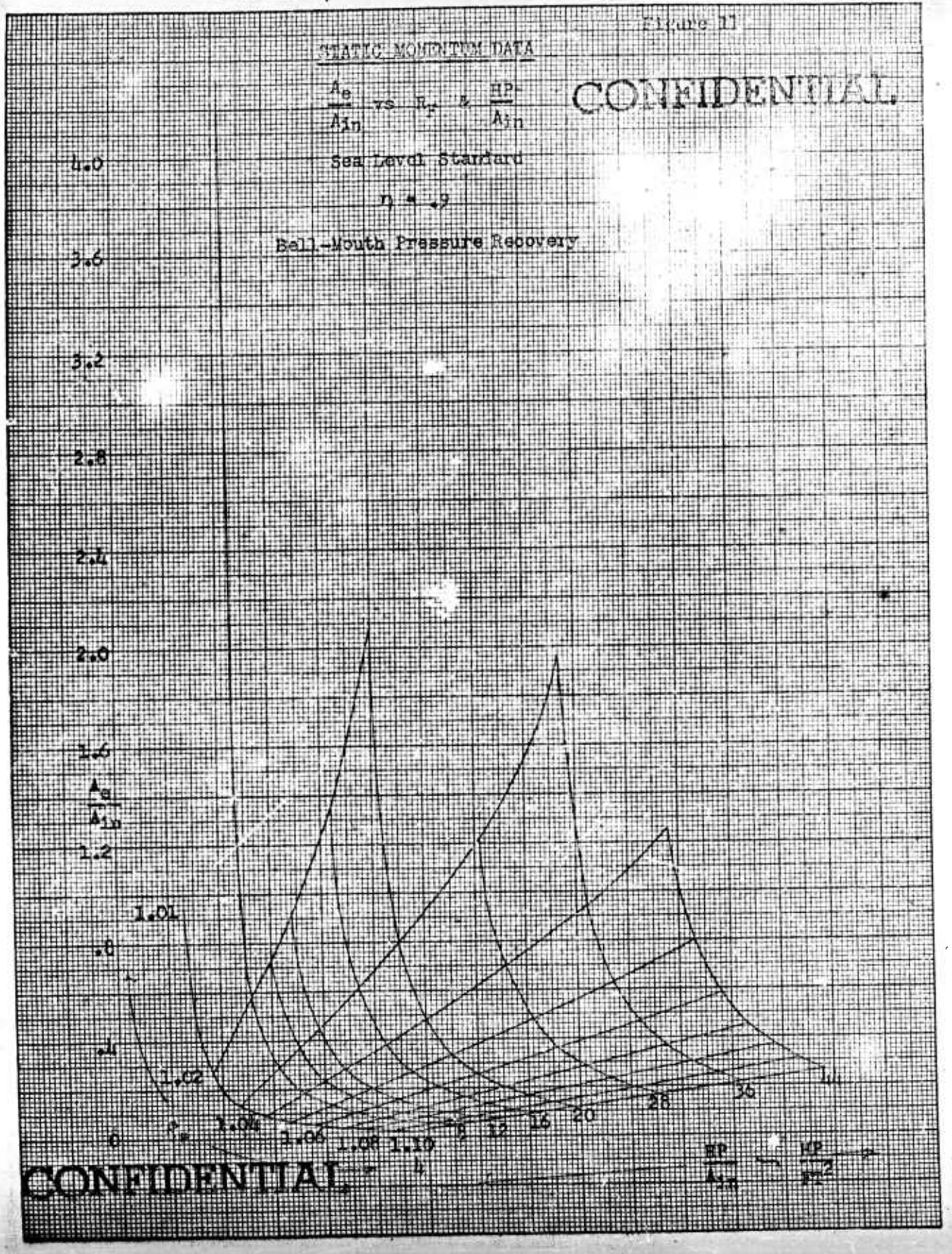

CONFIDENTIAL

Figure 12

STATIC MOMENTUM DATA

CONFIDENTIAL

$\frac{F_s}{HP}$ vs R_x & $\frac{HP}{A_1 n}$

Sea Level Standard

$\eta_c = .9$

Dell-Wouth Pressure Recovery

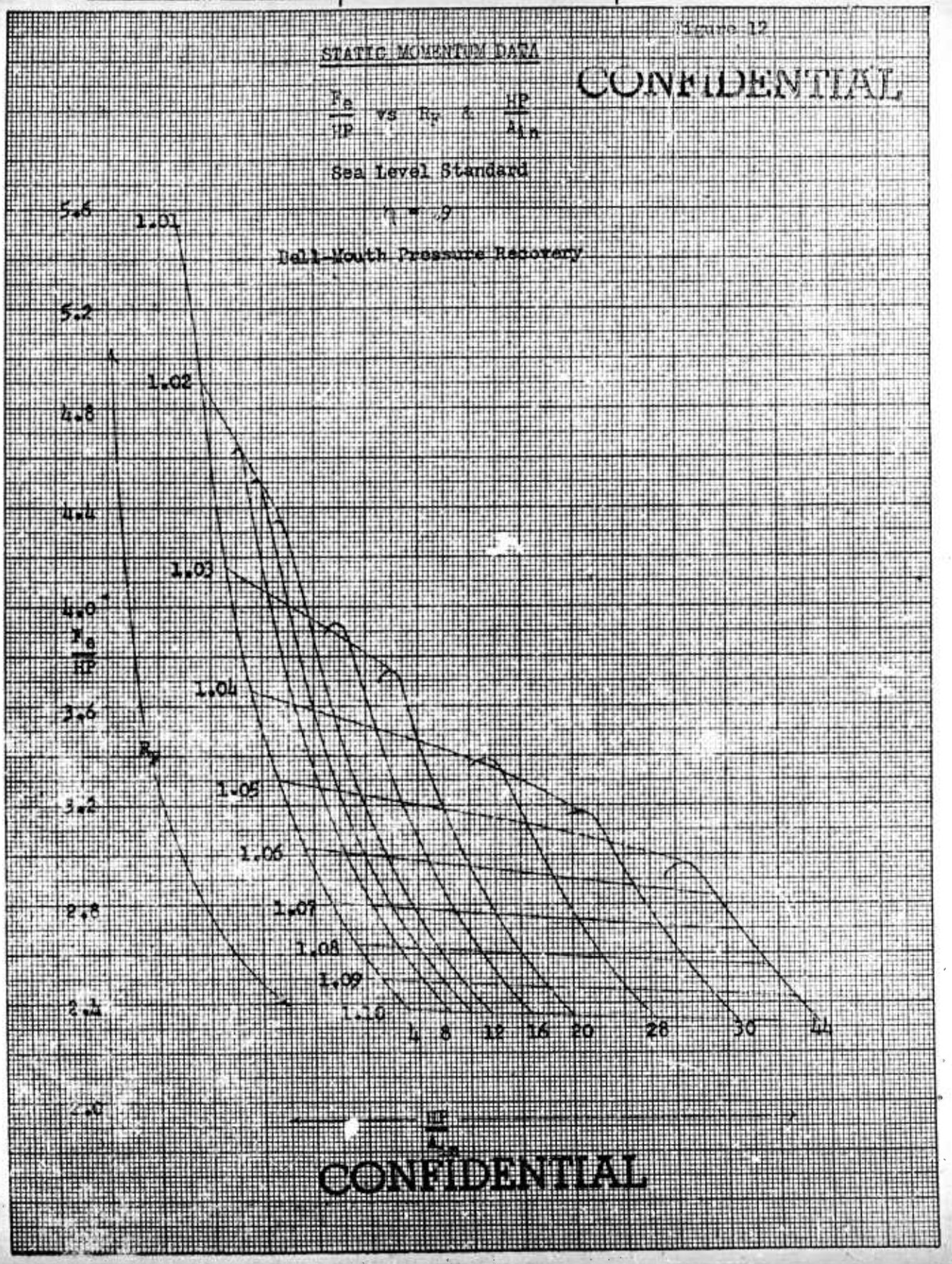

CONFIDENTIAL

CONFIDENTIAL

Figure 13

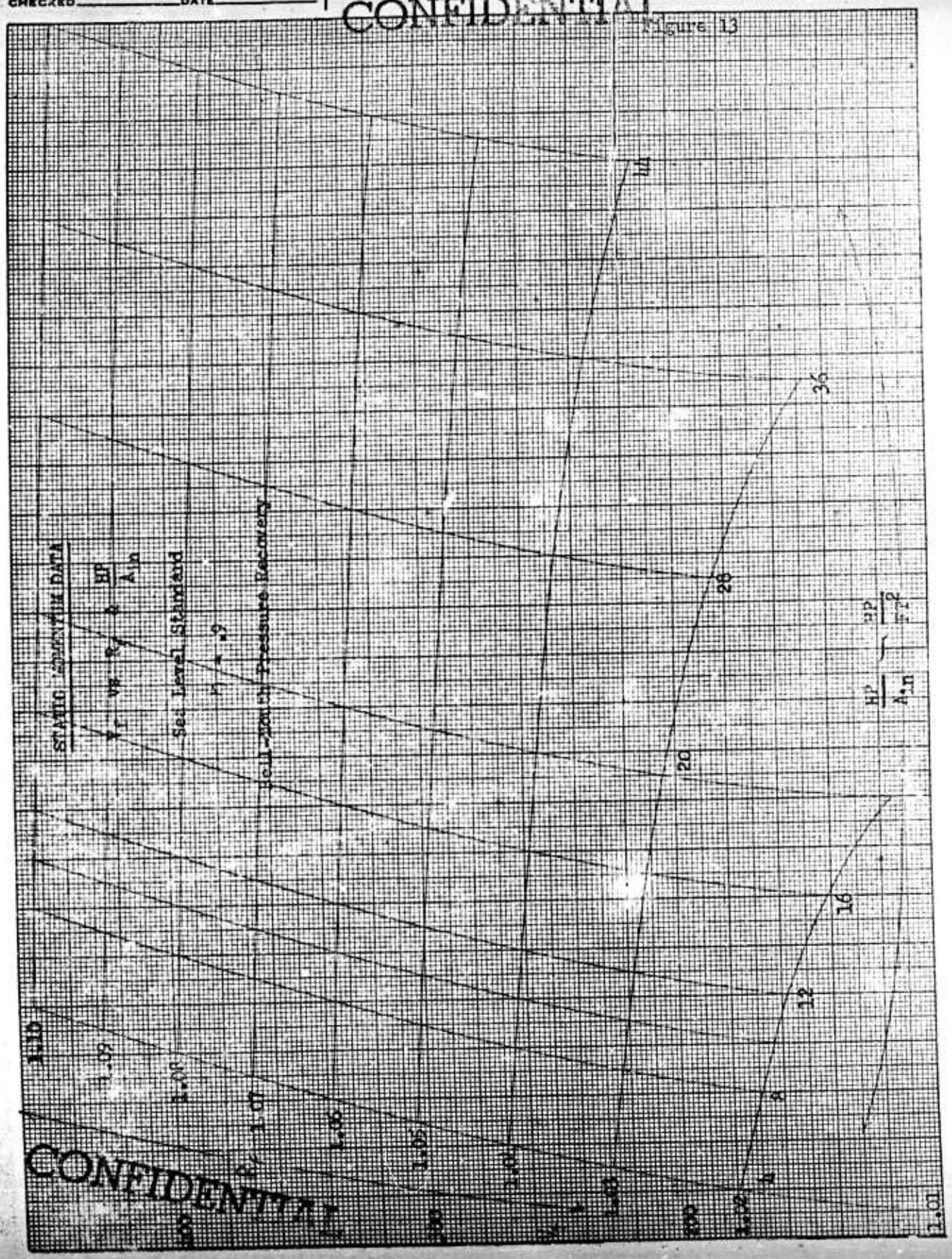

CONFIDENTIAL

the horsepower input and inlet diameter are known and a specific $\frac{F_e}{HP}$ is desired, the pressure ratio may be determined from Figure 12, and the area ratio and fan velocity from Figures 11 and 13 respectively.

The carpet plot in Figure 14 is a cross-plot of Figures 11 and 12, and may be used for any fan provided the assumptions used in the development of Figures 11 and 12 are retained. This carpet shows that the parameter $\frac{HP}{A_{in}}$ has a much greater effect on the thrust/horsepower ratio than the area ratio parameter. A specific example has been developed in Figure 15. The fan for this example has an 11.6 ft. exit diameter, absorbs 4500 HP and has a hub to tip ratio at the fan of .4. The curve shows the variation of static $\frac{F_e}{HP}$ with inlet diameter. Below an inlet diameter of about 13 ft., a bell-mouth pressure recovery can probably not be achieved and the thrust-horsepower ratio would fall off more rapidly than is shown by the calculations. Statically, this curve points up the desirability of a large inlet area, compared to the exit or fan area, for a fan of fixed diameter. Since a fixed inlet to meet such a requirement is in conflict with the desirability of a minimum drag shroud at high speeds, inlet flaps are considered as the most obvious solution.

CONFIDENTIAL

Figure 14

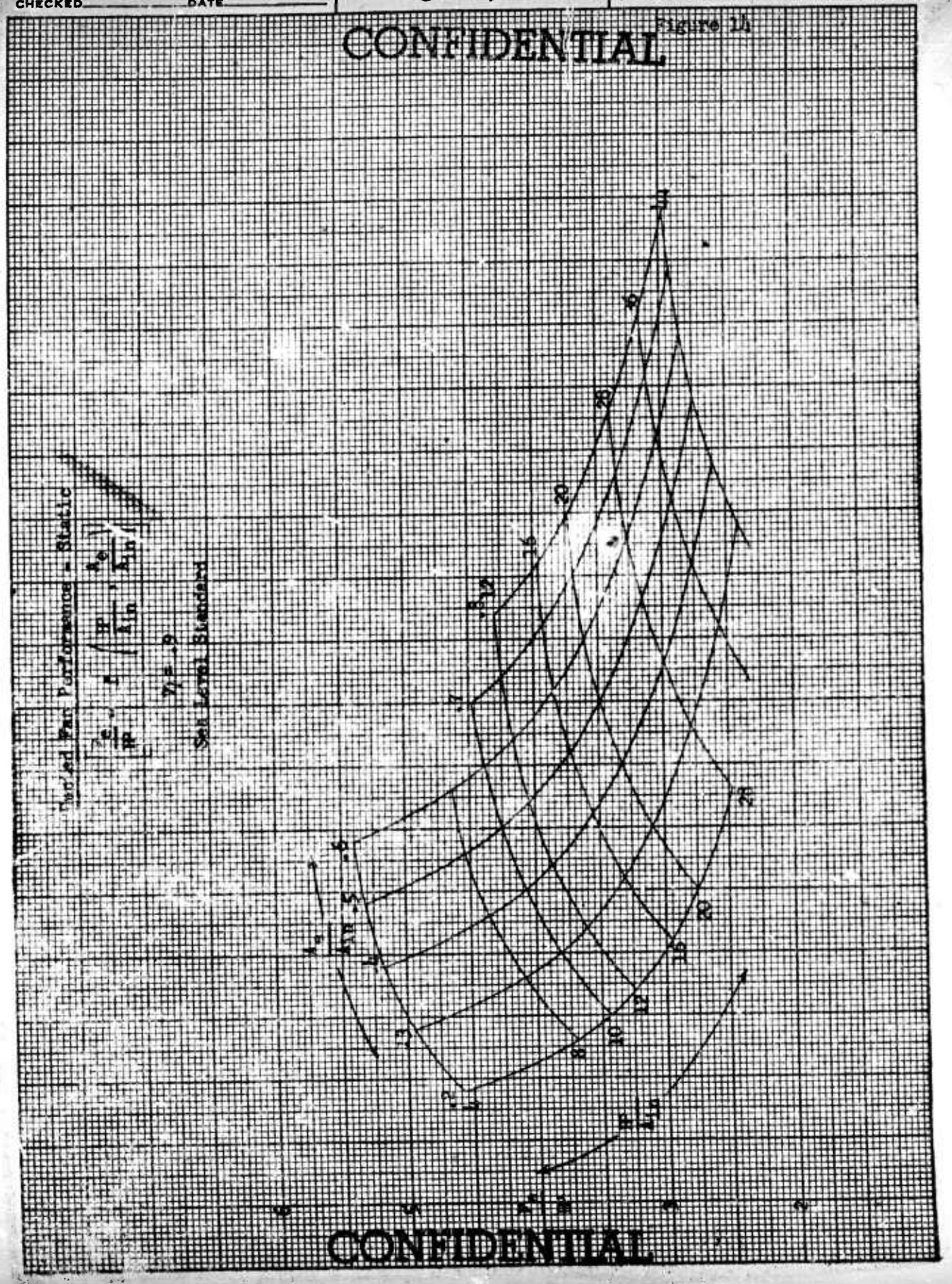

CONFIDENTIAL

CONFIDENTIAL

Figure 15

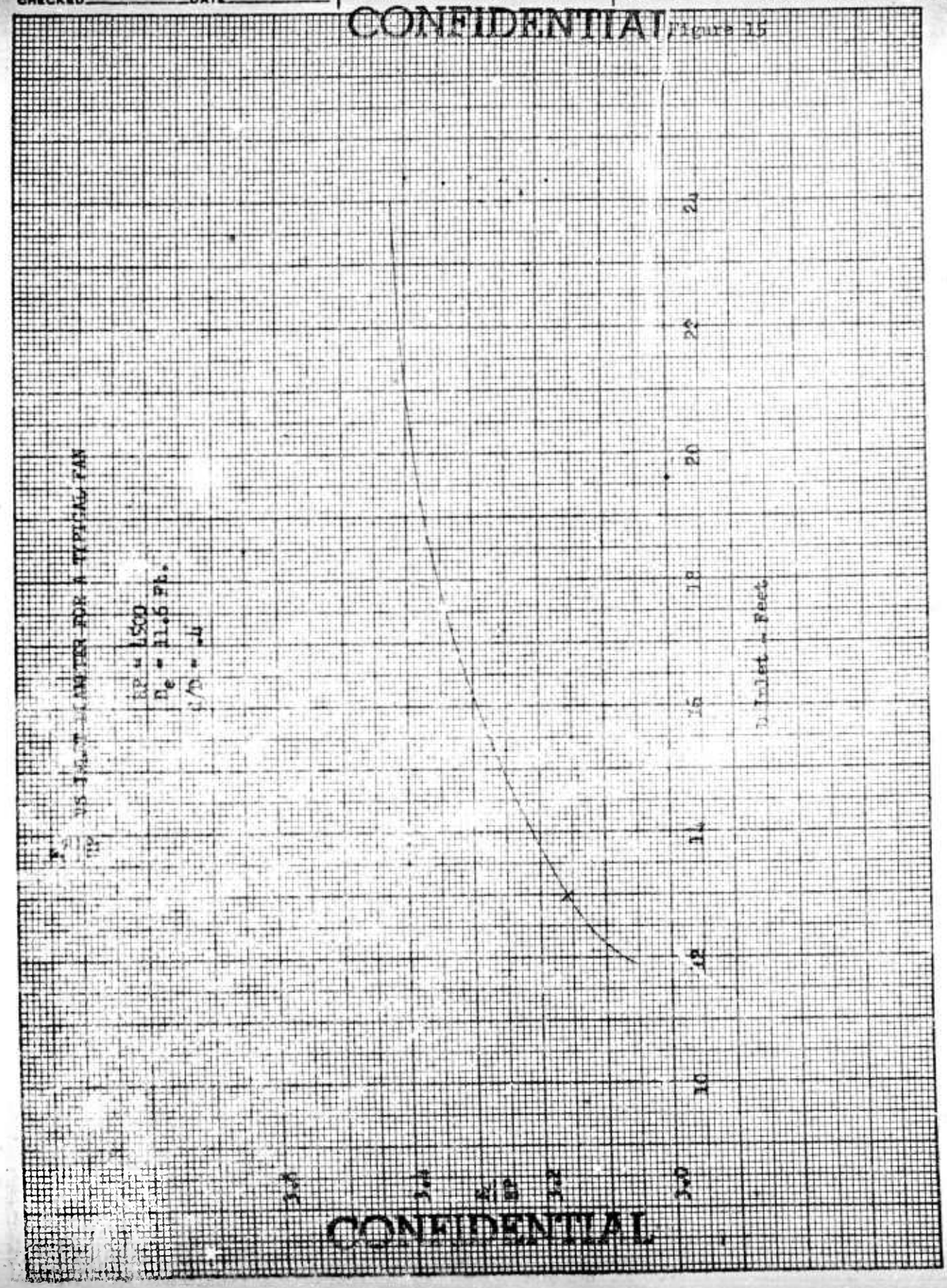

CONFIDENTIAL

C. In-Flight Momentum Analysis

A ducted propeller for use on a vertically rising aircraft is usually designed to operate in conjunction with a specific engine, and thus the horsepower available is known. Statically, an airplane thrust-weight ratio equal to or greater than 1.0 must be attained in order to achieve vertical take-off. The usual design procedure used in this study has been to determine the internal duct geometry from the static momentum data, knowing the horsepower input and the thrust-horsepower ratio desired, and then design the fan itself at some forward flight speed. In order to accomplish the detail design of the blading, it is essential that the velocity of the air entering the fan be known. This velocity, V_f, along with the thrust/horsepower ratio which is used in the airplane performance studies, may be determined by means of a momentum approach. The method used in these studies is somewhat different from that used in the static analysis, and is outlined in the following sections.

1. Method of Analysis

In Reference 7, it is shown that the tangential force on a rotor blade at any radial station is given by

$$F_t = \frac{c \rho V_f}{\sigma} \Delta w_u$$

where c = blade chord

σ = solidity

Δw_u = tangential whirl velocity

Then the total tangential force on the fan may be expressed as

$$F_t = NcR \int_{(r/R)}^{1.0} \frac{\rho V_f}{\sigma} \Delta w_u \, d(r/R)$$

where N is the number of blades and R is the radius. If constant chord blading is used, the solidity varies inversely with the radius. Assuming that the density and axial velocity are radially constant in front of the fan, the tangential force is then

$$F_t = \frac{Nc R \rho V_f}{\sigma_T} \int_{(r/R)}^{1.0} (r/R)\, \Delta w_U\, d(r/R)$$

where σ_T is the tip solidity. The torque, Q, at any point along a blade is equal to $F_t r$ or $F_t R\,(\frac{r}{R})$. Therefore

$$HP = \frac{Q\Omega}{550} = \frac{Nc\rho V_f R^2 \Omega}{550\sigma_T} \int_{(r/R)}^{1.0} (r/R)^2\, \Delta w_U\, d(r/R) \qquad (1\text{-}33)$$

If a free vortex velocity distribution is assumed, the whirl velocity also varies inversely with the radius, and (1-33) becomes

$$HP = \frac{Nc\rho V_f R^2 \Omega \Delta w_{U_I}}{550\sigma_T} \int_{(r/R)}^{1.0} (r/R)\, d(r/R) \qquad (1\text{-}34)$$

If free vortex blading is not used in the fan, the radial distribution of the fan velocity will not be constant. However, it is felt that, for any type of blading, the average axial velocity along the radius will be about the same as for the free vortex distribution, and therefore the power absorption will be the same.

Again from Reference 7, the whirl velocity may be written as

$$\Delta w_{U_t} = \frac{T_{t_1} (R_F^{\frac{\gamma-1}{\gamma}} - 1)\, g J C_p}{R\Omega} = \frac{T_{t_1} (R_F^{\frac{\gamma-1}{\gamma}} - 1)\, 10^4}{1.66\, R\Omega} \qquad (1\text{-}35)$$

where T_t, is in °K. Since $\sigma_T = \frac{Nc}{2\pi R}$ and $A_f = \pi R^2 \left[1 - (r/R)^2\right]$, upon integration (1-34) becomes

$$HP = \frac{\rho A_f V_f T_{t_1} \left(R_F^{\frac{\gamma-1}{\gamma}} - 1\right) 10^4}{1.66\,(550)} = \frac{m}{550} \frac{T_{t_1} \left(R_F^{\frac{\gamma-1}{\gamma}} - 1\right) 10^4}{1.66} \qquad (1\text{-}36)$$

Then for given values of HP and forward velocity, the ratio $\frac{m}{550}$ may be determined as a function of R_F. Taking into account the fan efficiency, the horsepower absorbed may be expressed as

$$\eta HP = \frac{m}{2\,(550)} \left[V_e^2 - V_o^2\right] \qquad (1\text{-}37)$$

from which

$$V_e = \sqrt{\frac{1100\,\eta HP}{m} + V_o^2} \qquad (1\text{-}38)$$

It is now possible to plot a curve of V_e vs. R_F or V_f, which defines the corresponding values of V_e and R_F or V_f for which the full horsepower input to the fan will be absorbed at any given forward velocity.

One of the assumptions which has been made in this analysis is that the mass flow is a constant. The mass flow may be expressed as

$$m = \rho AV = \frac{PAV}{gRT}$$

or, multiplying through by $\frac{T_t}{P_t}$

$$V = \frac{m}{A} \frac{T_t}{P_t} g R \left(\frac{P_t}{P}\right)^{\frac{1}{\gamma}}$$

Then the ratio of exit velocity to fan velocity may be expressed as

$$\frac{V_e}{V_f} = \frac{\left[\frac{m}{A}\frac{T_t}{P_t} gR\left(\frac{P_t}{P}\right)^{\frac{1}{\gamma}}\right]_e}{\left[\frac{m}{A}\frac{T_t}{P_t} gR\left(\frac{P_t}{P}\right)^{\frac{1}{\gamma}}\right]_f}$$

$$= R_F^{-\frac{1}{\gamma}} \frac{\left(P_t/P\right)_e^{\frac{1}{\gamma}}}{\left(P_t/P\right)_f^{\frac{1}{\gamma}}} \qquad (1\text{-}39)$$

$\left(P_t/P\right)_e = R_F \left(\frac{P_{t_o}}{P_o}\right)\left(\frac{P_{t_1}}{P_{t_o}}\right)$, where $\frac{P_{t_1}}{P_{t_o}}$ is the inlet pressure recovery. Using Equations (1-2) and (1-3), and using the values of R_F and V_f obtained from (1-36), V_e may be plotted as a function of R_F or V_f. The curve obtained from (1-38) fulfills the assumption of full horsepower absorption, while the curve obtained from (1-39) fulfills the assumption of constant mass flow. The intersection of these curves give the operating conditions of the fan at the given forward flight velocity. The thrust may then be obtained from (1-17)

An example of this type of calculation is shown in Figure 16 for sea level standard conditions. This particular fan had a horsepower input of 10,140 HP and a fan area of 82.1 ft.^{2}. The flight velocity was 200 knots. The curve with the negative slope represents the line of full horsepower absorption and the curve with positive slope represents the line of constant

CONFIDENTIAL

Figure 16

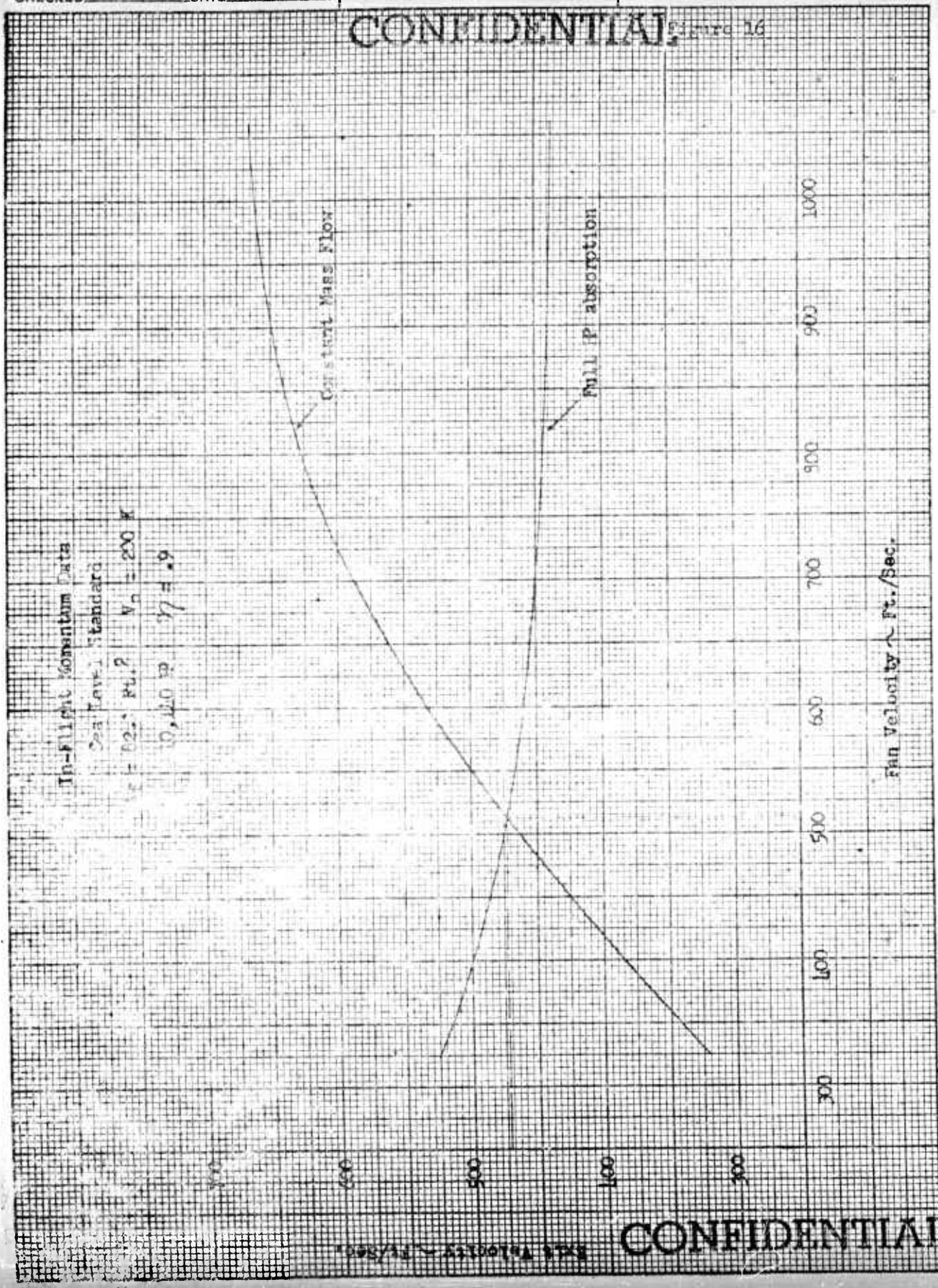

CONFIDENTIAL

mass flow. From this plot it may be seen that, for the given input conditions, the velocity at the fan is 513 ft/sec. and the velocity at the exit is 472 ft/sec. The inlet pressure recovery was assumed to be 97% for this case.

2. Generalized IBM Analysis

As in the static case, it is again desirable to have a completely generalized analysis so that the flow conditions in the duct may readily be ascertained for any operating condition. The equations contained in the previous section have been changed only slightly for IBM solution. As stated before, it has been assumed in this analysis that there is no change in total temperature except for energy addition at the fan. Knowing $\frac{HP}{A_f}$ and V_o, from Equation (1-36).

$$V_f = \frac{HP}{A_f} \frac{1}{K \rho T_{t_o} \left(R_F^{\frac{\gamma - 1}{\gamma}} \right)} \tag{1-40}$$

where K = 10.953 and $\frac{HP}{A_f}$ is the propeller power loading. Then from the relationship of (1-2)

$$M_f^2 = \frac{V_f^2 / T_{t_o}}{\gamma R g - \left(\frac{\gamma - 1}{2} \right) V_f^2 / T_{t_o}} \tag{1-41}$$

Since $m = \frac{W}{g}$, from (1-13)

$$\frac{m}{A_f} = \frac{\sqrt{\frac{\gamma}{gR}} \, k P_{t_o} M_f}{\left[1 + \frac{\gamma - 1}{2} M_f^2 \right]^{\frac{\gamma + 1}{2(\gamma - 1)}} \sqrt{T_{t_o}}} \tag{1-42}$$

where k is the inlet pressure recovery. An assumed value of k = .97 has

been used in this analysis. From (1-38)

$$V_e = \sqrt{1100\eta \frac{HP/A_f}{m/A_f} + V_o^2} \qquad (1\text{-}43)$$

Using the criterion of constant mass flow, from (1-39)

$$V_e = \frac{V_f}{R_F^{1/\gamma}} \left(\frac{P_{t_e}/P_e}{P_{t_f}/P_f} \right)^{\frac{1}{\gamma}}$$

where $\frac{P_{t_e}}{P_e} = R_F k \left(\frac{P_{t_o}}{P_o}\right)$ and $\frac{P_{t_f}}{P_f}$ is defined by (1-3).

The point of intersection of the curves defined by Equations (1-43) and (1-39) was found by an iterative process on the IBM equipment. Having determined V_e in this manner,

$$\frac{F}{A_f} = \left[m/A_f\right] (V_e - V_o) \qquad (1\text{-}44)$$

and

$$\frac{F}{HP} = \frac{F/A_f}{HP/A_f} \qquad (1\text{-}45)$$

The in-flight momentum analysis completed for this study covered a complete range of altitudes from sea level to 50,000 feet and a range of efficiencies from 50 to 100 percent. It was originally intended to also cover a range of inlet pressure recovery from .95 to 1.0, but the effect of this parameter upon the final results of the analysis proved to be

negligible. Plots of fan velocity and $\frac{F_e}{HP}$ as functions of the power loading, $\frac{HP}{A_f}$, and the free stream velocity are shown in Figures 17 and 18, for an efficiency of 90% at sea level standard conditions. From Figure 17 it may be seen that greater $\frac{F_e}{HP}$ ratios are obtained with the lower values of power loading. This figure also shows that $\frac{F_e}{HP}$ decreases as the forward speed of the airplane is increased, and the decrease is greater for the lower values of $\frac{HP}{A_f}$. Figure 18 shows that the fan velocity also decreases as the power loading decreases, and that the range of fan velocities is greater for the lower values of $\frac{HP}{A_f}$. This analysis points out that a given thrust may be obtained with the least power in a lightly loaded fan and that this fan will have low fan velocities. However, a highly loaded fan will have less drop off in thrust with forward speed and the fan will operate over a smaller velocity range. These conditions must be compromised for each configuration. A complete set of the carpet plots obtained from these calculations is presented in Appendix B.

CONFIDENTIAL

Figure 17

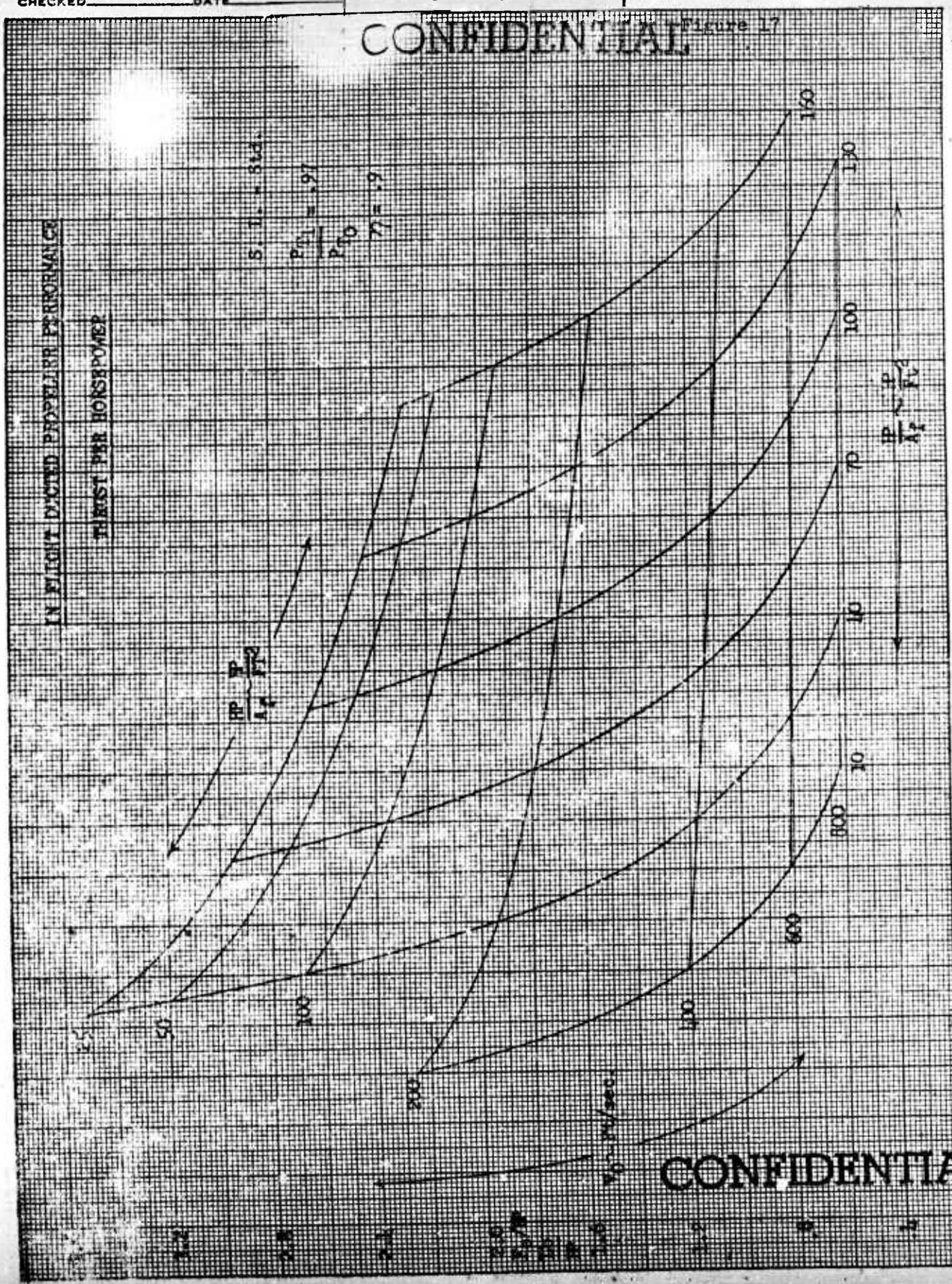

CONFIDENTIAL

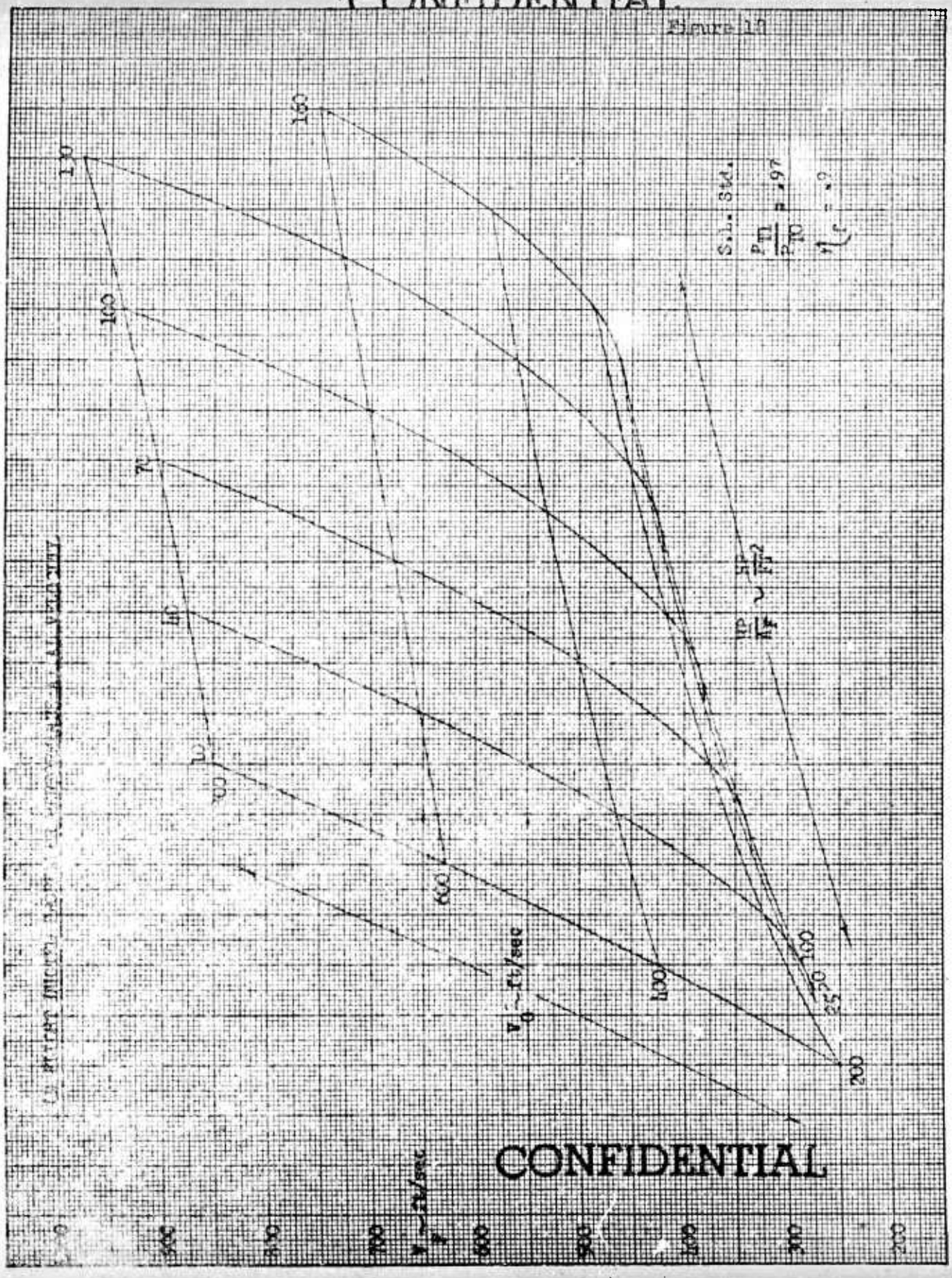

D. Discussion of IBM Results

In the design of a ducted propeller installation for use on an assault transport, the performance requirements and configuration of the airplane must be taken into consideration in the establishment of duct configuration and power requirements. In order to achieve a vertical take-off, a minimum static thrust-weight ratio of at least 1.0 is required, but it is good design practice to use a slightly higher value. Therefore, in order to reduce the power required and thus keep the aircraft gross weight at a minimum, a high value of static $\frac{F_e}{HP}$ is desirable. As shown in the static analysis, higher values of $\frac{F_e}{HP}$ may be obtained by decreasing HP/A_{in}, but the inlet area may be limited by the configuration of the aircraft or by the practical aspects of retracting the flaps for forward flight. The parameter HP/A_{in} may also be decreased by increasing the number of ducts for the same horsepower input. A preliminary study has indicated that, for a given required thrust, the weight of the propulsion system may actually be decreased by using a multiple duct arrangement.

In the forward flight analysis, it has been shown that low power loadings result in larger thrust-horsepower ratios. However, lower power loadings result in a greater range of fan velocities over which the propeller must operate, for forward speeds from V_o to V_{max}. This makes the actual blade design more difficult, since means of obtaining a greater variation in effective pitch angle must be provided. Any effort to alleviate this condition by the addition of power alone results in a decrease in $\frac{F_e}{HP}$ both statically and in forward flight.

From the above discussion, it is evident that many factors affecting fan performance must be compromised in the design of an optimum fan for a given aircraft. The most critical factors are the power input, fan or exit area and, statically, the inlet area. The momentum analyses presented in this report give a complete picture of the influence of these parameters on the fan performance. By judicious use of the graphs presented in Appendices A and B, it is possible to select the most practical values for these parameters in the design of any ducted propeller system.

PART II

PART II

DUCTED PROPELLER ANALYSIS

The design of a ducted propeller system may be accomplished in two phases. The first phase consists of the design of the duct or shroud, in conjunction with the selection of a suitable power plant. The second phase is the detail design of the propeller blading, together with the design of any non-rotating stages that are needed.

It is essential that the duct design and engine selection be carried out simultaneously, since, as pointed out in Part I - Section D, the internal geometry of the duct and the power available are critical factors in determining the amount of thrust available from the system. In order to attain the thrust level required, it is usually necessary to compromise these factors. As shown previously, it is desirable to have low values of $\frac{HP}{A_{in}}$ and power loading in order to realize the maximum thrust-horsepower ratio attainable. The value of $\frac{HP}{A_{in}}$ may be decreased by providing retractable inlet flaps, which would be extended under static conditions. Lower power loadings may be obtained by increasing the diameter of the duct, but duct size may be limited by several factors, such as airplane configuration, drag, stability or structural requirements. An alternative method of decreasing the power loading is to utilize several smaller ducts, thereby increasing the total disk area for the same power input. This method is also effective in decreasing $\frac{HP}{A_{in}}$. Once the flow conditions for the duct-powerplant combination are known, it is possible to design a propeller system to operate at maximum efficiency under these conditions.

Engine characteristics, duct configurations and propeller design methods are covered in the following sections. A survey of the available power plants is presented in table form, along with the pertinent characteristics of the particular engines used. Duct geometry, including huo size and the use of variable inlet area, is covered in Section B. Cascade methods used in the design of this report are covered in Section C, and include the use of low-solidity cascade data, limit-loading parameters, thickness distribution and exit stator design. Variations in the design procedure for three different types of ducted propeller are presented in Section D, including the calculation of off-design performance. Specific designs are presented in Section E, and these designs are discussed in Section F. The last section covers the forthcoming wind tunnel tests at the University of Wichita, and includes model specifications and photographs.

A. Power Plant Characteristics

A turboprop power plant has been selected as the most logical installation for ducted propeller applications. A turboprop engine has a lower weight/power ratio than the reciprocating engine, and the reduced frontal area results in less drag. Although the specific fuel consumption is higher, the later models are approaching S.F.C's which are competitive with reciprocating engines. The residual thrust available from the turboprop is also an advantage, particularly in the static case.

In setting up configuration studies for the Assault Transport application, it was useful to determine the major turboprop engines now available in the domestic and foreign markets. As a result, Table I has been prepared to show these engines and some of their major characteristics. It will be noted that several very small engines have been included. The tabulations range from a shaft horsepower of 210 for the Boeing T-50 engine to 13,340 for the Pratt and Whitney T-57. The majority of the available engines fall in the horsepower range from 4000 to 10,000 horsepower. It might also be noted that the Rolls-Royce RB-109 has been included twice in this tabulation. This engine was used as the power plant in one of the ducted propeller systems designed in this study, and at the time the design was initiated the later data was not available.

Three different engines were used in the design studies completed under this contract. They are the Wright T-49, the Rolls-Royce RB-109 and the Allison 550-B1. The important characteristics of these engines operating in conjunction with a ducted fan are shown in Figures 19 through 25. These curves have been corrected for gearing losses and engine inlet

CONFIDENTIAL

TABLE I

SUMMARY OF TURBOPROP ENGINES

Manufacturer	Designation	T.O. Shaft HP	Weight Lbs	Weight Power Lb/HP	Thrust Lbs	Thrust Weight	S.F.C. Lbs/Hr/S.HP	Length in.	R.P.M. T.O.	Power Turbine	R.P.M. at Partial Power	Reference	Date of Issue
American Engines													
Allison	[1]T54 (500 - C14)	7510	3150	0.420	1460	0.470	0.560	123.6	13820	Coupled	13820 at 60%	T54 Brochure	May 1955
												Spec. 382	Apr 1954
	T56 (501 - D8)	3755	1785	0.475	740	0.415	0.570	145.0	13820	Coupled	13820 at 50%	Spec. 377C	Apr 1955
	550 - B1	5166	2150	0.416	830	0.386	0.543	137.0	9900	Two Spool	8670 at 60%	Spec. 394B	Jan. 5, 195
Boeing	T50	210(ESHP)	240	1.140			1.3(per ESHP)	40.0				Aviation Week	Mar.12,1956
	502 - 10B	270(ESHP)	245	0.910			1.02(per ESHP)	43.0				Aviation Week	Mar.12,1956
Continental	XT51-T-3(Artouste II)	425	236	0.555	75	0.318	0.970	44.3	6000	Coupled	6000 at 60%	Spec. 2110	Sept 3,1954
	[2]Turmo II (260 - 2)	396	384	0.970	60	0.156	1.050	57.2	6000	Free	5020 at 60%	Spec. 2087	Dec. 1953
General Electric	T58-GE-2	998	325	0.326			0.660	59.0	19500	Free		Spec. SE-1	Sept 9,1954
Lycoming	T53 (LTC 1B)	825	460	0.560	102	0.222	0.710	48.0		Free		Spec. 104.2	Oct 15,1955
	T53 (LTC 1C)	960	460	0.480	118	0.256	0.680	52.0	26100	Free		Spec. 104.1	Aug 3,1955
	T55 (LTC 4B-1)	1600	600	0.375	190	0.317	0.680	45.0	18100	Free	16650 at 75%	Spec. 124.4	Jan 16,1956
Pratt & Whitney	T34 (T34-P-3)	5500	2590	0.471	1250	0.483	0.687	157.0	11000	Coupled	10250 at 50%	P & W Inst. Hdbk. (T34)	Apr 28,1954
	T57 (YT57-P-1)	11000	6600	0.471	5000	0.758	0.570	196.0	6525	Two Spool	5300 at 50%	P & W Inst. Man. Prel. Perf. Data	Aug 15,1955
Westinghouse	[3]R. Da. 7/2	1910	1201	0.630	500	0.416	0.730	98.0	14500	Coupled		Westinghouse R & T A1840	
												R. R. Sheets Sept 21, 1955	& Oct 4,1955
	RB-109	4020	1875	0.466	1000	0.533	0.505	98.0	14100	Two Spool	11000 at 50%	R. R. - T. S. D. Pub. 499	June 1953
	[4]RB-109	4020	1935	0.481	1175	0.610	0.567	100.3	14100	Two Spool	11000 at 50%	Brochure	Feb.10,1956
Wright Aeronautical	T47	11400	4825	0.423	3050	0.632	0.570	160.0	7700	Two Spool	6800 at 50%	Wright SP 876	July 20,1951
	T49 (YT 49-W-1)	9000	4466	0.496	3450	0.772	0.758	102.0	8000	Coupled	7350 at 50%	Wright Spec. 875E	Jan. 4,1954
Foreign Engines													
Armstrong-Siddeley	Mamba	1270(ESHP)			375		0.920						
	Double Mamba (ASMD.3)	3035(ESHP)	2200				0.75(per ESHP)	101.0					
	Python	4100										Aviation Week	Mar 12,1956
Bristol	BE-25	4000	3020	0.755	2730	0.905	0.815	110.0		Two Spool		BE-25 Ser. 1 Eng. Spec.	
Napier	Eland (N.E.L. 4)	3765	1800	0.478	610	0.339	0.595	121.0	12500	Coupled	10900 at 50%	Brochure P.S. XL118	Nov. 1953
Rolls-Royce	Dart	1640	1157	0.705	365	0.315	0.750	96.0		Coupled		R.R. - T.S.D. Pub. 500	
	RB-109	4020	1835	0.456	1000	0.545	0.505	98.0		Two Spool		R.R. - T.S.D. Pub. 499	June 1953

1. Rating to increase to 9000 ESHP by 1961 (T54 Brochure dated May 1955)
2. Turmo III prototype Max. rating 750 SHP at .78 S.F.C. (Engine Summary dated Sept. 25, 1955)
3. Advanced R. Da. 8 will have a Max. ESHP rating of 2500 HP.
4. RB-109 has growth potential to 5000 SHP by 1964.

CONFIDENTIAL

Figure 19

POWER AVAILABLE
WRIGHT T49-W-1
97% Pressure Recovery
2% Gear Losses
Military Rating

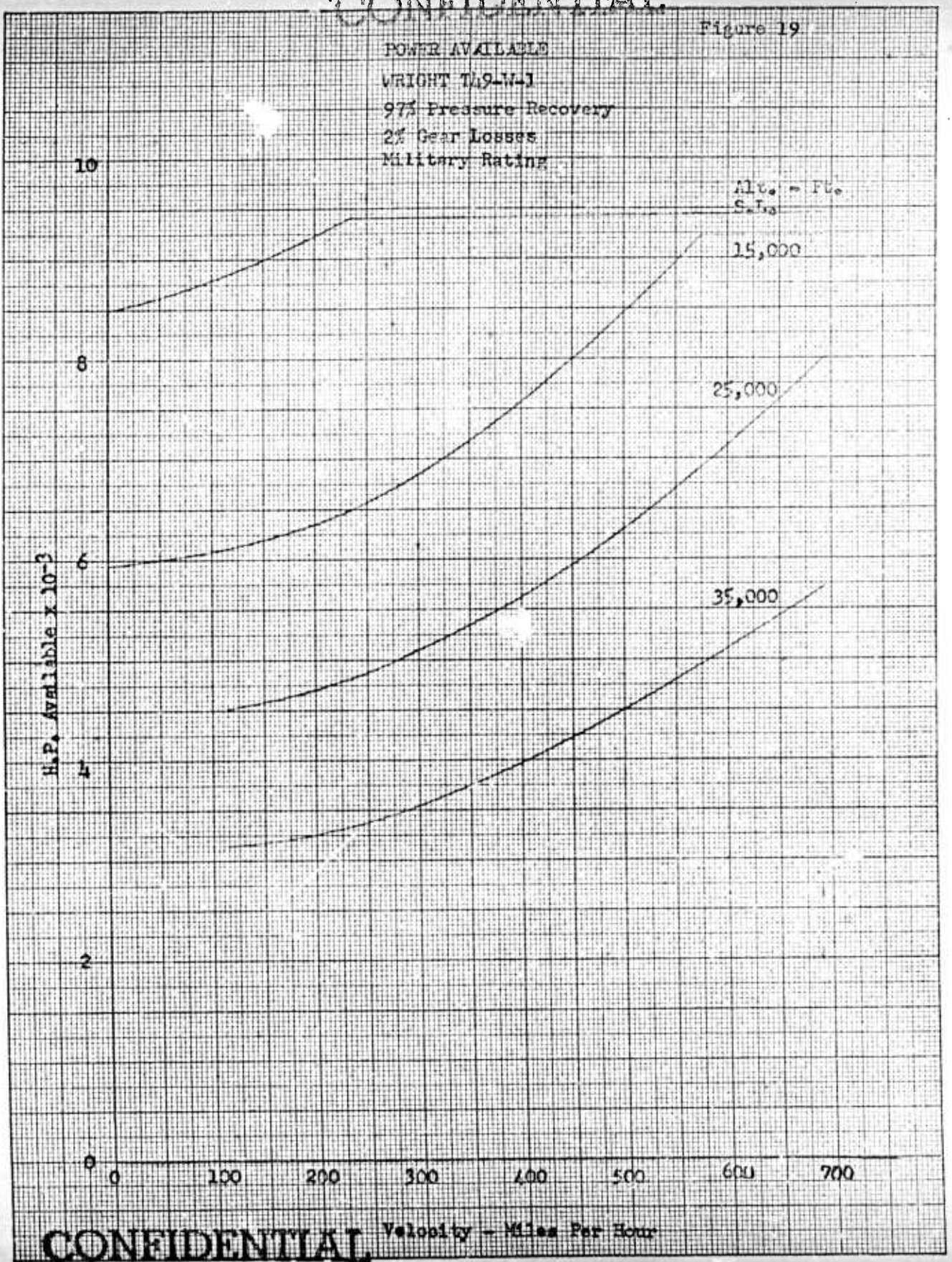

CONFIDENTIAL

Figure 20

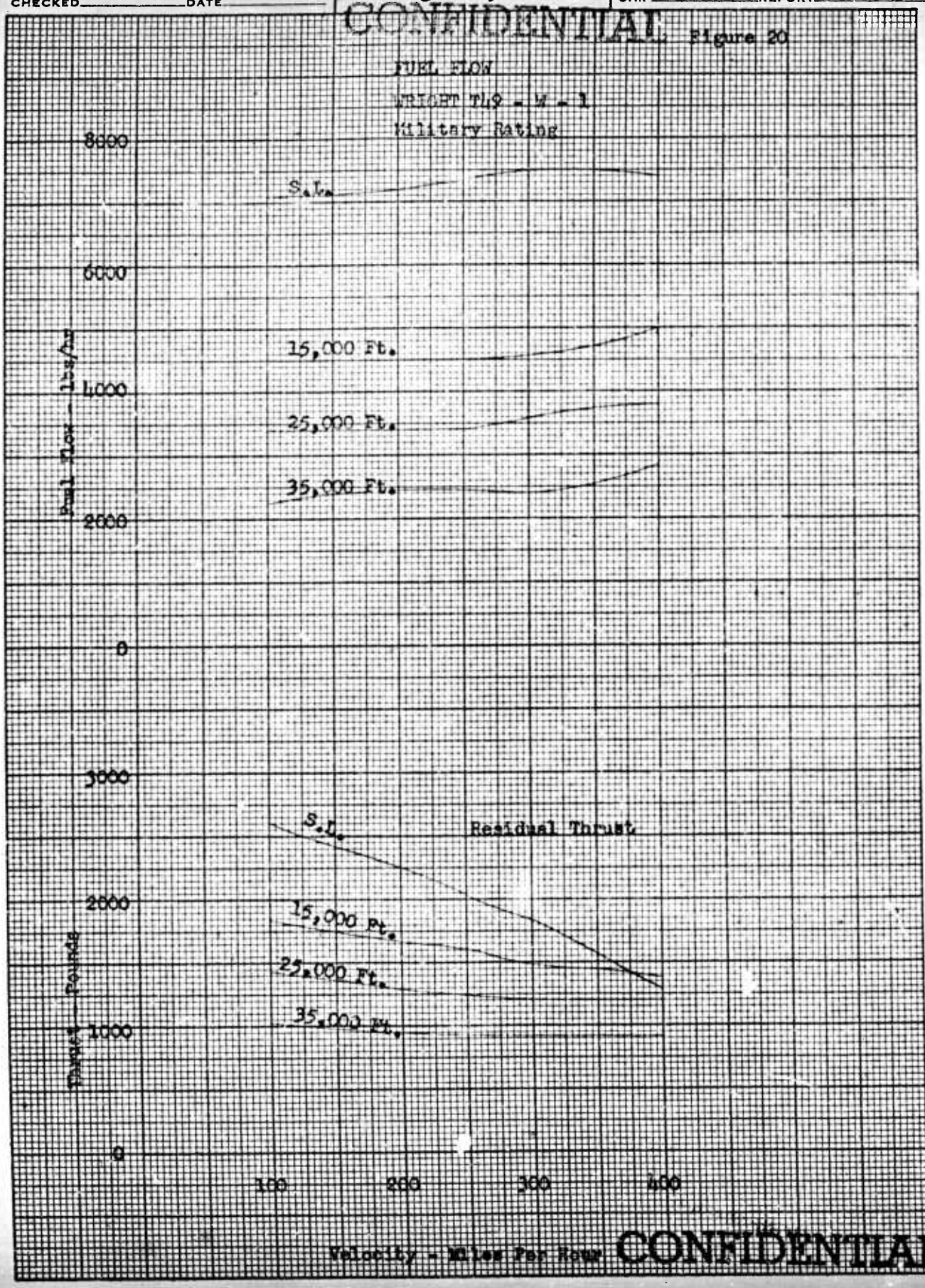

CONFIDENTIAL

CONFIDENTIAL

Figure 21

POWER AVAILABLE
ROLLS ROYCE RB-109
97% Pressure Recovery
2% Gear Losses
13,200 RPM

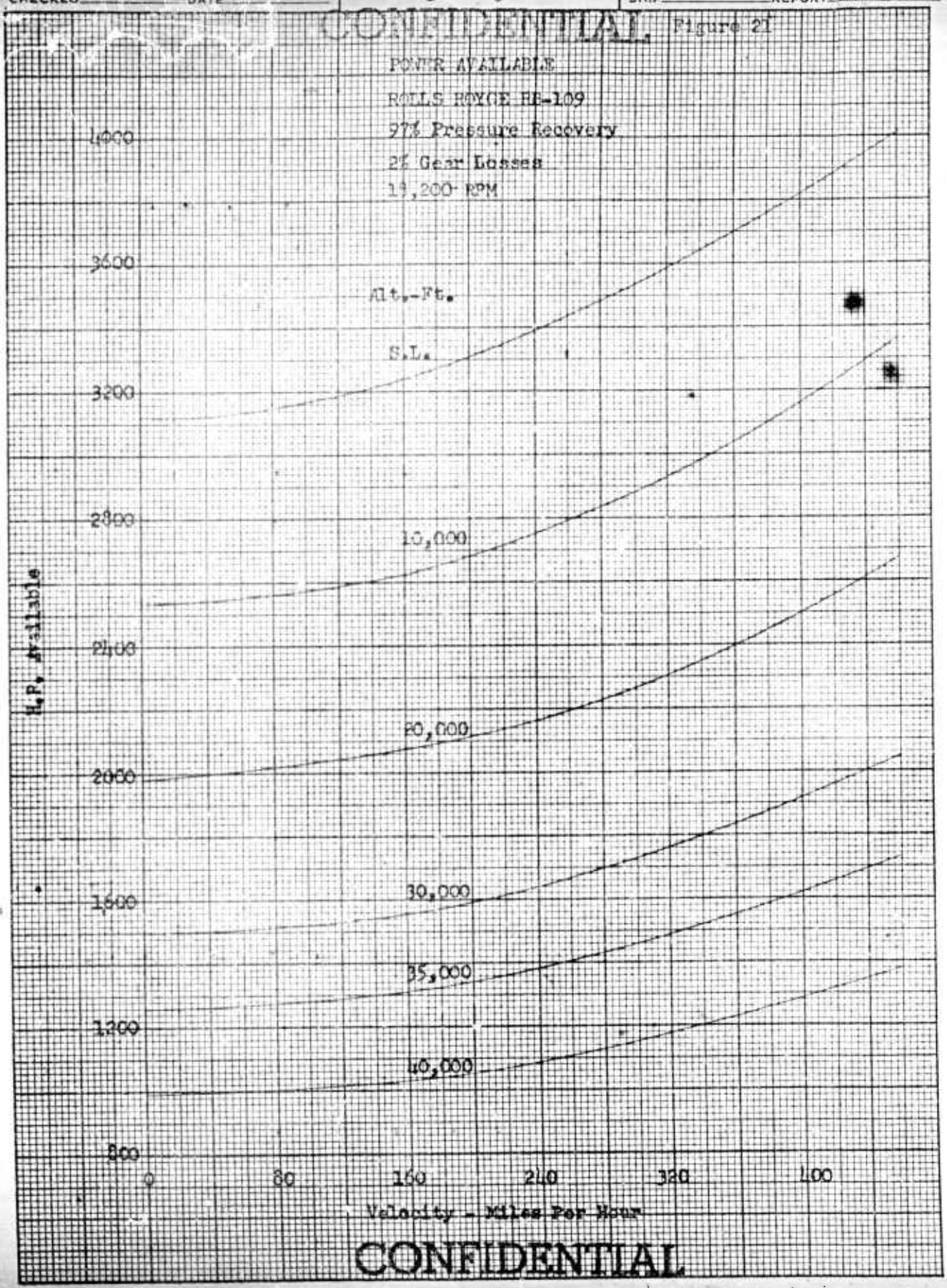

Figure 22

ROLLS ROYCE RB-109

18,200 RPM

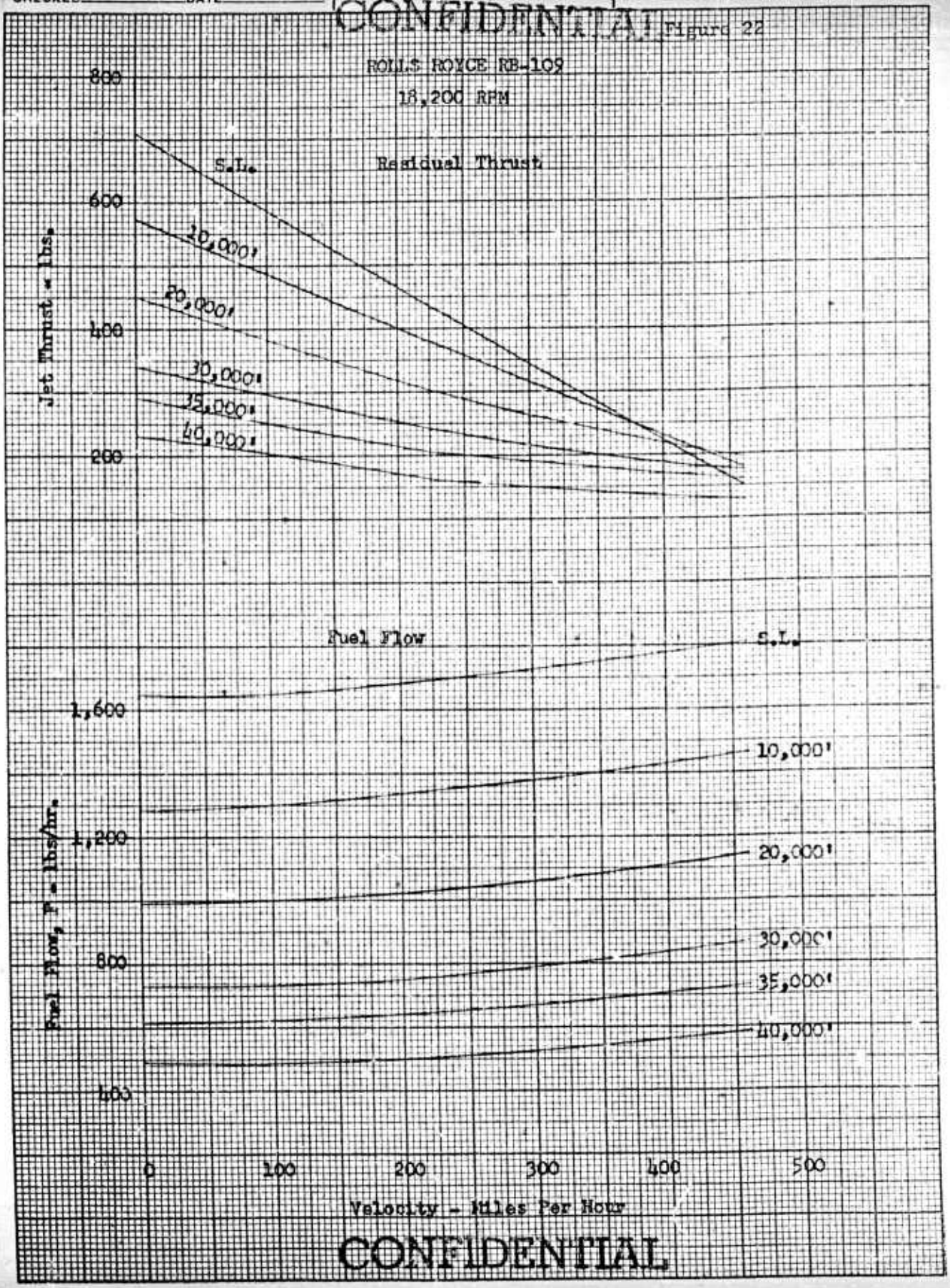

Figure 23

POWER AVAILABLE ALLISON 550-E1

97% Pressure Recovery
2% Gear Losses
Military Rating

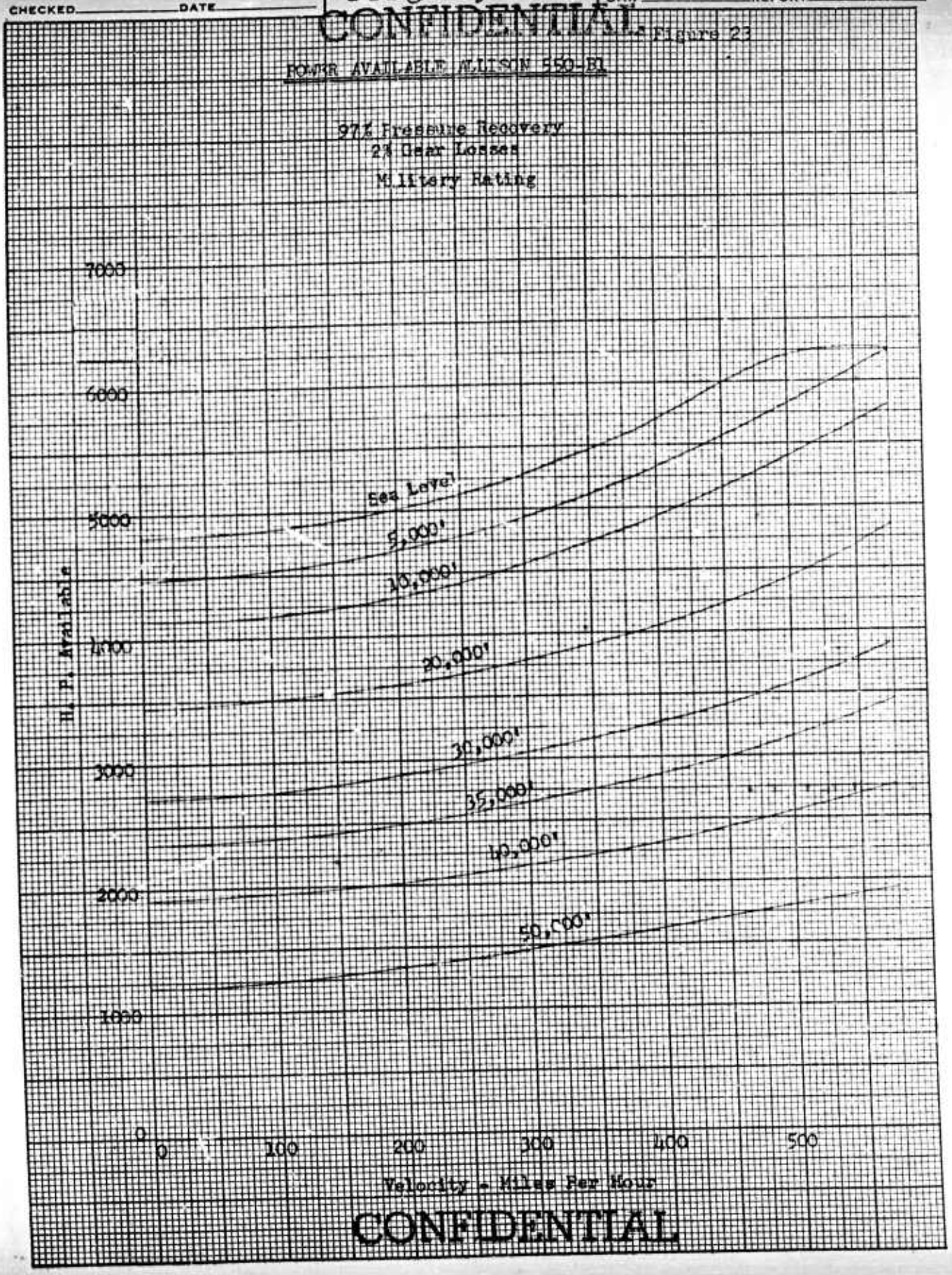

CONFIDENTIAL

Figure 24

RESIDUAL THRUST ALLISON 550-B1

97% Pressure Recovery
2% Gear Losses
Military Rating

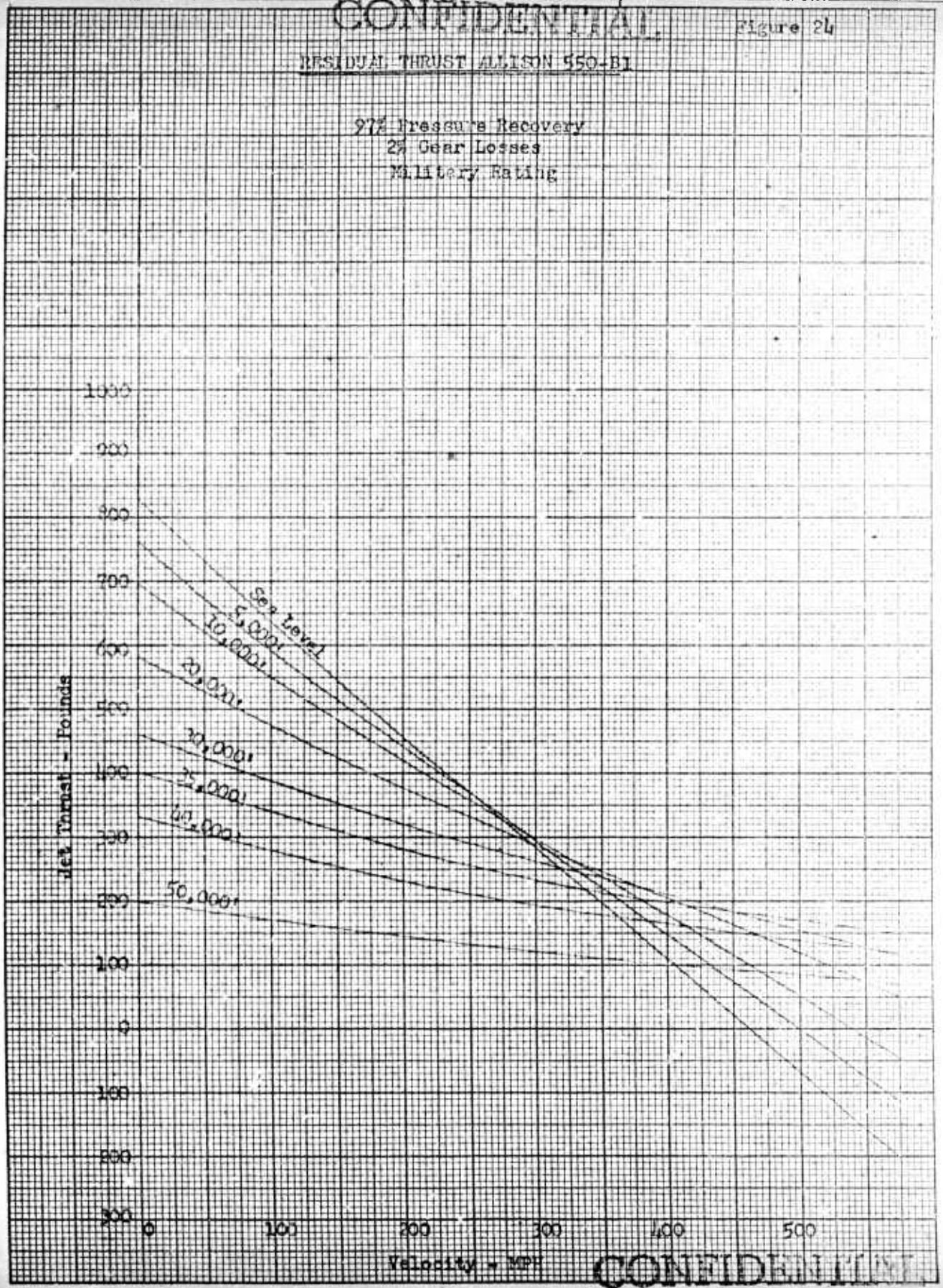

CONFIDENTIAL

CONFIDENTIAL

Figure 25

FUEL FLOW
ALLISON 550-81
97% Pressure Recovery
2% Comp. Losses
Military Rating

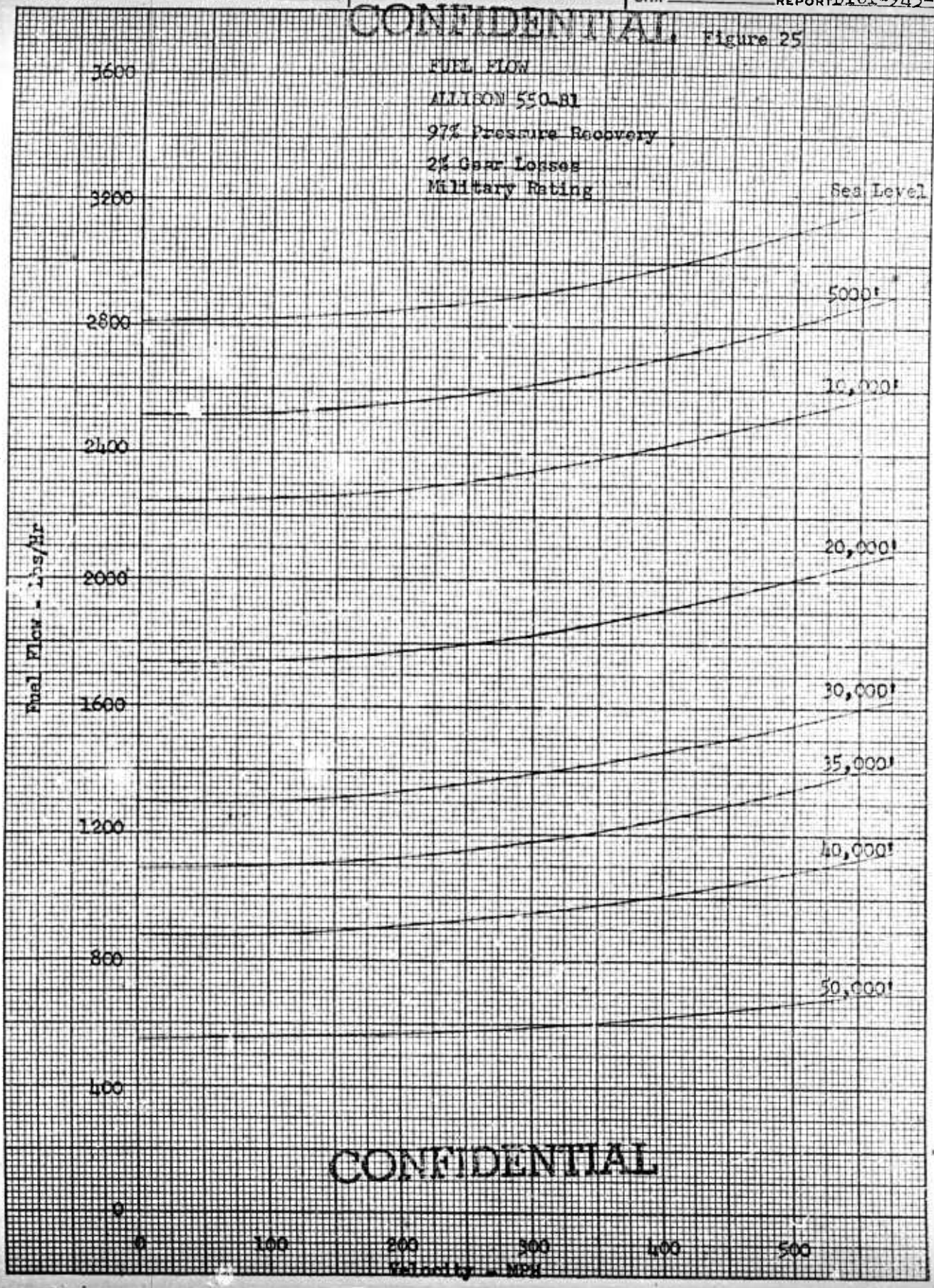

CONFIDENTIAL

losses. The power available at the fan for the Wright T-49 engine is shown in Figure 19. The fuel flow and residual thrust for the T-49 is shown in Figure 20. These curves were obtained from information contained in Reference 8. The horsepower available at the fan and the residual thrust and fuel flow for the Rolls-Royce RB-109 are shown in Figures 21 and 22 respectively, and were obtained from Reference 9. The same parameters for the Allison 550-B1 are shown in Figures 23, 24 and 25, and were taken from data contained in Reference 10.

The requirements of this study specify that the aircraft configurations proposed must be able to perform a vertical take-off at 6000 feet on a 95° day. It has been assumed in this study that the full sea level horsepower output of the engine may be regained under 6000 feet - 95° conditions by the use of water injection. In several of the conferences held during the course of this study it has been agreed that such an assumption is entirely feasible, and engine manufacturers have agreed that their engines could be modified to regain sea level power at 6000 feet and 95°F The main limitation on the use of water injection is the strength of the engine gearing. It has been analytically shown (Reference 11) that power augmentation up to 200%, at a compressor tip speed of 1800 ft/sec., is possible by use of water injection. To obtain this magnitude of power augmentation, it is necessary to completely saturate the air at the compressor outlet. In the same report, it is also shown that a total water flow of 4.5 times the initial fuel flow is required to attain a thrust

augmentation of 78%. In order to realize these augmentation possibilities, it would be necessary to modify any of the present day engines so that the engine gearing could withstand the additional stresses imposed.

B. Duct Design

In the design of a duct for the assault transport configuration, two factors are involved. First, as shown in Part I, it is desirable to have larger values of $\frac{HP}{A_{in}}$ under static conditions. Secondly, a low drag shroud is desirable in order to attain high forward speeds. These two requirements are in conflict, and must be compromised in order to obtain a configuration which is satisfactory over the complete flight regime.

The obvious solution to this situation is the use of retractable inlet flaps, which may be extended under static conditions to give low values of $\frac{HP}{A_{in}}$ and retracted in flight to give a low drag configuration. Such a system has been incorporated into the designs investigated during this study. In Part I, a bell-mouth pressure recovery was assumed in the static momentum analysis. A bell-mouth inlet has a very favorable pressure gradient, and would be the most desirable inlet shape under static conditions. However, a simpler type flap which also gives a favorable pressure gradient has been used in the present designs. It is believed that the pressure recovery of this practical flap will approach that of a bell-mouth, and experimental work to verify this assumption is underway at the University of Wichita. Sketches of the various flap arrangements to be tested may be seen in Figure 62, Section C . It will be noted that the inlet contour is notched when the flaps are in the open position. Kruger (Reference 6) has shown that good results can be obtained with this split flap arrangement.

Kruger (Reference 6) has also shown that fan efficiencies can be improved by using thin shroud profiles with small chord lengths. The length/diameter ratio of the shrouds covered in this report are of the

order of .5, which is a reasonably small value. It has been assumed that the cross-sectional profile of the in-flight configuration will be that of a thin airfoil, and preliminary ordinates for the present designs have been established.

Up to this time, nothing has been said of the duct hub. The ratio of the hub diameter to the fan diameter, usually called the hub-tip ratio, is an important parameter in the detail design of the blading. In ducted propeller design, a large hub has several advantages. For a given number of constant chord blades, a large hub size results in a smaller solidity variation from hub to tip and less blade twist. In addition, a high hub-tip ratio results in less sensitivity of the system to off-design operation. Also a large hub may permit the installation of the engines in the hub, thereby eliminating some of the gearing problems present in other installations. The disadvantages of a high hub-tip ratio are the adverse effects of drag and the weight of a large hub. These factors must be taken into account in the selection of hub size.

C. Development of Design Procedure

Once the powerplant has been selected and other duct geometry established, the detail design of the propeller itself may be accomplished. The flow conditions in the duct are determinable from the momentum data, and the propeller blading must be designed to fit these flow conditions.

Due to the over-all size limitations imposed on the design, it was necessary that high power loadings be employed. These high power loadings require solidities which are much higher than those used in classical propeller theory, and result in pressure ratios which are high in comparison with those obtained on present day propellers. It was, therefore, decided that a detail design method must be established which would permit the use of multi-bladed propellers of moderately high pressure ratio. Since high solidities and high pressure ratios are normally used in the design of axial-flow fans and compressors, it was decided to use a similar design method for the ducted propeller. Due to the limited amount of time available for this feasibility study, only designs with a free vortex velocity distribution at the design point were considered. The method used is outlined in the following sections.

1. Design Procedure Using Available Cascade Data

In the design of axial-flow fans and compressors, low speed cascade data, such as that contained in Reference 12, has been used rather extensively. This data has also been used in the ducted fans designed for the Assault Transport application. An adiabatic fan efficiency of .9 has been assumed throughout.

All of the designs in this report utilize the NACA 65-series compressor blade section, modified to incorporate a trailing edge radius equal to 10% of the maximum thickness. It has been established in Reference 13 that such a modification will not appreciably alter the characteristics of the blade.

For a given aircraft configuration, the number of ducts and the maximum duct diameters allowable are predetermined. Knowing the estimated take-off gross weight and the power plants to be used, it is then possible to determine the duct geometry which will give a static thrust-horsepower ratio sufficient for vertical take-off from the static momentum data. Thus, the static flow conditions in the duct have also been established. It is now possible to design a fan which will operate at these flow conditions or, since $\frac{HP}{A_f}$ is also known, any forward flight speed may be chosen as the design point.

A typical vector diagram for an axial-flow rotor may be seen in Figure 26. In the fans designed for this study, the relative tip velocity $(w_1)_{tip}$ has been limited. Since the fan velocity is given by the momentum data, the maximum tangential velocity at the tip ($R\Omega$) is thus determined.

$$R\Omega = \sqrt{(w_1^2)_{limit} - V_f^2} \qquad (2\text{-}1)$$

The maximum relative tip velocity may be specified at any value of V_o. A rated military power setting at the design point has been assumed for all designs, and therefore, since a turboprop engine is essentially a constant speed device, the tangential velocity thus obtained is the same at any other value of V_o chosen as a design point.

Figure 26

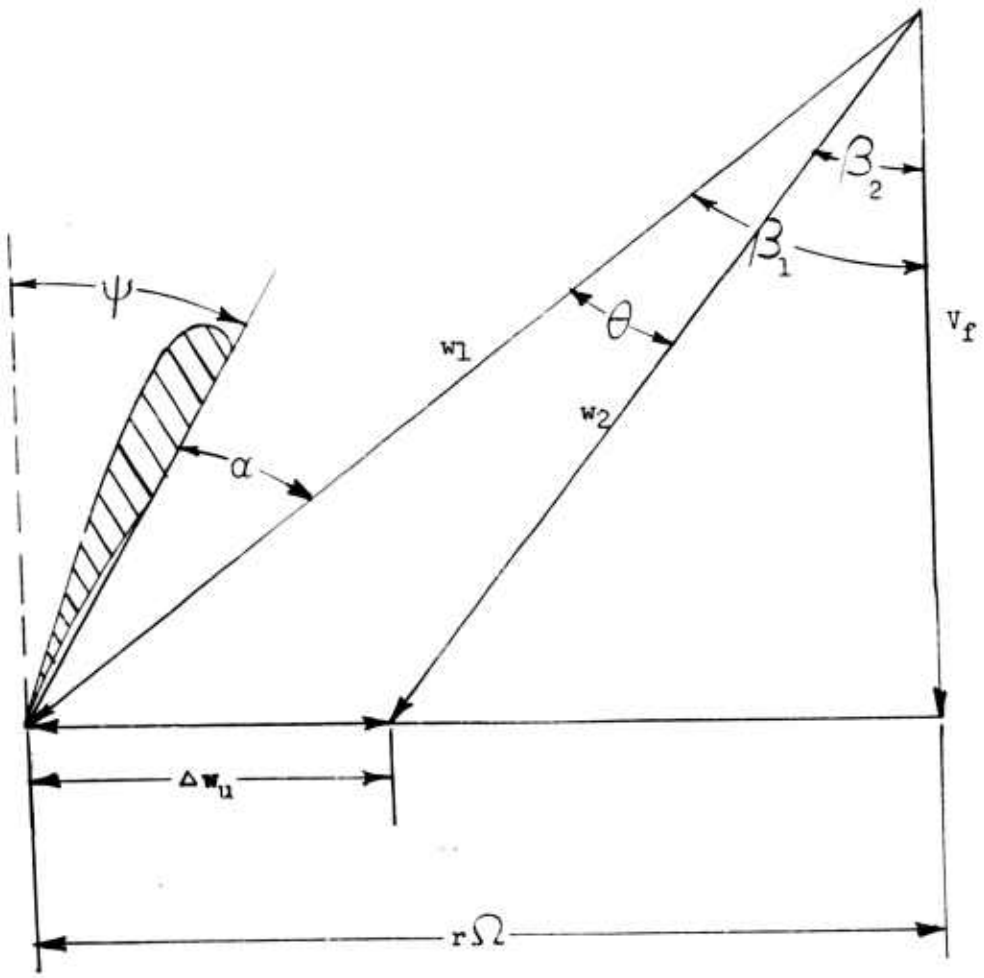

Typical Axial-Flow Rotor Vector Diagram

Equation (1-36) may be written

$$HP = \frac{\rho A_f V_f R \Omega \Delta w_{u_T}}{550}$$

from which

$$\Delta w_{u_T} = 550\left(\frac{HP}{A_f}\right)\frac{1}{\rho V_f R \Omega} \qquad (2\text{-}2)$$

The tangential velocity varies directly with the radius. In a free vortex design, the whirl velocity varies inversely with the radius. Thus the variation of tangential velocity and whirl velocity from hub to tip may be determined. Denoting these velocities at any radial station by $r\Omega$ and Δw_{u_f} respectively, the inlet angle, β_1, and exit angle, β_2, at that station are given by

$$\beta_1 = \tan^{-1}\frac{r\Omega}{V_f} \qquad (2\text{-}3)$$

$$\beta_2 = \tan^{-1}\frac{r\Omega - \Delta w_{u_f}}{V_f} \qquad (2\text{-}4)$$

and from Figure 26, the turning angle is

$$\theta = \beta_1 - \beta_2 \qquad (2\text{-}5)$$

As mentioned previously, the fans considered in this report were assumed to have constant chord blading. As a result, the solidity also varies inversely with the radius of the blade. Nominal values of tip solidity have been chosen for each particular design. Normally these solidities were within the range of the data contained in Reference 12,

but in some instances lower values were used. The method used to obtain data at these lower solidities is covered in the next section.

The cascade data of Reference 12 has been summarized in a more convenient form in Reference 14. The carpets presented in that report have been used in all the designs accomplished under this study contract. Having determined the inlet angle, turning angle and solidity, the design chamber (C_{l_o}) and design angle of attack (α_d) at each radial station may be found from Figures 1 and 2 of Reference 14. Since these curves were developed from experimental data, the values thus obtained were plotted vs. radial station and a curve was faired through the points to give the final results. Finally the angle between the blade chord and the center line of the duct is given by

$$\psi_d = \beta_1 - \alpha_d \qquad (2\text{-}6)$$

The above method is presented in tabular form in Table II.

The off-design performance of the rotor may also be determined from Figure 3 (f) of Reference 14. However, since the methods used to determine off-design performance differ slightly for fans using inlet guide vanes and those having variable pitch, they are presented in Section D.

2. Low - Solidity Cascade Data

The use of higher power loadings in ducted propeller installations necessitates the use of solidities which are somewhat higher than those ordinarily used for a bare propeller. It is felt, however, that these solidities need not be as high as those ordinarily used in axial-flow compressor design. High solidities obviously impose a greater weight

TABLE II

Rotor Design Procedure

Radial Station r/R	$r\Omega$	Δw_{u_f}	β_1	β_2	θ	σ	c_{l_o}	α_d	ψ_d	t/c	C-Factor
1.0 ←	$R\Omega$ (r/R)	$\frac{1}{(r/R)} \Delta w_{u_T}$	Equation (2-3)	Equation (2-4)	Equation (2-5)	$\frac{1}{(r/R)} \sigma_T$	Fig. 1, Ref. 14 or Fig. 28	Fig. 2, Ref. 14 or Fig. 27	Equation (2-6)	Section C-4	Section C-3

Given:

V_f - determined from momentum data

$R\Omega$ - Equation (2-1)

Δw_{u_T} - Equation (2-2)

σ_T - Selected

penalty, and the problems inherent in the design of any variable pitch mechanism are greatly increased. It was therefore decided to investigate several fan designs which had tip solidities in the range of values between those used in compressor work and those common to bare propellers.

The cascade data of References 12 and 14 cover a range of solidities from .5 to 1.5. No design charts covering solidities less than .5 are available. However, in Figure 108 of Reference 12, the design angle of attack data for various design cambers has been extrapolated to a value of $\sigma = 0$. Using this plot, it is a simple matter to construct a low solidity design angle of attack chart. The carpet thus obtained is shown in Figure 27. In Figure 109 of the same report, the design turning angle has been similarly extrapolated for various values of C_{l_o} and β_1. The low solidity design chart obtained from this curve is plotted in Figure 28. These curves are used in the same manner as those of Reference 14.

It was somewhat more difficult to construct a low solidity carpet showing off-design performance characteristics. The test data contained in Reference 12 were cross-plotted and extrapolated in several different ways, and the results were compared with each other and with extrapolations of the carpet plots of Reference 14. This procedure was repeated until the faired curves were in reasonably good agreement with each other. By this tedious procedure it was possible to construct an off-design chart which was felt to be good enough to give approximate results until futher test data was available. The off-design chart thus obtained is reproduced in large size and placed in the envelope attached to the back cover of this report.

CONFIDENTIAL

LOW SOLIDITY DESIGN ANGLE OF ATTACK

Figure 27

Ref. : L5103

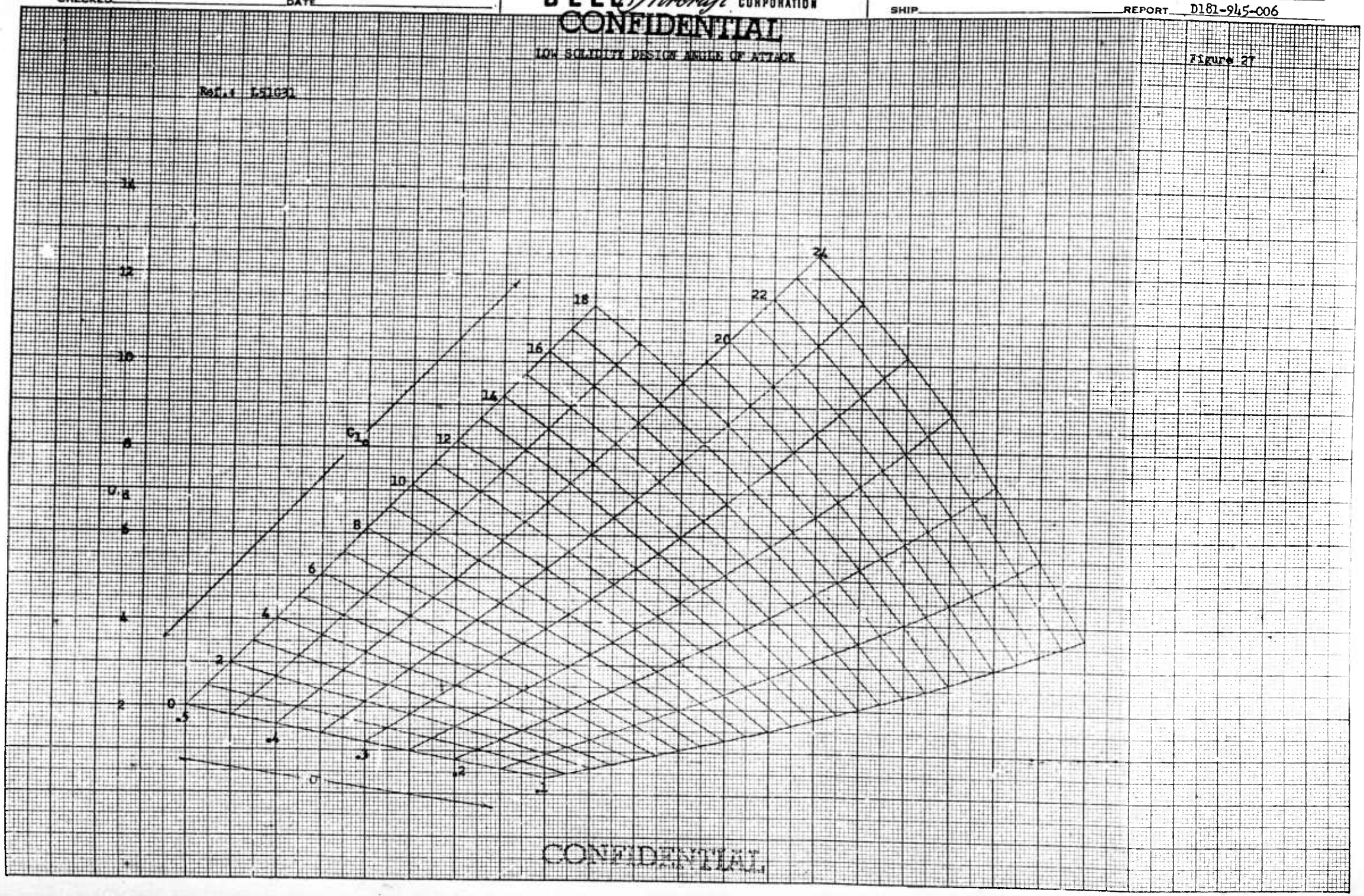

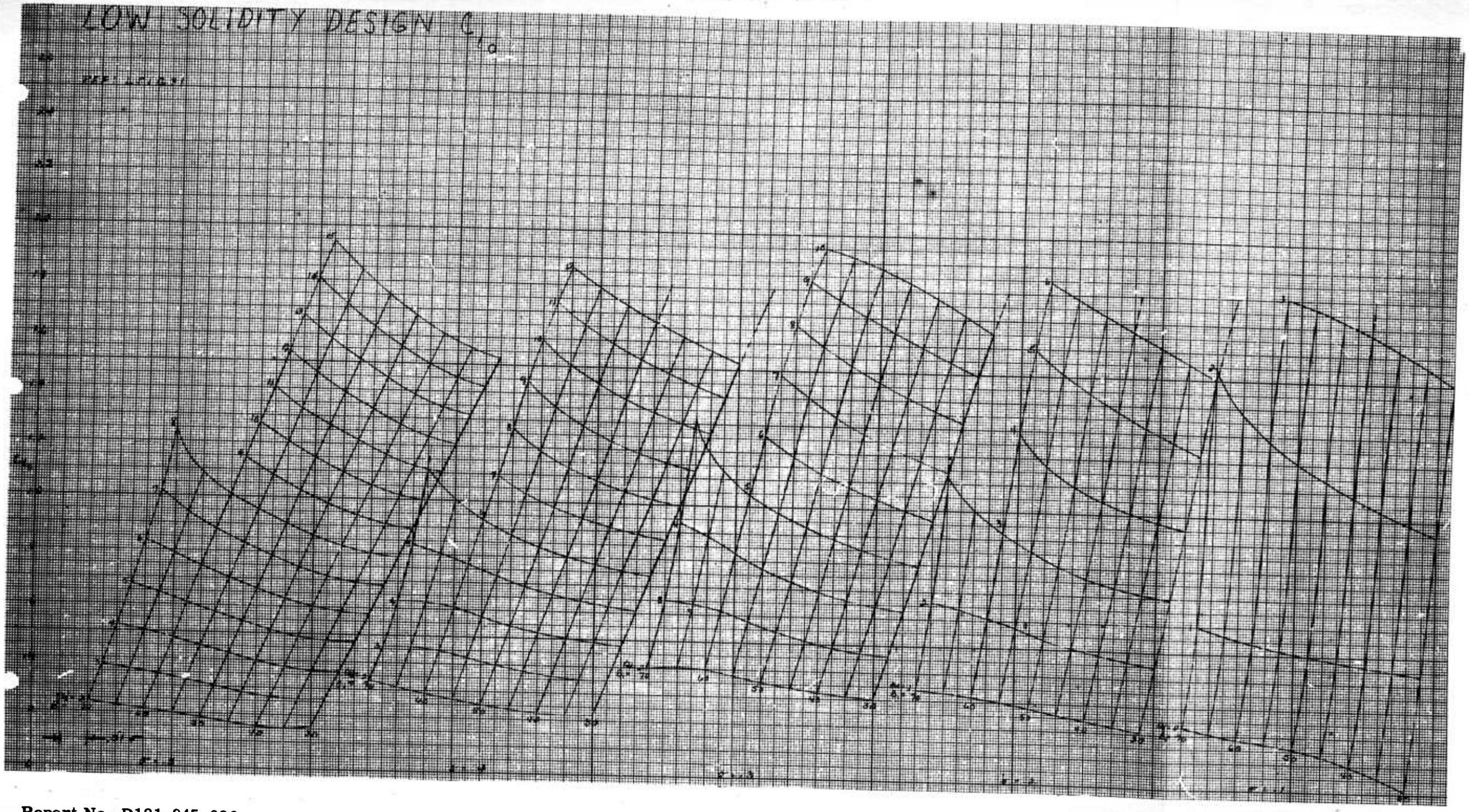

Report No. D181-945-006

Figure 28

Its manner of use is the same as for the off-design chart presented in Reference 14.

Since all of the low-solidity carpets were based on extrapolated data, it was highly desirable to obtain some experimental data to substantiate the results. Consequently, the Cascade Aerodynamics Section of the NACA at Langley Field was requested to conduct some experimental tests to check a few of the extrapolated points. This request was granted, and the results of the check runs are shown in Figure 29. The tests were run for σ = .25 and β_1 = 60°. As shown by the curves, the values obtained for θ_d at the design angle of attack are in fairly good agreement, especially at lower values of C_{l_o}, the largest discrepancy being 1.1 degrees at a C_{l_c} = 1.8. However, the slopes of the curves vary considerably, the error of the extrapolated data ranging from 25 to 83%. This would indicate that the low solidity design charts will give approximate results, but considerable error may be encountered in using the off-design chart at values of α which are considerably higher or lower than α_d. However, the low-solidity data is intended primarily for use with variable pitch configurations. The angle of attack variation over the speed range is much less for this type configuration than for a configuration using inlet guide vanes. It is, therefore, felt that the results obtained using this data are valid within the scope of this study. Nevertheless, some refinement of this data, supported by experiment, would be necessary before applying it to a prototype configuration. Some experimental verification of the predicted performance of a ducted fan design incorporating this data should be forthcoming from the wind tunnel tests of the second model to be tested

CONFIDENTIAL

Figure 29

C_{L_0}	α_d deg.	ϵ_d Extrapolated	ϵ_d Test	$\frac{d\epsilon}{d\alpha}$ Extrapolated	$\frac{d\epsilon}{d\alpha}$ Test	ϵ_d	$\partial C_m/\partial C_L$
.4	3.2	2.2	2.8	.55	.3	27.	83
1.2	7.5	5.4	5.8	.46	.33	7.5	39
1.8	9.0	6.7	7.8	.35	.44	16.	25

$\tilde{\epsilon} = .25$

$\beta_1 = 60°$

$C_{L_0} = .4$

$C_{L_0} = 1.2$

$C_{L_0} = 1.8$

Extrapolated

Test

CONFIDENTIAL

at the University of Wichita. (See Section G).

3. Blade Limit - Loading Parameter

The loading limit for a compressor-blade section is defined as the blade loading above which high losses will occur. In order to obtain high fan efficiencies, it is therefore essential that some index of the blade loading be determined. Limit-loading factors which indicate the region of high blade losses are presented in References 15 and 16. The C- Factor of Reference 16 was used to check the designs in this report, and is defined as

$$C = \frac{\Delta P}{P_t - P_p} = \frac{\Delta P/q_1}{(P_t - P_p)/q_1} \qquad (2-7)$$

$\Delta P/q_1$ may be obtained from Figure 4 of Reference 14. Values of $\frac{P_t - P_p}{q_1}$ are plotted in Reference 16. These curves have been replotted in carpet form, and are shown in Figures 30 through 34.

4. Blade Thickness Distribution

The experimental cascade data of Reference 12 was obtained from blades having a 10% thick section. However, it was felt that a 10% section is too thick for the tip speeds which were being incorporated into the fan design. Reference 12 shows that a small change in section thickness will not significantly effect the rotor performance. This small influence of changes in section thickness was also mentioned at one of the conferences held during the study, and it was suggested that a linear variation of $\frac{t}{c}$ from .04 to .10, depending upon the relative Mach number, be used. This suggestion was adopted, and the variation in

BY _____ DATE _____
CHECKED _____ DATE _____

BELL Aircraft CORPORATION

MODEL _____ PAGE 84
SHIP _____ REPORT D181-945-006

CONFIDENTIAL

PEAK PRESSURE COEFFICIENT

Ref.: RM8L52A

Figure 30

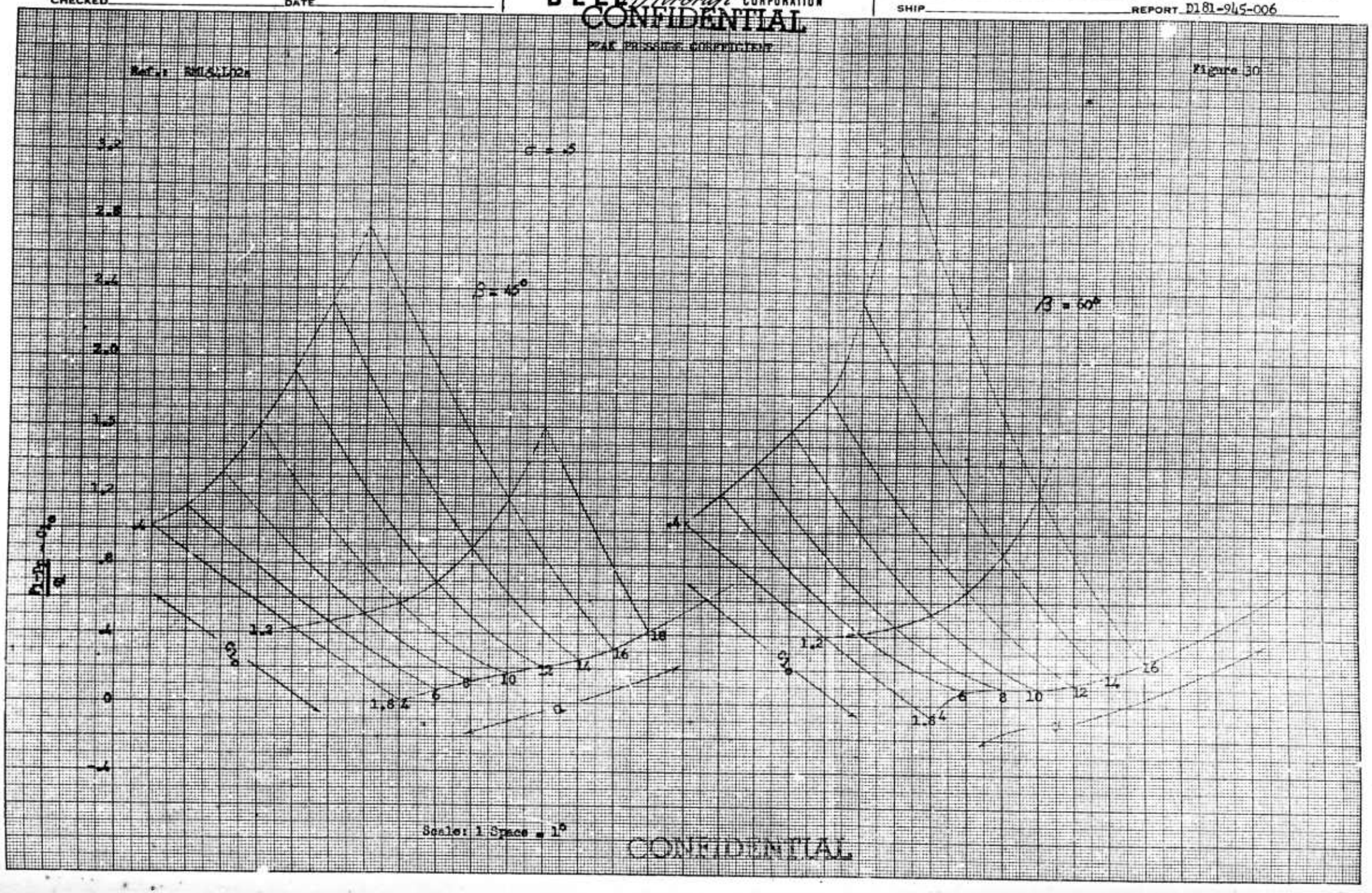

Scale: 1 Space = 1°

CONFIDENTIAL

BY _____ DATE _____
CHECKED _____ DATE _____

BELL Aircraft CORPORATION

MODEL _____ PAGE 57
SHIP _____ REPORT D181-945-006

CONFIDENTIAL
PEAK PERSONNEL ONLY

Figure 31

Ref. RM 54J20a

$C_l = .75$

$\beta = 45°$

$\beta = 60°$

C_{l_α}

C_{l_C}

Scales: 1 Space 1

CONFIDENTIAL

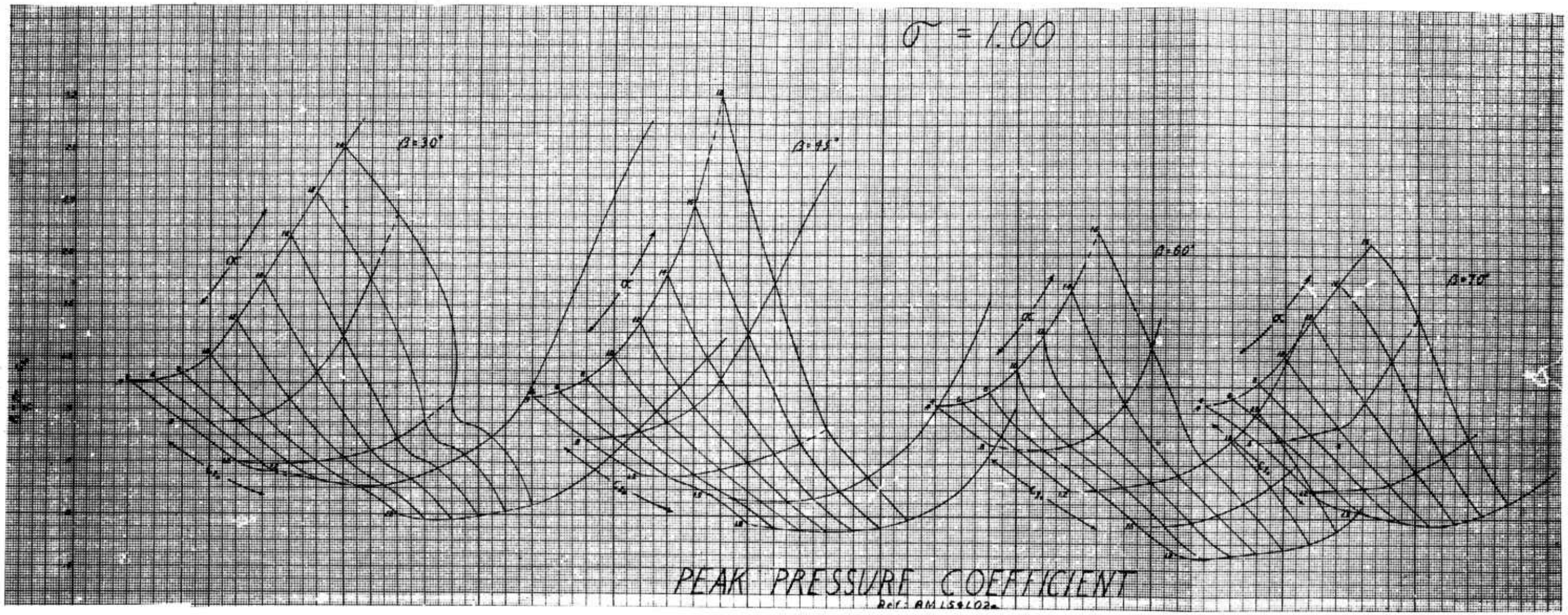
σ = 1.00
β=30°
β=45°
β=60°
β=70°
PEAK PRESSURE COEFFICIENT
Ref: AM 1581.02

Figure 32

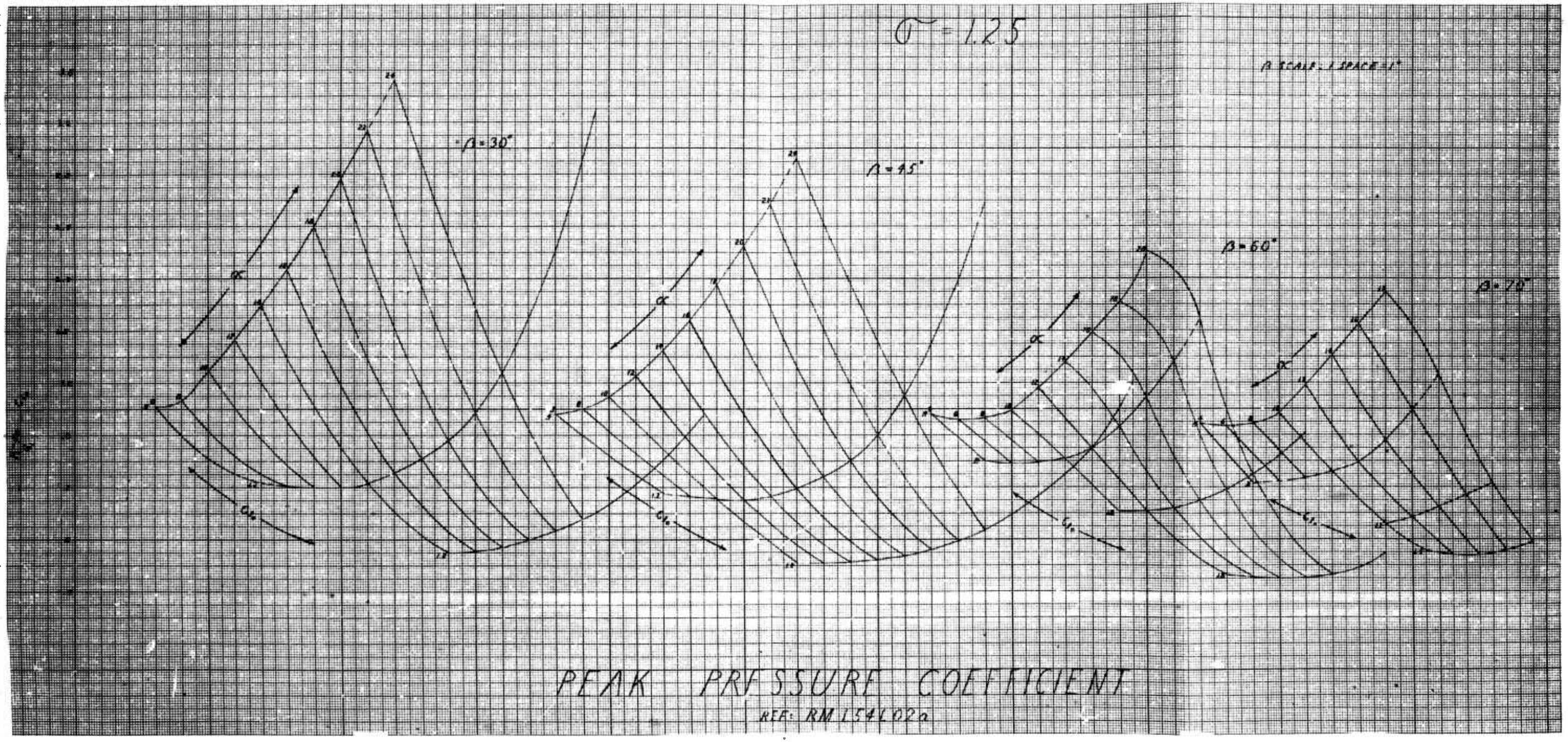

Report No. D181-945-006

Figure 33

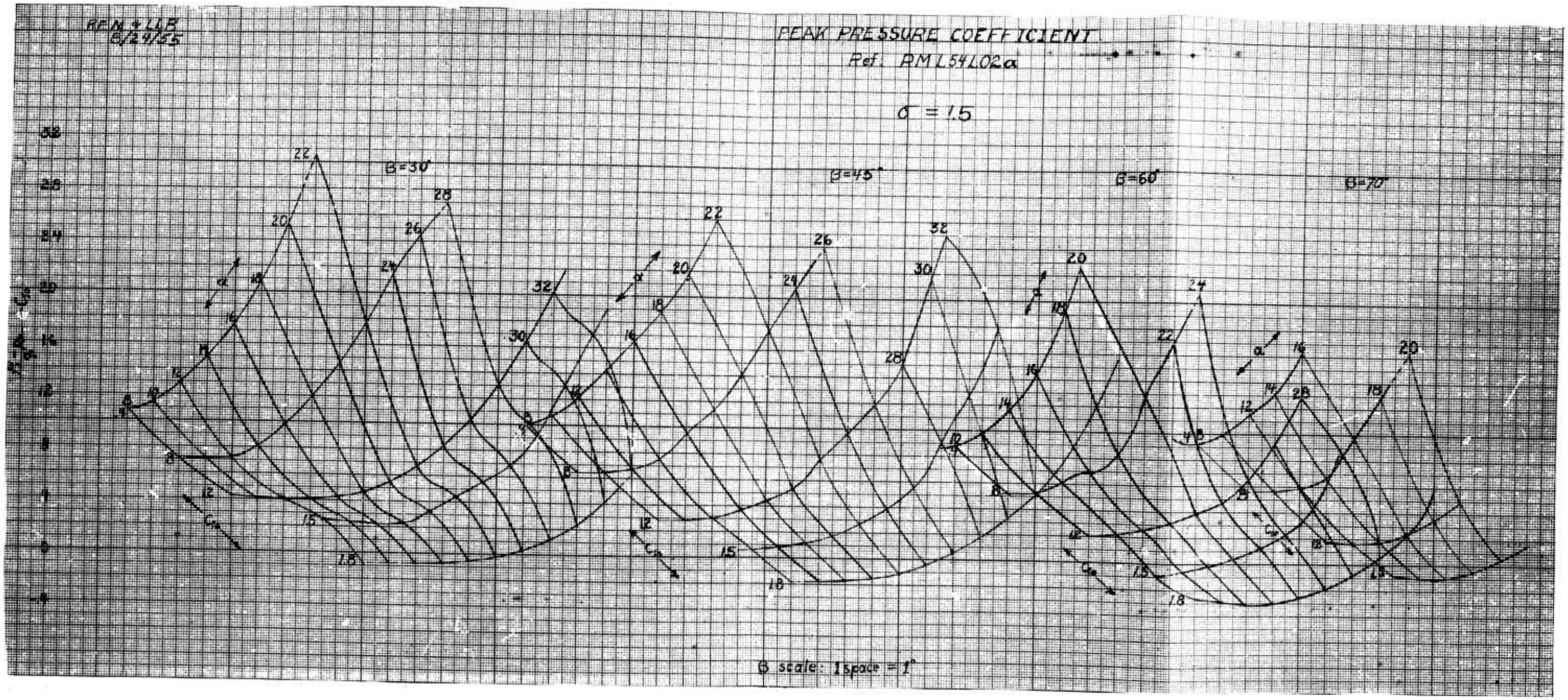
RFN & LLR
6/24/55
PEAK PRESSURE COEFFICIENT
Ref. RM L54L02a
σ = 1.5
β=30°
β=45°
β=60°
β=70°
β scale: 1 space = 1°

Figure 34

$\frac{t}{c}$ which was used is shown in Figure 35. The use of this criteria usually resulted in a slightly non-linear variation of $\frac{t}{c}$ from hub to tip. A straight line was then faired through these points to give a linear variation in blade thickness from hub to tip.

5. Exit Stator Design

In order to turn the flow in the axial direction, and thus gain in the amount of resultant thrust, it was necessary to include exit stators in all of the fans designed except those configurations employing contra-rotation. Since maximum thrust is desired under static conditions, all exit stators were designed to remove all of the residual whirl under static conditions at 6000 feet on a 95° day. Other operating points represent off-design operation of the exit stators, so that only a portion of the residual whirl will be removed. However, as shown in the several fan designs contained in Section E, it was found that the greater part of the residual whirl was removed under most operating conditions.

A typical exit stator vector diagram is shown in Figure 36. As seen from this diagram, in order to remove all of the residual whirl the turning angle must equal the inlet angle. The same design procedure used for the rotor is applicable to the exit stators, with $R\Omega$ and β_2 equal to zero. A constant thickness was assumed. Some difficulty in the use of the charts from Reference 14 was experienced, since the inlet angles for an exit stator are normally smaller than those for a rotor. It was again necessary to extrapolate the data, and these extrapolations were made directly on the design charts.

CONFIDENTIAL

Figure 35

Blade Thickness Distribution

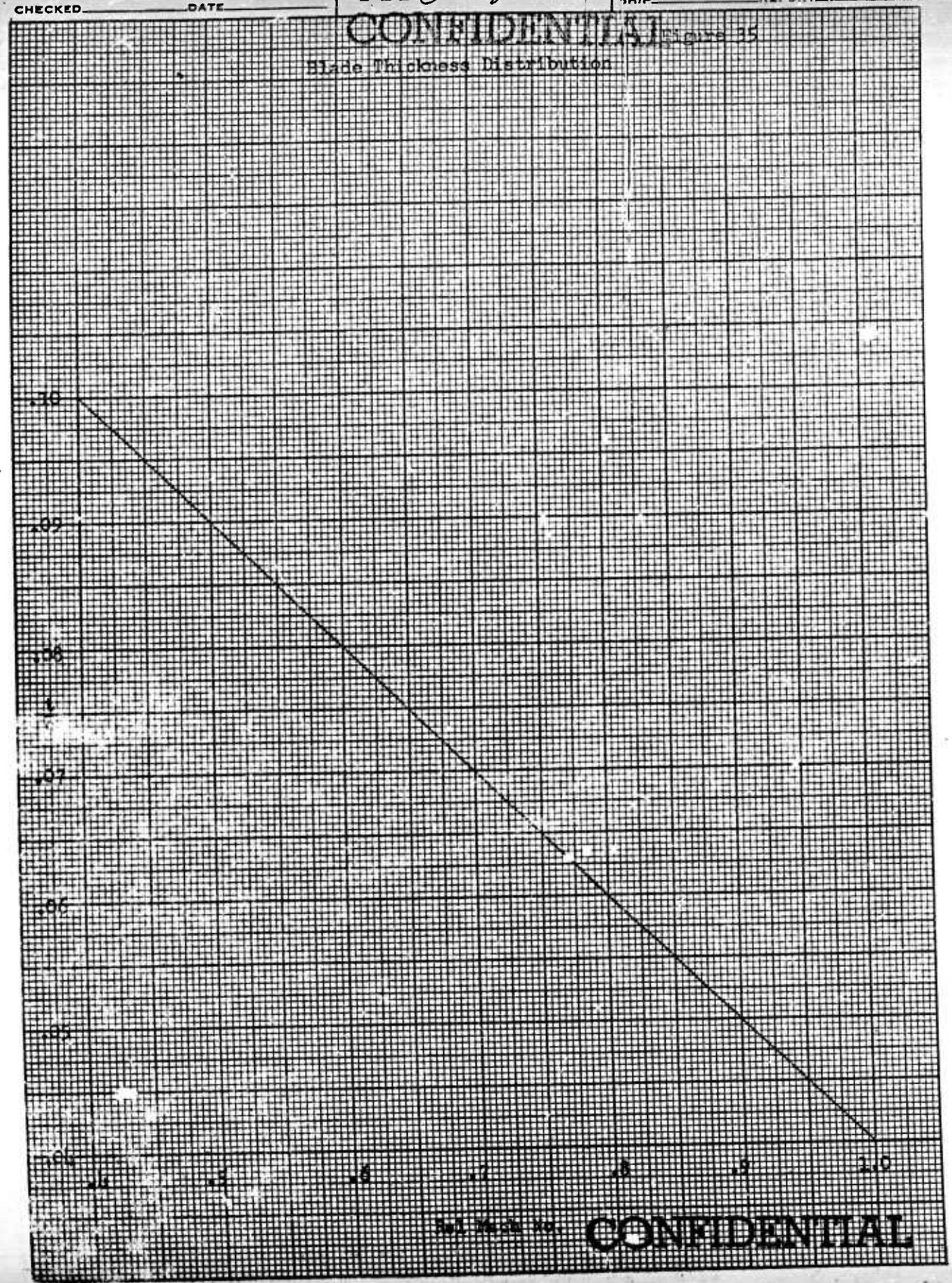

CONFIDENTIAL

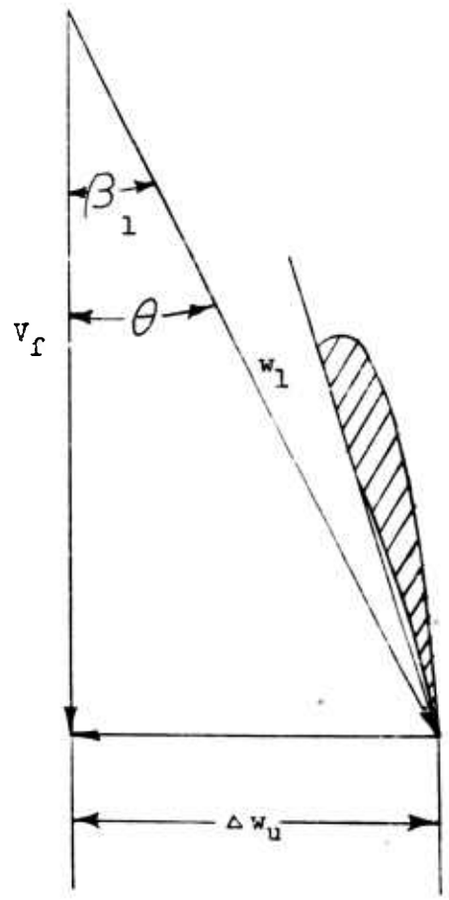

Exit Stator Vector Diagram

D. Ducted Propeller Configurations

The method outlined in the preceeding section may be used to design a ducted propeller installation which will absorb all of the horsepower available and perform satisfactorily at the design point. At other points in the flight regime, however, the forward velocity, altitude, horsepower input, rotational velocity, or a combination of these parameters may be different than at the design point. Thus, if a fixed pitch configuration is considered, the propeller will operate inefficiently and, over a large range of operating conditions, may overspeed or suffer a drastic reduction in thrust due tc blade stall. This situation might be alleviated by varying the engine RPM, but, with a direct-drive constant-speed engine such as a turboprop, this would necessitate contending with engine surge, poor engine specifics, poor acceleration characteristics, etc. A variable-drive gear box between the propeller and engine is another possibility, but this would entail a long development program and might result in too great a weight penalty. The most practical way to solve the off-design problem is to incorporate some means of varying the effective angle of attack of the blades, such as the use of variable pitch or inlet guide vanes. Both type configurations were designed during this study. The off-design methods used for each type are covered in the following sections.

1. Inlet Guide Vane Configurations

The first fans designed under this study contract employed inlet guide vanes as a means of obtaining satisfactory off-design performance. These fans were designed with symmetrical guide vane sections set at zero angle of attack at the design point. Under off-design conditions, the guide

vanes were rotated in positive or negative directions to insure full power absorption at flight speeds lower or higher than design speed. The rotor vector diagrams for positive and negative vane deflection are shown in Figure 37. The diameter of the duct at the leading edge of the guide vanes is the same as that at the rotor, and it has been assumed that there is no change in axial velocity between these two points.

Figure 107 of Reference 12 shows the variation of $\frac{dc_l}{d\alpha}$ with blade solidity for moderate cambers and various values of β_1. The curve for β_1 equal to 30 or 45 degrees was found to be in very good agreement with data contained in References 17 and 18 for $\beta_1 = 0$ and cambers as low as $C_{l_o} = .10$. This curve is reporduced in Figure 38, and was used in determining the vane angle required for full power absorption.

Equation (1 - 3) may be written

$$HP = \frac{Nc\rho V_f^2 R (R\Omega)}{550\sigma_T} \int_{(r/R)}^{1.0} (r/R)^2 \frac{\Delta w_{u_f}}{V_f} d(r/R)$$

from which

$$\int_{(r/R)}^{1.0} (r/R)^2 \frac{\Delta w_{u_f}}{V_f} d(r/R) = \frac{550\sigma_T HP}{Nc\rho V_f^2 R\, R\Omega} \qquad (2 - 8)$$

The integral on the left hand side of the above equation will be referred to hereafter as the Power Factor, (PF). For a particular ducted fan design,

Figure 37

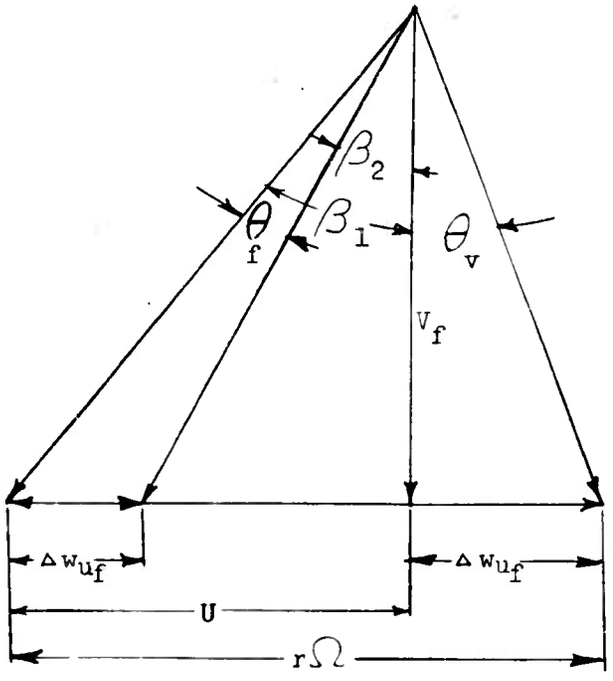

a. Rotor Vector Diagram for Positive Inlet Guide Vane Angle

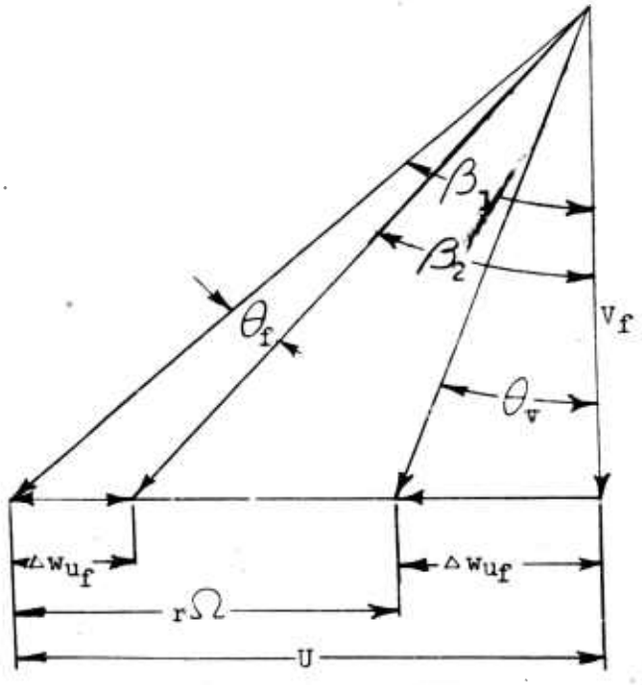

b. Rotor Vector Diagram for Negative Inlet Guide Vane Angle

CONFIDENTIAL

Figure 38

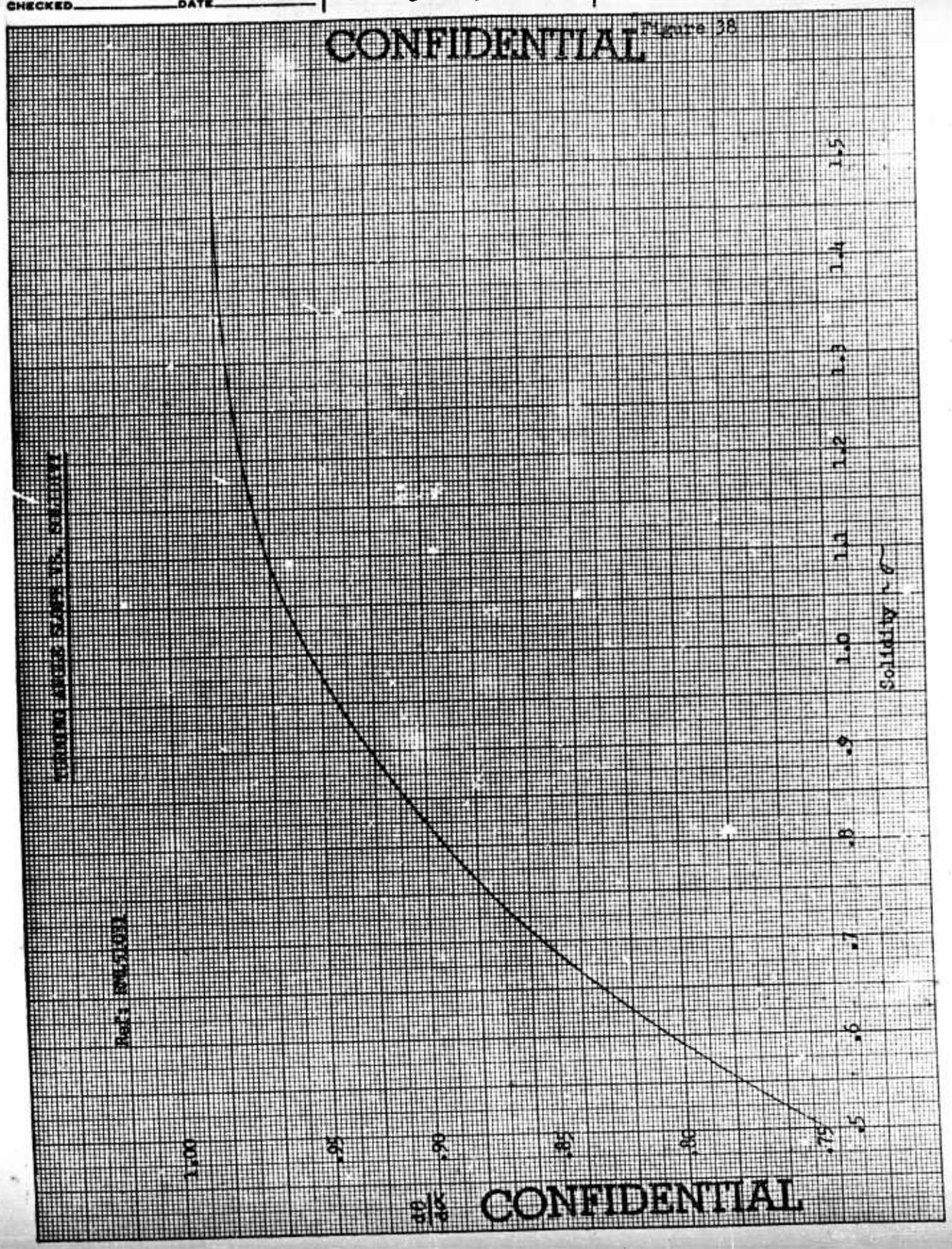

CONFIDENTIAL

The Power Factor may also be expressed as a function of the blade setting of the inlet guide vanes and $\frac{R\Omega}{V_f}$, as shown in the following procedure.

The whirl velocity imparted to the air by the rotor may be written as

$$\Delta w_{U_f} = U - \left(U - \Delta w_{U_f}\right) \qquad (2 - 9)$$

From Figure 37,

$$U = r\Omega - V_f \tan\theta_v$$

and,

$$U - \Delta w_{U_f} = V_f \tan\beta_2$$

Then, from Equation (2 - 9)

$$\frac{\Delta w_{U_f}}{V_f} = \frac{r\Omega}{V_f} - \tan\theta_v - \tan\beta_2 \qquad (2 - 10)$$

For a given flight condition, $\frac{r\Omega}{V_f}$ at each station is known. Now, for a given inlet guide vane setting, θ_v at each station may be determined since the solidity is known. Using Figure 38,

$$\theta_v = \alpha_v \left(\frac{d\theta}{d\alpha}\right)_v \qquad (2 - 11)$$

Also, from Figure 37

$$\beta_1 = \tan^{-1} \frac{r\Omega - V_f \tan\theta_v}{V_f}$$

$$= \tan^{-1}\left(\frac{r\Omega}{V_f} - \tan\theta_v\right) \qquad (2 - 12)$$

At each station, by varying α, a plot of θ_f vs β_1 may be obtained from the off-design charts. Then, since $\beta_2 = \beta_1 - \theta_f$ and β_1 and θ_f are now known, β_2 may be plotted as a function of β_1 at each station, or better yet, $\tan\beta_2$ may be plotted as a function of $\tan\beta_1$. Thus, using equation (2 - 10), it is now possible to determine the quantity $(r/R)^2 \frac{\Delta w_{u_f}}{V_f} d(r/R)$ at each radial station. This quantity may then be plotted vs radial station and graphically integrated to obtain the Power Factor. This process is repeated for several values of α_v and $\frac{R\Omega}{V_f}$, and the results may be plotted in carpet form, showing PF as a function of α_v and $\frac{R\Omega}{V_f}$. This procedure must be repeated for each new fan design. A typical carpet of this type is shown in Figure 42, Section E.

The Power Factor variation discussed above may be obtained by varying only α_v and V_f, while rotational velocity, horsepower input and altitude are considered constant. However, the carpet thus obtained is completely general for the particular fan involved, and may be used for any value of HP input, $R\Omega$ or V_f, at any desired altitude. This may be seen from equation (2 - 8), which shows that

$$PF = \frac{550\,\eta_I HP}{N c \rho V_f^2 R (R\Omega)} \qquad (2 - 13)$$

For a particular fan under consideration, knowing $R\Omega$ and the horsepower input at a given altitude, V_f may be determined from the momentum data. Then the value of PF may be calculated from equation (2 - 13). Knowing

the value of PF and $\frac{R\Omega}{V_f}$, the inlet guide vane angle required to absorb all the available horsepower may be determined from the carpet. In this manner, the carpet plot may also be used to determine the vane angles necessary to operate at reduced power and RPM.

It will be noted that as the inlet angle (β_1) changes due to rotation of the inlet guide vanes, the angle of attack (α) of the rotor blades also changes. As a general rule, it was considered that the maximum allowable α of the rotor was determined by the same criteria used in References 12 and 14. The maximum angle of attack data contained in these references was plotted in carpet form, and is shown in Figure 39.

2. Variable-Pitch Configurations

As shown previously in this report, the attainment of low disk power loadings in a ducted propeller design is very desirable. It has been noted during this study, however, that as the power loading is decreased the range of angles over which the inlet guide vanes are required to operate is increased. Therefore, it was decided to investigate the use of lower solidity fans incorporating variable pitch. The design procedure for a variable pitch configuration is the same as that for the fixed-pitch fans with no guide vane turning at the design point but the determination of off-design performance is somewhat different.

The vector diagram for a variable pitch configuration is the same as that shown in Figure 26. For a given flight condition, V_f and $R\Omega$ are known. Therefore, β_1 at each station is also known. Knowing the camber and solidity at each station, the turning angle corresponding to various angles of attack may be obtained from the off-design charts.

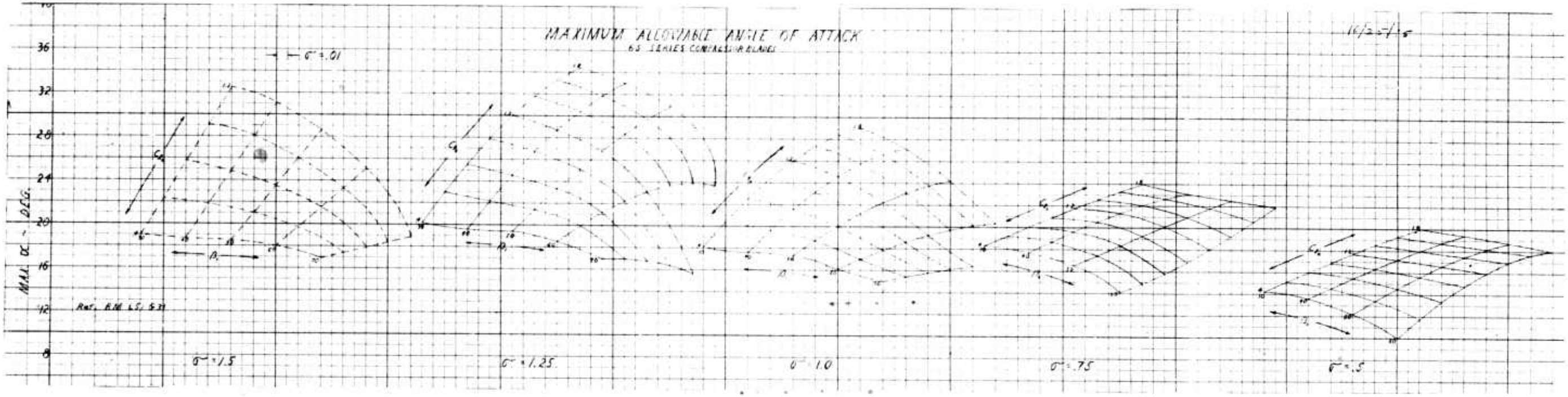
MAXIMUM ALLOWABLE ANGLE OF ATTACK
65 SERIES COMPRESSOR BLADES
MAX. α DEG.
Ref. RM LS. 5-21
σ = 1.5
σ = 1.25
σ = 1.0
σ = .75
σ = .5

Figure 39

Repeating this procedure for several values of V_o, a rotor performance carpet of θ vs α and V_o may be plotted for each radial station. A typical rotor performance chart is shown in Figure 51, Section E.

Since the variable pitch rotor has been designed in the same manner as the fixed-pitch configuration, $r\Omega$, β_1, and ψ_d are known at each radial station for a given flight condition. Then if the pitch angle of the blade is varied (i.e., if ψ_d is changed by some amount $\Delta\psi$), the resulting pitch angle is given by

$$\psi' = \psi_d + \Delta\psi \qquad (2 - 14)$$

and the resulting blade angle of attack is

$$\alpha = \beta_1 - \psi'$$

The turning angle, ϵ, may now be determined at each station from the rotor performance chart. Then, using equation (2 - 5) and referring to Figure 26,

$$\frac{\Delta w_{uf}}{V_f} = \tan\beta_2 \qquad (2 - 15)$$

Using graphical integration, the Power Factor is then given by

$$PF = \int_{(r/R)}^{1.0} (r/R)^2 \frac{\Delta w_{uf}}{V_f}\, d(r/R) \qquad (2 - 16)$$

Repeating the above procedure for various values of $\Delta\psi$ and V_f, a carpet of PF vs $\Delta\psi$ and $\frac{R\Omega}{V_f}$ may be obtained. This is again a completely general plot, and may be used in the same manner as that obtained for the inlet guide vane configurations. This graph shows the change in pitch angle necessary to absorb full horsepower under all flight conditions. A typical plot may be seen in Figure 52 , Section E.

3. Contra-Rotating Configurations

Another type of fan design studied during this contract was the contra-rotating configuration. This type of fan configuration eliminates the use of exit stators, since the rear rotor is designed to remove all of the residual whirl added to the air flow by the front rotor. Typical vector diagrams for a contra-rotating fan are shown in Figure 40.

The contra-rotating configuration has been designed so that the relative tip speed ($w_{1_{R2}}$) of the rear rotor will not exceed a limiting value. Also, since the rear rotor must remove all of the residual swirl added to the air stream by the front rotor,

$$\Delta w_{U_{R1}} = \Delta w_{U_{R2}}$$

and

$$\left(R\Omega + \Delta w_{U_{R1}}\right)^2 = w_{1_{R2}}^2 - V_f^2 \qquad (2 - 17)$$

Integrating equation (1 - 34) and simplifying, the HP absorbed may be

Figure 40

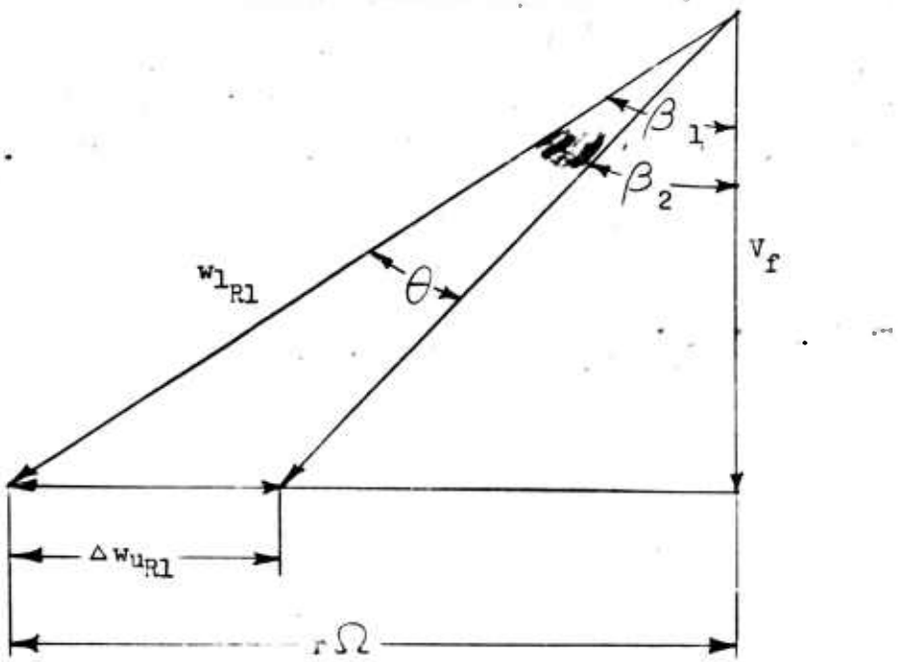

a. Contra-Rotating Fan - Front Rotor

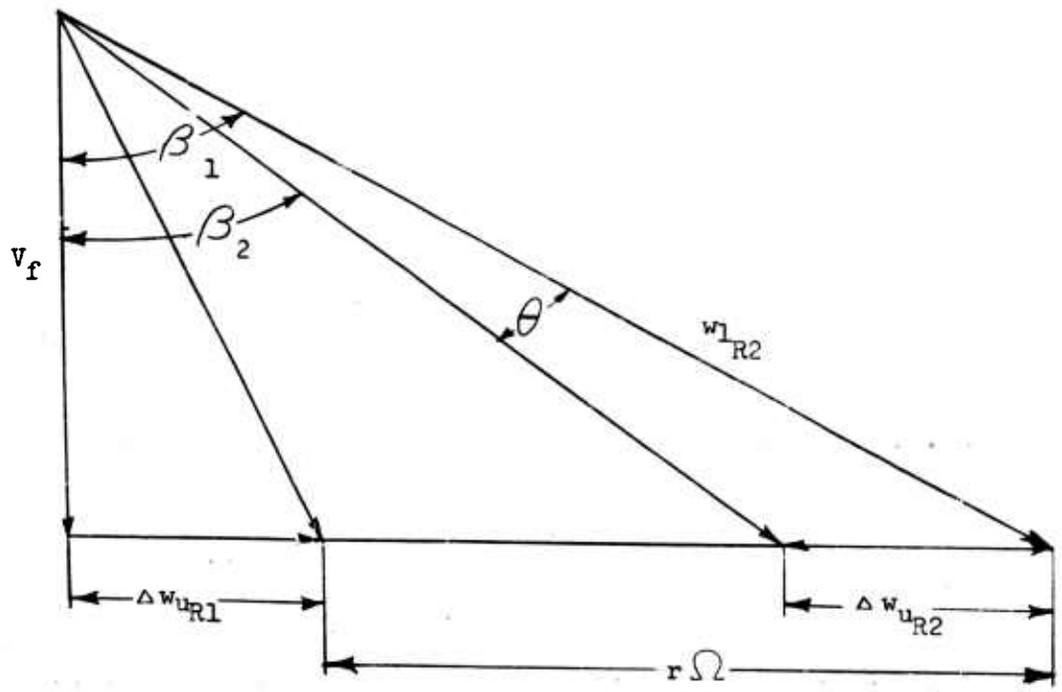

b. Contra-Rotating Fan - Rear Rotor

expressed as

$$HP = \frac{A_f}{550} \rho V_f (R\Omega)(\Delta W_{U_T}) \qquad (2 - 18)$$

and, since half of the horsepower is absorbed by each rotor,

$$\Delta W_{U_T} = \Delta W_{U_{R1}} + \Delta W_{U_{R2}}$$

Choosing an arbitrary value for $\Delta W_{U_{R1}}$, $R\Omega$ may be found from (2 - 17). Then the horsepower absorbed at a given design flight condition may be determined from (2 - 18). Repeating this process, a plot of HP vs $\Delta W_{U_{R1}}$ may be obtained. Knowing the HP available, the required value of $\Delta W_{U_{R1}}$ may be found from this curve and the required $R\Omega$ from (2 - 17). The design procedure is then the same as for the variable pitch configurations. Since the inlet angles are different, rotor performance charts and power factor carpets must be determined for both front and rear rotors.

In the design of the contra-rotating configuration, an additional simplifying assumption has been made. It has been assumed that the axial fan velocity at the rear rotor is the same as at the front rotor. It is believed that this assumption will have a negligible effect on the over-all fan performance.

E. DUCTED PROPELLER DESIGNS

The main purpose of the detailed fan analyses was to determine a configuration suitable for incorporation into the aircraft configuration studies. A total of five basic ducted fan configurations were investigated, and several design variations were studied for most of the configurations. As mentioned previously, three power plants have been considered for use with a ducted propeller system during this study. They are the Wright Aeronautical T-49, the Rolls Royce RB-109 and the Allison 550-B1. The fans designed for use with these engines are covered in the following paragraphs.

1. Configuration No. 1

The first detailed design of a ducted propeller system carried out during this study incorporated a T-49 engine as the power source and was a fixed pitch configuration designed for a static fan thrust of 17,370 pounds at 6000 feet on a 95° day. At this stage of the study the use of water injection to recover sea level power output at the higher altitude and temperature requirements was not considered, so that severe penalties were imposed upon the design. Despite this fact, it was possible to develop a configuration which would fulfill the design requirements.

Four variations of this configuration were studied. The first attempt was to design a fan with axial inlet velocity at the required static conditions. It was found, however, that this design would not absorb the power available at high speed conditions. The use of symmetrical inlet guide vanes to change the inlet angle for high speed conditions resulted in blade angles of attack which were prohibitive. Since the duct

geometry had already been dictated by the static requirements, it was then decided to design the system for some flight speed other than zero.

Three fan designs were investigated at forward flight speeds, the design points being 100, 200 and 300 knots at sea level standard conditions. The operating range of the designs was considered to be from 0 to 300 knots, the static point being at 6000 feet and 95°F. The inlet guide vanes consisted of untwisted, symmetrical 6% thick sections. The flow into the fixed-pitch rotor was axial at the design point, the pitch of the inlet guide vanes being varied to enable off-design operation. The exit stators were designed to give axial flow at the exit under static conditions at 6000 feet, and 95°F. The configuration data for these fans are shown in Table III.

The most satisfactory configuration obtained was that having a design point of 200 knots. Under static conditions, it is necessary to set the inlet vanes at an angle of attack of approximately 18°, while for the 300 knot condition it is necessary to rotate them approximately 15° in the opposite direction. While this particular configuration is not considered to be an optimum design, it is nevertheless an acceptable design which will operate satisfactorily over the required speed range. The 300 knot design would operate over the entire range but appeared to be marginal at static conditions. The 100 knot design was severely limited at the high speed end, as was the earlier static design. In the case of the 100 knot design, satisfactory operation was obtained at the design point and under static conditions at 6000 feet and 95°, but the high guide vane deflection angle required to prevent negative lift coefficients at the 300 knot condition was considered to be prohibitive.

TABLE III

Configuration Data - Fan No. 1

Design Point	Static (6000'-95°)	100 Knots (S.L.-Std.)	300 Knots (S.L.-Std.)	200 Knots (S.L.-Std.)
Power Plant	T-49	T-49	T-49	T-49
HP available at Design Point	6095	8806	9440	9383
Fan Diameter	11.6'	11.6'	11.6'	11.6'
Inlet Diameter (Static)	15.5'	15.5'	15.5'	15.5'
R.P.M.	1395	1235	1235	1235
Hub/Tip Ratio	.4	.4	.4	.4
No. of Rotor Blades	17	17	17	17
Inlet Stators (Variable)	21	21	21	21
Exit Stators	19	19	19	19
Tip Mach No.	.8 (static)	.85 @ 300K	.85 @ 300K	.85 @ 300K
Design Fan Velocity in ft/sec	339	371	582	458
Static Fan Thrust, lb. (6000'-95°F)	17,370	17,370	17,370	17,370

The 300 knot configuration was considered to be marginal at the static condition, since an angle of attack of 24° was required on the inlet stators at this condition.

As would be expected, a positive guide vane deflection was required to reduce the rotor angle of attack at speeds lower than design while at speeds above the design point the opposite was true. At the lower design speeds, a large variation in camber was required. This entailed extreme camber at the root with very moderate camber at the tips. With increased design speed the camber at the root was progressively reduced resulting in less camber variation along the blade. The blade twist was also reduced for higher design speeds.

One of the troubles encountered with the less successful designs involved negative lift on the rotor. At speeds greater than design speed, insufficient guide vane deflection caused the tip section of the rotor blade to operate at negative lift coefficients. This resulted in the induced rotation from the rotor having one direction at the root and the opposite direction at the tip. It would appear that such a flow pattern would absorb power without producing full thrust. For the 100 knot design, this negative lift condition was not eliminated until a vane deflection of -30.6°, at a flight velocity of 300 knots, was attained. Since the assumption of linear guide vane turning could not be considered valid to an angle of attack of this magnitude, the 100 knot design was limited to some speed less than 300 knots and was therefore eliminated.

The 200 knot design was considered successful since it operated satisfactorily over the entire speed range, with guide vane deflections of +18° statically and -15° at 300 knots, and did not encounter any

negative lift region. The design parameters for this configuration are shown in Table IV. The inlet guide vanes are NACA 63-006 sections, modified to have a trailing edge radius equal to 10 percent of the maximum thickness. The exit stators were designed for operation under static conditions at 6000 feet and 95°F. This was the condition of maximum flow rotation behind the rotor and therefore was the condition under which the angle of attack of the stators was maximum. A plot of flow rotation for the stators as a function of inlet angle for the 200 knot design is shown in Figure 41. As shown in Section C, the inlet angle (β_1), and turning angle (θ) are equal at the design point. The dashed line in Figure 41 shows the ideal operating line for the exit stator, where $\theta = \beta_1$. The solid line shows the estimated stator performance, and indicates that there is very little residual whirl behind the stator under any operating condition. The performance curve is extrapolated beyond the available data as is shown by the centerline curve.

The Power Factor for the 200 knot design is shown in Figure 42. This fan has been completely analyzed over a range of flight speeds from 0 to 300 knots, altitudes from sea level to 35,000 feet, and power settings from 30 percent to maximum. The variation of engine RPM vs. HP for lower power settings was obtained from Reference 8. Figures 43 through 47 show the operating conditions for this fan. Figures 43 through 46 are carpets showing the inlet guide vane setting for 100%, 60%, 40% and 30% power as a function of forward speed and altitude. The operating range for the inlet guide vanes was considered to be $\pm$ 20°. These carpets show that the fan will operate satisfactorily at altitudes from sea level to 35,000

TABLE IV

Configuration No. 1

Inlet Guide Vanes

Chord = 1.04 feet, Thickness = 6 %, Modified 63-006 section.
Linear variation in solidity, σ = 1.5 at hub , .6 at tip.

Rotor

Chord = 1.070 feet, Modified 65 - series section.

Radial Station	σ	C_{l_c}	α_c	t/c	ψ
.4	1.250	.890	11.5	.091	21.8
.5	1.000	.650	8.3	.086	31.1
.6	.833	.605	6.9	.081	37.6
.7	.714	.490	5.9	.076	42.9
.8	.625	.440	5.0	.071	47.6
.9	.555	.360	4.2	.066	51.6
1.0	.500	.290	3.5	.061	55.1

Exit Stators

Chord = 1.15 feet, Modified 65 - series section.

Radial Station	σ	C_{l_c}	α_c	t/c	ψ
.4	1.500	1.50	18.4	.06	13.6
.5	1.200	1.60	18.9	.06	12.6
.6	1.000	1.64	19.7	.06	11.7
.7	.856	1.75	20.7	.06	10.7
.8	.750	1.95	21.8	.06	9.7
.9	.666	2.13	22.9	.06	8.8
1.0	.600	2.35	24.0	.06	7.8

Figure 11

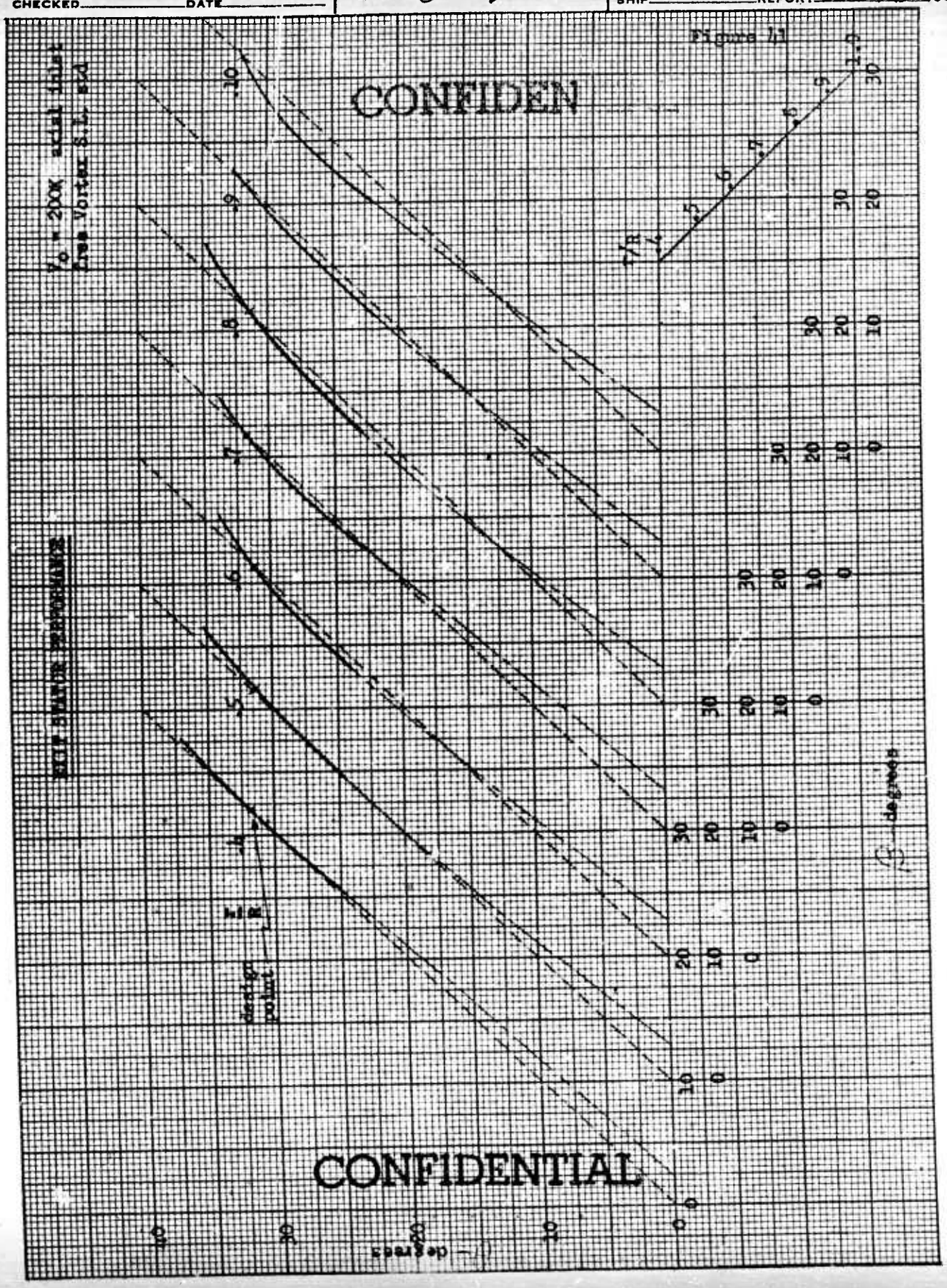

Figure 42

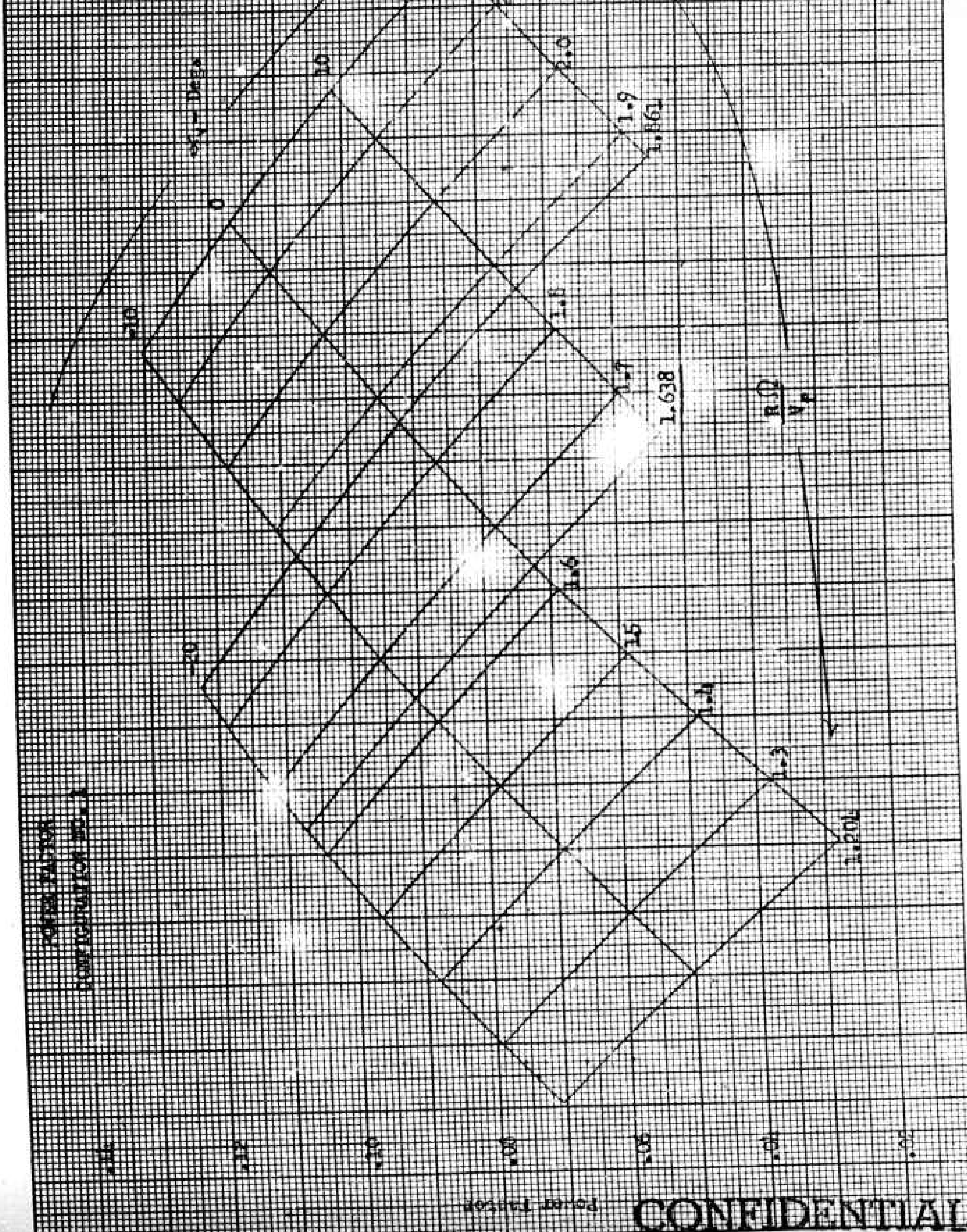

Figure 43

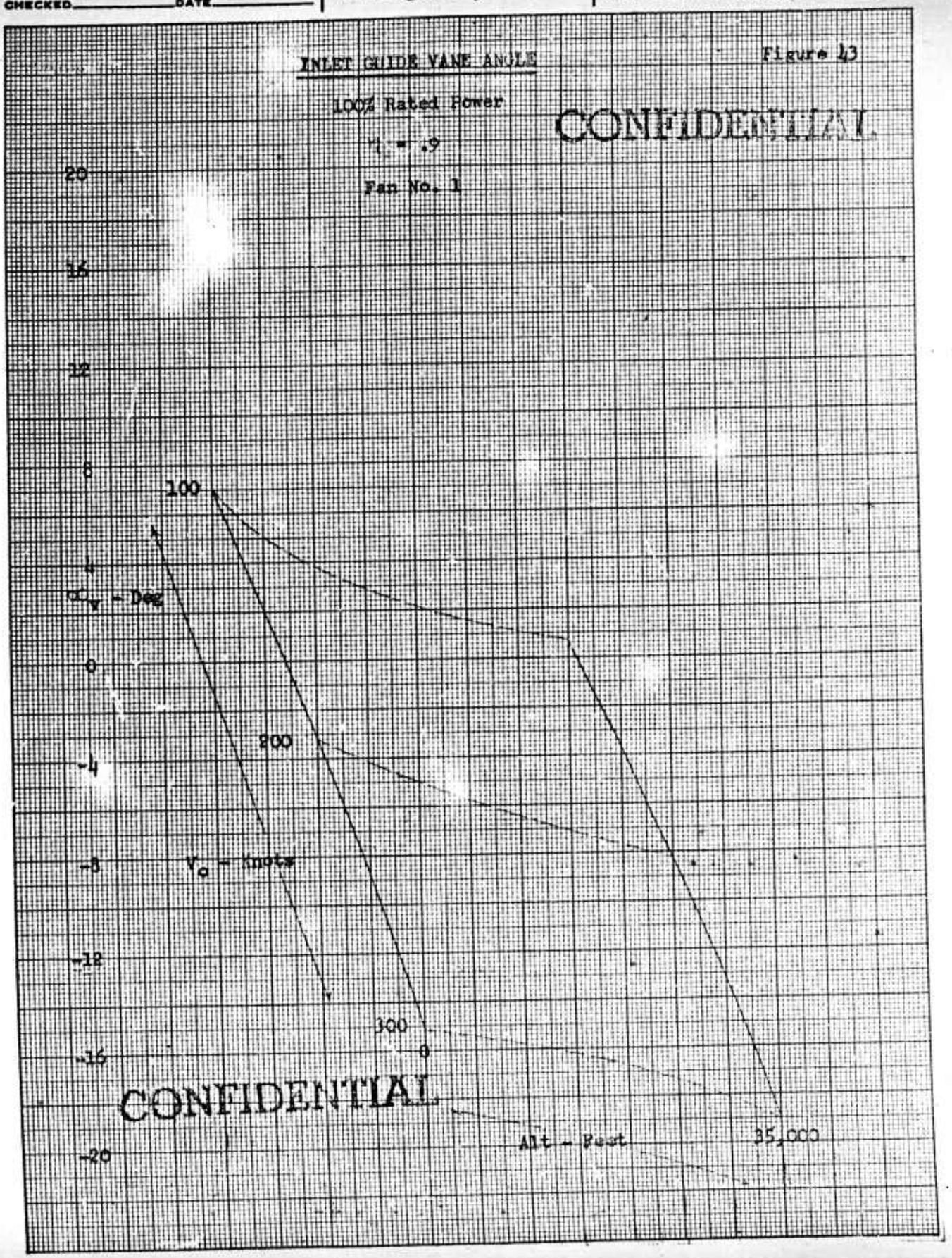
INLET GUIDE VANE ANGLE
100% Rated Power
η = .9
Fan No. 1
CONFIDENTIAL
20
16
12
8
4
0
-4
-8
-12
-16
-20
α_v - Deg
100
200
300
0
V_o - Knots
Alt - Feet
35,000
CONFIDENTIAL

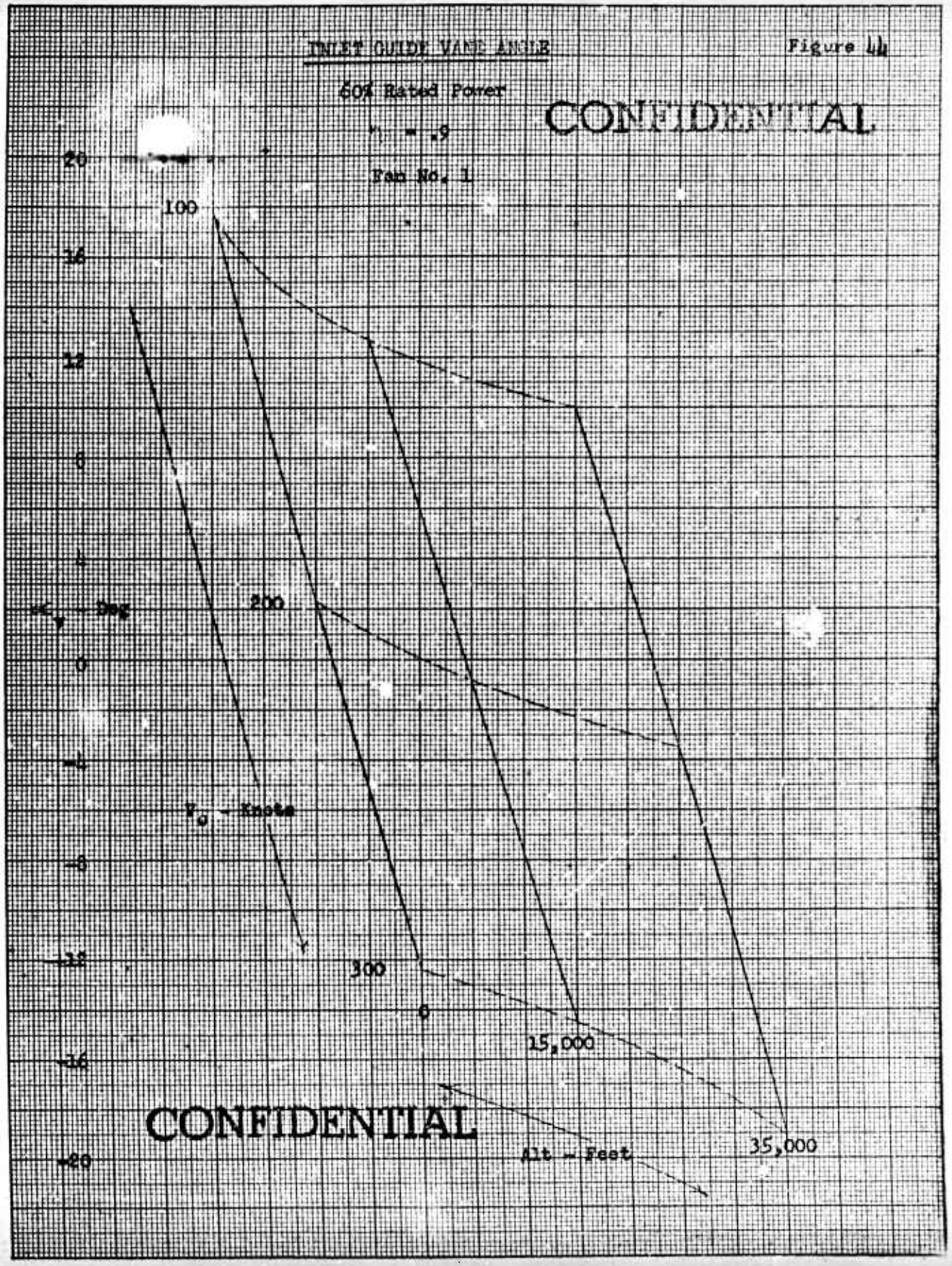
INLET GUIDE VANE ANGLE
Figure 44
60% Rated Power
η_c = .9
Fan No. 1
CONFIDENTIAL
20
16
12
8
4
0
-4
-8
-12
-16
-20
α_v - Deg
100
200
300
V_o - Knots
0
15,000
35,000
Alt - Feet
CONFIDENTIAL

Figure 45

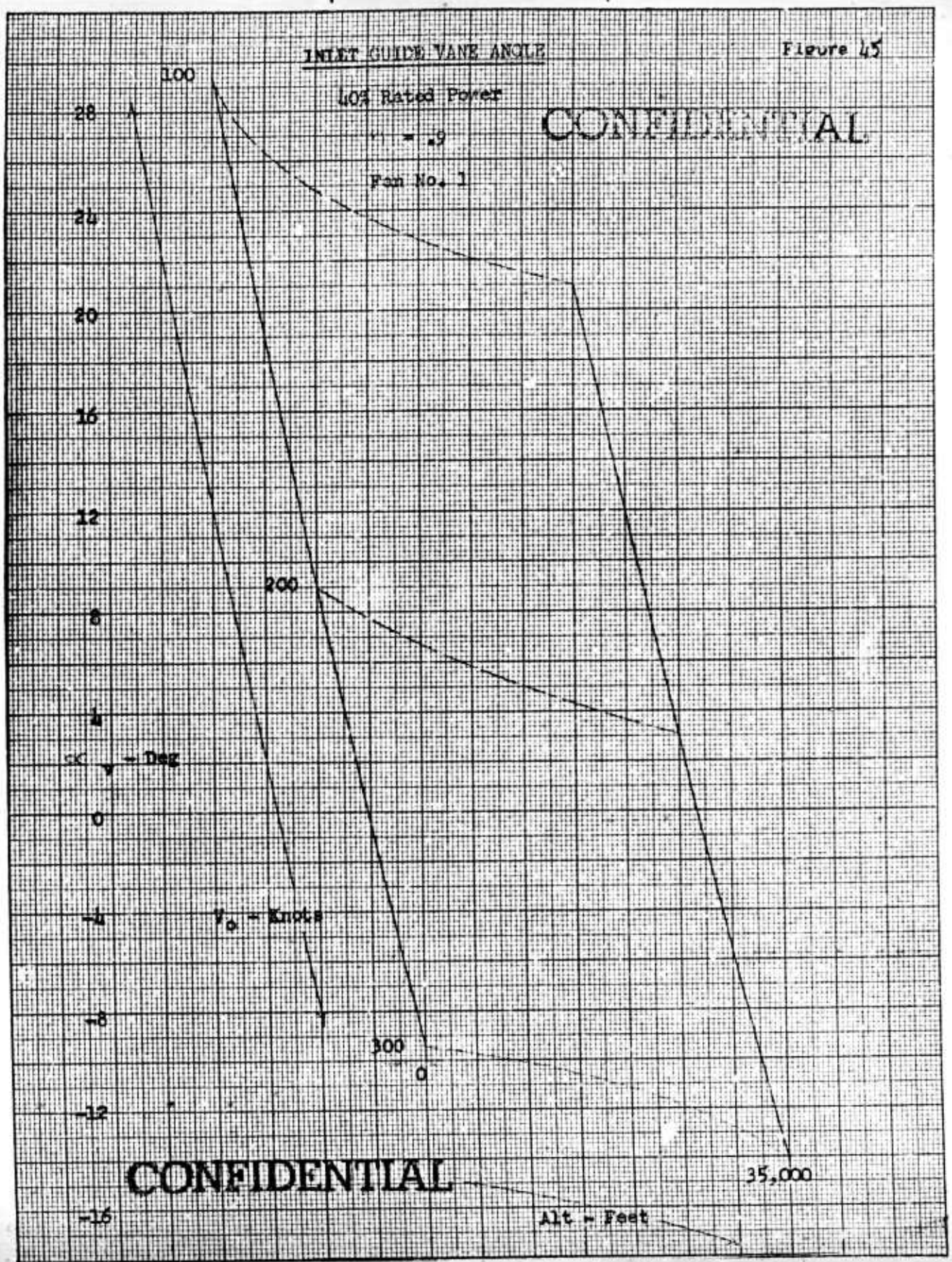
INLET GUIDE VANE ANGLE
40% Rated Power
r = .9
Fan No. 1
CONFIDENTIAL
100
200
300
0
28
24
20
16
12
8
4
0
-4
-8
-12
-16
α_K - Deg
V_o - Knots
Alt - Feet
35,000
CONFIDENTIAL

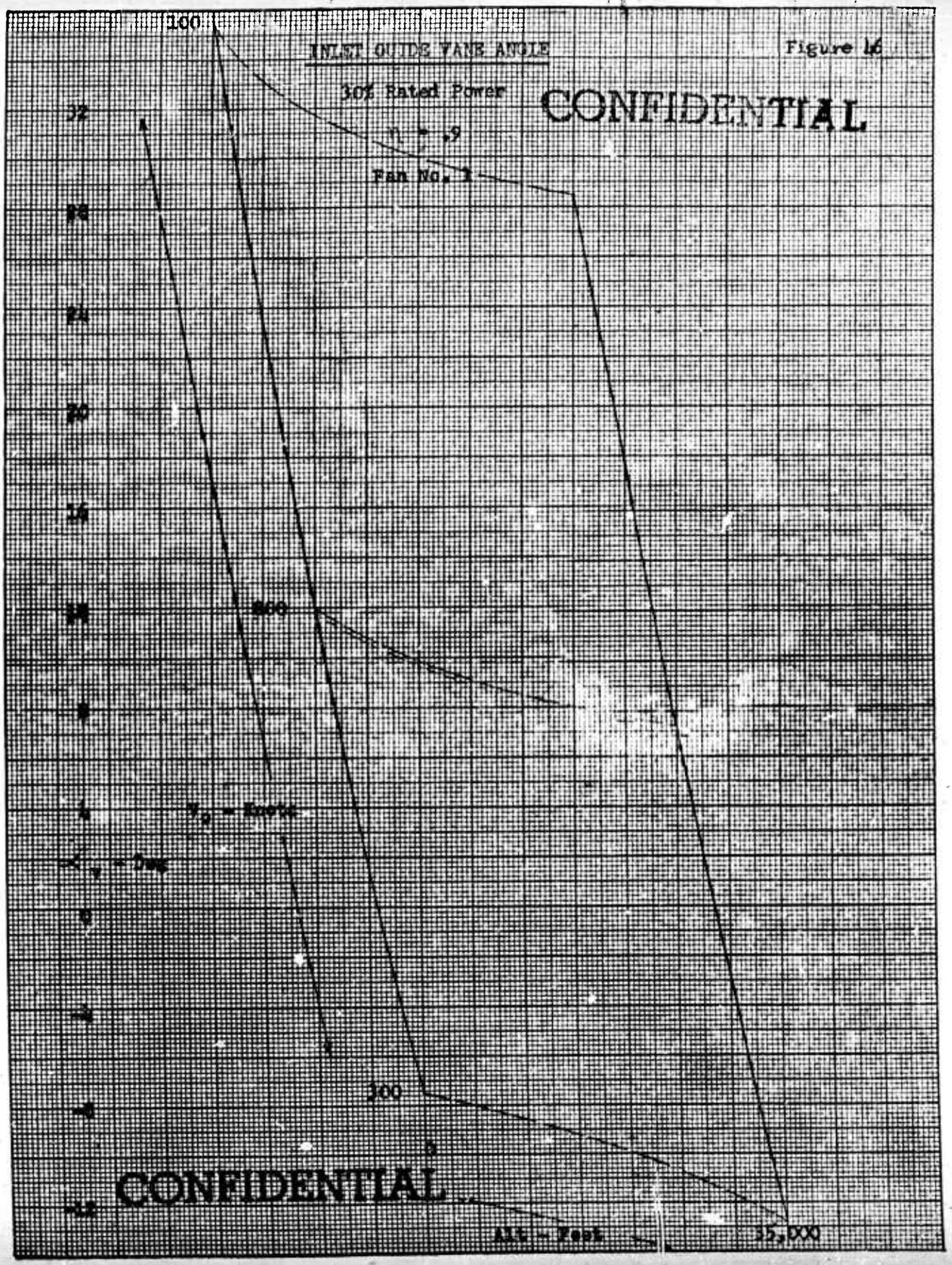
INLET GUIDE VANE ANGLE
Figure 16
30% Rated Power
CONFIDENTIAL
η = .9
Fan No. 1
100
32
28
24
20
16
12
8
4
0
-4
-8
-12
800
300
V_g = Knots
α_v = Deg
Alt = Feet
35,000
CONFIDENTIAL

Figure 47

INLET GUIDE VANE ANGLE REQUIRED
AT VARIOUS POWER SETTINGS

Sea Level Standard Conditions

η = .9

Fan No. 1

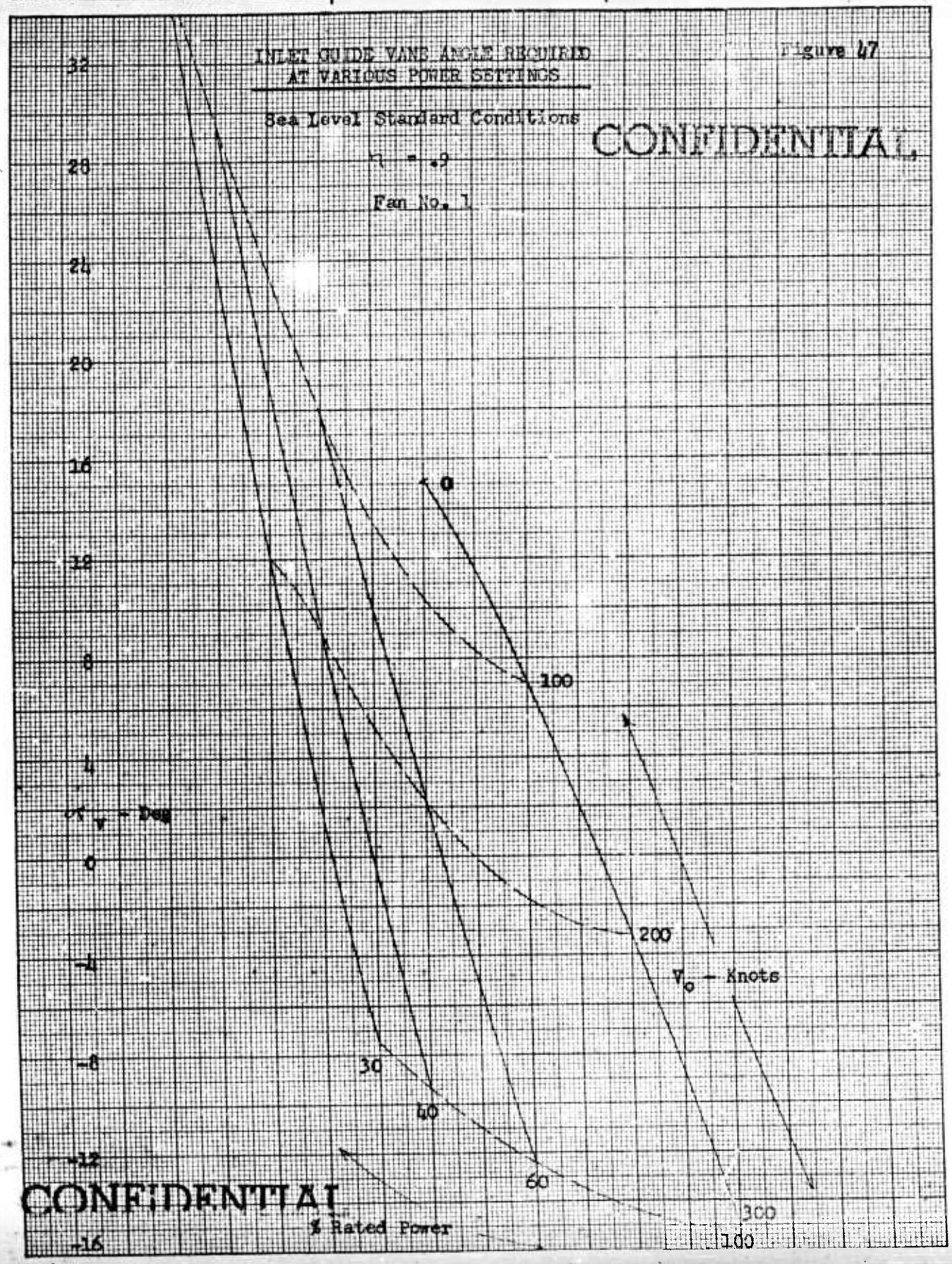

CONFIDENTIAL

CONFIDENTIAL

feet at full rated and at 60% rated power. At 40% rated power, the fan operation will be marginal at 35,000 feet and 100 knots forward speed. At the same power at sea level the inlet guide vane angles necessary to absorb the available power are prohibitive at flight speeds lower than 140 knots and therefore the fan will not function efficiently. Excessive guide vane angles are required in the low flight speed regime at all altitudes at 30% power. This power setting is not too significant, however, since it is very close to the idle point on the engine. When considering this fan design in conjunction with a specific aircraft configuration, it is evident that the cruise condition of the aircraft must be at a power setting somewhere between 60 and 100% rated power. This fan would be satisfactory for the operational flight regime of the airplanes being considered in this study. Figure 47 is a composite curve which shows the vane angle required under standard sea level conditions as a function of forward speed and power setting. It can be seen from the curve that the low speed flight regime requires the higher guide vane angles, and is therefore the more critical area as far as satisfactory fan operation is concerned.

2. Configuration No. 2

The second fan configuration which was studied incorporated the Rolls-Royce RB-109 engine as a power source. Three variations of this design were investigated, two of the configurations employing inlet guide vanes and one being a variable pitch arrangement. All of these variations had a lower disk power loading than the T-49 design, and were designed for a static fan thrust of 11,317 lbs.

The configuration data for these fans are shown in Table V. As can be seen from this table, the inlet and fan diameters are the same as for the previous design. Since the use of a .3 hub-tip ratio resulted in

TABLE V

CONFIGURATION DATA - FAN NO. 2

	Inlet Guide Vanes	Inlet Guide Vanes	Variable Pitch
Design Point	200 Kts.	150 Kts.	200 Kts.
Power Plant	RB-109	RB-109	RB-109
Available at Design Point	3365	3250	3365
Fan Diameter	11.6'	11.6'	11.6'
Inlet Diameter	15.5'	15.5'	15.5'
RPM	1143	1143	1143
Hub/Tip Ratio	.3	.3	.3
No. of Rotor Blades	10	10	10
Inlet Stators	13	13	
Exit Stators	15	15	15
Tip Mach No. at 300 knots	.8	.8	.8
Design Fan Velocity	408 fps	350 fps	408 fps
Static Fan Thrust (6000', 95°F.)	11317lbs.	11317lbs.	11317 lbs.

lower solidities along the blade, it was necessary to utilize the low-solidity cascade data in the design of this configuration. Ten rotor blades and fifteen exit stators were employed in both the variable pitch and inlet guide vane designs, and thirteen inlet guide vanes were used in the versions which required them.

Figures 48 and 49 show the Power Factor variation for the 150 and 200 knot inlet guide vane designs, respectively. Figure 50 shows the variation of the inlet guide vane angle which was required at various forward speeds for these designs. Inspection of this plot indicates that the inlet guide vane angle required for operation over the complete range desired is unsatisfactory. This situation is due to the high power loading.

The most successful design using the RB-109 powerplant was the variable pitch configuration, with a design point of 200 knots. The design parameters for this configuration are shown in Table VI. The Rotor Performance Chart for this design is shown in Figure 51, while the Power Factor variation is presented in Figure 52. Figure 53 shows the change in pitch angle required as a function of flight speed. As shown by this plot, the greatest change in pitch angle required is -16° at a forward speed of 400 knots. The pitch change required under standard sea level conditions, at various power settings is shown in Figure 54. Even at 30% rated power, it may be seen that the maximum pitch change required is only -17.5°. It may therefore be concluded that this fan will operate satisfactorily over the entire flight regime required, with a maximum speed in excess of 400 knots. A comparison of the inlet guide vane angles

Figure 48

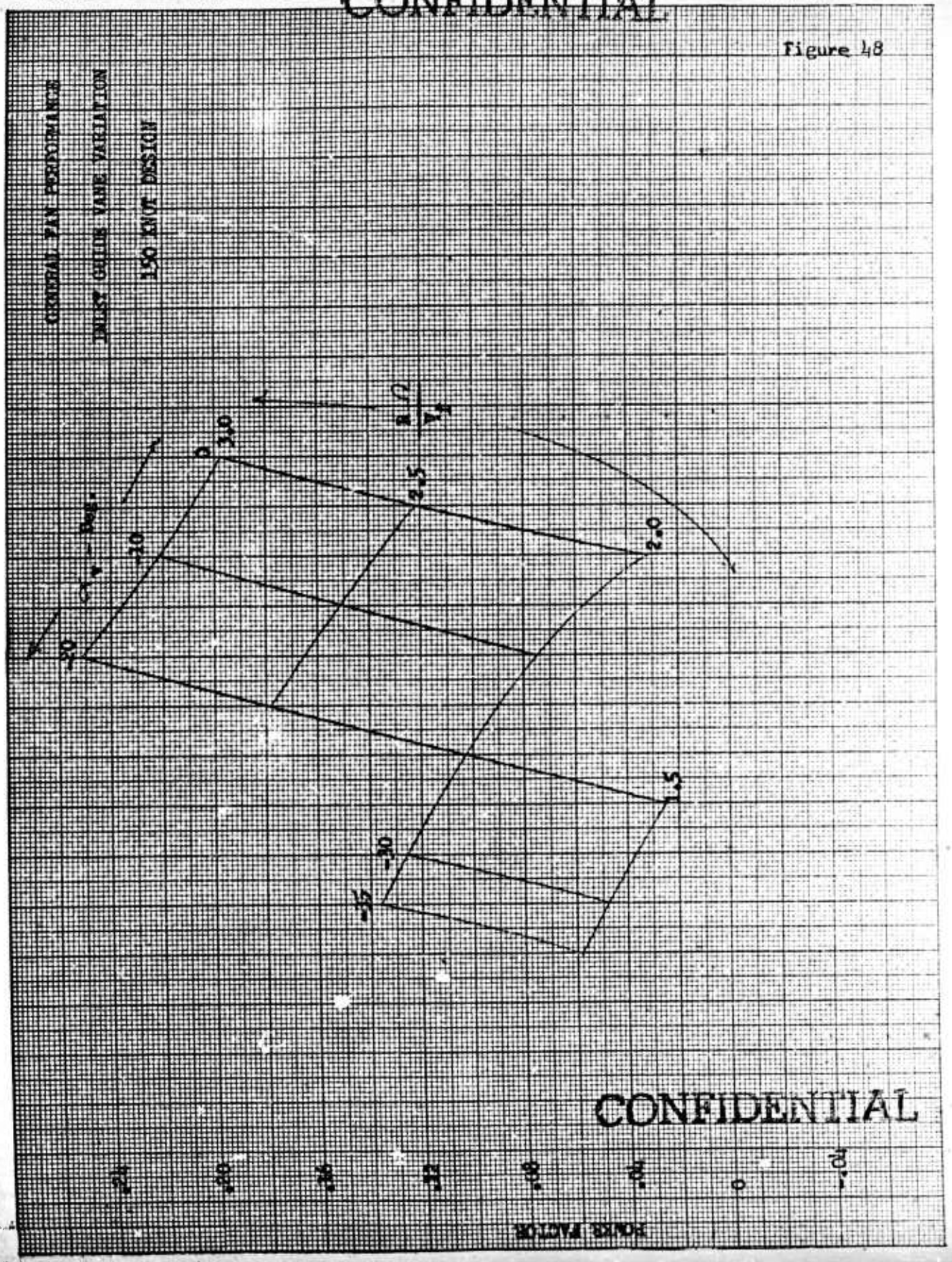

Figure 10

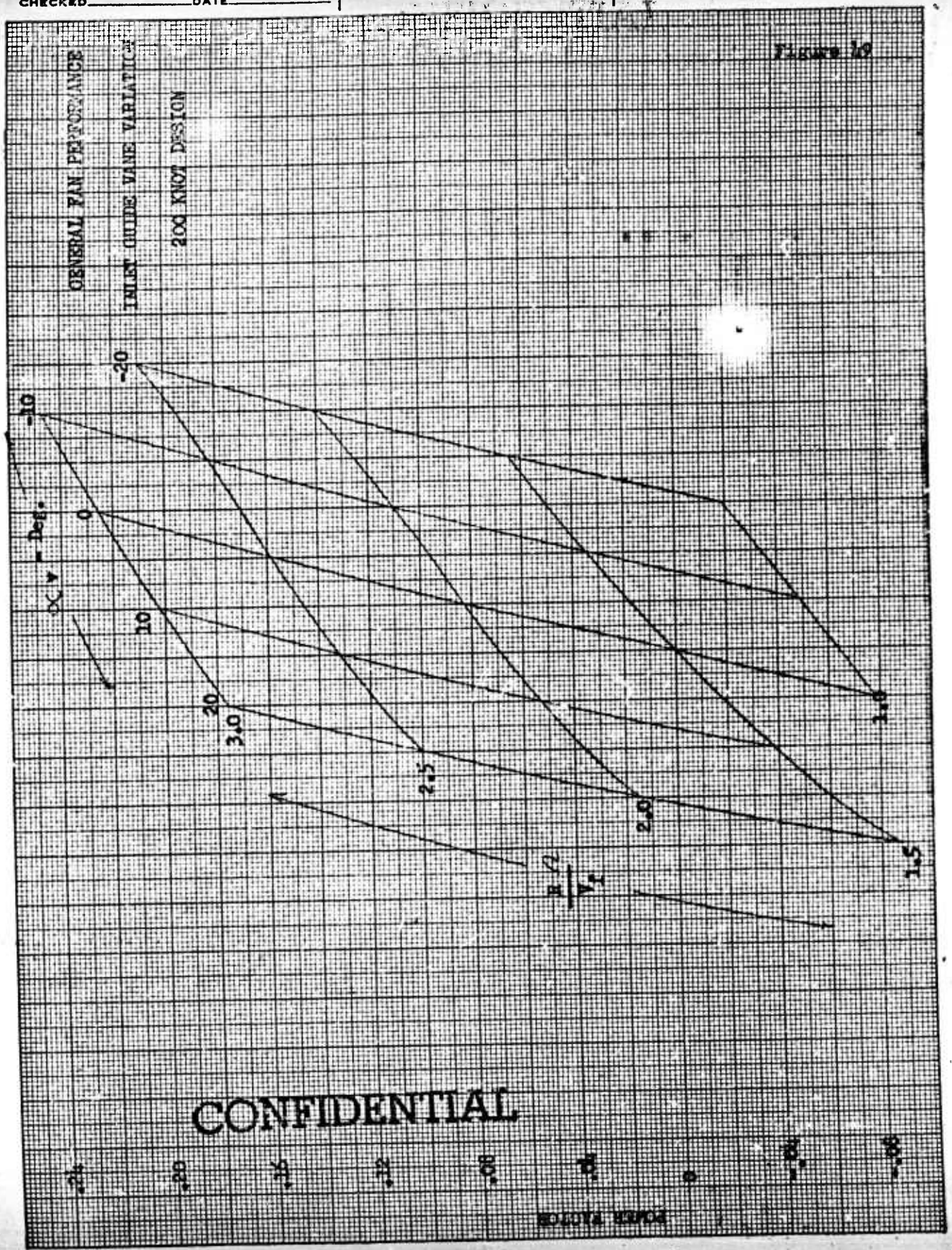
GENERAL FAN PERFORMANCE
INLET GUIDE VANE VARIATION
200 KNOT DESIGN
-20
-10
0
10
20
3.0
2.5
2.0
1.5
1.0
CONFIDENTIAL

CONFIDENTIAL

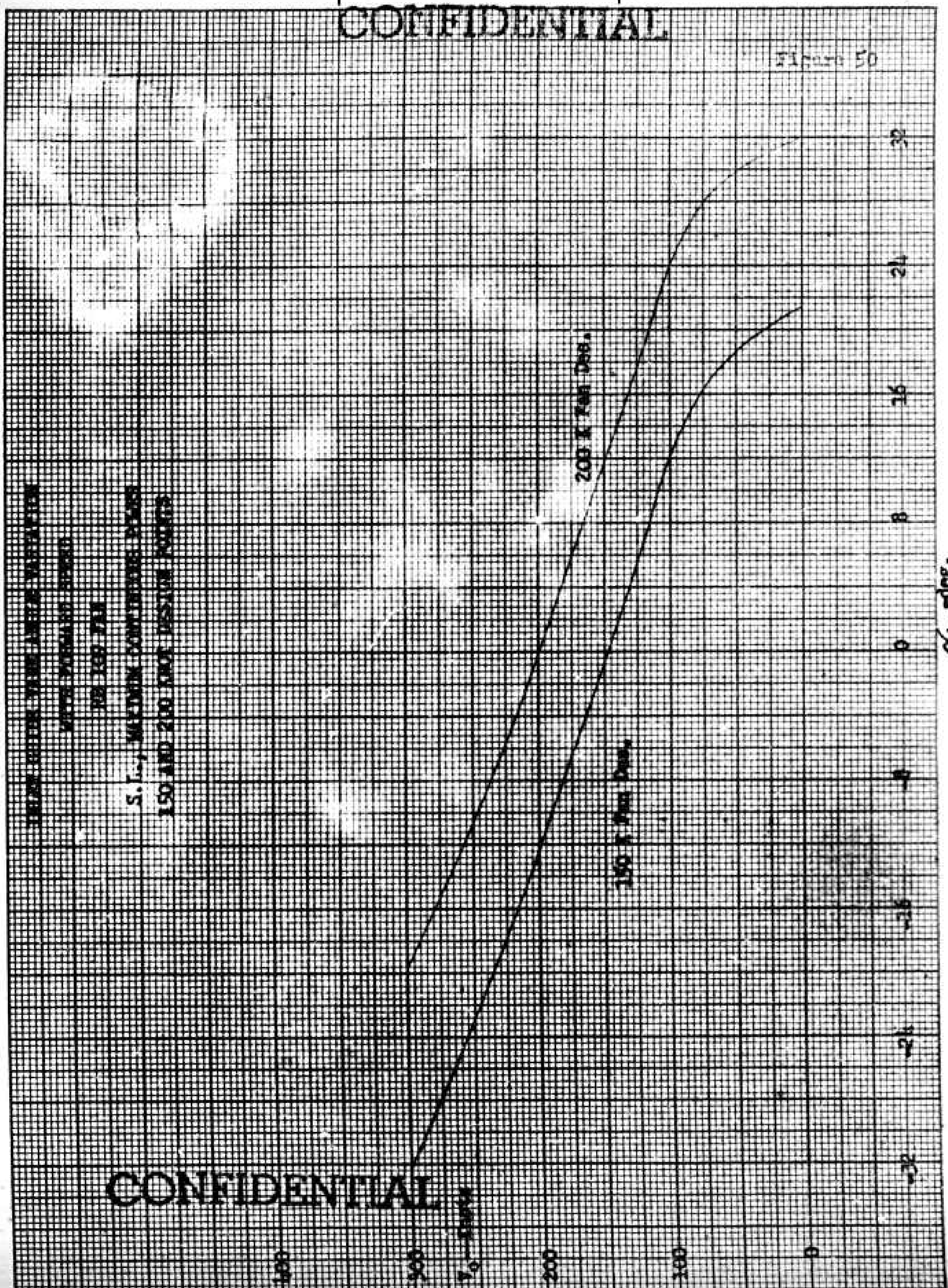

CONFIDENTIAL

TABLE VI

Configuration No. 2

Variable pitch fan, 200 K axial inlet.

Rotor

Chord = 1.093 feet. Modified 65 - Series section.

Radial Station	σ	C_{l_o}	α_d	t/c	ψ
.3	1.0	.56	7.65	.0675	19.35
.4	.75	.48	5.95	.0644	28.15
.5	.60	.408	4.7	.0613	35.7
.6	.50	.35	3.79	.0582	41.81
.7	.429	.31	3.05	.0551	46.95
.8	.375	.277	2.5	.0521	51.2
.9	.333	.244	2.2	.0490	54.6
1.0	.30	.212	1.88	.0460	57.72

Exit Stators

Chord = 1.093 feet. Modified 65 - Series section.

Radial Station	σ	C_{l_o}	α_d	t/c	ψ
.3	1.5	.82	12.1	.06	6.2
.4	1.125	.92	11.0	.06	6.2
.5	.900	.955	9.9	.06	6.2
.6	.750	1.04	9.50	.06	6.2
.7	.642	1.19	9.55	.06	6.2
.8	.562	1.38	9.81	.06	6.2
.9	.500	1.675	10.62	.06	6.2
1.0	.450	2.100	11.99	.06	6.2

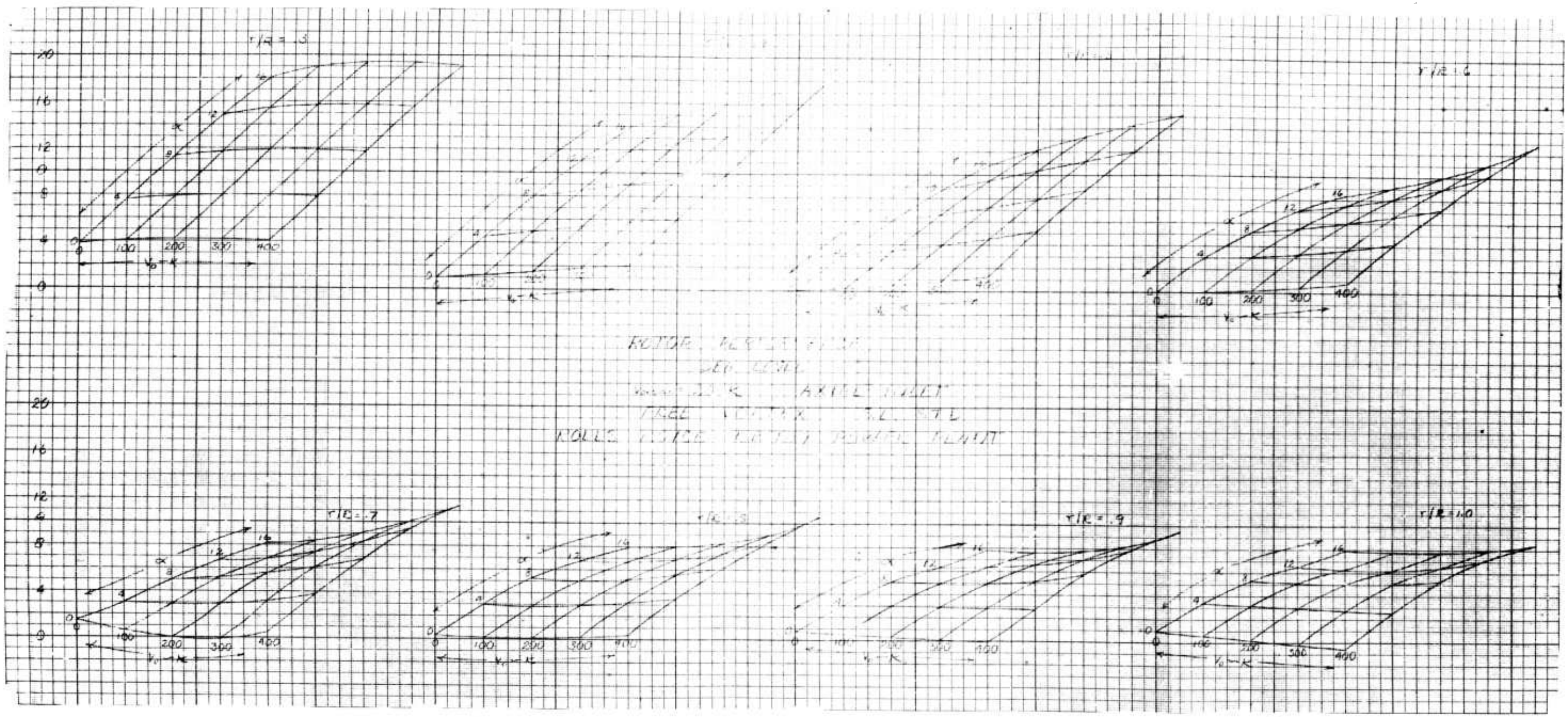

Report No. D181-945-006

Figure 51

Figure 52

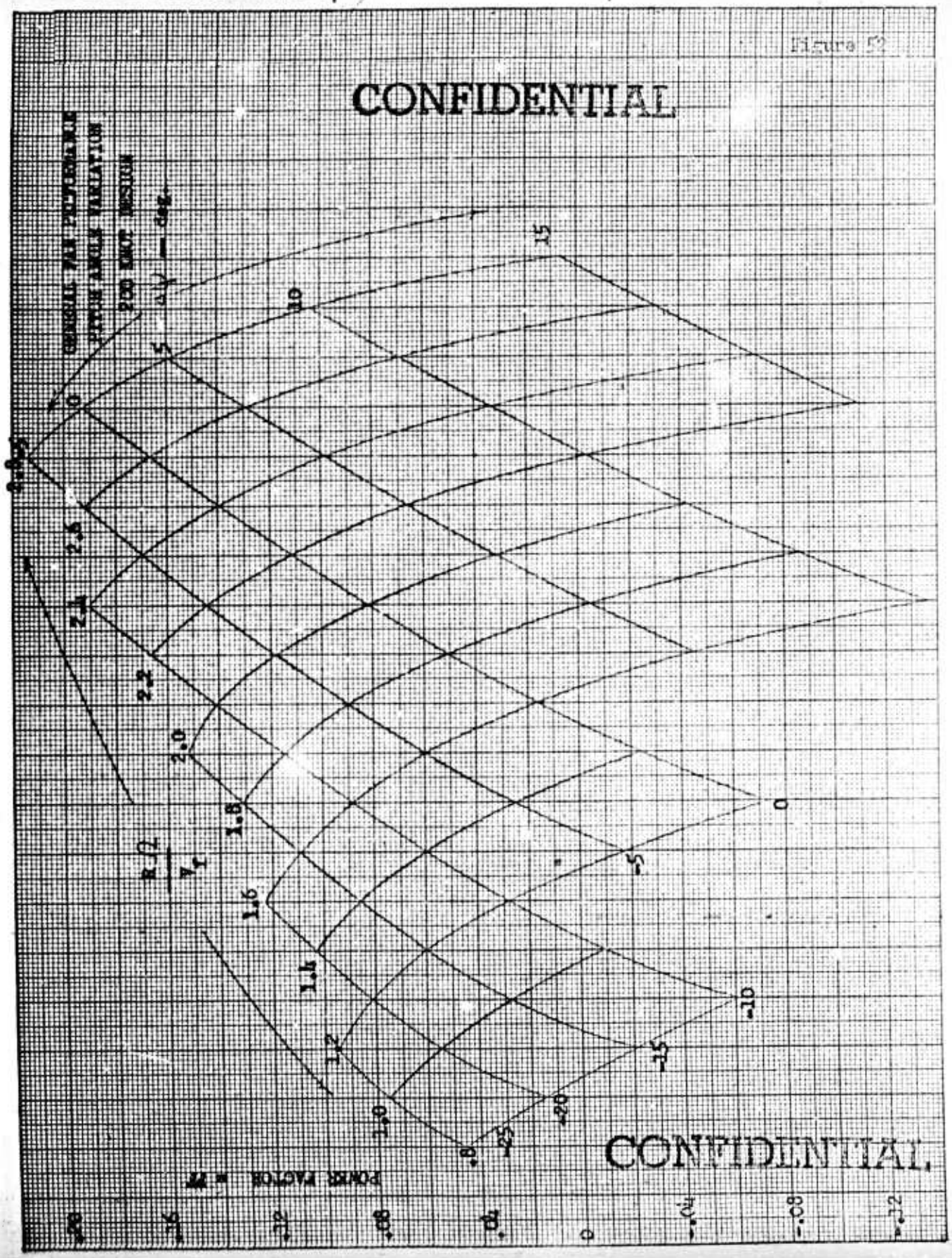

Figure 53

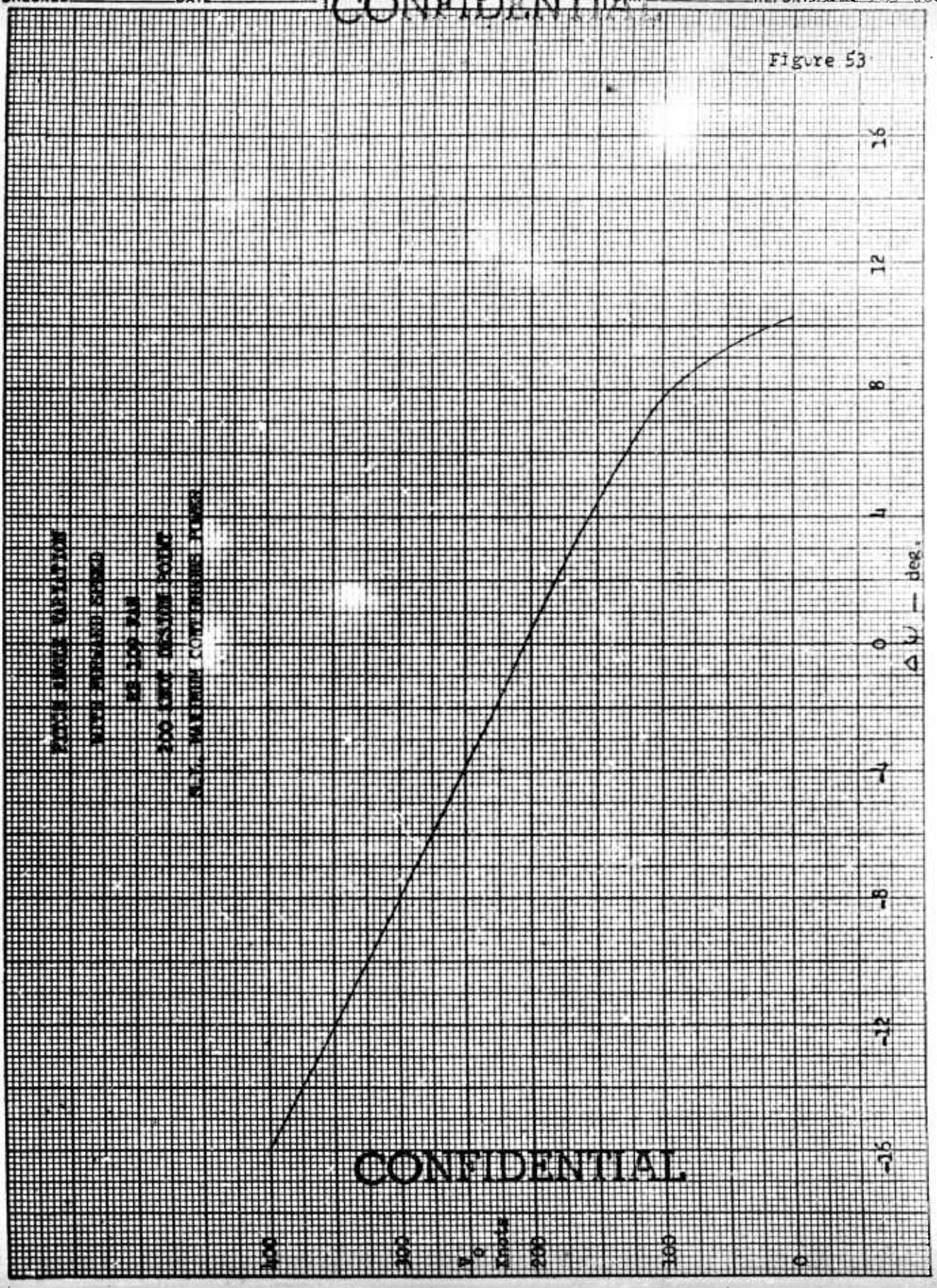

CONFIDENTIAL

PITCH CHANGE REQUIRED AT VARIOUS POWER SETTINGS

Figure 54

d.L. Std. - .9

FAN NO. 2

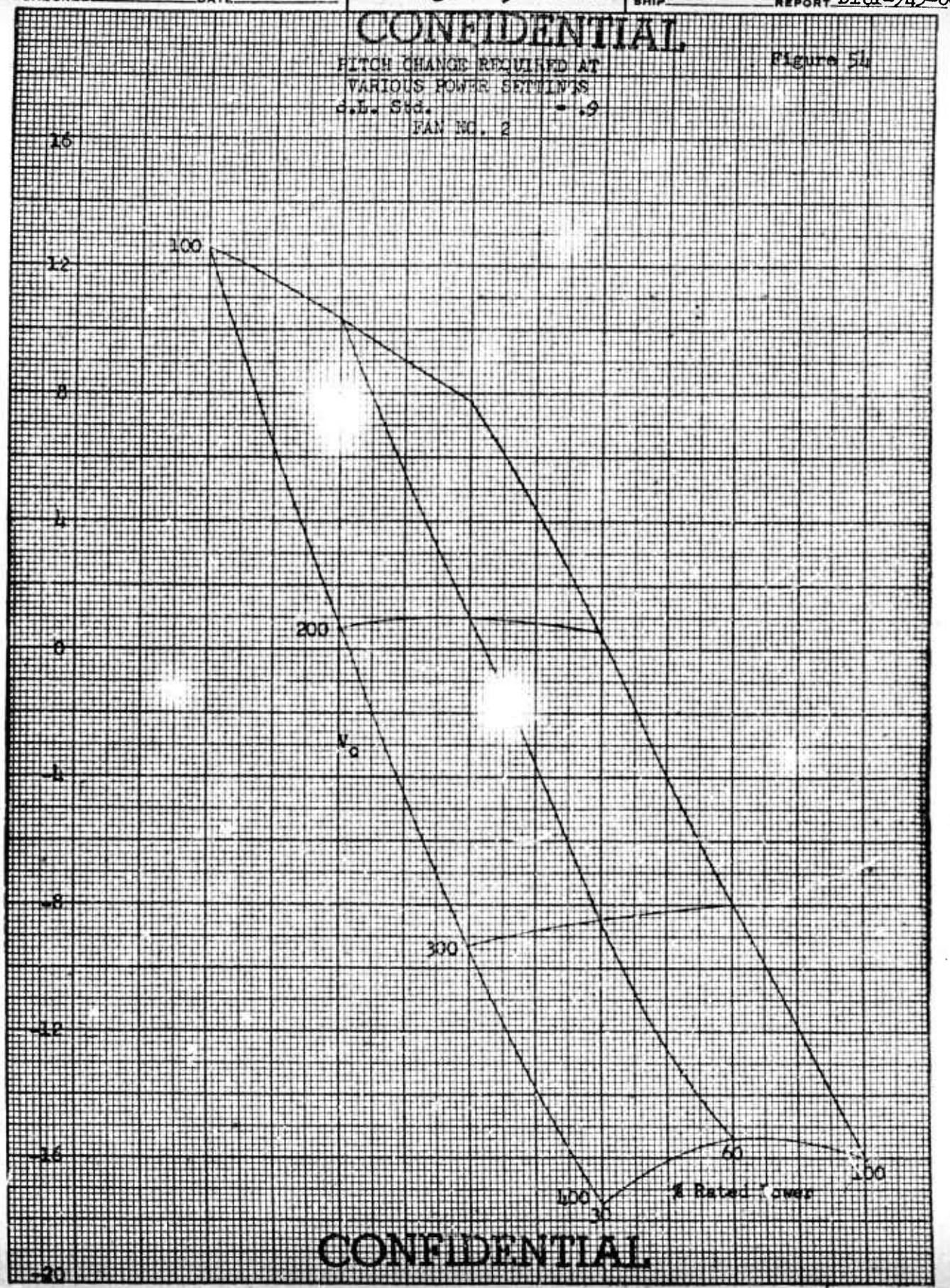

CONFIDENTIAL

and pitch angles required for the three design variations investigated is shown in Table VII.

3. Configuration No. 3

A contra-rotating configuration, designated as Configuration No. 3, was also designed during this study. This configuration uses two Allison 550-B1 powerplants, each rotor absorbing the power from one engine. The design point was at 200 knots at standard sea level conditions, and the fan was designed for a static fan thrust of 22,550 lbs. at 6000 feet and a temperature of 95°F. The diameter of the fan is 11.8 feet, the static inlet diameter is 15 feet, and the hub-tip ratio is .5. Each of the 10-bladed rotors rotates at 996 RPM. The design parameters for this configuration are shown in Table VIII.

The Rotor Performance Charts for the front and rear rotors of this fan are shown in Figures 55 and 56 respectively, and the Power Factor carpets are shown in Figures 57 and 58. The change in pitch angle required for both the front rotor and rear rotor, for various forward flight speeds, are given in Table IX for both sea level and 30,000 feet conditions. Due to a lack of available powerplant information, the pitch changes required at reduced power settings were not calculated. From Table IX it may be seen that the maximum total pitch angle change over the flight spectrum is less than 20° on each fan. Since this is an acceptable variation, it may be concluded that this configuration will perform satisfactorily over the flight regime under consideration.

In the design of the contra-rotating configuration, the rear rotor was designed to remove all of the rotational velocity induced by the front rotor at the design point. In the off-design calculations, it

TABLE VII

COMPARISON OF INLET VANE ANGLE AND PITCH ANGLE VARIATION

	V_o ~ Knots	α_v - Deg.	$\Delta\psi$ - Deg.
200 K Fan Design	0	32° *	10.25
	100	24°	7.75
	200	0	.5
	300	-19.6	-8
	400	----	-16
150 K Fan Design	0	21.5	Not Calculated
	100	12.25	
	200	-12.5	
	300	-32.3 *	
	400	----	

Note: * Beyond usable angle of attack range.

TABLE VIII

Configuration No. 3

Contra-Rotating Fan

Front Rotor

Chord = 1.13 feet. Modified 65 - Series section.

Radial Station	σ	c_{l_o}	α_d	t/c	ψ
.5	.60	.68	6.26	.0620	24.64
.6	.50	.57	4.94	.0598	30.76
.7	.429	.51	4.00	.0574	36.0
.8	.375	.464	3.33	.0546	40.47
.9	.333	.425	2.81	.0518	44.39
1.0	.30	.39	2.45	.0487	47.75

Rear Rotor

Chord = 1.13 feet. Modified 65 - Series section.

Radial Station	σ	c_{l_o}	α_d	t/c	ψ
.5	.60	.59	5.73	.0568	32.07
.6	.50	.50	4.59	.056	36.21
.7	.429	.456	3.70	.0547	40.3
.8	.375	.42	3.19	.0529	43.81
.9	.333	.39	2.72	.0508	46.98
1.0	.30	.365	2.40	.0483	49.8

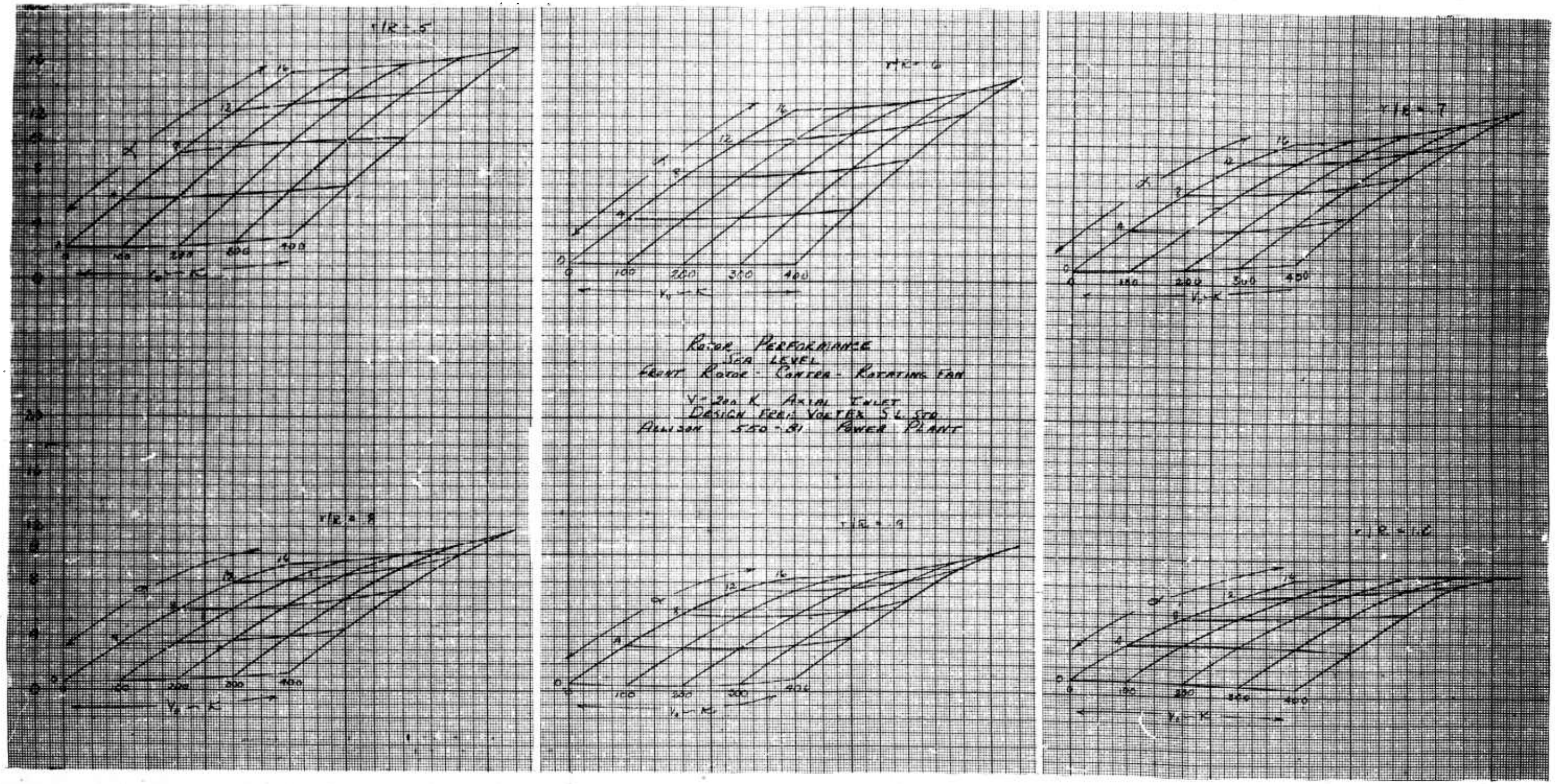

Report No. D181-945-006

Figure 55

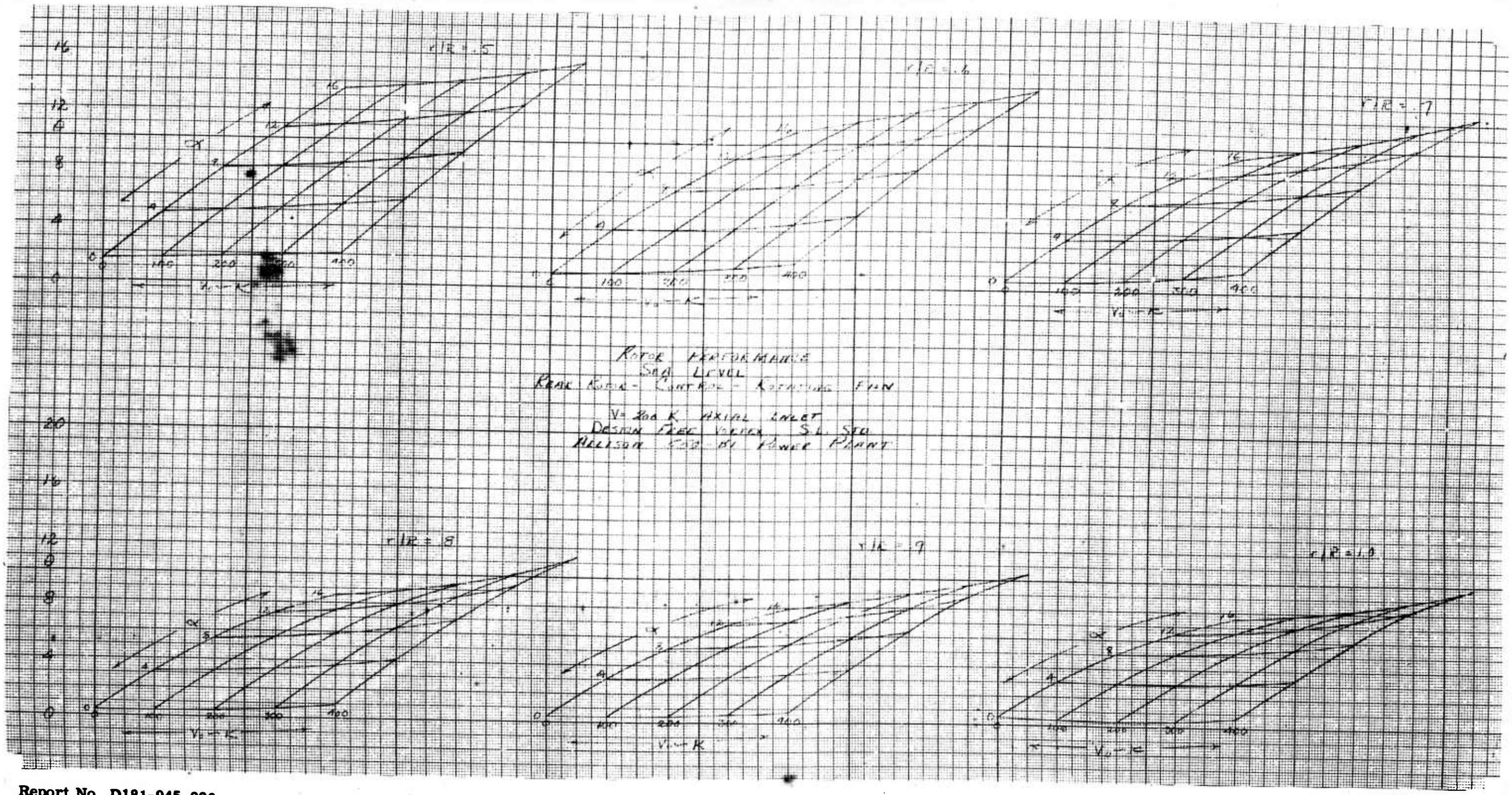

Report No. D181-945-006

Figure 56

Figure 57

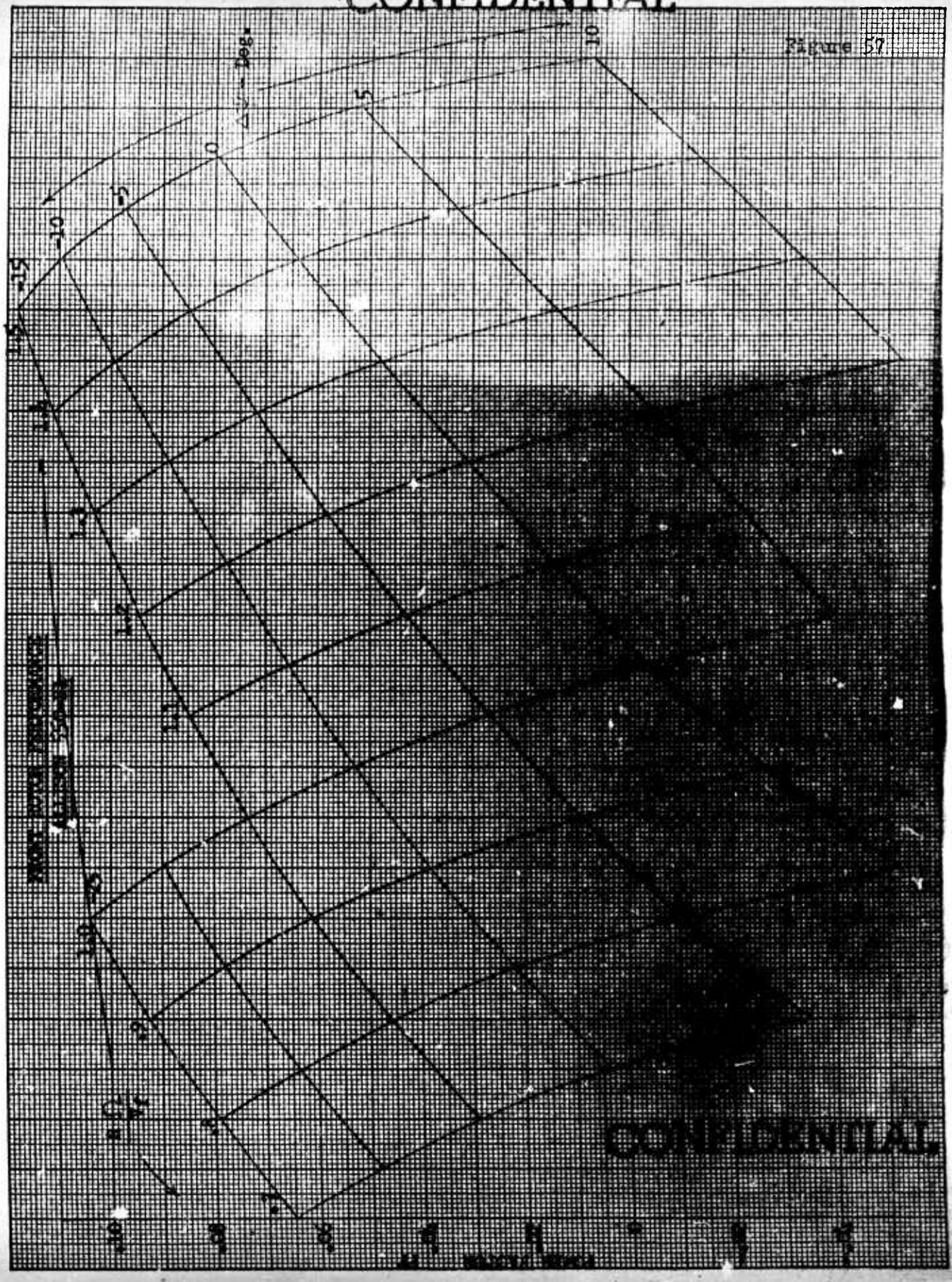

CONFIDENTIAL

Figure 58

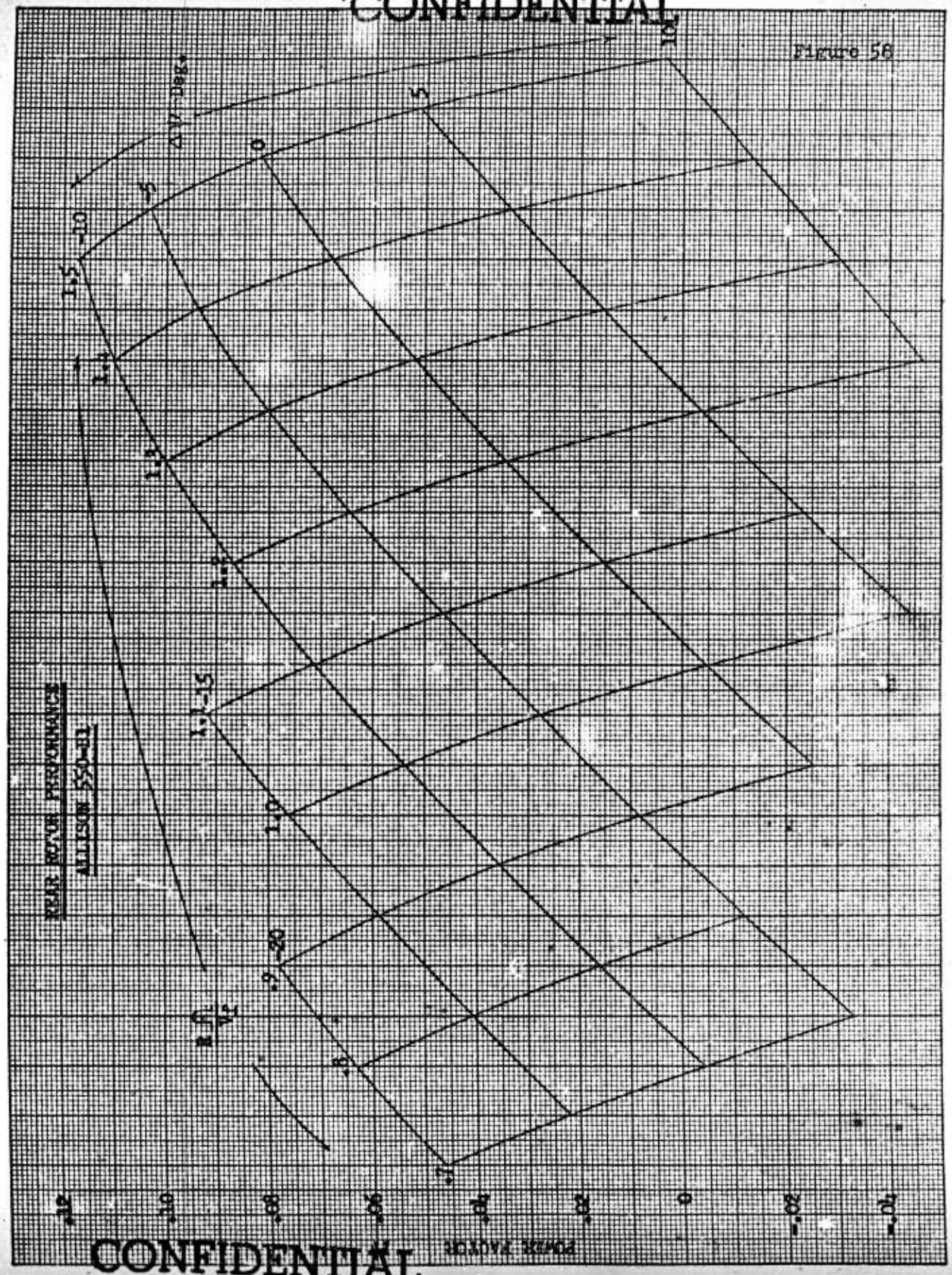

TABLE IX

ROTOR PITCH ANGLES, FAN NO. 3

V_o ~ Knots	$\Delta\psi$ ~ Deg. S.L.	$\Delta\psi$ ~ Deg. (30,000')
Front Rotor		
0	4.75	--
100	3.3	- 3.3
200	- .3	- 5.9
300	- 5.25	-10.8
400	-10.25	--
Rear Rotor		
0	5.3	--
100	3.5	- 1.6
200	- .38	- 5.2
300	- 6.0	-11.2
400	-11.75	--

TABLE X

V_o ~ Knots	S.L. Residual Whirl % HP	% Rated Thrust	(30,000 ft) Residual Whirl % HP
0	1.098		--
100	2.1		1.13
200	4.47		.87
300	1.285		2.7
400	7.043	.45	--

was noted that the rear rotor did not remove this rotational velocity completely at other than design conditions, thus leaving a quantity which was called residual whirl. The amount of residual whirl was determined for sea level and 30,000 feet conditions and is listed in Table X as a percentage of the total available horsepower and as a percentage of the rated thrust at the point where the whirl was greatest.

4. Configuration No. 4

Toward the end of this contract period, it was decided to investigate the use of highly cambered inlet guide vanes to impart a high pre-whirl to the flow entering the rotor. High pre-whirl makes it possible to operate a fixed-pitch rotor over a wide range of velocity and power settings with only small changes in the inlet guide vane angle. Obviously, the use of high pre-whirl would permit the design of an inlet guide vane configuration which would have a much greater operating range than the symmetrical-vane configurations. However, all the high pre-whirl designs which were attempted were unsuccessful. This was primarily due to the fact that the large guide vane turning angles resulted in supersonic relative velocities on the rotor blades. While this condition might not actually be prohibitive, a lack of sufficient time prevented further investigation.

As the last design investigated under this study contract, symmetrical inlet guide vanes were used in conjunction with the duct designed for the high pre-whirl fans. This design had an inlet diameter of 11.1 ft., a fan diameter of 8.4 ft., and a hub-tip ratio of .5. The design point was chosen to be 250 knots at sea level, and the powerplant used was the Allison 550-B1. The fan was designed for a static fan thrust

of 11,275 lbs. at 6000 feet on a 95° day, and has 12 rotor blades and 13 inlet guide vanes. The rotor operates at 1542 RPM. Although exit stators are a necessity with this type of configuration, a lack of sufficient time precluded their design in this instance. The design data for this configuration is given in Table XI. The Power Factor is plotted in Figure 59. The guide vane angles required for full power absorption range from 12.85° at static conditions to -12.9° at 400 knots, all at sea level. No reduced power vane angle settings were obtained for this fan.

TABLE XI

Configuration No. 4

Inlet Guide Vanes

Chord = 1.014 feet, Thickness = 6%. Modified 63-006 section.

Linear Variation in Solidity, σ = 1.0 at root, .5 at tip.

Rotor

Chord = 1.1 feet. Modified 65 - Series section.

Radial Station	σ	C_{l_o}	α_d	t/c	ψ
.5	1.00	.63	8.16	.0736	22.5
.6	.833	.580	7.00	.0691	28.42
.7	.714	.525	6.00	.0646	33.69
.8	.625	.470	5.20	.0601	38.28
.9	.556	.408	4.40	.0556	42.45
1.0	.500	.330	3.70	.0511	46.15

Exit Stators

Not Designed.

CONFIDENTIAL

Figure 59

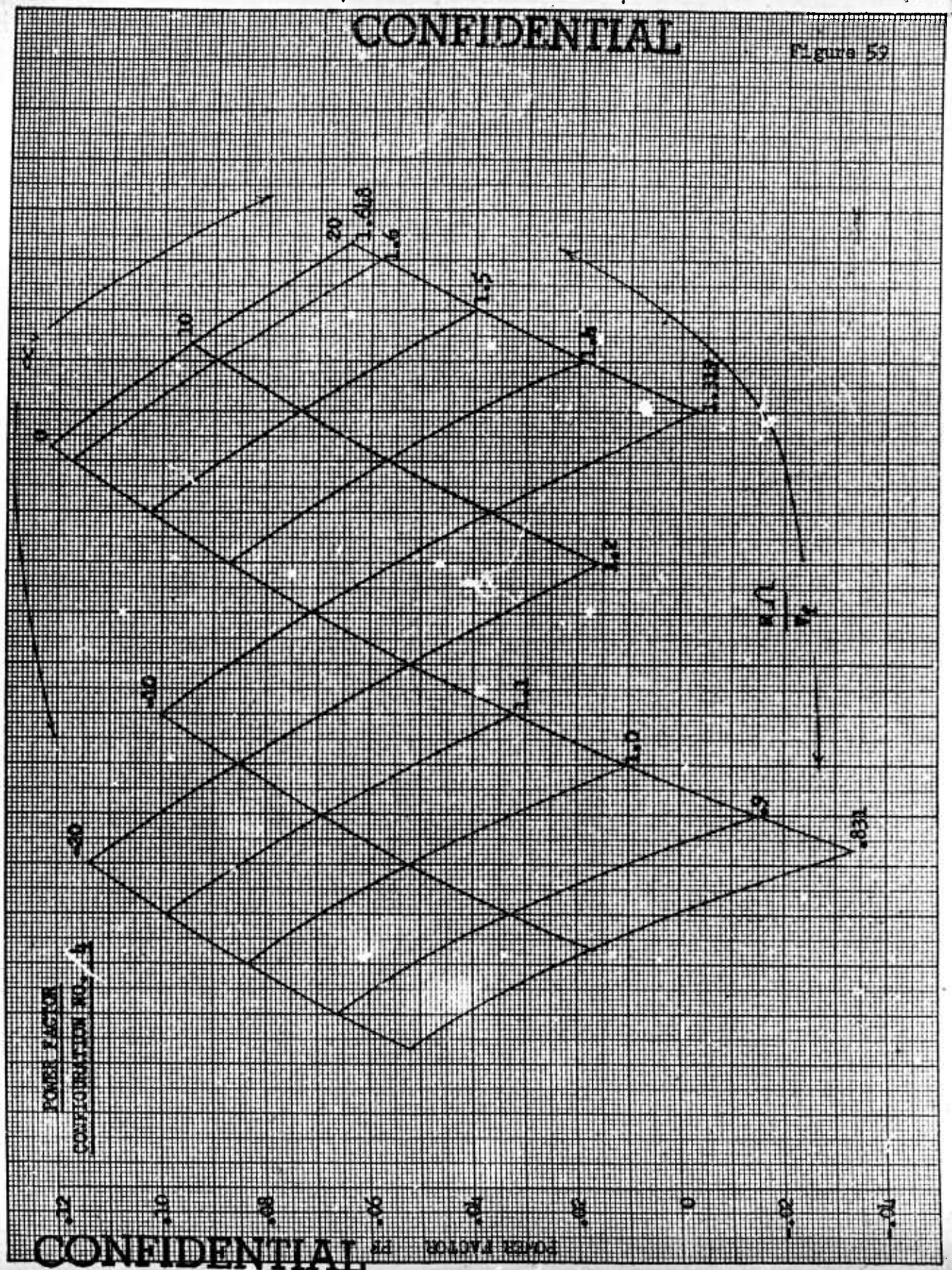

F. Comparison of Ducted Propeller Designs

Basically, three different types of ducted propeller systems have been considered during this study program. They consist of configurations which use inlet guide vanes to turn the entering flow, those which employ variable pitch, and contra-rotating configurations. Two variations in the inlet guide vane designs were studied, those using symmetrical vanes set at zero angle of attack at the design point and those using highly cambered vanes to impart a high pre-whirl to the flow under all conditions.

Probably the most satisfactory configuration obtained was the contra-rotating fan, Configuration No. 3. This particular fan required relatively small pitch changes over the entire flight regime, and would operate satisfactorily over a range of forward speeds form zero to a speed in excess of 400 knots. In addition, the large hub provides ample room for installation of the required variable pitch mechanism. This configuration would be suitable for the Assault Transport application, providing not only the static thrust required but a high speed capability as well. The large hub-tip ratio also permits installation of two Allison power plants in the hub. This is an ideal situation, since it eliminates some of the gearing problems inherent in other type installations and also permits utilization of the engine residual thrust as an additional lifting force when the ducts are rotated for vertical take-off.

The variable pitch configurations and those using inlet guide vanes could also be successfully applied to the Vertical Take-Off Assault Transport. The variable pitch fans have an advantage over those employing symmetrical inlet guide vanes in that they require a smaller pitch change

and thus have a higher speed potential. As a result of these studies, however, it is felt that the potentialities of the inlet guide vane concept have not been fully exploited, especially with regard to the application of high pre-whirl vanes. A lack of time prevented any concerted effort to overcome the difficulties which were encountered. The application of a smaller amount of pre-whirl should be investigated. The extension of the present design methods into the area of higher relative Mach number on the blades would also improve this approach, since axial-flow fans and compressors having this type blading have been successfully designed by the NACA (Ref. 19). In any event, a further investigation of this concept is highly desirable.

G. Wind Tunnel Test Program

In August, 1955, negotiations were begun with the University of Wichita with a view toward obtaining experimental data to complement the theoretical studies covered by this report. Subsequently, it was agreed that a wind tunnel program, under sponsorship of the Office of Naval Research, should be undertaken. Two models to be tested during the program have been designed by Bell Aircraft Corporation, and Bell personnel will be present to observe the tests.

The models to be tested are 1/10 scale models of two of the configurations presented in this report. Model No. 1 is the 1/10 scale version of Configuration No. 1, with the exception that the number of inlet guide vanes has been reduced from 21 to 18. A sketch of this model is shown in Figure 60. Model No. 2 is the scaled-down replica of Configuration No. 2, and is shown in Figure 61. Since the inlet and fan diameters of these configurations are the same, it will be possible to use the same shroud for both models. This shroud has an interchangeable inlet section, so that both the static and high speed configurations may be tested. The inlet arrangements to be tested are shown in Figure 62. Figure 62a shows the high speed shroud, while the bell-mouth inlet is shown in Figure 62b. Figure 62c shows the static practical flap, which is a split flap arrangement as can be seen from Figure 62d. A split Bell-Mouth flap will also be tested. The specifications for the practical flap are shown in Figure 63.

CONFIDENTIAL

Figure 60

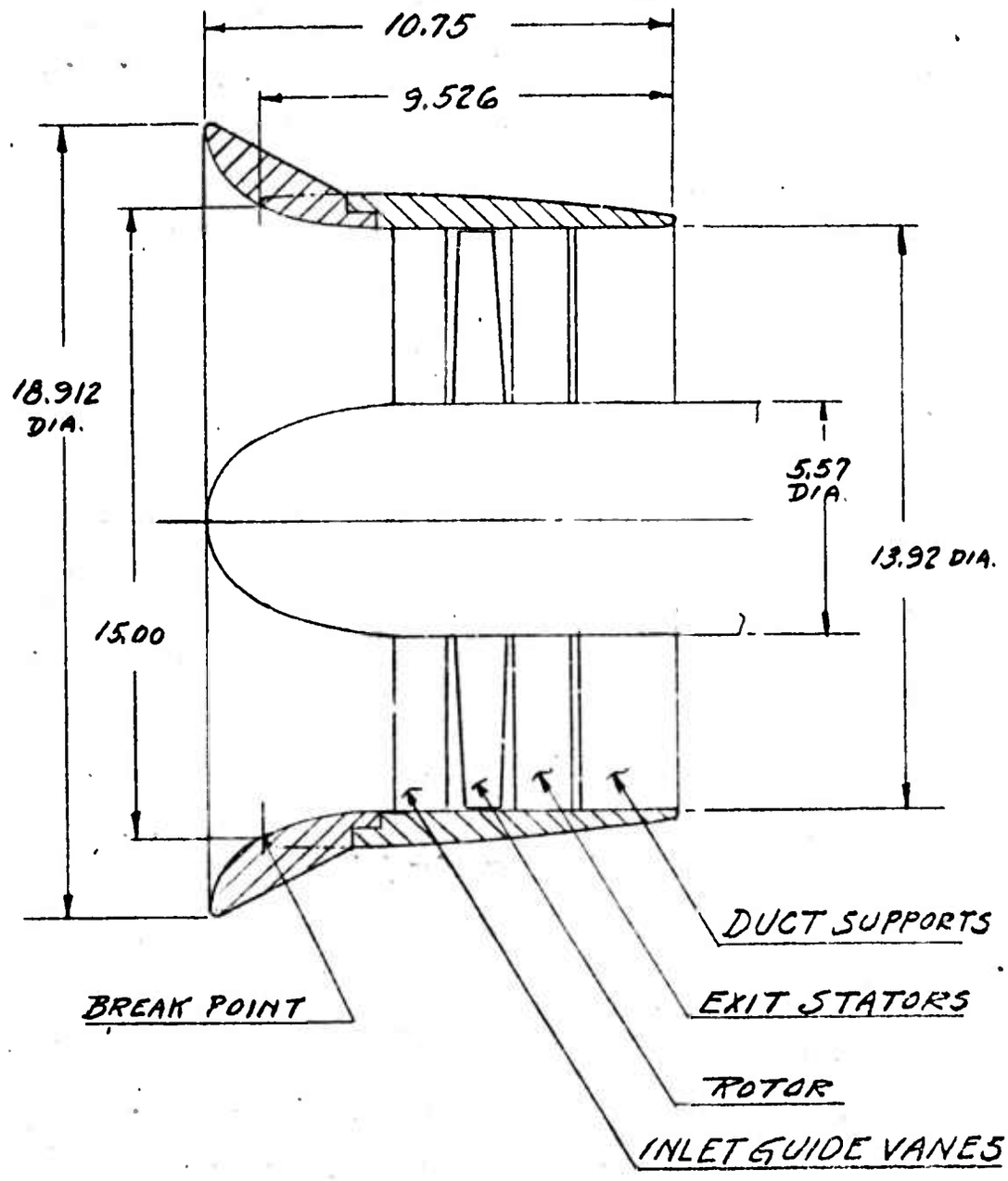

WIND TUNNEL MODEL NO. 1

Form E4-1 Rev. 353

CONFIDENTIAL

Figure 61

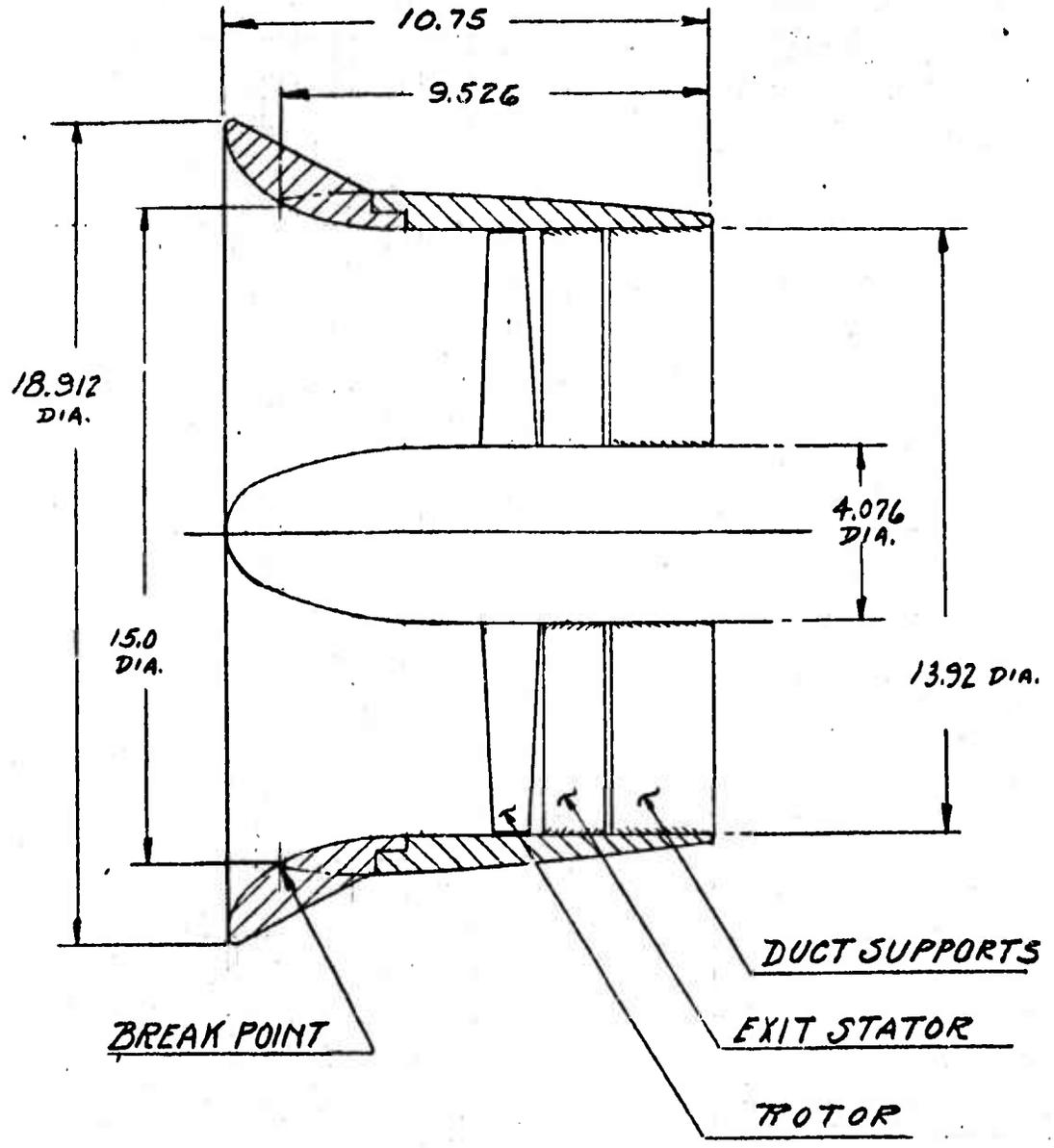

WIND TUNNEL MODEL NO. 2

Form Ed-1 Rev. 353

CONFIDENTIAL

Figure 62

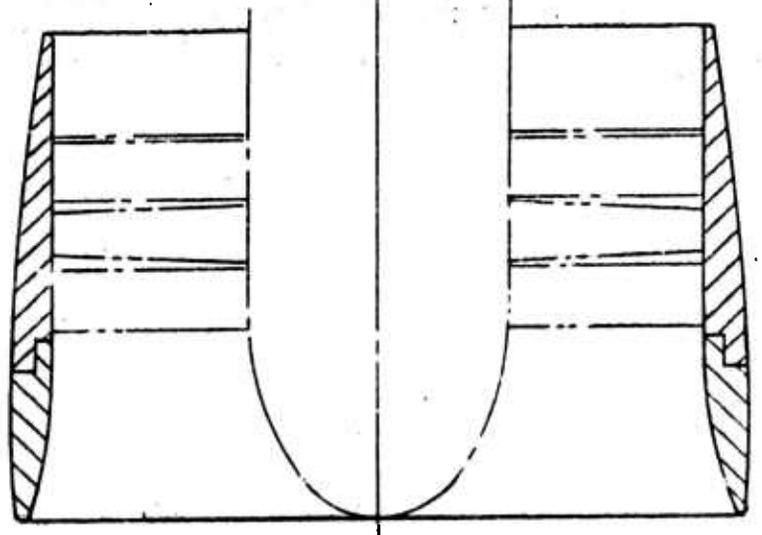

a. High Speed Shroud

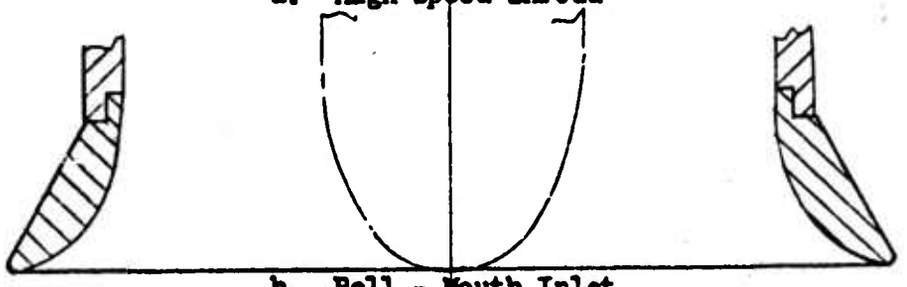

b. Bell - Mouth Inlet

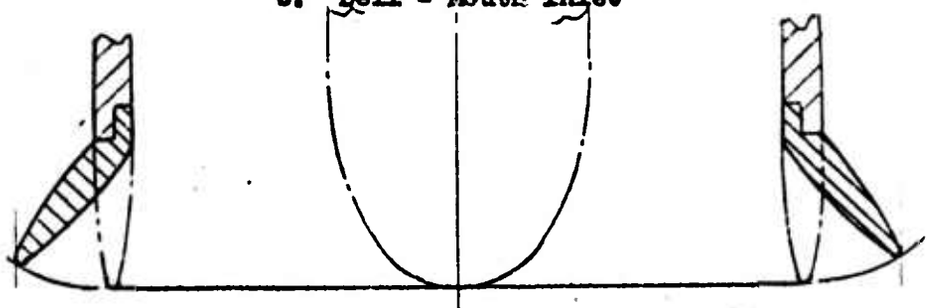

c. Practical Flap

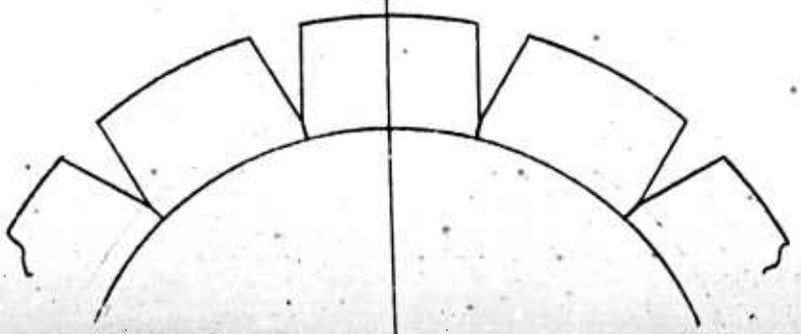

d. Split Static Flap

CONFIDENTIAL

D181-945-006

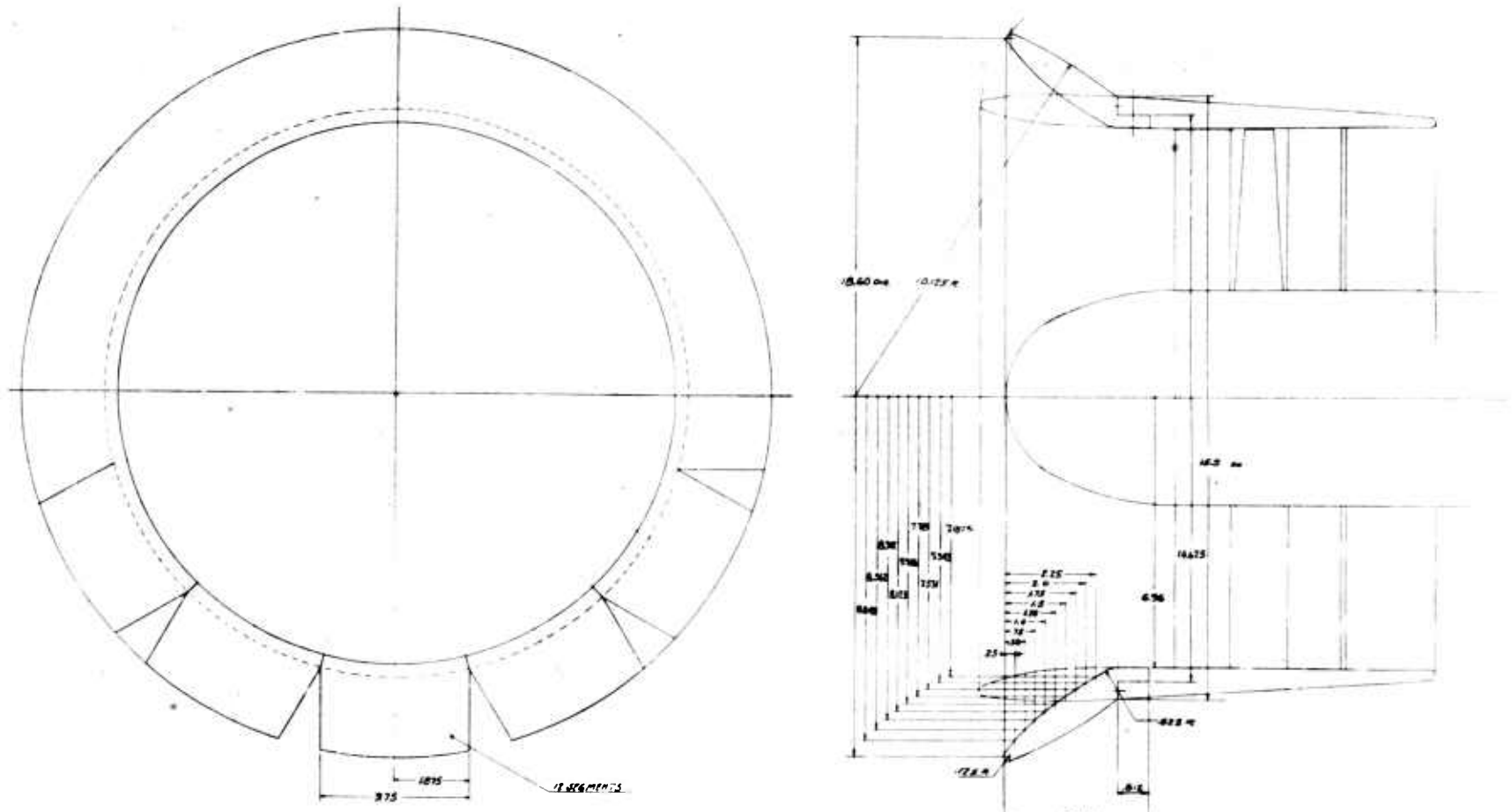

Figure 63. Dwg. No. D181-960-008: Modified Static Duct Inlet, 0.1-Scale Tunnel Test Model

The fabrication of the first model has been completed. Model specifications were determined by Bell Aircraft Corporation and blade templates were also furnished by that facility. Actual fabrication of the model was done under the supervision of the University of Wichita. Blade specifications for the first model are shown in Tables XII, XIII and XIV. Load distributions on the inlet guide vanes, rotor and exit stators are shown in Figures 64, 65 and 66 respectively. The model rotor is shown being balanced in Figure 67, and is shown mounted on the motor and shaft assembly in Figure 68. The practical flap and split Bell-Mouth inlets are shown in Figure 69. Figures 70 and 71 show the high speed configuration and the Bell-Mouth configuration, respectively, mounted in the tunnel.

At the present time, work is progressing on the fabrication of the second model. Templates have been completed and have been sent to the University. Specifications for the rotor and exit stators are shown in Tables XV and XVI.

Actual tests on the first model were begun on April 23, 1956. Both force and pressure tests will be conducted during this program over a range of yaw angles from 0 to 90°, and at tunnel speeds from zero to the maximum attainable. The testing program, as originally outlined, is shown in Table XVII. Since that time, however, the program has been modified so that the tests may be run at a series of basic vane settings as the

yaw angles, speeds and RPM are varied over a given range. This modified program is shown in Table XVIII. As yet, no data from the preliminary runs are available. The final results of these tests will be published by the University of Wichita in a future report.

TABLE XII

Inlet Guide Vane Ordinates

Section: 63-006 With Thickened Trailing Edge

(Zero Camber, 6% Thick)

x/c % Chord	x in.	Y Ordinates All Stations in.
0	0	0
1.25	.0170	.0105
2.5	.0340	.0144
5.0	.0680	.0199
10	.1360	.0273
15	.2040	.0324
20	.2720	.0361
25	.3400	.0386
30	.4080	.0402
35	.4760	.0408
40	.5440	.0404
45	.6120	.0391
50	.6800	.0370
55	.7480	.0342
60	.8160	.0313
65	.8840	.0284
70	.9520	.0254
75	1.0200	.0225
80	1.0880	.0196
85	1.1560	.0166
90	1.2240	.0137
95	1.2920	.0108
100	1.3600	0
Leading Edge Radius:		.0040
Trailing Edge Radius:		.0082

Chord = 1.36 in.

No. of Blades = 18

Sta.	σ
.4	1.400
.5	1.120
.6	.932
.7	.800
.8	.700
.9	.622
1.0	.560

Y = Distance above and below Mean Camber Line

All dimensions are in inches.

TABLE XIII

Model No. 1 - Rotor

Mean Camber Line Ordinates

		r/R →	.4	.5	.6	.7	.8	.9	1.0
x/c	x	$R_{in.}$ →	2.784	3.480	4.176	4.872	5.568	6.264	6.960
% Chord	in.	C_{l_o} →	.890	.650	.575	.505	.435	.360	.290
0	0		0	0	0	0	0	0	0
.5	.0064		.0029	.0021	.0018	.0016	.0014	.0012	.0009
.75	.0096		.0040	.0029	.0026	.0023	.0020	.0016	.0013
1.25	.0161		.0061	.0045	.0040	.0035	.0030	.0025	.0020
2.50	.0321		.0106	.0078	.0069	.0060	.0052	.0043	.0035
5	.0642		.0181	.0132	.0117	.0103	.0088	.0073	.0059
7.5	.0964		.0242	.0177	.0157	.0138	.0118	.0098	.0079
10	.1285		.0296	.0216	.0191	.0168	.0144	.0120	.0096
15	.1927		.0385	.0281	.0249	.0218	.0188	.0156	.0125
20	.2569		.0455	.0332	.0294	.0258	.0222	.0184	.0148
25	.3212		.0512	.0374	.0331	.0290	.0250	.0207	.0167
30	.3854		.0556	.0406	.0359	.0315	.0272	.0225	.0181
35	.4496		.0589	.0430	.0380	.0334	.0288	.0238	.0192
40	.5139		.0612	.0447	.0396	.0347	.0299	.0248	.0200
45	.5781		.0626	.0457	.0404	.0355	.0306	.0253	.0204
50	.6424		.0631	.0461	.0407	.0358	.0308	.0255	.0205
55	.7066		.0626	.0457	.0404	.0355	.0306	.0253	.0204
60	.7708		.0612	.0447	.0396	.0347	.0299	.0248	.0200
65	.8351		.0589	.0430	.0380	.0334	.0288	.0238	.0192
70	.8993		.0556	.0406	.0359	.0315	.0272	.0225	.0181
75	.9635		.0512	.0374	.0331	.0290	.0250	.0207	.0167
80	1.0278		.0455	.0332	.0294	.0258	.0222	.0184	.0148
85	1.0920		.0385	.0281	.0249	.0218	.0188	.0156	.0125
90	1.1562		.0296	.0216	.0191	.0168	.0144	.0120	.0096
95	1.2205		.0181	.0132	.0117	.0103	.0088	.0073	.0059
100	1.2847		0	0	0	0	0	0	0
Angle of Base Line with Duct ℄ :			21.8°	31.1°	37.6°	42.9°	47.6°	51.6°	55.1°
Solidity:			1.25	1.00	.833	.714	.625	.555	.500

No. of Blades = 17

Chord = 1.2847 in.

All dimensions are in inches.

Report No. D181-945-006

TABLE XIII (Cont'd)

Model No. 1 - Rotor

Section Ordinates Above & Below (⊥) Mean Camber Line

		r/R →	.4	.5	.6	.7	.8	.9	1.0
x/c	x	$R_{in.}$ →	2.784	3.480	4.176	4.872	5.568	6.264	6.960
% Chord	in.	t/c →	.091	.086	.081	.076	.071	.066	.061
0	0		0	0	0	0	0	0	0
.5	.0064		.0091	.0086	.0082	.0077	.0071	.0067	.0062
.75	.0096		.0110	.0104	.0098	.0092	.0086	.0081	.0075
1.25	.0161		.0137	.0130	.0123	.0115	.0108	.0101	.0094
2.5	.0321		.0185	.0174	.0165	.0155	.0144	.0135	.0125
5.0	.0642		.0255	.0241	.0227	.0213	.0199	.0185	.0171
7.5	.0964		.0310	.0293	.0276	.0258	.0241	.0225	.0208
10	.1285		.0355	.0336	.0316	.0297	.0277	.0258	.0238
15	.1927		.0429	.0405	.0381	.0358	.0334	.0310	.0287
20	.2569		.0484	.0458	.0431	.0404	.0378	.0351	.0324
25	.3212		.0526	.0497	.0468	.0439	.0410	.0381	.0352
30	.3854		.0556	.0526	.0495	.0464	.0434	.0403	.0373
35	.4496		.0576	.0544	.0512	.0481	.0449	.0417	.0386
40	.5139		.0584	.0552	.0520	.0488	.0456	.0424	.0392
45	.5781		.0581	.0549	.0517	.0485	.0453	.0422	.0390
50	.6424		.0563	.0532	.0502	.0471	.0440	.0410	.0379
55	.7066		.0531	.0502	.0473	.0444	.0415	.0387	.0358
60	.7708		.0486	.0459	.0434	.0407	.0380	.0356	.0329
65	.8351		.0443	.0420	.0396	.0373	.0348	.0325	.0301
70	.8993		.0397	.0376	.0356	.0334	.0312	.0292	.0271
75	.9635		.0351	.0332	.0315	.0295	.0276	.0259	.0240
80	1.0278		.0305	.0289	.0274	.0257	.0240	.0227	.0210
85	1.0920		.0256	.0242	.0229	.0215	.0201	.0190	.0176
90	1.1562		.0210	.0199	.0188	.0177	.0166	.0157	.0146
95	1.2205		.0160	.0151	.0147	.0138	.0129	.0124	.0111
100	1.2847		0	0	0	0	0	0	0
Leading Edge Radius:			.0072	.0068	.0056	.0053	.0049	.0034	.0031
Trailing Edge Radius:			.0117	.0110	.0104	.0098	.0091	.0085	.0078

All dimensions are in inches.

NOTE: Section ordinates are measured perpendicular to Mean Camber Line.

TABLE XIV

Model No. 1 - Exit Stators

Mean Camber Line Ordinates

		r/R →	.4	.5	.6	.7	.8	.9	1.0
x/c	x	$R_{in.}$ →	2.784	3.480	4.176	4.872	5.568	6.264	6.960
% Chord	in.	C_{1_o} →	1.50	1.60	1.64	1.75	1.95	2.13	2.35
0	0		0	0	0	0	0	0	0
.5	.0069		.0052	.0055	.0057	.0060	.0067	.0073	.0081
.75	.0104		.0072	.0077	.0079	.0085	.0094	.0103	.0114
1.25	.0173		.0111	.0118	.0121	.0129	.0144	.0157	.0174
2.50	.0345		.0193	.0205	.0210	.0225	.0250	.0273	.0302
5	.0690		.0327	.0349	.0358	.0382	.0425	.0464	.0512
7.5	.1035		.0439	.0468	.0480	.0512	.0570	.0623	.0688
10	.1380		.0535	.0571	.0585	.0624	.0696	.0760	.0838
15	.2070		.0697	.0743	.0762	.0813	.0906	.0989	.1091
20	.2760		.0824	.0879	.0901	.0961	.1071	.1170	.1291
25	.3450		.0926	.0988	.1013	.1081	.1204	.1315	.1451
30	.4140		.1006	.1073	.1100	.1174	.1308	.1429	.1576
35	.4830		.1066	.1137	.1166	.1244	.1386	.1514	.1670
40	.5520		.1108	.1182	.1212	.1293	.1441	.1574	.1737
45	.6210		.1133	.1209	.1239	.1322	.1473	.1609	.1776
50	.6900		.1142	.1218	.1248	.1332	.1484	.1621	.1789
55	.7590		.1133	.1209	.1239	.1322	.1473	.1609	.1776
60	.8280		.1108	.1182	.1212	.1293	.1441	.1574	.1737
65	.8970		.1066	.1137	.1166	.1244	.1386	.1514	.1670
70	.9660		.1006	.1073	.1100	.1174	.1308	.1429	.1576
75	1.0350		.0926	.0988	.1013	.1081	.1204	.1315	.1451
80	1.1040		.0824	.0879	.0901	.0961	.1071	.1170	.1291
85	1.1730		.0697	.0743	.0762	.0813	.0906	.0989	.1091
90	1.2420		.0535	.0571	.0585	.0624	.0696	.0760	.0838
95	1.3110		.0327	.0349	.0358	.0382	.0425	.0464	.0512
100	1.3800		0	0	0	0	0	0	0
Angle of Base Line with Duct ℄ :			13.6	12.6	11.7	10.7	9.7	8.8	7.8
Solidity:			1.50	1.20	1.00	.856	.750	.666	.600

No. of Blades = 19

Chord = 1.38 in.

All dimensions are in inches.

TABLE XIV (Cont'd)

Model No. 1 - Exit Stators

Section Ordinates Above and Below (⊥) Mean Camber Line

x/c	x	All Stations
% Chord	in.	t/c ⟶ .06
0	0	0
.5	.0069	.0066
.75	.0104	.0079
1.25	.0173	.0099
2.50	.0345	.0132
5	.0690	.0181
7.5	.1035	.0219
10	.1380	.0252
15	.2070	.0303
20	.2760	.0343
25	.3450	.0372
30	.4140	.0394
35	.4830	.0407
40	.5520	.0414
45	.6210	.0412
50	.6900	.0400
55	.7590	.0378
60	.8280	.0347
65	.8970	.0318
70	.9660	.0286
75	1.0350	.0254
80	1.1040	.0222
85	1.1730	.0186
90	1.2420	.0153
95	1.3110	.0120
100	1.3800	0
Leading Edge Radius:		.0033
Trailing Edge Radius:		.0083

All dimensions are in inches.

NOTE: Section ordinates are measured perpendicular to Mean Camber Line.

CONFIDENTIAL

INLET GUIDE VANES
BLADE LOADING
MODEL NUMBER 1

Figure 64

11,180 RPM 60 HP

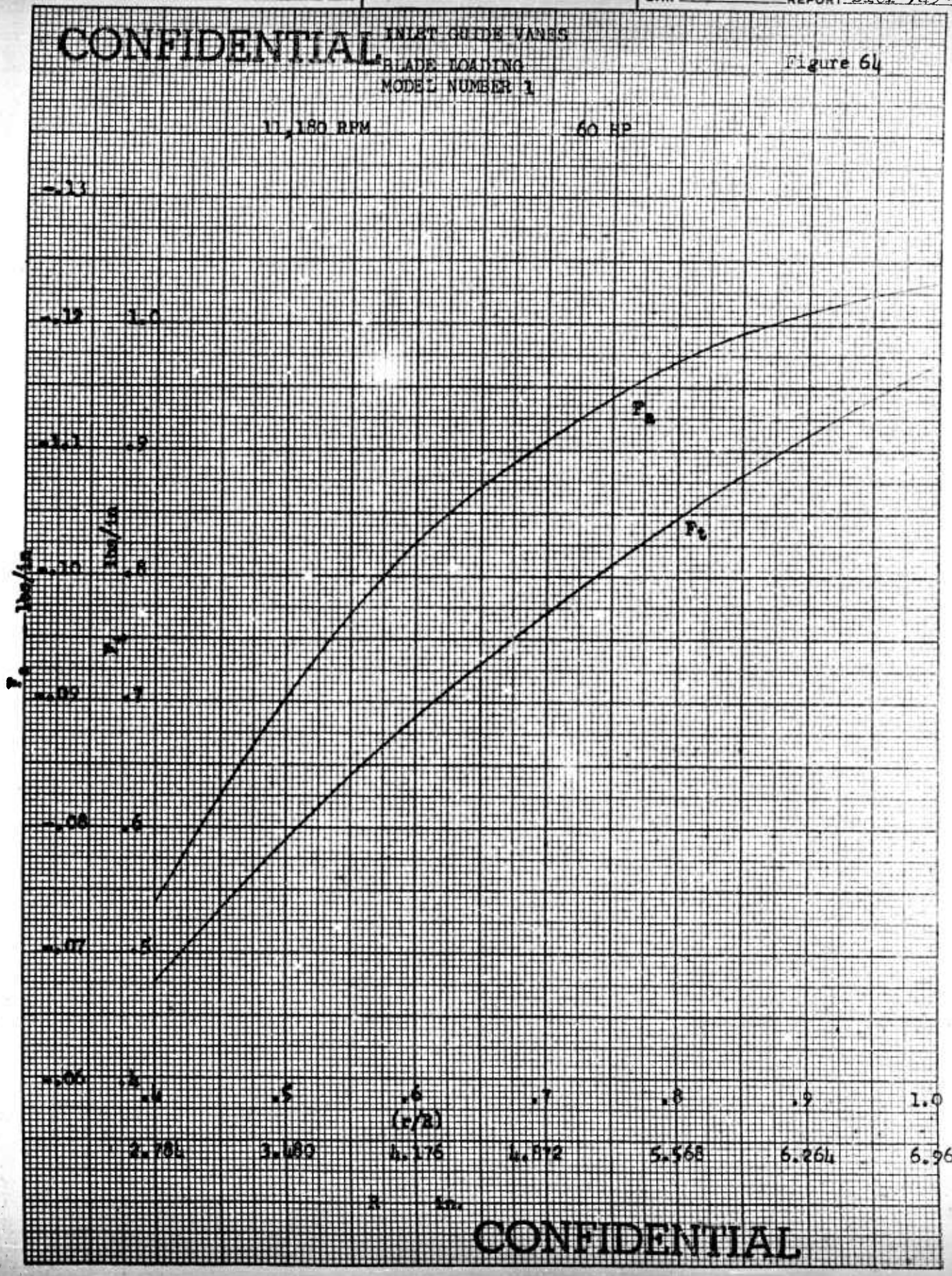

CONFIDENTIAL

CONFIDENTIAL

ROTOR

Figure 65

BLADE LOADING

MODEL NUMBER 1

11,180 RPM 60 MP

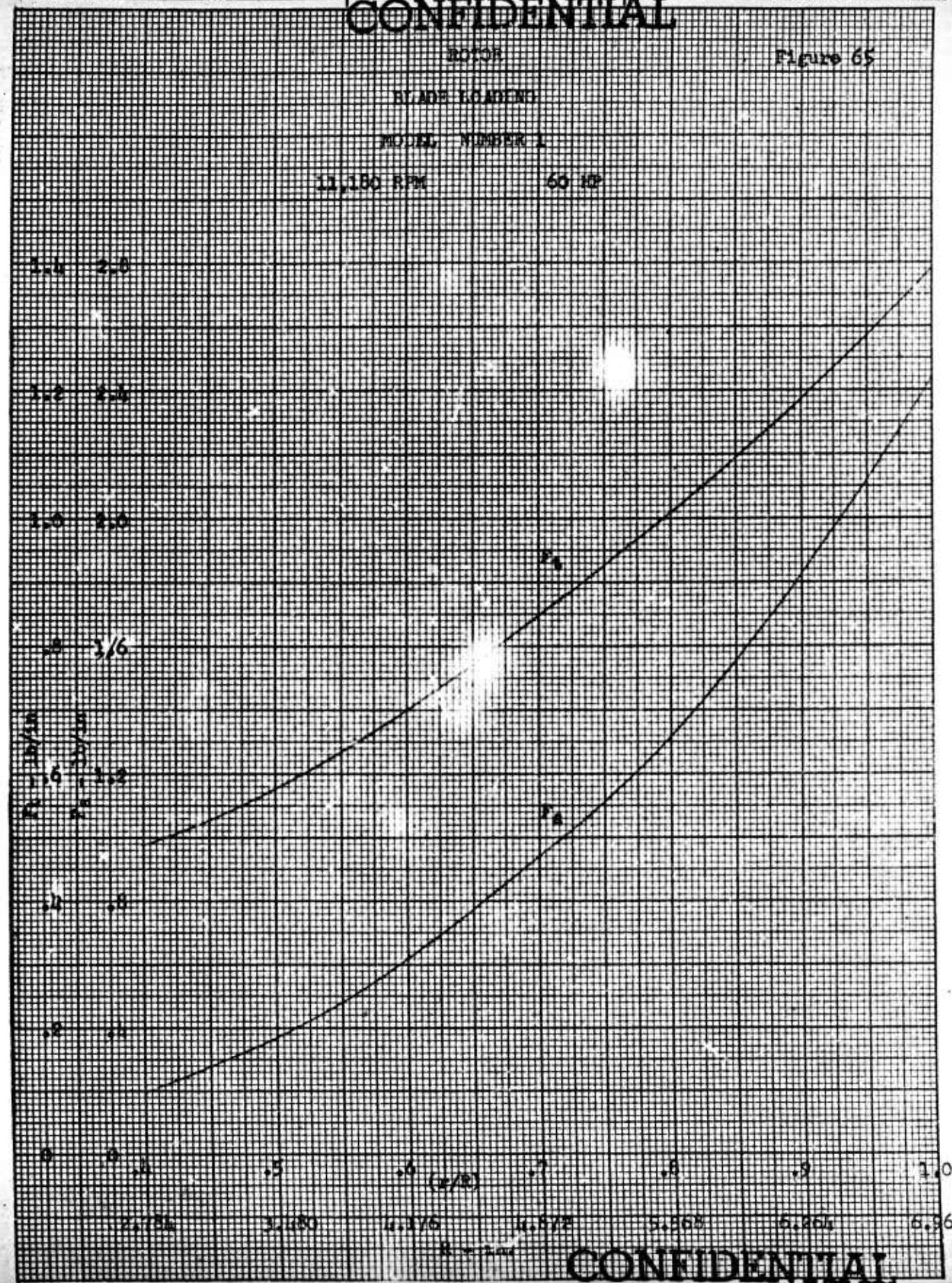

CONFIDENTIAL

CONFIDENTIAL

ROTOR STATIONS

Figure 66

BLADE LOADING

MODEL NUMBER 1

11,180 RPM 60°F

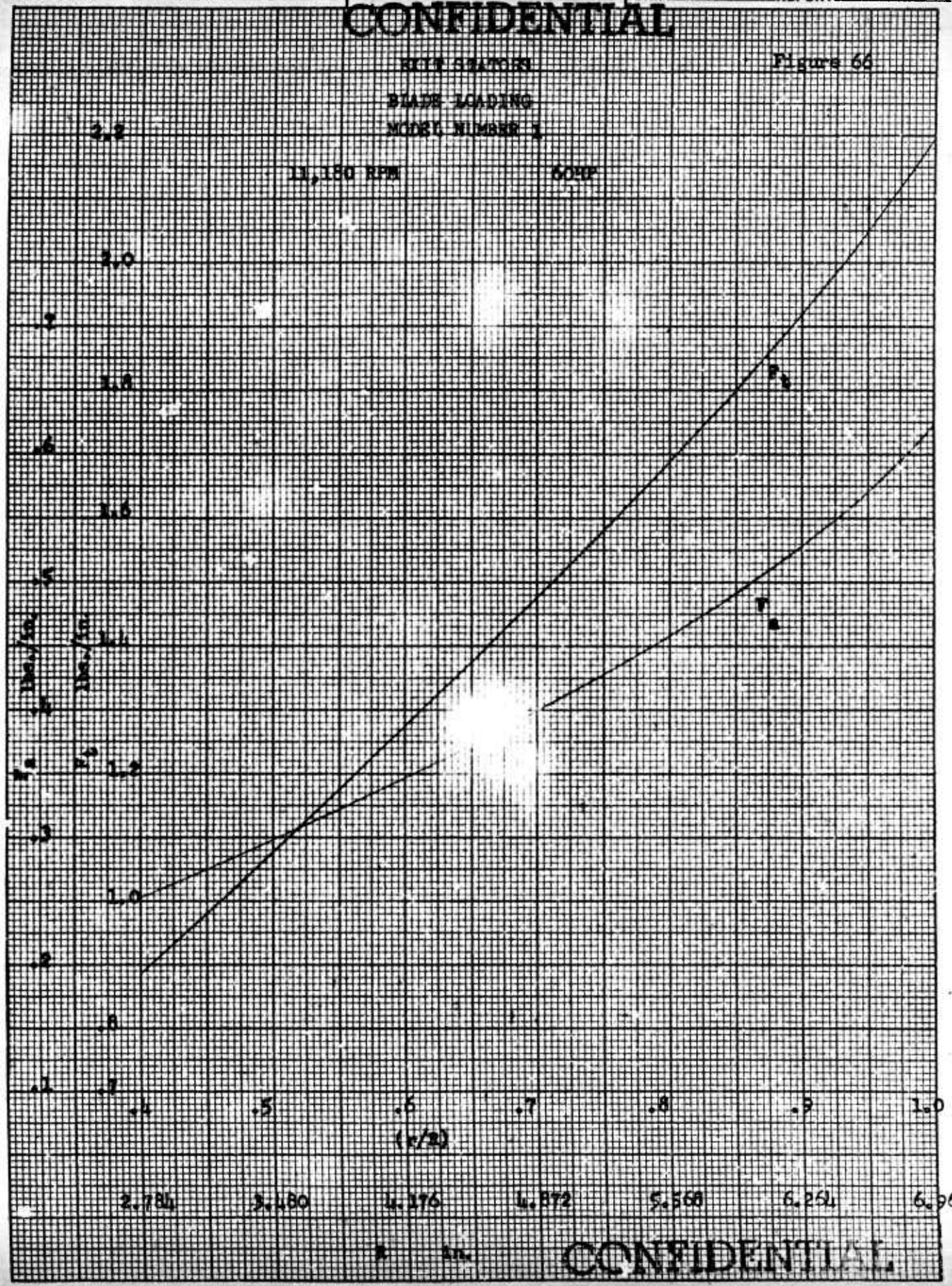

CONFIDENTIAL

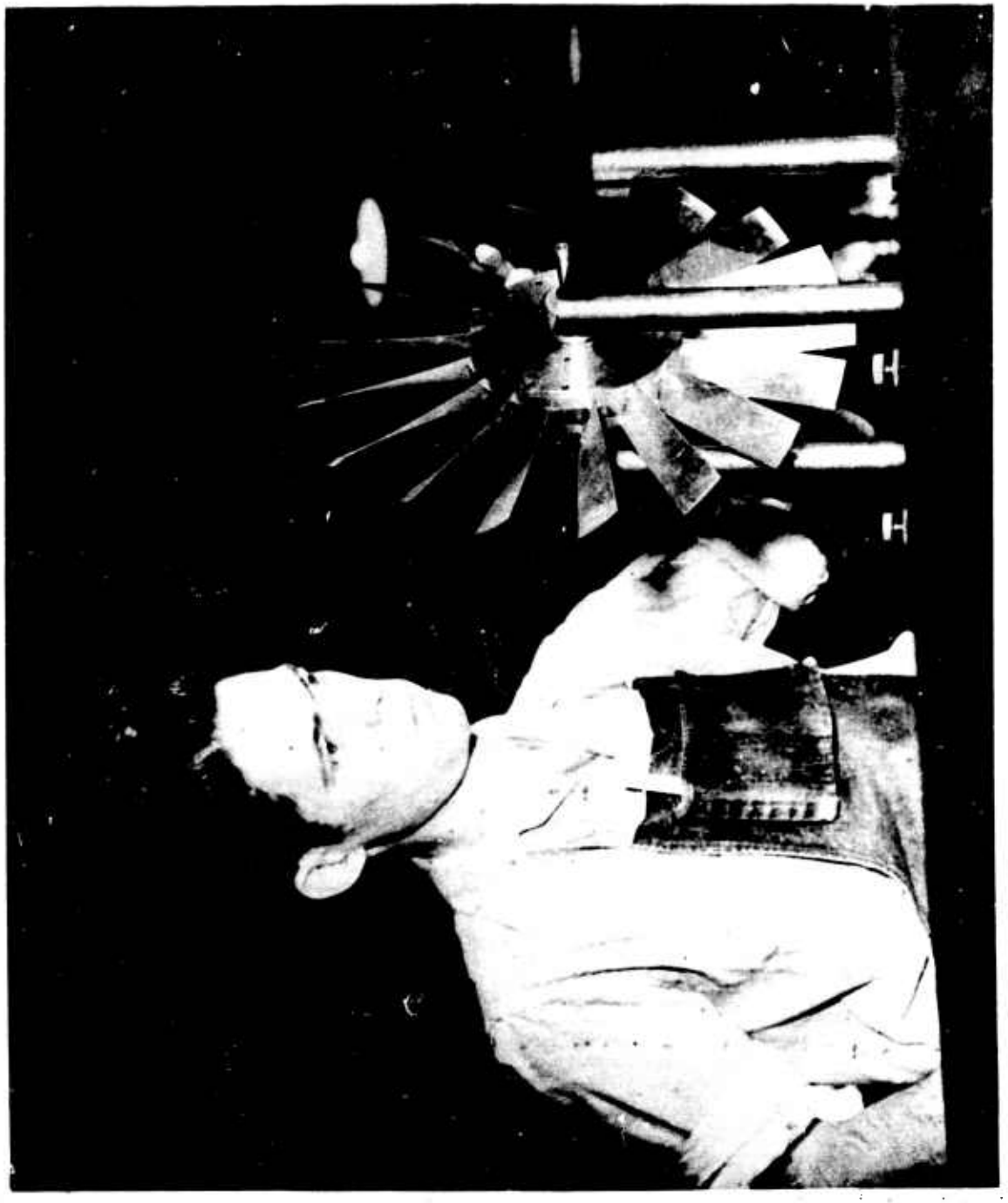

Figure 67. Model Rotor Balancing

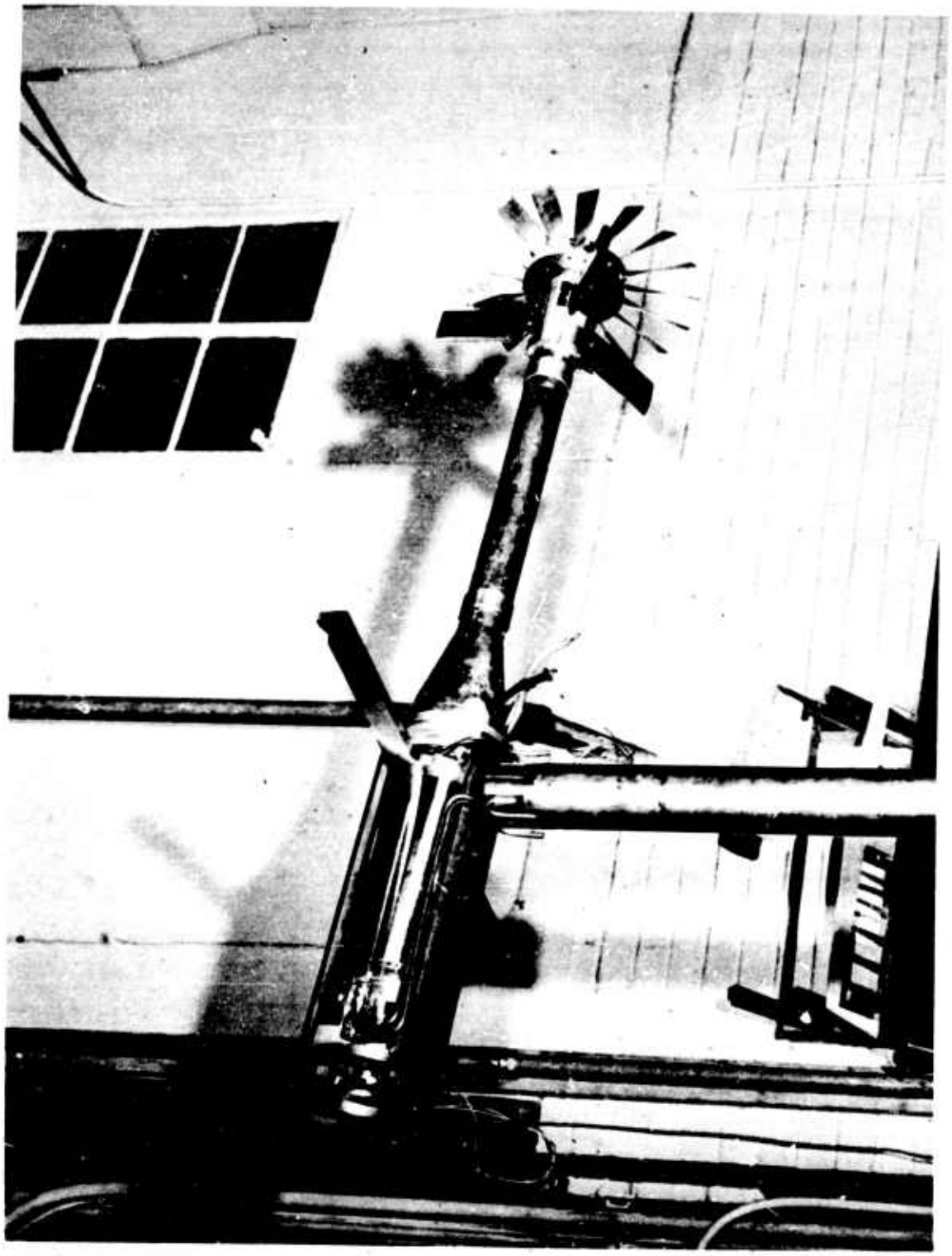

Figure 68. Partial Model Assembly

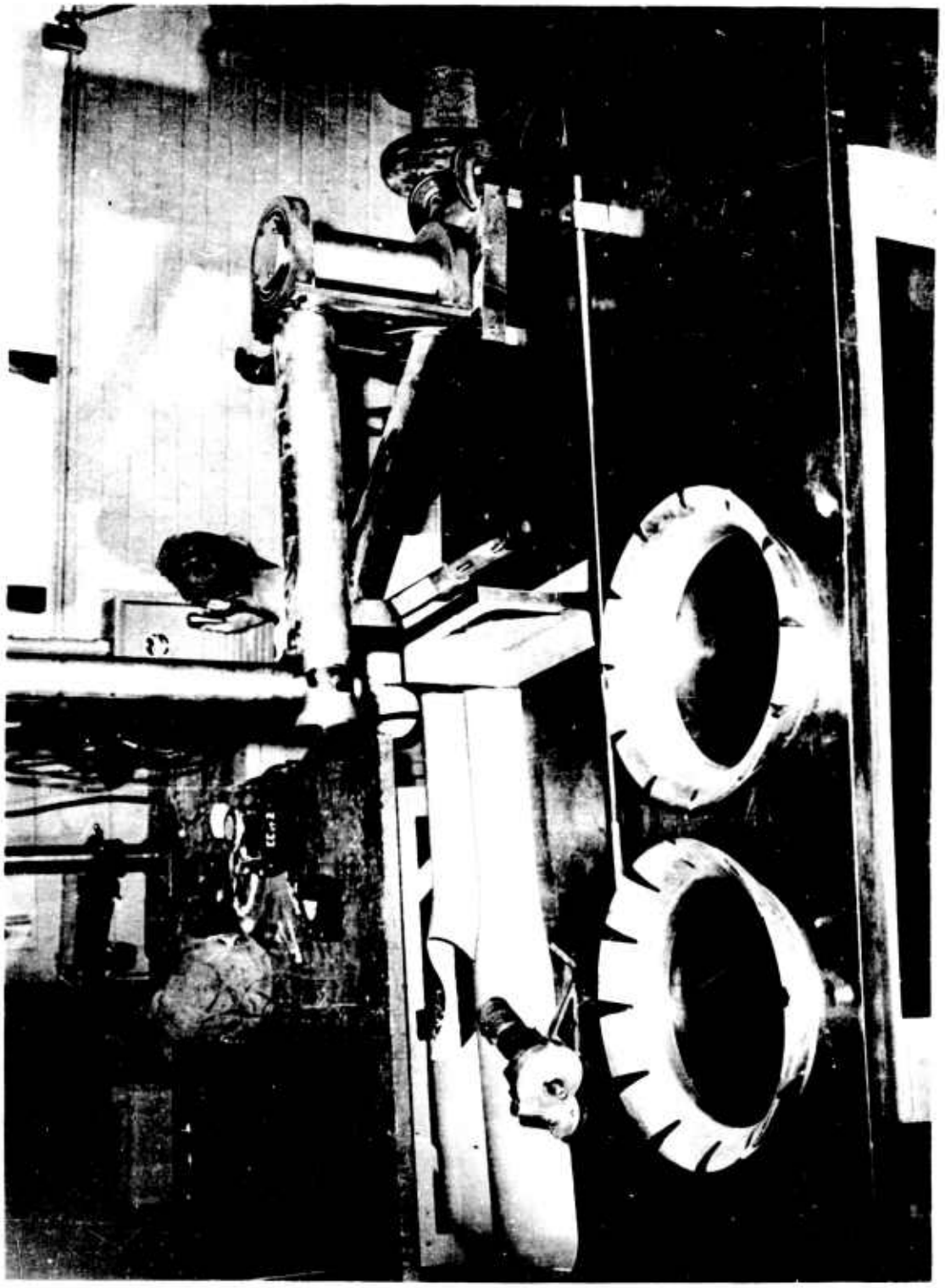

Figure 69. Practical Flap and Split Bell-Mouth Inlets

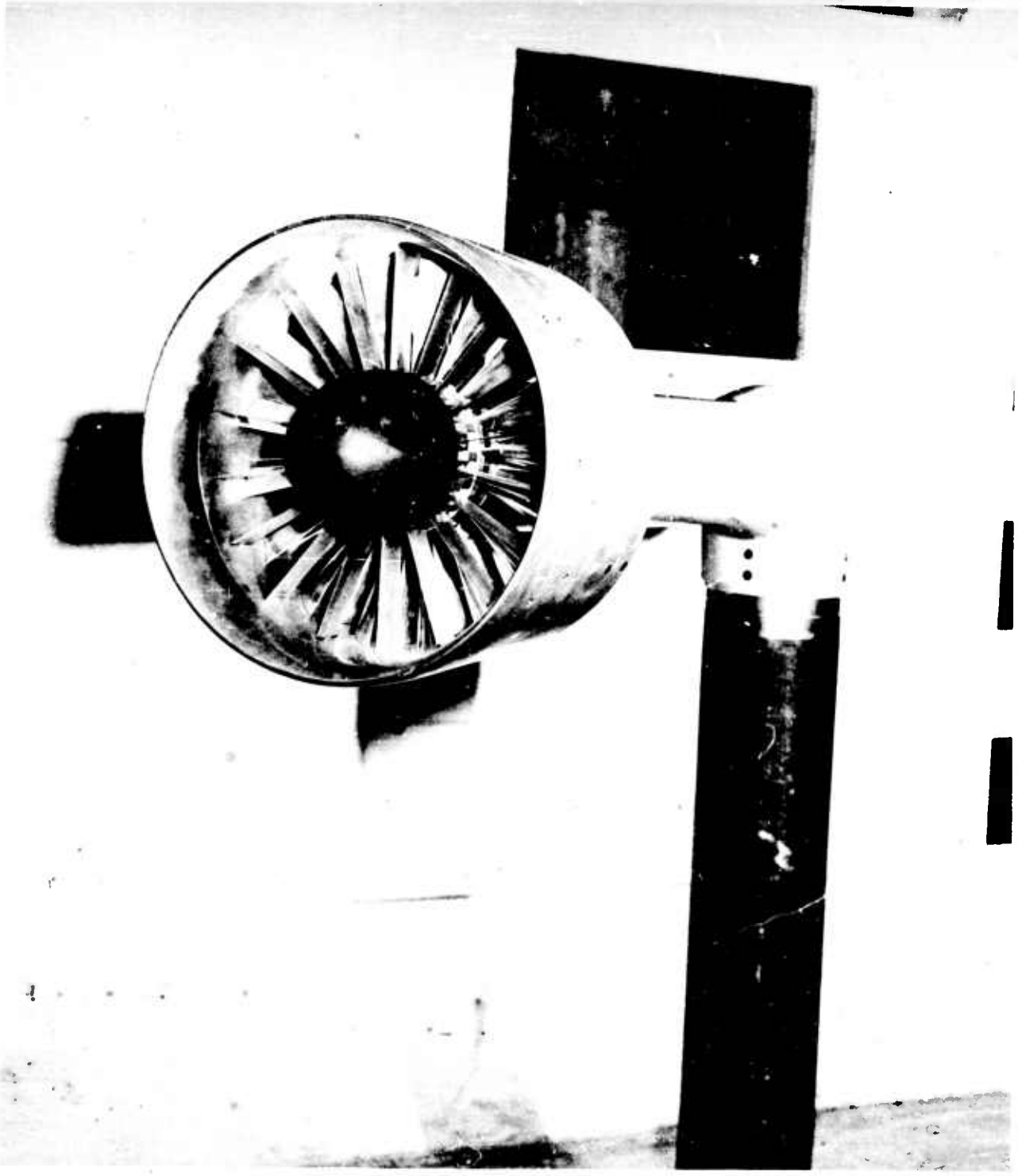

Figure 70 Wind Tunnel Duct Model

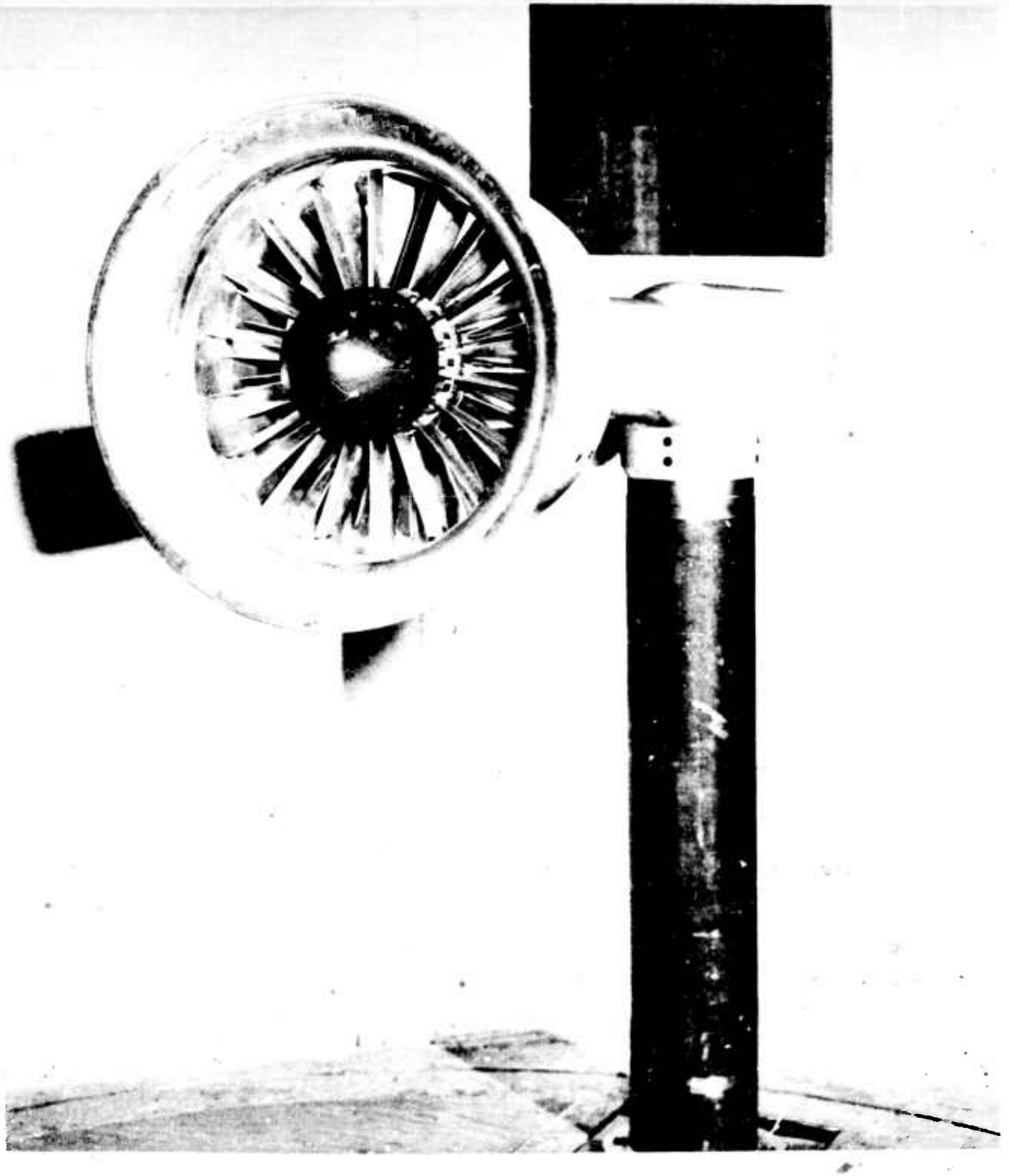

Figure 71 Wind Tunnel Duct Model

TABLE XV

Model No. 2 - Rotor

Mean Camber Line Ordinates

		r/R →	.3	.4	.5	.6	.7	.8	.9	1.0
x/c	x	$R_{in.}$ →	2.088	2.784	3.480	4.176	4.872	5.568	6.264	6.960
% Chord	in.	C_{l_o} →	.560	.480	.408	.350	.310	.277	.244	.212
0			0	0	0	0	0	0	0	0
.5	.0066		.0018	.0016	.0013	.0011	.0010	.0009	.0008	.0007
.75	.0098		.0026	.0022	.0019	.0016	.0014	.0013	.0011	.0010
1.25	.0164		.0039	.0034	.0029	.0025	.0022	.0019	.0017	.0015
2.50	.0328		.0068	.0059	.0050	.0043	.0038	.0034	.0030	.0026
5	.0656		.0116	.0099	.0085	.0073	.0064	.0057	.0051	.0044
7.5	.0984		.0156	.0133	.0113	.0097	.0086	.0077	.0068	.0059
10	.1312		.0190	.0163	.0138	.0119	.0105	.0094	.0083	.0072
15	.1967		.0247	.0212	.0180	.0154	.0137	.0122	.0108	.0094
20	.2623		.0292	.0251	.0213	.0183	.0162	.0145	.0127	.0111
25	.3279		.0329	.0282	.0239	.0205	.0182	.0163	.0143	.0124
30	.3935		.0357	.0306	.0260	.0223	.0198	.0177	.0156	.0135
35	.4591		.0378	.0324	.0276	.0236	.0209	.0187	.0165	.0143
40	.5246		.0393	.0337	.0287	.0246	.0218	.0195	.0171	.0152
50	.6558		.0405	.0347	.0295	.0253	.0224	.0200	.0176	.0153
55	.7214		.0402	.0345	.0293	.0251	.0223	.0199	.0175	.0152
60	.7870		.0393	.0337	.0287	.0246	.0218	.0195	.0171	.0149
65	.8525		.0378	.0324	.0276	.0236	.0209	.0187	.0165	.0143
70	.9181		.0357	.0306	.0260	.0223	.0198	.0177	.0156	.0135
75	.9837		.0329	.0282	.0239	.0205	.0182	.0163	.0143	.0124
80	1.0493		.0292	.0251	.0213	.0183	.0162	.0145	.0127	.0111
85	1.1149		.0247	.0212	.0180	.0154	.0137	.0122	.0108	.0094
90	1.1804		.0190	.0163	.0138	.0119	.0105	.0094	.0083	.0072
95	1.2460		.0116	.0099	.0085	.0073	.0064	.0057	.0051	.0044
100	1.3116		0	0	0	0	0	0	0	0
Angle of Base Line with Duct Center Line at Design Speed (200K)			19.35°	28.15°	35.7°	41.81°	46.95°	51.2°	54.6°	57.72°
Solidity			1.00	.750	.600	.500	.429	.375	.333	.300

No. of Blades = 10

Chord = 1.3116 in.

All dimensions are in inches.

TABLE XV (Cont'd)

Model No. 2 - Rotor

Section Ordinates Above & Below (⊥) Mean Camber Line

		r/R →	.3	.4	.5	.6	.7	.8	.9	1.0
	x	$R_{in.}$ →	2.088	2.784	3.480	4.176	4.872	5.568	6.264	6.960
% Chord	in.	C_{l_o} →	.0675	.0644	.0613	.0582	.0551	.0521	.0490	.0460
0	0		0	0	0	0	0	0	0	0
.5	.0066		.0070	.0067	.0064	.0061	.0057	.0054	.0051	.0048
.75	.0098		.0085	.0081	.0077	.0073	.0069	.0065	.0061	.0058
1.25	.0164		.0106	.0101	.0096	.0091	.0086	.0082	.0077	.0072
2.5	.0328		.0141	.0135	.0128	.0122	.0115	.0109	.0102	.0096
5.0	.0656		.0193	.0184	.0176	.0167	.0158	.0149	.0140	.0132
7.5	.0984		.0234	.0224	.0213	.0202	.0191	.0181	.0170	.0160
10	.1312		.0269	.0257	.0244	.0232	.0220	.0208	.0195	.0183
15	.1967		.0324	.0309	.0294	.0280	.0280	.0250	.0235	.0221
20	.2623		.0366	.0349	.0333	.0316	.0299	.0283	.0266	.0250
25	.3279		.0398	.0380	.0361	.0343	.0325	.0307	.0289	.0271
30	.3935		.0421	.0401	.0382	.0363	.0344	.0325	.0305	.0287
35	.4591		.0436	.0416	.0396	.0376	.0356	.0336	.0316	.0297
40	.5246		.0442	.0422	.0402	.0381	.0361	.0341	.0321	.0301
45	.5902		.0440	.0420	.0400	.0380	.0359	.0340	.0320	.0300
50	.6558		.0428	.0408	.0389	.0369	.0349	.0330	.0311	.0292
55	.7214		.0404	.0386	.0367	.0349	.0330	.0312	.0294	.0276
60	.7870		.0372	.0354	.0337	.0320	.0303	.0287	.0270	.0253
65	.8525		.0340	.0324	.0309	.0294	.0278	.0263	.0247	.0232
70	.9181		.0306	.0291	.0277	.0263	.0250	.0236	.0222	.0209
75	.9837		.0271	.0258	.0247	.0234	.0221	.0210	.0197	.0185
80	1.0493		.0237	.0227	.0215	.0205	.0194	.0182	.0172	.0162
85	1.1149		.0200	.0190	.0181	.0172	.0162	.0154	.0145	.0136
90	1.1804		.0164	.0157	.0149	.0142	.0133	.0127	.0120	.0111
95	1.2460		.0129	.0120	.0116	.0111	.0102	.0098	.0093	.0089
100	0		0	0	0	0	0	0	0	0
Leading Edge Radius			.0035	.0034	.0032	.0031	.0029	.0027	.0026	.0024
Trailing Edge Radius			.0088	.0084	.0080	.0076	.0072	.0068	.0064	.0060

All dimensions are in inches

NOTE: Section ordinates are measured perpendicular to Mean Camber Line

TABLE XVI

Model No. 2 - Exit Stators

Mean Camber Line Ordinates

		r/R →	.3	.4	.5	.6	.7	.8	.9	1.0
x/c	x	$R_{in.}$ →	2.088	2.784	3.480	4.176	4.872	5.568	6.264	6.960
% Chord	in.	C_{l_o} →	.820	.920	.955	1.040	1.190	1.380	1.675	2.100
0	0		0	0	0	0	0	0	0	0
.5	.0066		.0027	.0030	.0031	.0034	.0039	.0045	.0055	.0069
.75	.0098		.0038	.0042	.0044	.0048	.0055	.0063	.0077	.0096
1.25	.0164		.0058	.0064	.0067	.0073	.0084	.0097	.0118	.0147
2.50	.0328		.0100	.0112	.0116	.0127	.0145	.0168	.0204	.0256
5	.0656		.0170	.0191	.0198	.0216	.0247	.0286	.0347	.0435
7.5	.0983		.0228	.0256	.0266	.0289	.0331	.0384	.0466	.0584
10	.1311		.0278	.0312	.0324	.0352	.0403	.0468	.0568	.0712
15	.1967		.0362	.0406	.0421	.0459	.0525	.0609	.0739	.0927
20	.2623		.0428	.0480	.0498	.0543	.0621	.0720	.0874	.1096
25	.3278		.0481	.0540	.0560	.0610	.0698	.0810	.0983	.1232
30	.3934		.0523	.0586	.0609	.0663	.0758	.0880	.1068	.1338
35	.4590		.0554	.0621	.0645	.0702	.0804	.0932	.1131	.1418
40	.5245		.0576	.0646	.0671	.0730	.0836	.0969	.1176	.1475
45	.5901		.0589	.0660	.0686	.0747	.0854	.0991	.1212	.1508
50	.6557		.0593	.0665	.0691	.0752	.0861	.0998	.1211	.1519
55	.7212		.0589	.0660	.0686	.0747	.0854	.0991	.1202	.1508
60	.7868		.0576	.0646	.0671	.0730	.0836	.0969	.1176	.1475
65	.8523		.0554	.0621	.0645	.0702	.0804	.0932	.1131	.1418
70	.9179		.0523	.0586	.0609	.0663	.0758	.0880	.1068	.1338
75	.9835		.0481	.0540	.0560	.0610	.0698	.0810	.0983	.1232
80	1.0490		.0428	.0480	.0498	.0543	.0621	.0720	.0874	.1096
85	1.1146		.0362	.0406	.0421	.0459	.0525	.0609	.0739	.0927
90	1.1802		.0278	.0312	.0324	.0352	.0403	.0468	.0568	.0712
95	1.2457		.0170	.0191	.0198	.0216	.0247	.0286	.0347	.0435
100	1.3113		0	0	0	0	0	0	0	0
Angle of Base Line with Duct Center Line			6.2°	6.2°	6.2°	6.2°	6.2°	6.2°	6.2°	6.2°
Solidity			1.500	1.125	.900	.750	.642	.562	.500	.450

No. of Blades = 15

Chord = 1.3113 in.

All dimensions are in inches

TABLE XVI (Cont'd)

Model No. 2 - Exit Stators

Section Ordinates Above and Below (⊥) Mean Camber Line

x/c	x	All Stations
% Chord	in.	t/c ⟶ .06
0	0	0
.5	.0066	.0062
.75	.0098	.0075
1.25	.0164	.0094
2.50	.0328	.0125
5	.0656	.0172
7.5	.0983	.0208
10	.1311	.0239
15	.1967	.0288
20	.2623	.0326
25	.3278	.0354
30	.3934	.0374
35	.4590	.0387
40	.5245	.0393
45	.5901	.0391
50	.6557	.0380
55	.7212	.0359
60	.7868	.0330
65	.8523	.0302
70	.9179	.0272
75	.9835	.0241
80	1.0490	.0211
85	1.1146	.0177
90	1.1802	.0146
95	1.2457	.0114
100	1.3113	0

Leading Edge Radius: .0032

Trailing Edge Radius: .0078

All dimensions are in inches.

NOTE: Section ordinates are measured perpendicular to Mean Camber Line.

TABLE XVII

WIND TUNNEL TEST PROGRAM

Force tests

Data to be collected

Forces and moments on the shroud
Forces and moments on the blades
Combined forces and moments
Total pressure ratio across the duct

Model Configuration Identification

code order

(Angle of attack) (Inlet) (Guidevane) (Rotor) (Stator) (Flaps exit)

Angle of attack	-	subscript identifies angle
Inlets	B -	bell mouth, subscripts would indicate notch size. Two sizes will be tested. C none, 1 small notch, 2 large notch.
	F -	practical flap
	H -	high speed inlet
Guide Vanes	G -	superscripts identify blade setting angle. Subscripts no. of blades
Rotor	R	
Exit Stators	F -	subscripts show no. of blades
Exit Flaps	D -	subscripts 0 no exit flap .8, 1.2, & 1.4 show multiples of unflapped exit area. Exit flap tests to be extra if time allows mfg. of the shroud extensions

I Velocities in feet/second

A. Static V = 0

B. Low speed - Velocities from 0 to approaching stall speed. Three speeds approximately:

V = 30, 60, 85 ft/second

C. High speed - Velocities in the normal flight range, approximately:

V = 130, 180, & tunnel max

Model test points in the above Velocity requires

I Static - Design power only.

A. Test bell mouth on basic blade and exit configuration. Test basic bell mouth configuration with a change in inlet vane setting of ±5° and a change in motor RPM.

$B_0\ G_{18}\ R\ E_{19}\ D_0$

Vary inlet notch size over predetermined range, on the basic configuration

$B\ \left[G_{18}\ R\ E_{19}\ D_0\right]$

B. Test the practical flap with the basic configuration

$F\ \left[G_{18}\ R\ E_{19}\ D_0\right]$

C. Bell mouth with basic blades and exit area variation. This will be extra.

$\left[B_0\ G_{18}\ R\ E_{19}\right]\ D_{8,\ 1.2,\ 1.4}$

D. High speed inlet with the basic blade configuration.

$H\ \left[G_{18}\ R\ E_{19}\ D_0\right]$

E. Remove exit stators in steps from basic configuration.

$\left[B_0\ C_{18}\ R\right]\ E_{15,\ 8,\ 0}\ \left[D_0\right]$

F. Decrease inlet guide vanes on basic configuration

$$\left[B_0\right] \; G_9 \; \left[R \;\; E_{19} \; D_0\right]$$

guide vane setting will vary with number of blades due to solidity change.

II Low Speed - Design Power. 60 and 40% Power

A. With design power at the three velocity points, (V = 30, 60, and 85 ft/sec) test the basic configuration over the angle of attack range from 0 to 90 degrees.

$$\alpha_x \left[B_0 \; G_{18} \; R \;\; E_{19} \; D_0\right]$$

x = 90, 87.5, 85, 80, 75, 65, 50, 30, 15, 0

B. Same as A. with practical flap at one velocity over a reduced angle attack range.

$$\alpha_{60,\ 70,\ 85,\ 87.5,\ 90,} \;\; F \;\; \left[G_{18} \; R \;\; E_{19} \; D_0\right]$$

C. Same as B with exit area increase. This will be extra

$$\alpha_{50,\ 70,\ 80,\ 87.5,\ 90} \;\; \left[F \;\; G_{18} \; R \;\; E_{19}\right] \;\; D_{1.2,\ 1.4}$$

D. At 60 and 40% power and 1 velocity, check the basic configuration over the reduced angle of attack range.

$$\alpha_{60,\ 70,\ 80,\ 87.5,\ 90} \;\; \left[B_0 \; G_{18} \; R \;\; E_{19} \; D_0\right]$$

III High Speed - Design power and 1 Reduced power

A. The basic configuration with the high speed nose at design power over the velocity range. Test over the angle of attack range to stall angle.
(V = 130, 180, and tunnel max)

$$\alpha_{0,\ 5,\ 10,\ 15,\ 20} \;\; \left[H \;\; G_{18} \; R \;\; E_{19} \; D_0\right]$$

B. The reduced exit area over the velocity range with max power and reduced power at zero angle of attack. This will be extra.

$$\left[\alpha_0 \; H \; G_{18} \; R \; E_{19}\right] \; D_{0.8}$$

C. At reduced power and at one velocity check basic configuration over the angle of attack range.

$$\alpha_{0,\ 5,\ 10,\ 15,\ 20} \left[H \; G_{18} \; R \; E_{19} \; D_0\right]$$

TABLE XVIII

MODIFIED TEST PROCEDURE

Range of Variables:

Inlet Guide Vane Angle (α_{vane}) -20° to +20°

Velocity 0 to 250 ft/sec

RPM 6000 to 12,000

Yaw Angle (ψ) 0 to 90° (0 - 30° at Vo > 90 ft/sec)

Inlet Lips - bell mouth, notched bell mouth, practical flap, high speed lip

I Set inlet vane angle and test over complete range.

A. Bell Mouth Inlet

1. Static - vary RPM over range

2. Velocities 20, 40, 60, 90, 130, 180, 250 ft/sec - vary RPM over range and yaw angle over range.

B. Notched Bell Mouth

1. Static - vary RPM over range

2. Velocities 20, 45, 90, - vary RPM over range and yaw angles over range.

C. Practical Flap

1. Static - vary RPM over range

2. Velocities 20, 45, 90, 130, 180, 250 - vary RPM over range and yaw angles over range.

D. High Speed Nose

1. Static - vary RPM over range

2. Velocities 20, 45, 90, 130, 180, 250 - vary RPM and yaw angle over range.

II Reset inlet guide vane angle to new setting and repeat.

LIST OF SYMBOLS

a	-	Speed of sound, ft/sec
A	-	Area, sq ft
c	-	Blade chord, ft
C	-	C - factor for blade limit-loading
C_{l_o}	-	Blade design camber
C_p	-	Specific heat at constant pressure
D	-	Diameter, ft
F_e	-	Thrust, lbs
g	-	Acceleration due to gravity, ft/sec^2
HP	-	Horsepower
J	-	Joule's constant
k	-	Inlet pressure recovery P_{t_1}/P_{t_o}
K	-	Constant, equal to 10.95
m	-	Mass flow, slugs/sec
M	-	Mach number
N	-	Number of blades
P	-	Pressure, lbs/ft^2
PF	-	Power factor
q	-	Dynamic pressure, lbs/ft^2
Q	-	Torque, ft/lbs
r	-	Radius at any blade station, ft
R	-	Tip radius, ft

R - Universal gas constant

R_F - Fan pressure ratio, P_{t_2}/P_{t_1}

(r/R) - Radial station

t - Blade thickness

T - Temperature

U - Resultant rotational velocity, ft/sec

V - Velocity, ft/sec

w - Flow velocity relative to blades, ft/sec

Δw_u - Tangential whirl velocity, ft/sec

W - Weight flow, lbs/sec

α - Blade angle of attack, deg

β - Angle between flow direction and duct axis, deg

γ - Ratio of specific heats for air

η - Adiabatic fan efficiency

θ - Turning angle, deg

ρ - Density, slugs/ft^3

σ - Solidity

φ - Angle between blade chord and center line of duct, deg

Ω - Rotational velocity, ft/sec

SUBSCRIPTS

d - Design

e - Exit

f	-	Fan
in	-	Inlet
o	-	Free stream
p	-	Peak
t	-	Total or tangential
T	-	Tip
v	-	Vane
R1	-	Front rotor
R2	-	Rear rotor
1	-	Station immediately in front of fan
2	-	Station immediately behind fan

REFERENCES

1. Jackes, A.: "Unpublished Momentum Studies". Bell Aircraft Corporation, 1955.

2. Küchemann, D. and Weber, J.: "Aerodynamics of Propulsion". McGraw-Hill, 1953.

3. Mililo, J. R.: "Some Internal - Flow Characteristics at Zero Flight Speed of an Annular Supersonic Inlet and an Open-Nose Inlet with Sharp and Rounded Lips". NACA RM L54E19, 1954.

4. Platt, R. J., Jr.: "Static Tests of a Shrouded and an Unshrouded Propeller". NACA RM L7H25, February 9, 1948.

5. Zabinsky, J.: "Ducted Propeller Assault Transport Study - Survey of the State of the Art". Bell Aircraft Corporation Report No. D181-945-003, April 11, 1956.

6. Krüger, W.: "On Wind Tunnel Tests and Computations Concerning the Problem of Shrouded Propellers". NACA TM 1202, 1949.

7. Morley, A. W.: "Aircraft Propulsion Theory and Performance". Longmans, Green and Co., 1953.

8. Wright Aeronautical Corporation: "Model Specification, Engine, Aircraft, YT49-W-1 Turbo-Prop". W.A.D. Specification 875-E, March 20, 1951. Revised January 4, 1954.

9. Rolls-Royce: R.B. 109 Engine. "Initial Project Performance Data and Installation Notes". T.S.D. Publication 499, June 1953.

10. Allison Division, General Motors Corporation: "Preliminary Model Specification No. 394-B, Allison Model 550-B1 Turbo-Prop Engine". February 15, 1955, Revised January 5, 1956.

11. Ross, A. O. and Huppers, M. C.: "Analytical Determination of Effect of Water Injection on Power Output of Turbine Propeller Engine". NACA TN 3403, March 1955.

12. Herrig, L. J.; Emery, J. C.; Erwin, J. R.: "Systematic Two-Dimensional Cascade Tests of NACA 65-Series Compressor Blades at Low Speeds". NACA RM L51G31, September 14, 1951.

13. Herrig, L. J.; Emery, J. C.; Erwin, J. R.: "Effect of Section Thickness and Trailing Edge Radius on the Performance of NACA 65-Series Compressor Blades in Cascade at Low Speeds". NACA RM L51J16, December 13, 1951.

14. Felix, A. R.: "Summary of 65-Series Compressor-Blade Low-Speed Cascade Data by Use of the Carpet-Plotting Technique". NACA RM L54H18a, November 2, 1954.

15. Lieblein, S.; Schwenk, F. C.; Broderick, R. L.: "Diffusion Factor for Estimating Losses and Limiting Blade Loadings in Axial-Flow-Compressor Blade Elements". NACA RM E53D01, June 3, 1953.

16. Savage, M.: "Analysis of Aerodynamic Blade-Loading-Limit Parameters for NACA 65- (C_{1_o} A_{10}) 10 Compressor-Blade Sections at Low Speeds". NACA RM L54L02a, April 25, 1955.

17. Zimmey, C. M. and Lappi, V. M.: "Data for Design of Entrance Vanes from Two-Dimensional Tests of Airfoils in Cascade". NACA ACR L5G18, October 1945.

18. Dunavant, J. C.: "Cascade Investigation of a Related Series of 6-Percent-Thick Guide-Vane Profiles and Design Charts". NACA RM L54I02, November 26, 1954.

19. Lieblein, S.; Lewis, G. W., Jr.; Sandercock, D. M.: "Experimental Investigation of an Axial-Flow Compressor Inlet Stage Operating at Transonic Relative Inlet Mach Numbers". "I - Over-all Performance of Stage with Transonic Rotor and Subsonic Stators up to Rotor Relative Inlet Mach Number of 1.1". NACA RM E52A24, March 10, 1952.

20. Zabinsky, J. M. and Laszewski, M. M.: "Ducted Propeller Assault Transport Study - Performance". Bell Aircraft Corporation Report No. D181-945-004, May 15, 1956.

21. Vollo, S. D. and Brassaw, L. L.: "Ducted Propeller Assault Transport Study - Stability and Control". Bell Aircraft Corporation Report No. D181-945-005, May 15, 1956.

22. Sing, E.: "Ducted Propeller Assault Transport Study - Design Report". Bell Aircraft Corporation Report No. D181-945-002, May 15, 1956.

23. Bell Aircraft Corporation: "Ducted Fan Power Plant Study Proposal". Bell Aircraft Corporation Preliminary Design Report No. M29-001. July 30, 1954.

24. Bell Aircraft Corporation: "D-182A Ducted Propeller Test Airplane". Bell Aircraft Corporation Report No. D182-945-002, August 26, 1955.

25. Kane, J. B.; Vollo, S. D.; Roehrs, F. S.; Isom, J.: "Hovering Stability and Control". Bell Aircraft Corporation Report No. D139-945-103. December 1954.

26. Kane, J. B. and Vollo, S. D.: "Level Flight Stability and Control". Bell Aircraft Corporation Report No. D139-945-104, December 1954.

27. O'Malley, J. A.; Zabinsky, J.; Roehrs, F.; Isom, J.; Landphair, L.: "Aerodynamics of the Bell VTOL Air Test Vehicle". Bell Aircraft Corporation Report No. 65-978-008, October 26, 1953.

28. Roehrs, F. S.; Zabinsky, J. M.; O'Malley, J. A., Jr.: "A General Dynamic Stability and Control Analysis of Jet Powered VTOL Aircraft - Part I". Bell Aircraft Corporation Report No. 65-978-002, October 31, 1952.

29. Roehrs, F. S. and Landphair, L. C.: "A General Dynamic Stability and Control Analysis of Jet Powered VTOL Aircraft - Part II". Bell Aircraft Corporation Report No. 65-978-006, February 28, 1953.

30. Zabinsky, J. M.; Isom, J.; Landphair, L. C.; O'Malley, J. A., Jr.: "A General Performance Analysis of Jet Powered VTOL Aircraft - Part I", Bell Aircraft Corporation Report No. 65-978-003, November 30, 1952.

31. Zabinsky, J. M. and Isom, J., Jr.: "A General Performance Analysis of Jet Powered VTOL Aircraft - Part II". Bell Aircraft Corporation Report No. 65-978-005, February 20, 1953.

32. Wynn, W.; Isom, J., Jr.; Zabinsky, J. M.; O'Malley, J. A., Jr.: "A Preliminary Study of the Tactical Applications of Jet Powered VTOL Aircraft as Affected by Size and Weight". Bell Aircraft Corporation Report No. 65-978-007, February 20, 1953.

33. Zabinsky, J. M. and O'Malley, J. A., Jr.: "A Review of Available Literature on Jet Propeller Vertical Take-Off and Landing Aircraft". Bell Aircraft Corporation Report No. 65-978-004, January 1, 1953.

34. Payne, R. L.: "Evaluation of Control Methods for VTOL Aircraft". Bell Aircraft Corporation Report No. 65-989-001, December 29, 1952.

35. Dufort, R. H. and Buddenhagen, T. F.: "Control System Considerations for VTOL Aircraft". Bell Aircraft Corporation Report No. 65-989-002, February 28, 1953.

36. Bell Aircraft Corporation: "VTOL, A Review of the Study Program". Contract AF33(616)-84, December 1952.

37. Bell Aircraft Corporation: "Final Summary Report on the Study Program, Vertical Take-Off and Landing Aircraft". Bell Aircraft Corporation Report No. 65-989-003, March 9, 1953.

38. Whedon, R.: "Preliminary Specifications for an Air Test Vehicle". Bell Aircraft Corporation Report No. 65-947-001, February 27, 1953.

39. Dufort, R. H. and Meullen, N. F.: "Jet Convertiplane, Vertical Take-Off Fighter". Bell Aircraft Corporation Report No. D-109-945-003, November 9, 1951.

40. O'Malley, J. A.; Zabinsky, J.; et. al: "VTOL Dayfighter Weapon System - Aerodynamic Data". Bell Aircraft Corporation Report No. D139-945-028, July 15, 1954.

APPENDIX A

APPENDIX A

SUMMARY OF STATIC IBM PROCEDURE

Input Values: P_o, T_o, R_F, η, $\frac{HP}{A_{in}}$

Constants: $R = 53.3$, $\gamma = 1.4$, $g = 32.2$

Step	Calculation	Equation
1.	$\frac{HP}{W}$	(1-12)
2.	$\frac{W}{A_{in}}$	(1-25)
3.	$\frac{m}{m^*}$	(1-14)
4.	$\frac{P_{t_1}}{P_{t_o}}$	(1-26)
5.	$\frac{P_{t_e}}{P_e}$	(1-16)
6.	M_e	(1-27)
7.	$\sqrt{T_{t_e}}$	(1-19)
8.	$\left(\frac{W\sqrt{T_t}}{A\ P_t}\right)_e$	(1-28)
9.	$\frac{W\sqrt{T_t}}{A_{in}\ P_{t_e}}$	(1-29)
10.	$\frac{A_e}{A_{in}}$	⑨ / ⑧
11.	$\left(\frac{W\sqrt{T_t}}{A\ P_t}\right)_1$	(1-23)

Step	Calculation	Equation
12.	M_1	(1-13)
13.	V_f	(1-30)
14.	V_e	(1-31)
15.	$\frac{F_e}{A_{in}}$	(1-32)
16.	$\frac{F_e}{HP}$	(15) / $\frac{HP}{A_{in}}$

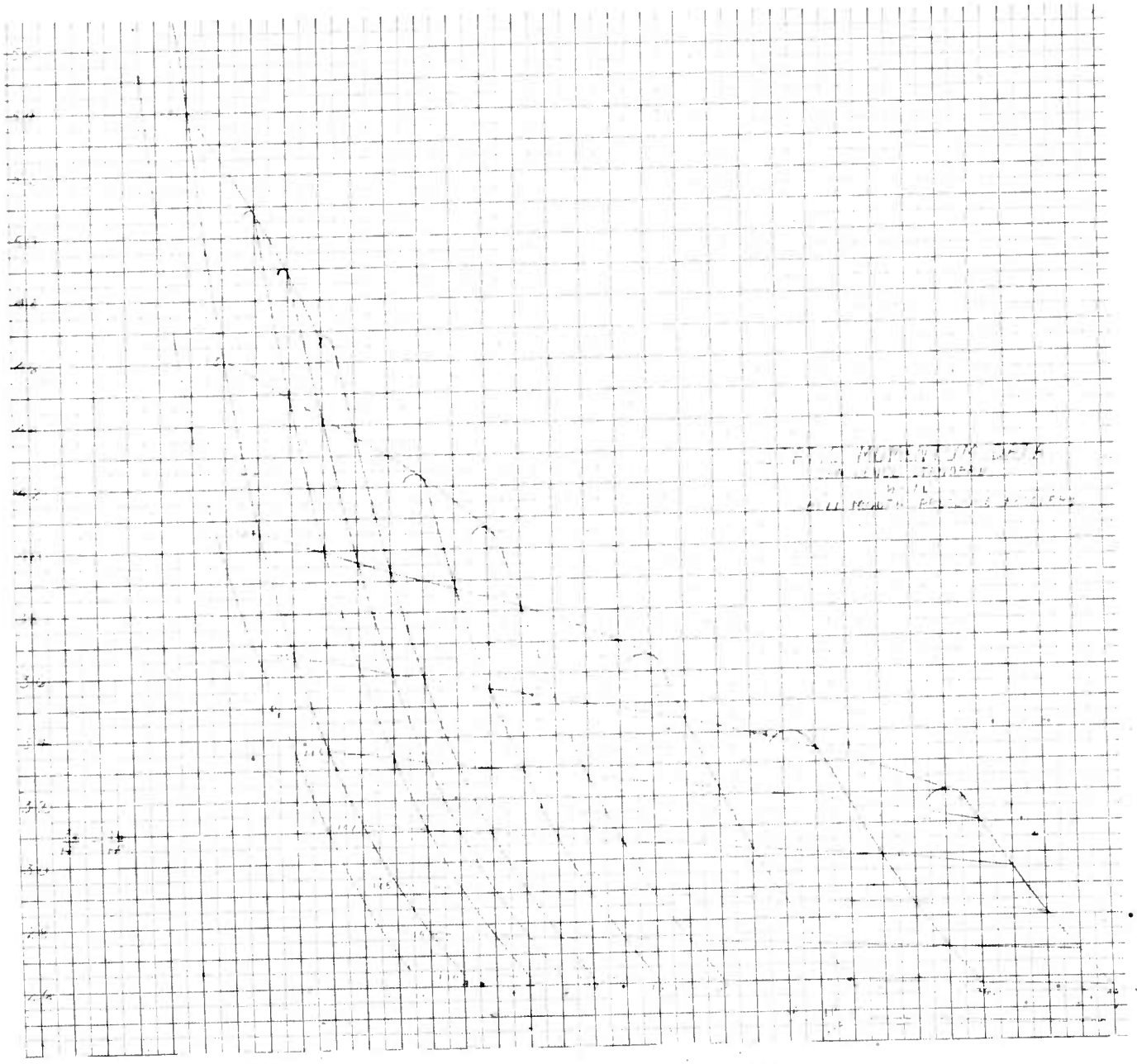

Report No. D181-945-006

Figure A 1

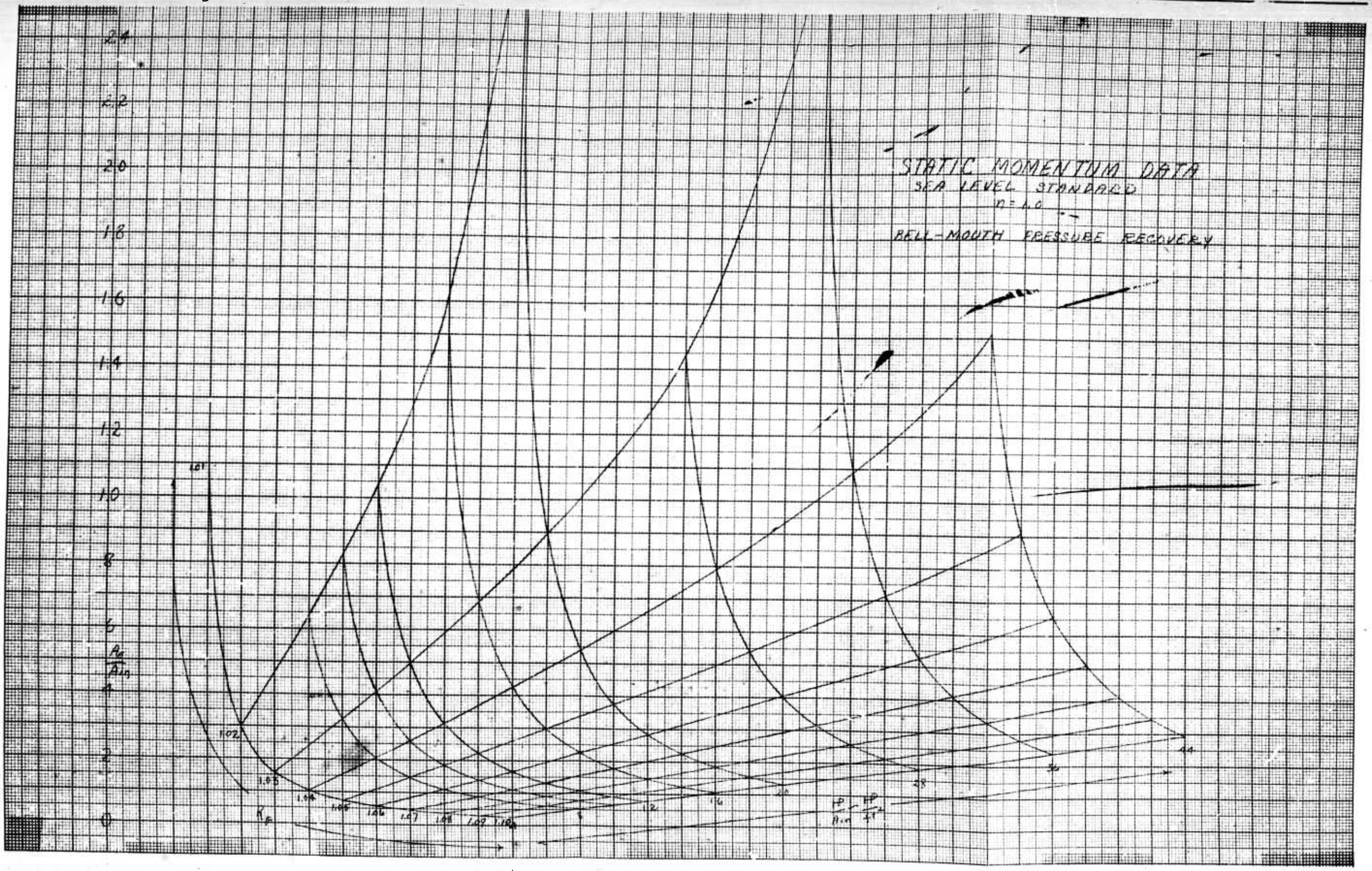

Figure A 1 cont

CONFIDENTIAL

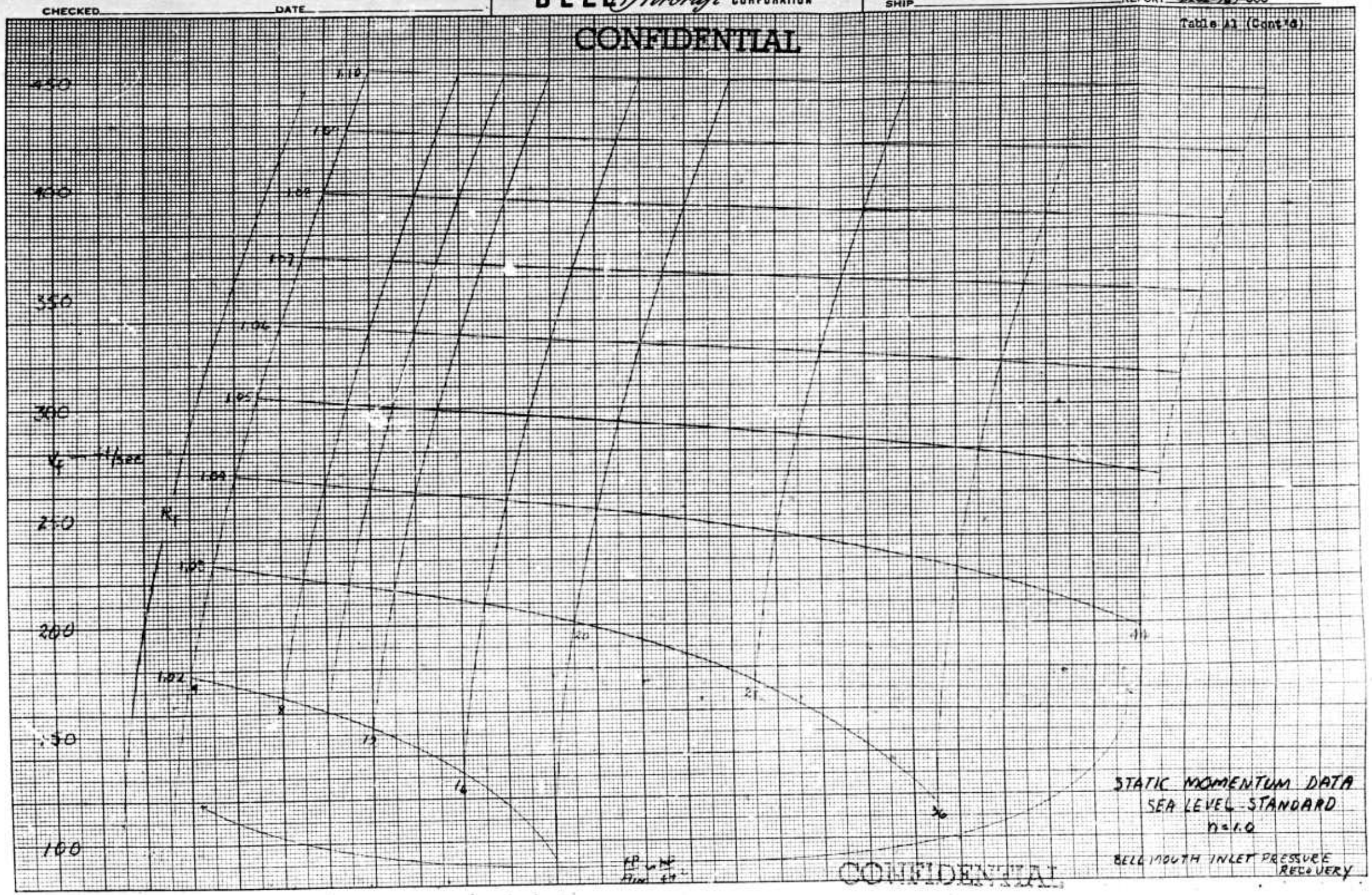

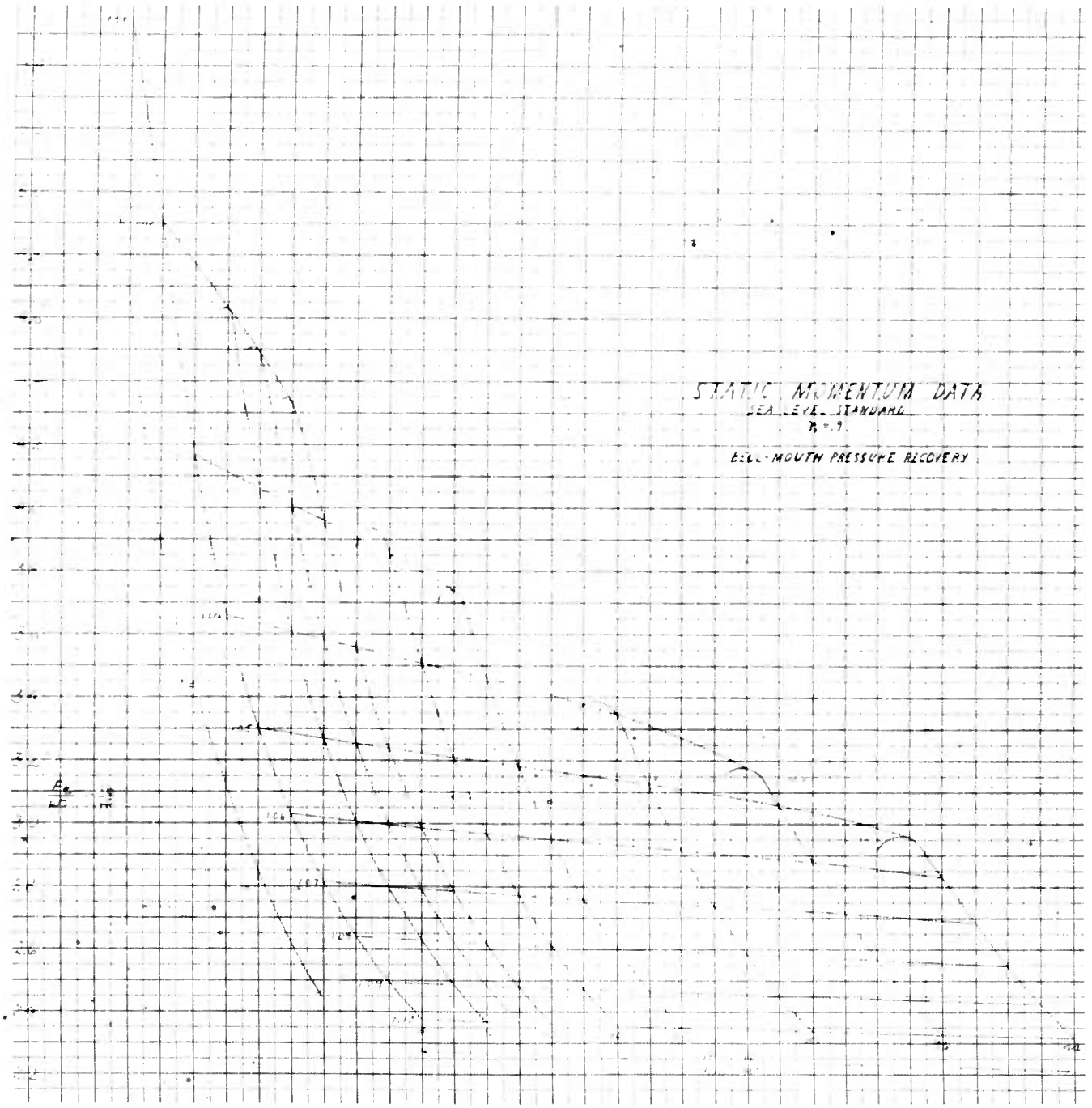

Report No. D181-945-006

Figure A 2

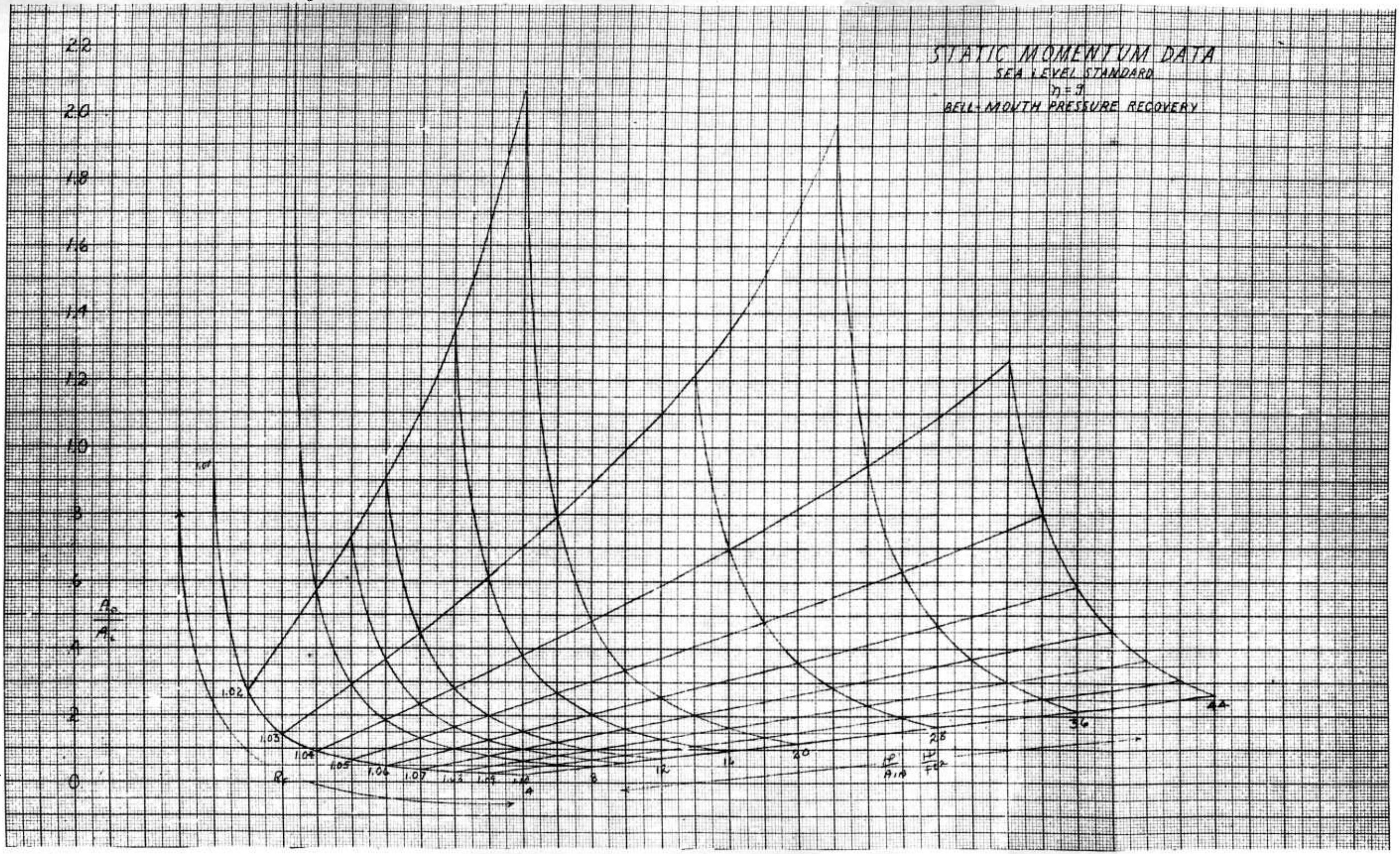

Report No. D181-945-006

Figure A 2

BY _____ DATE _____
CHECKED _____ DATE _____

BELL Aircraft CORPORATION

CONFIDENTIAL

MODEL _____ PAGE 188
SHIP _____ REPORT D181-945-066

Figure A2 (Cont'd)

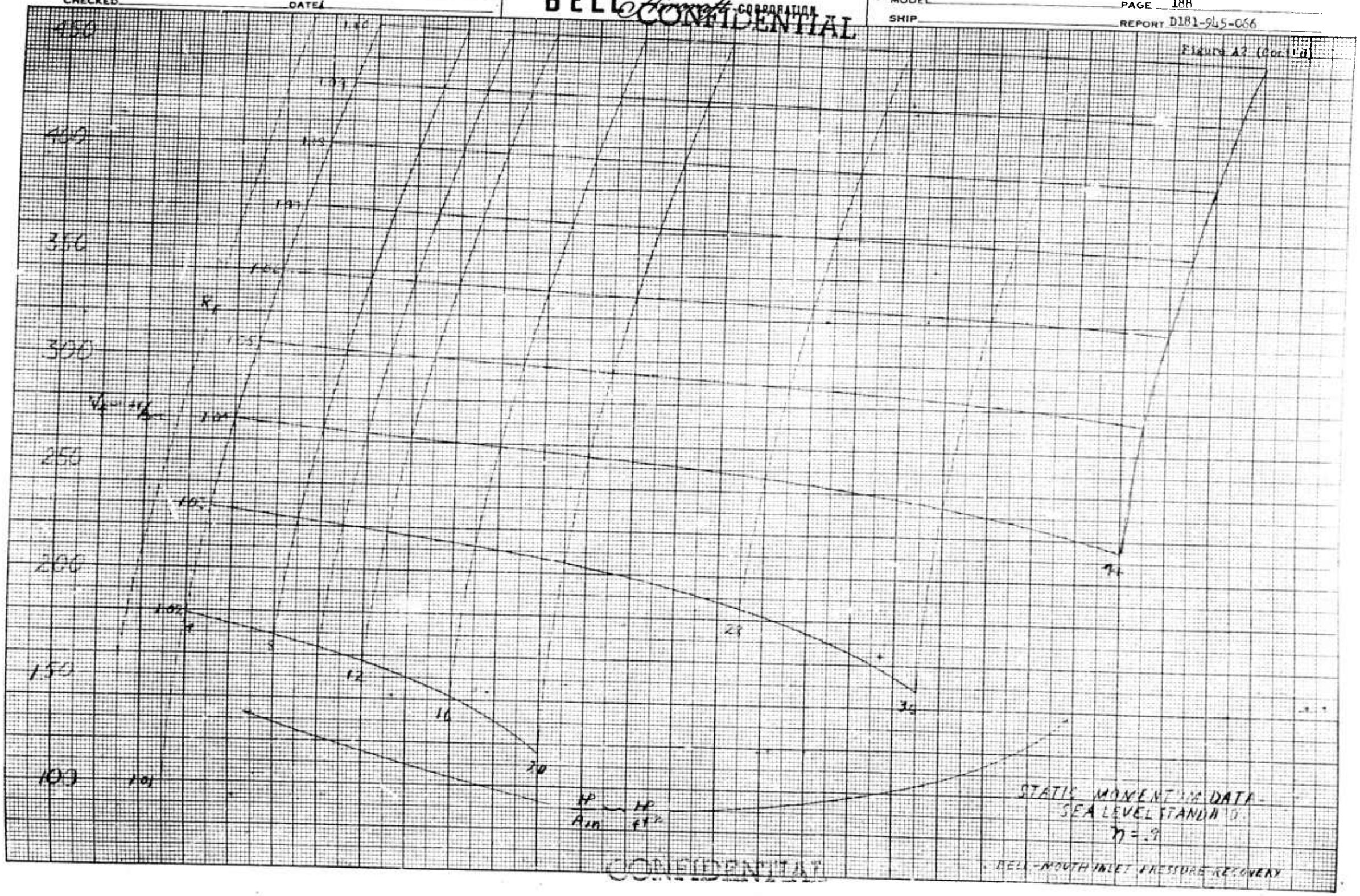

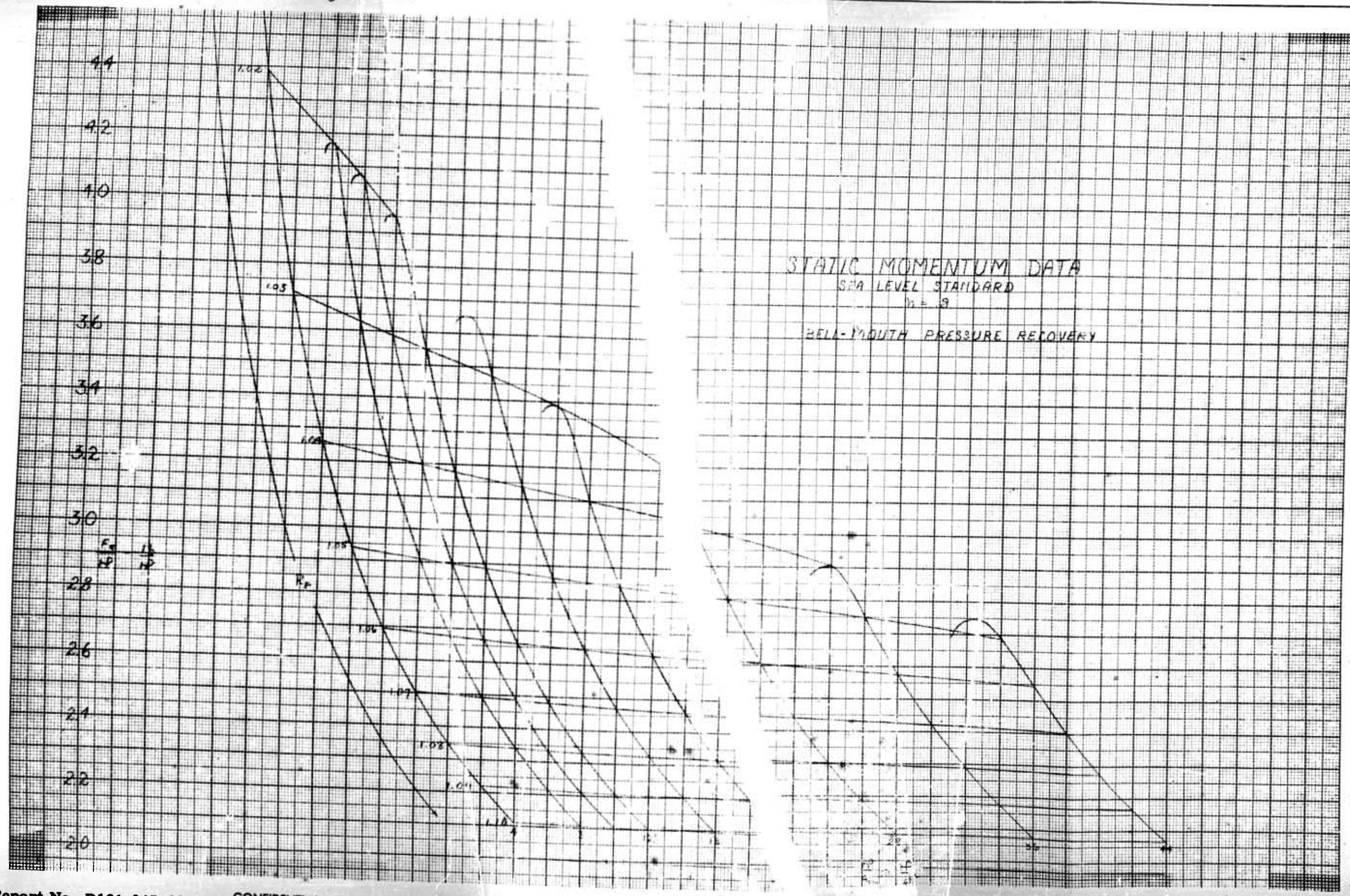
STATIC MOMENTUM DATA
SEA LEVEL STANDARD
h = 0
BELL-MOUTH PRESSURE RECOVERY
4.4
4.2
4.0
3.8
3.6
3.4
3.2
3.0
2.8
2.6
2.4
2.2
2.0
1.02
1.03
1.04
1.05
1.06
1.07
1.02
1.01
1.0
$\frac{F_s}{HP}$
$\frac{lb}{HP}$
R_F

Figure A-3

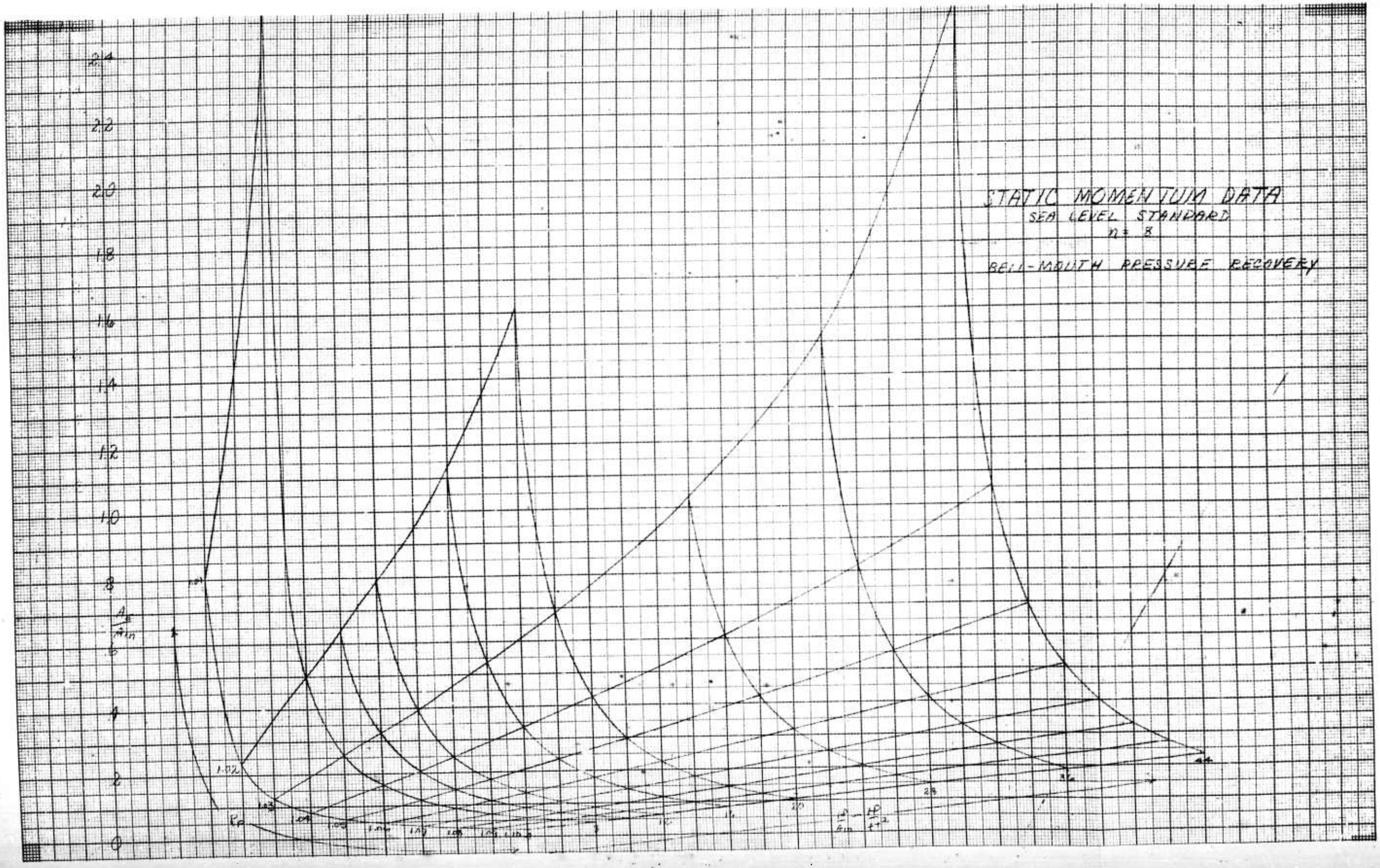

Figure A 3 cont

BY _____ DATE _____

CHECKED _____ DATE _____

BELL AIRCRAFT CORPORATION

MODEL _____ PAGE 191

SHIP _____ REPORT D181-945-006

Table A3 (Contd)

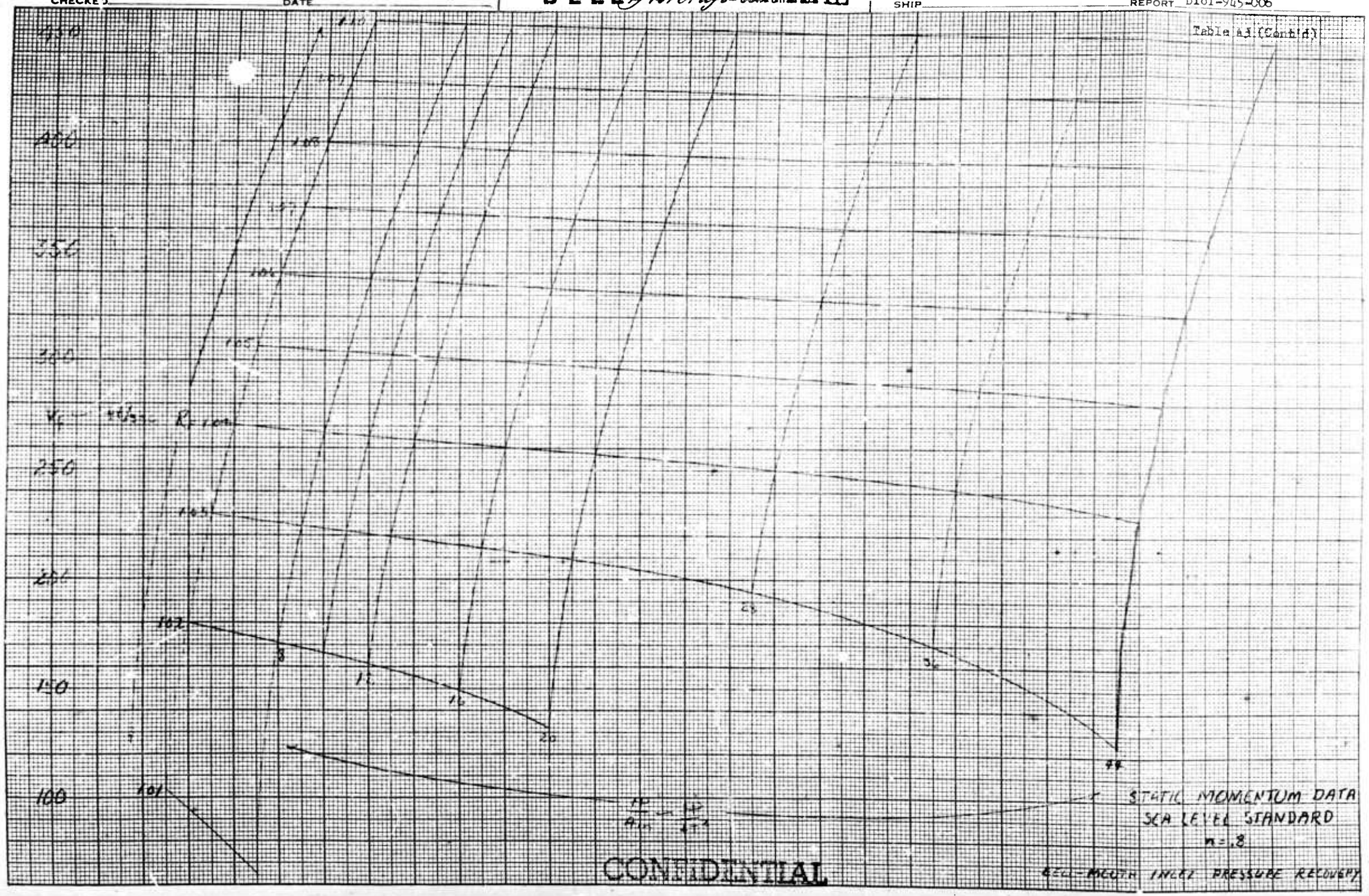

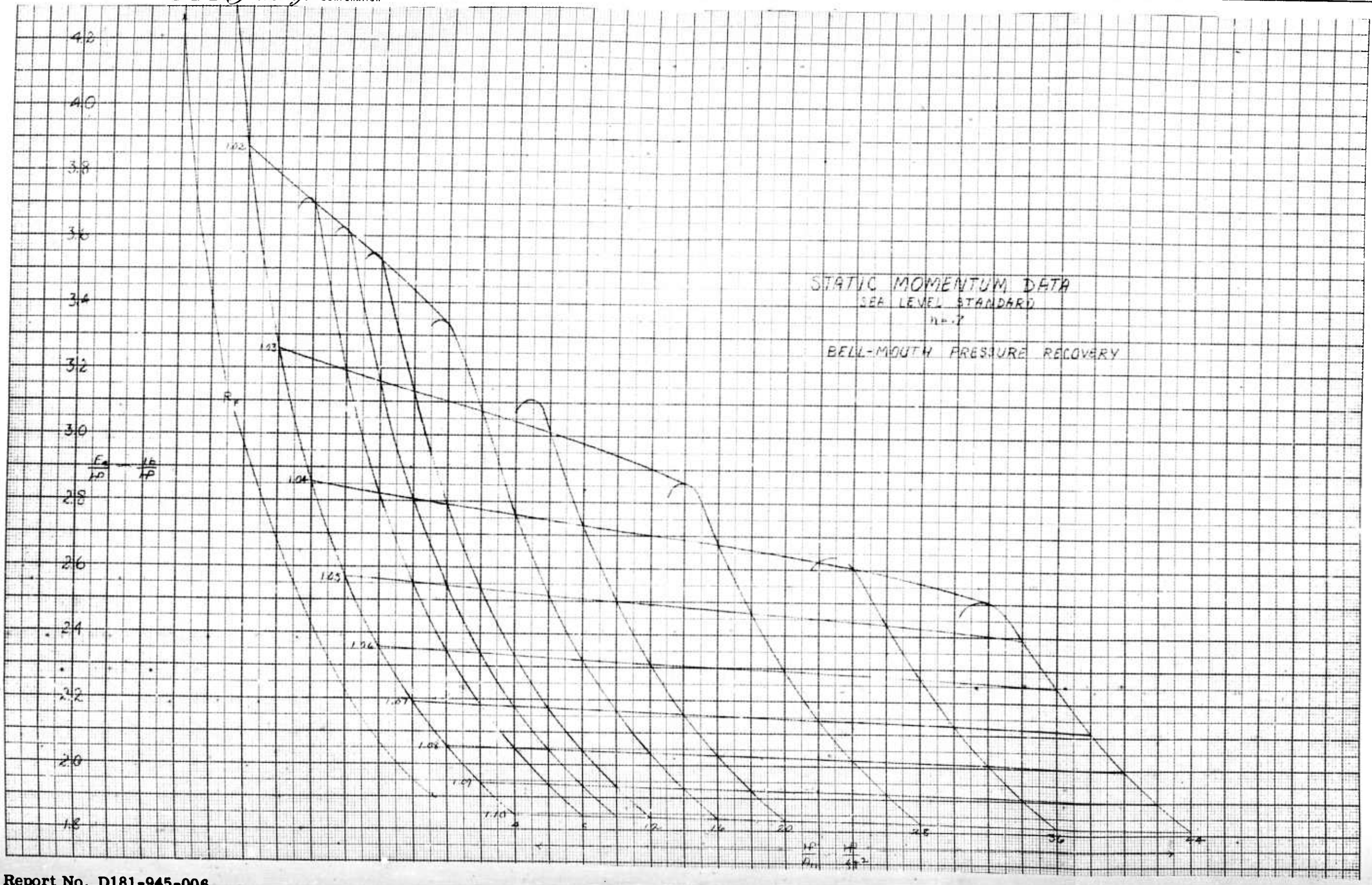

Report No. D181-945-006

Figure A4

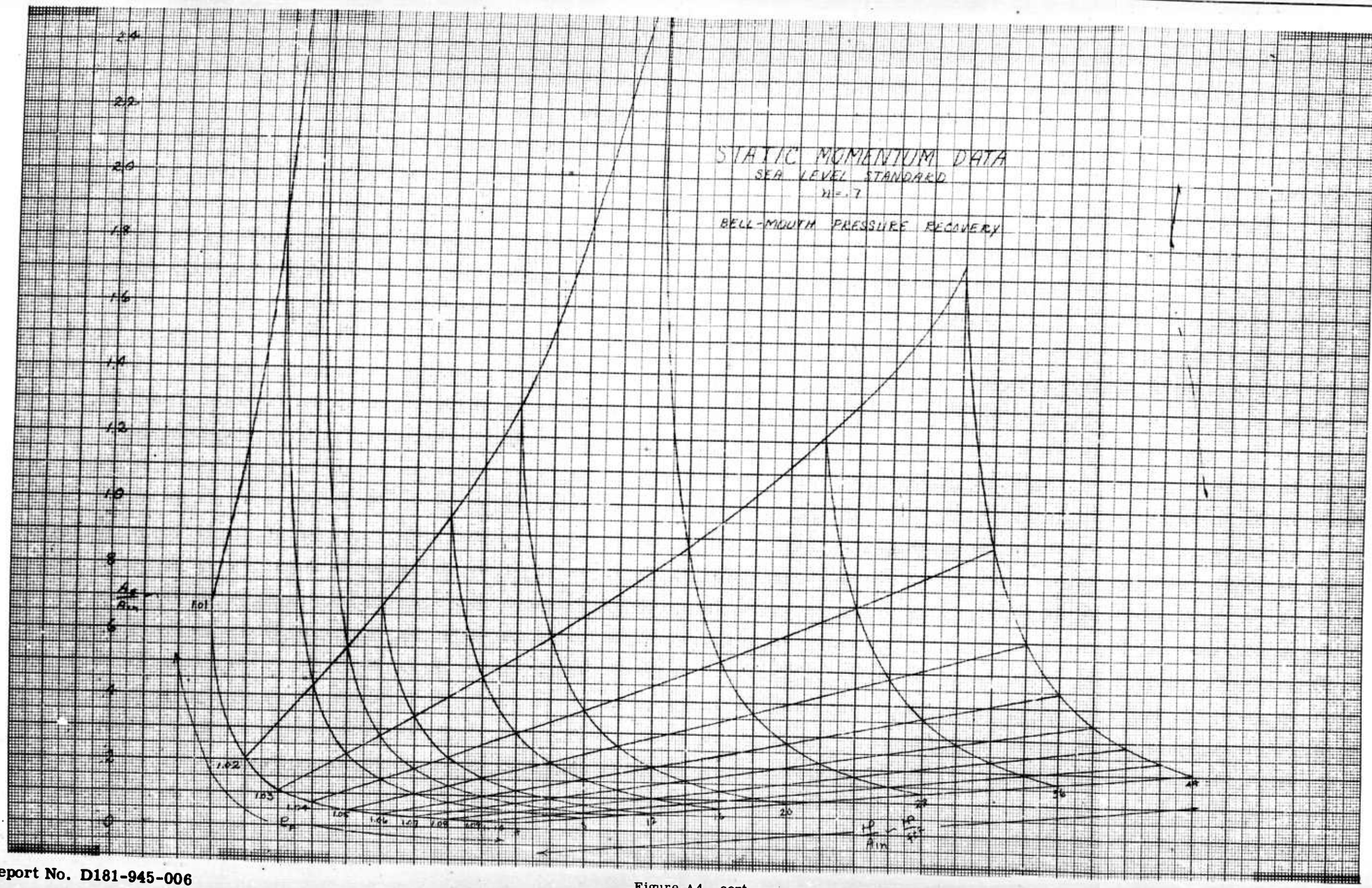

Figure A4 cont

Figure 44 (Cont'd)

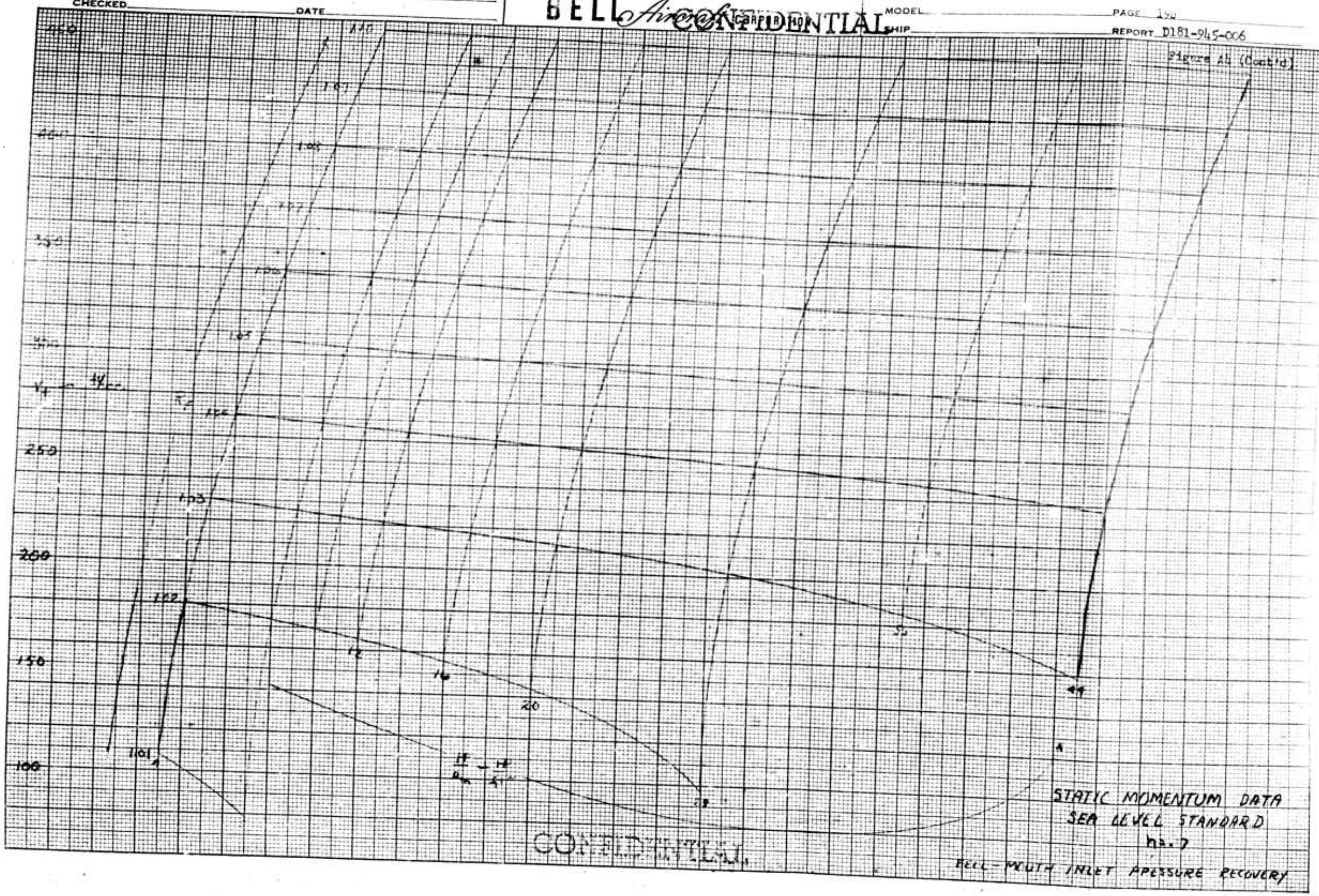

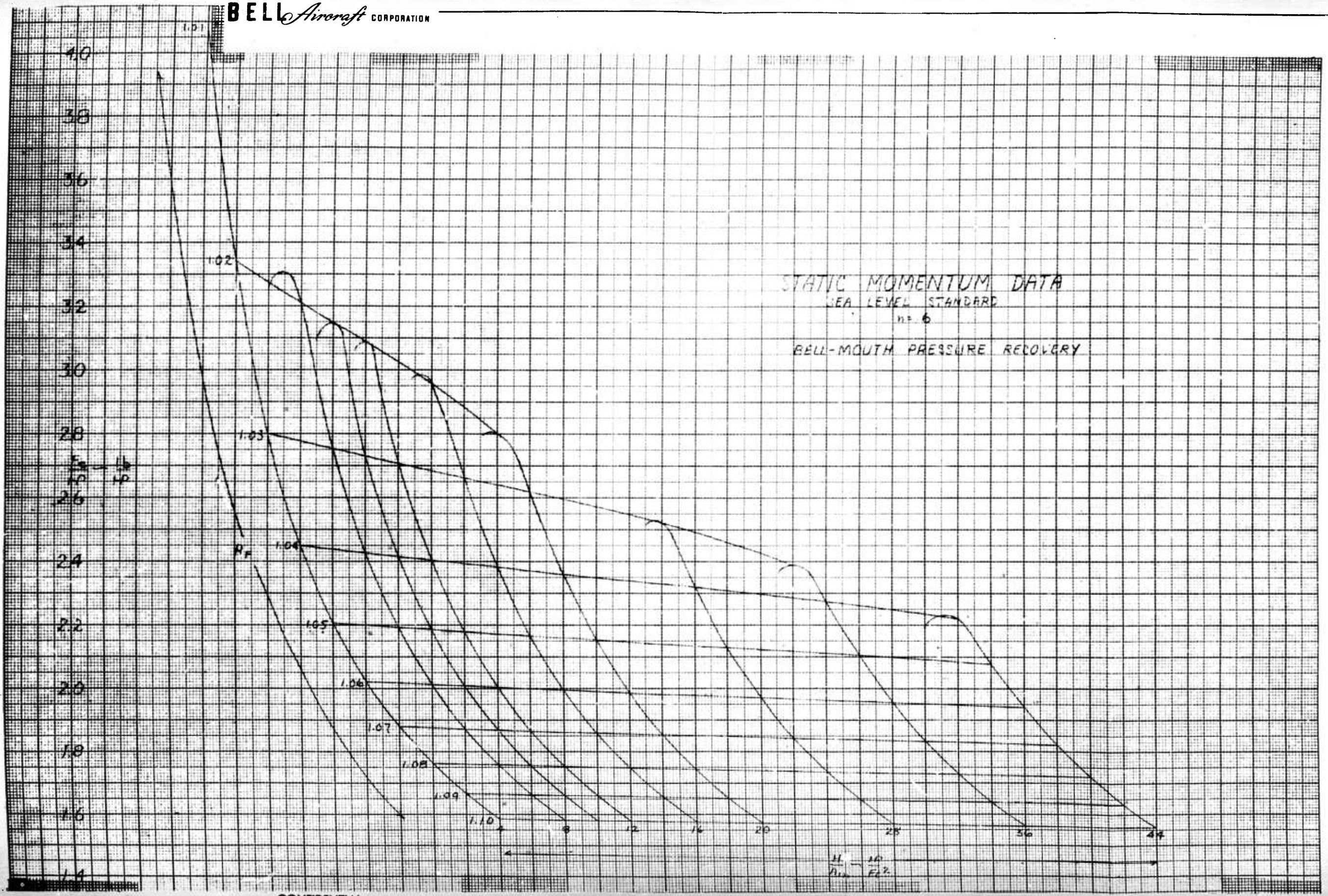
STATIC MOMENTUM DATA
SEA LEVEL STANDARD
n = 6
BELL-MOUTH PRESSURE RECOVERY
1.01
1.02
1.03
1.04
1.05
1.06
1.07
1.08
1.09
1.10
4.0
3.8
3.6
3.4
3.2
3.0
2.8
2.6
2.4
2.2
2.0
1.8
1.6
1.4
4
8
12
16
20
25
36
44

Figure A 5

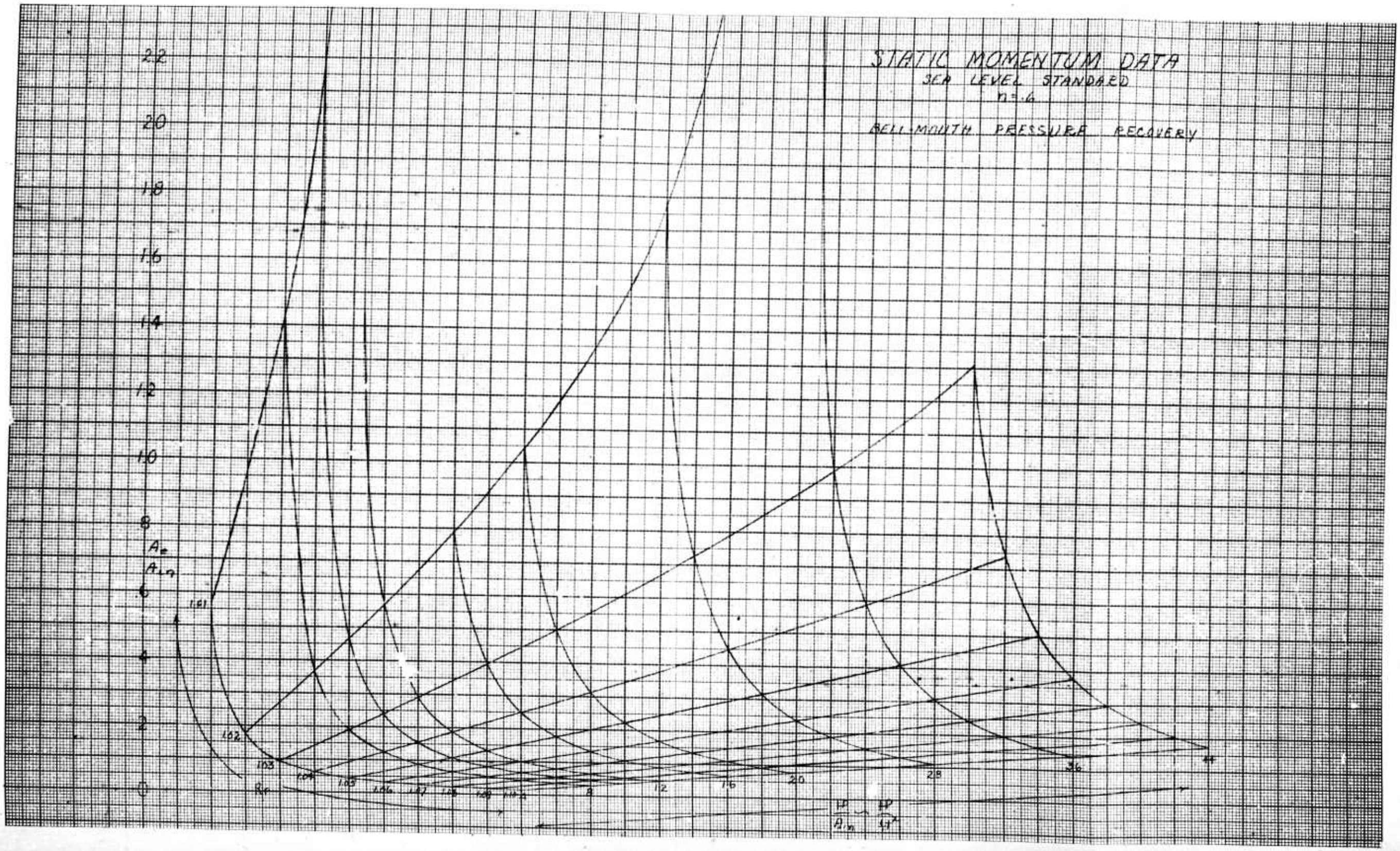

Figure A 5 cont

Figure 45 (Cont'd)

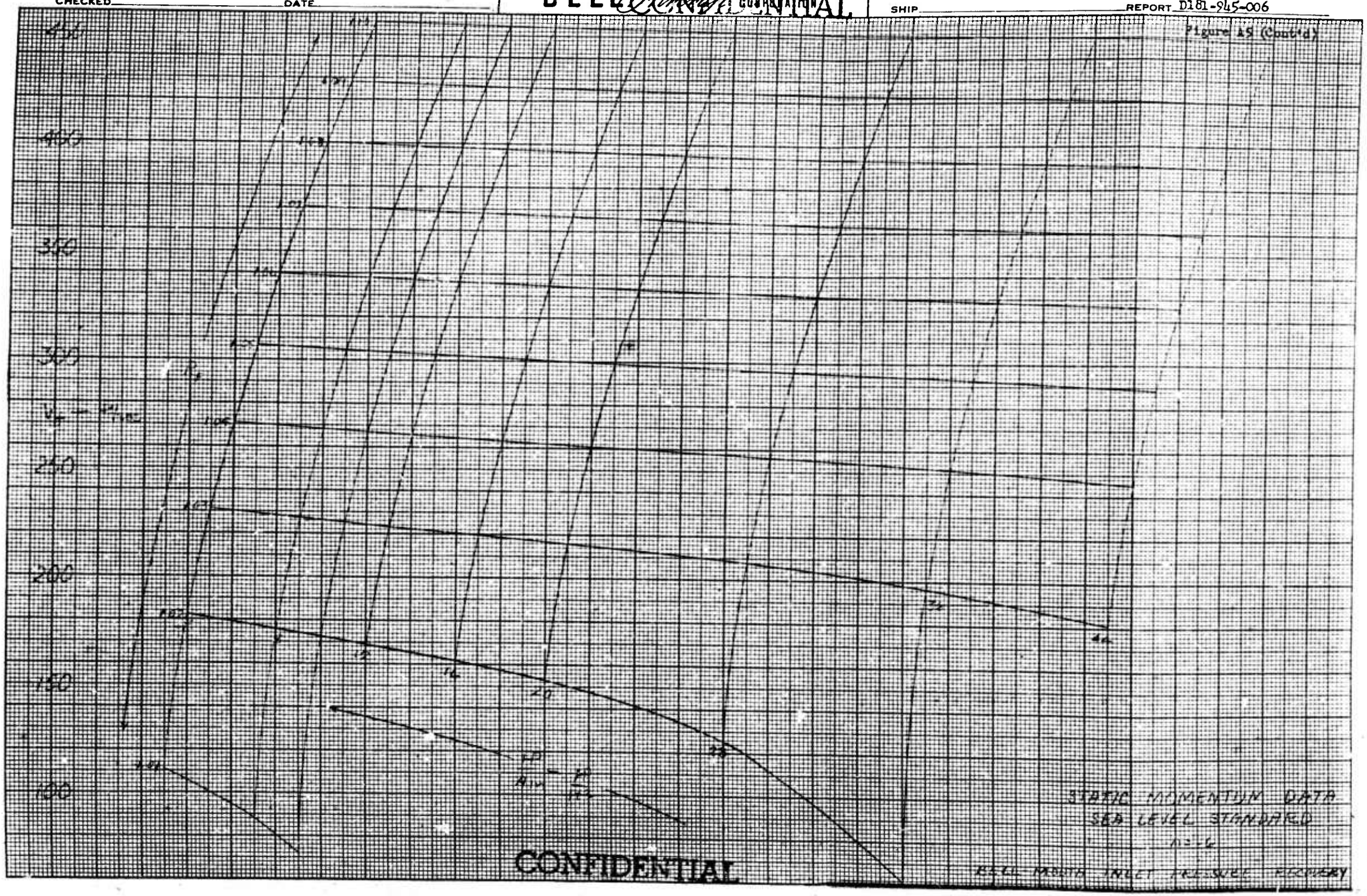

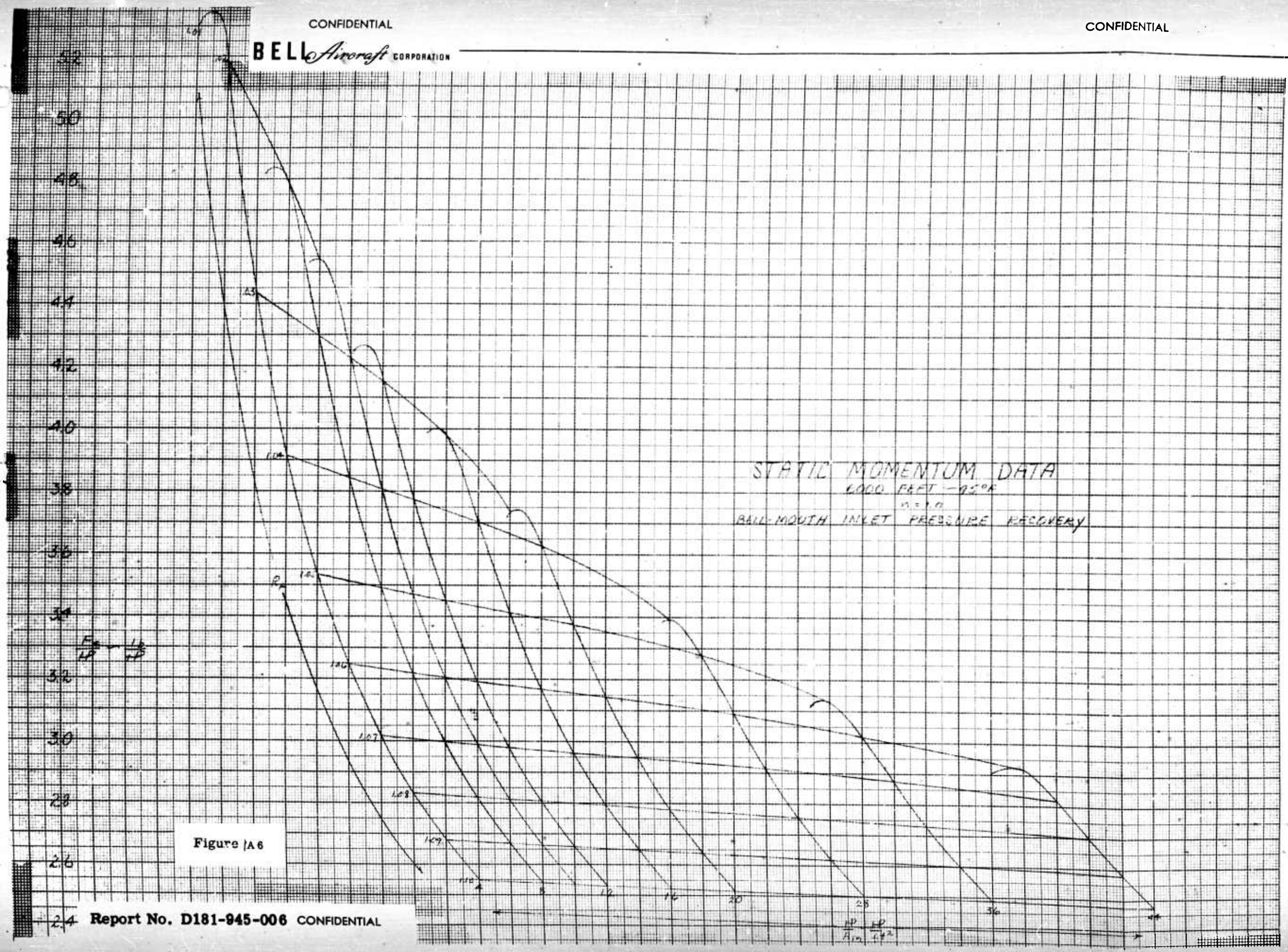
STATIC MOMENTUM DATA
6000 FEET -92°F
BELL-MOUTH INLET PRESSURE RECOVERY
5.2
5.0
4.8
4.6
4.4
4.2
4.0
3.8
3.6
3.4
3.2
3.0
2.8
2.6
2.4
105
110
115
120
125
130
135
140
145
150
155
160
165

Figure 1A6

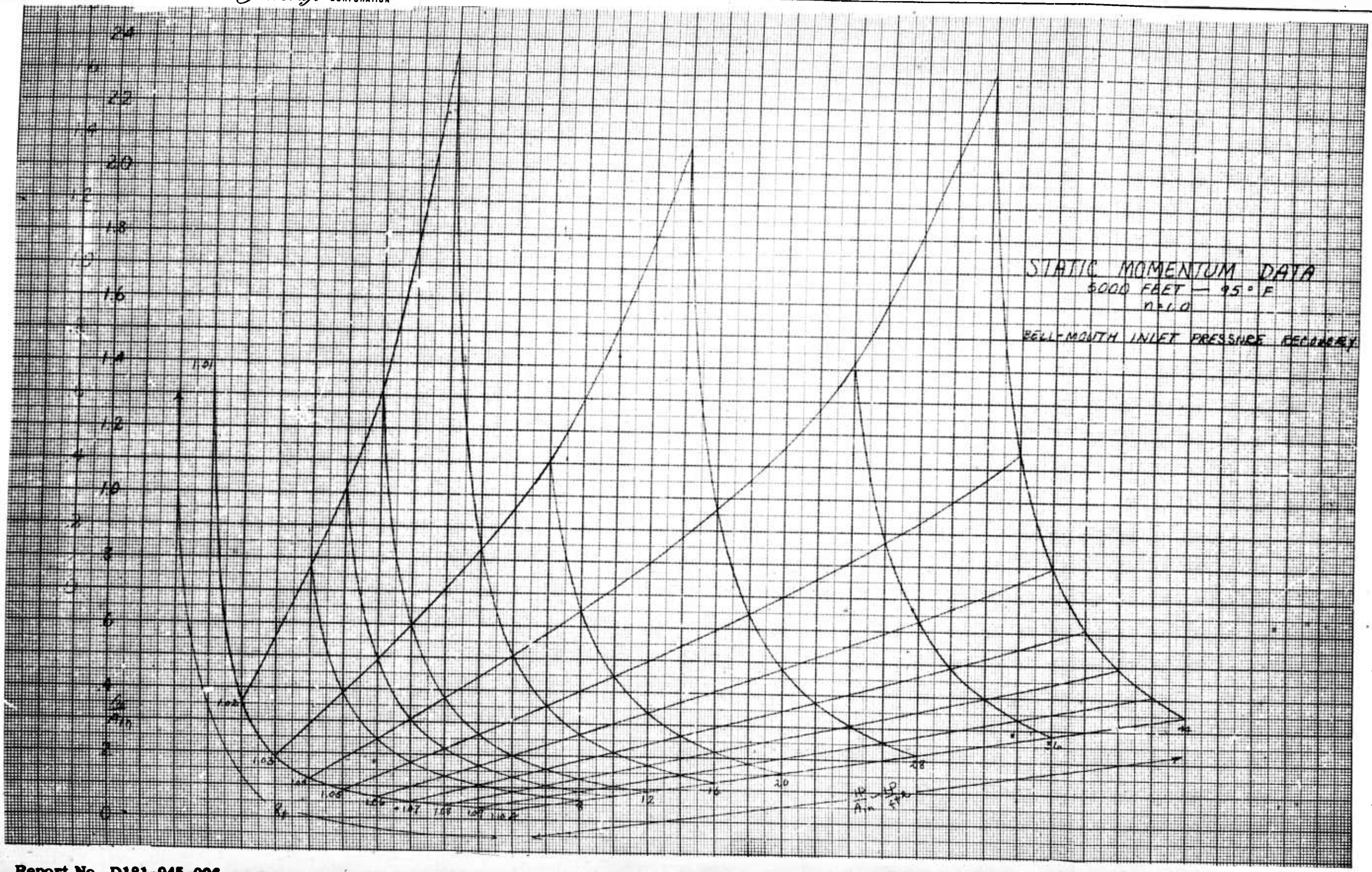

Figure A 6 cont

BY _____ DATE _____
CHECKED _____ DATE _____

BELL Aircraft CORPORATION

CONFIDENTIAL

MODEL _____ PAGE 60
SHIP _____ REPORT D181-945-006

Figure 15 (Cont'd)

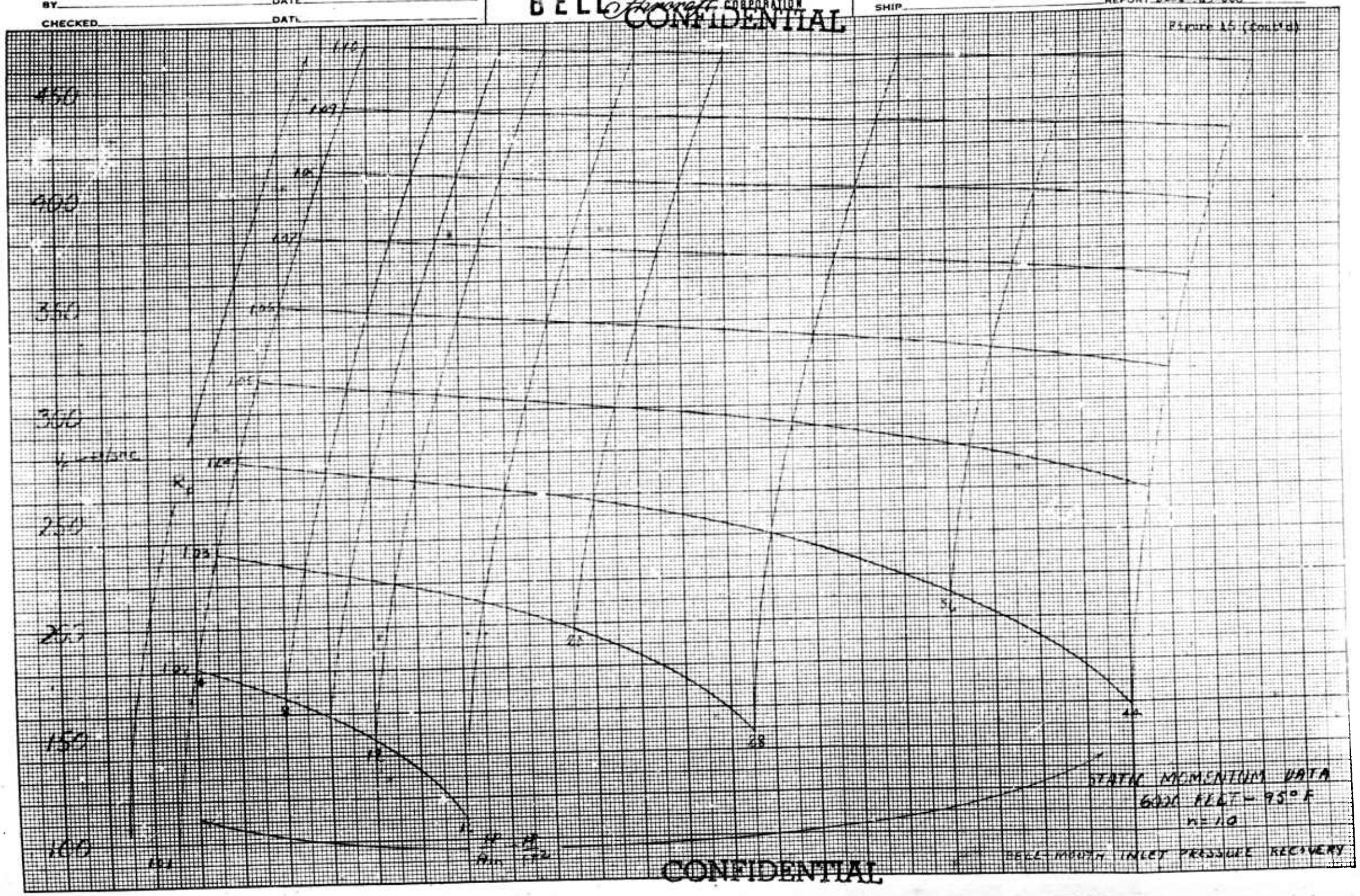

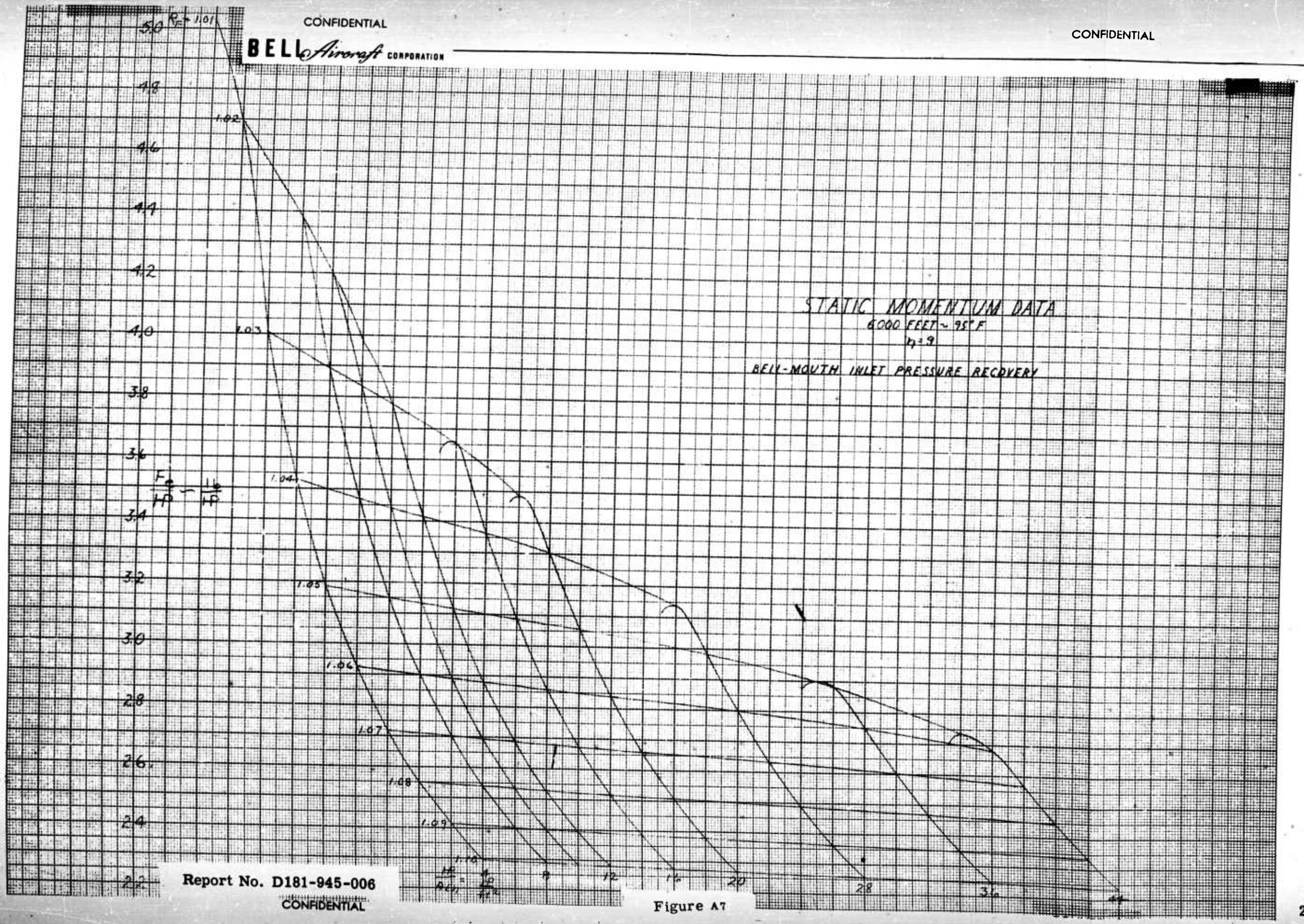
STATIC MOMENTUM DATA
6000 FEET ~ 95° F
$h_1 = 9$
BELL-MOUTH INLET PRESSURE RECOVERY
$R_F = 1.01$
1.02
1.03
1.04
1.05
1.06
1.07
1.08
1.09
1.10
$\frac{F_g}{HP} - \frac{V_0}{HP}$
$\frac{HP}{A_{H_1}} = \frac{V_0}{V_{H_2}}$
5.0
4.8
4.6
4.4
4.2
4.0
3.8
3.6
3.4
3.2
3.0
2.8
2.6
2.4
2.2
4
8
12
16
20
28
36
44

Figure A7

BELL Aircraft CORPORATION

CONFIDENTIAL

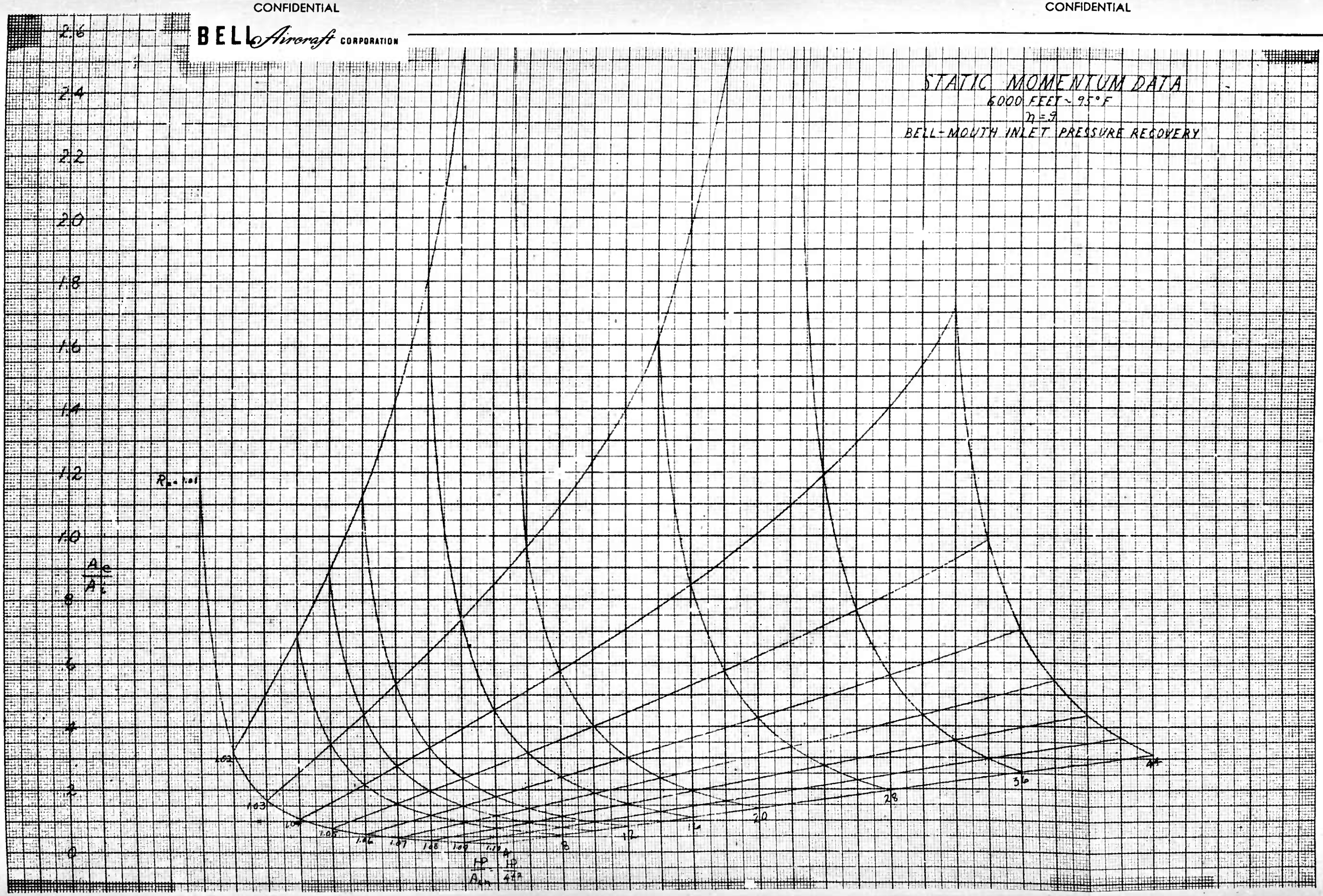

Figure A 7 cont

CONFIDENTIAL

Figure A7 (cont'd)

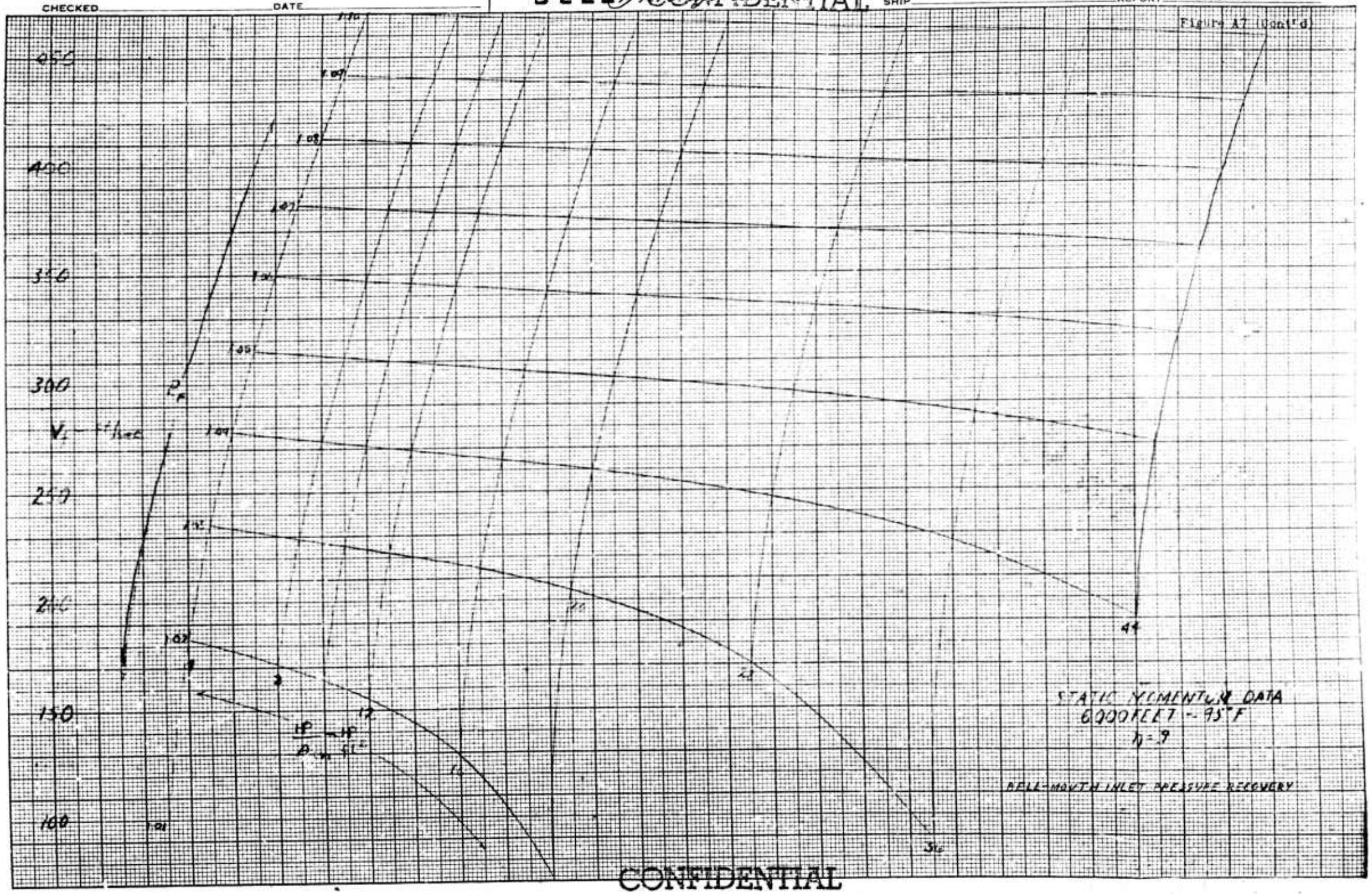

BELL Aircraft CORPORATION

STATIC MOMENTUM DATA
6000 FEET – 95°F
h = .8
BELL-MOUTH INLET PRESSURE RECOVERY

Figure A 8

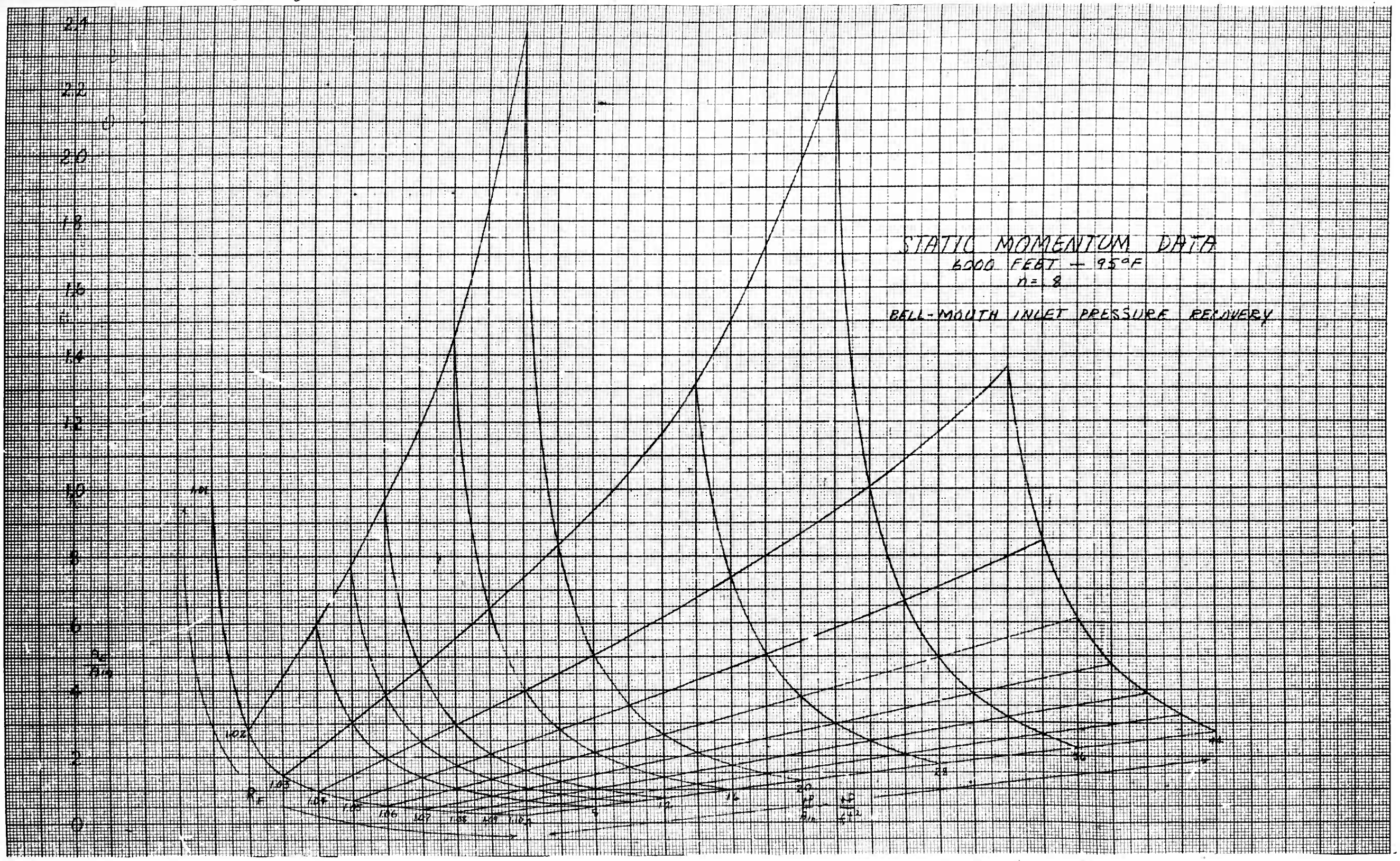

Figure A 8 cont

Figure 48 (Concld)

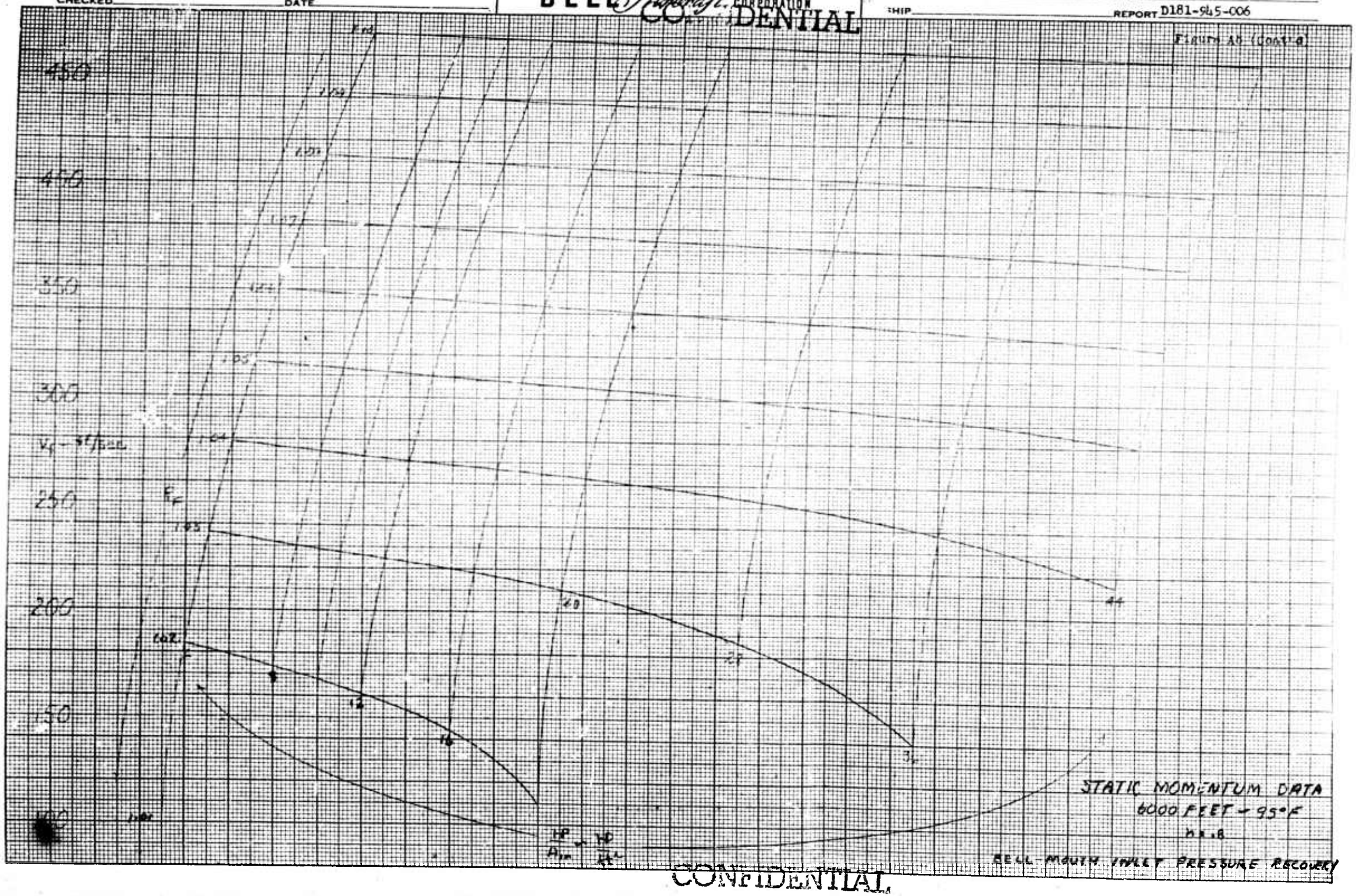

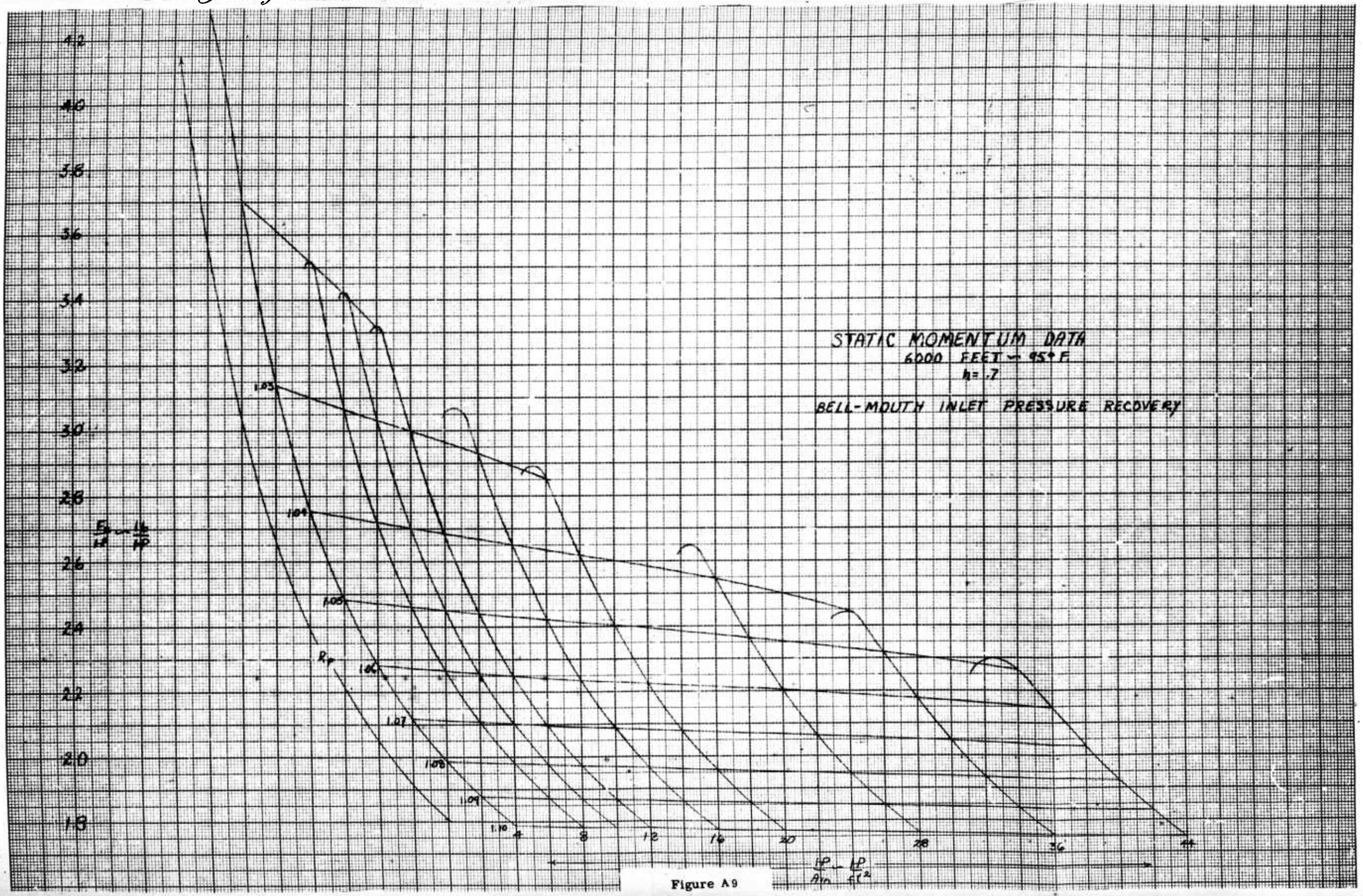
STATIC MOMENTUM DATA
6000 FEET — 95° F.
h = .7
BELL-MOUTH INLET PRESSURE RECOVERY
4.2
4.0
3.8
3.6
3.4
3.2
3.0
2.8
2.6
2.4
2.2
2.0
1.8
$\frac{F_g}{\dot{w}a} - \frac{V_0}{g}$
1.03
1.04
1.05
R_p
1.06
1.07
1.08
1.09
1.10
4
8
12
16
20
28
36
44
$\frac{HP - HP_0}{A_{10}\ q(2)}$

Figure A9

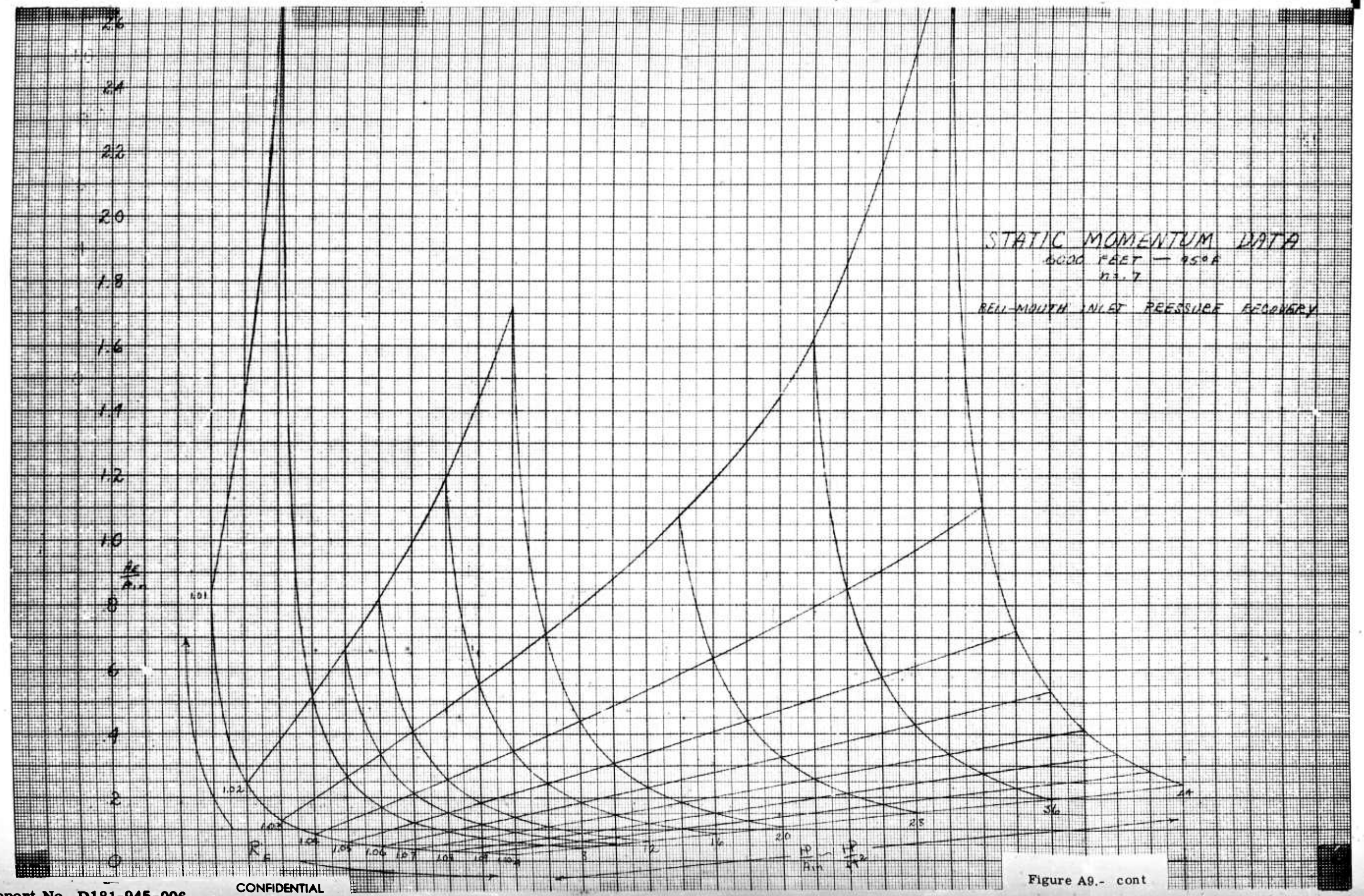

Figure A9.- cont

FIGURE 82 (CONTD)

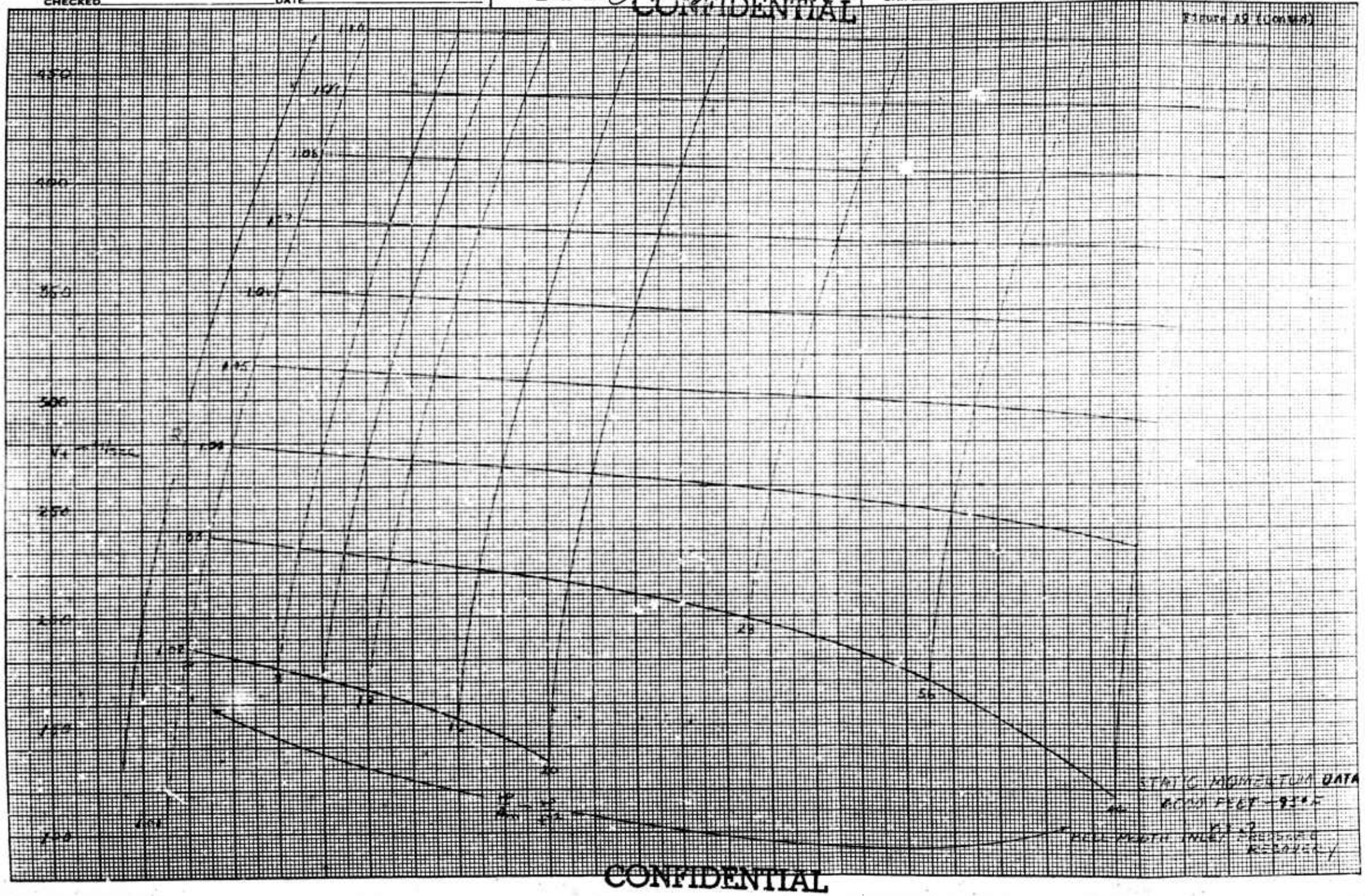

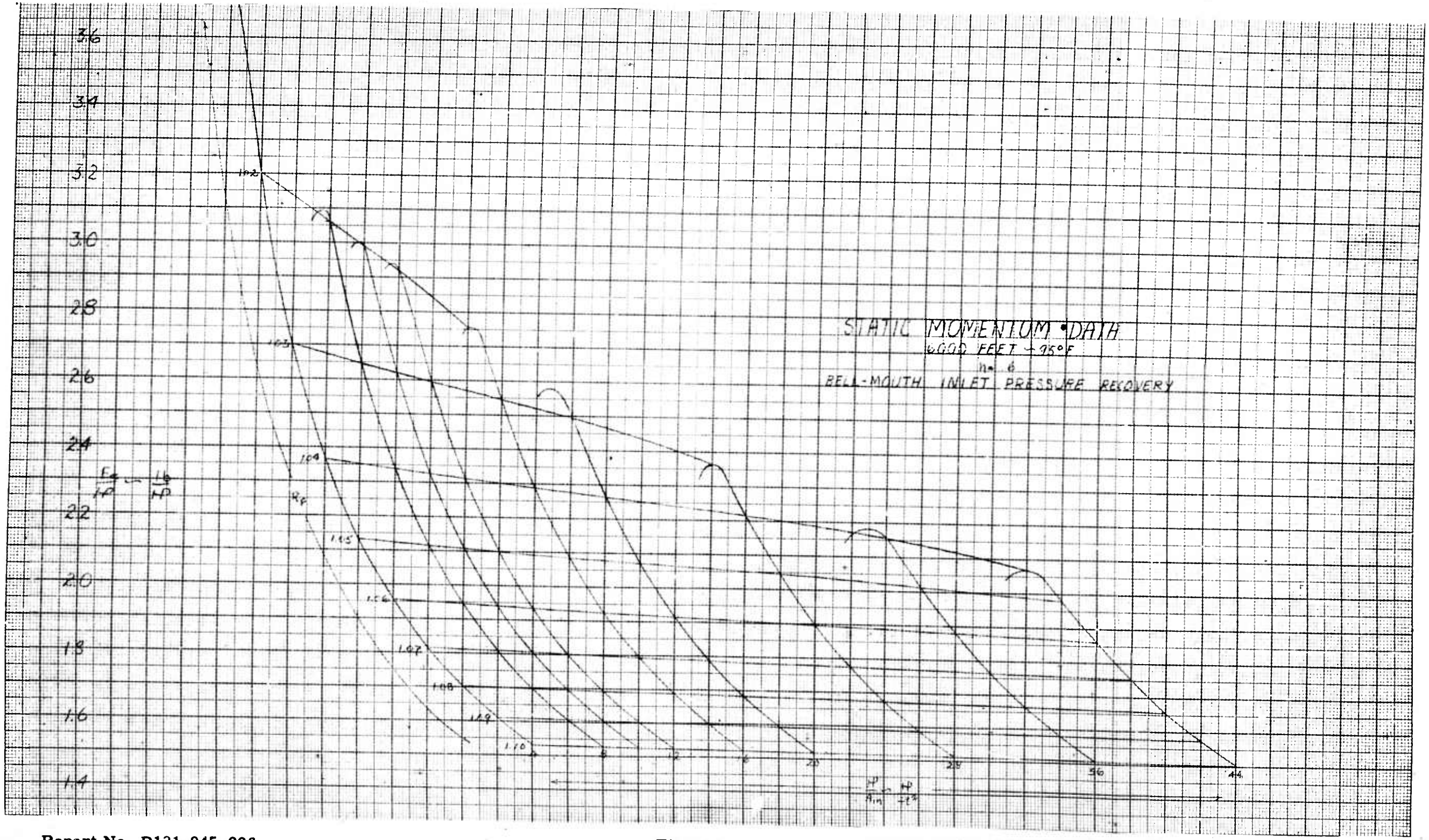
STATIC MOMENTUM PATH
6000 FEET - 95°F
BELL-MOUTH INLET PRESSURE RECOVERY
3.6
3.4
3.2
3.0
2.8
2.6
2.4
2.2
2.0
1.8
1.6
1.4
1.02
1.03
1.04
1.05
1.06
1.07
1.08
1.09
1.10
56
44

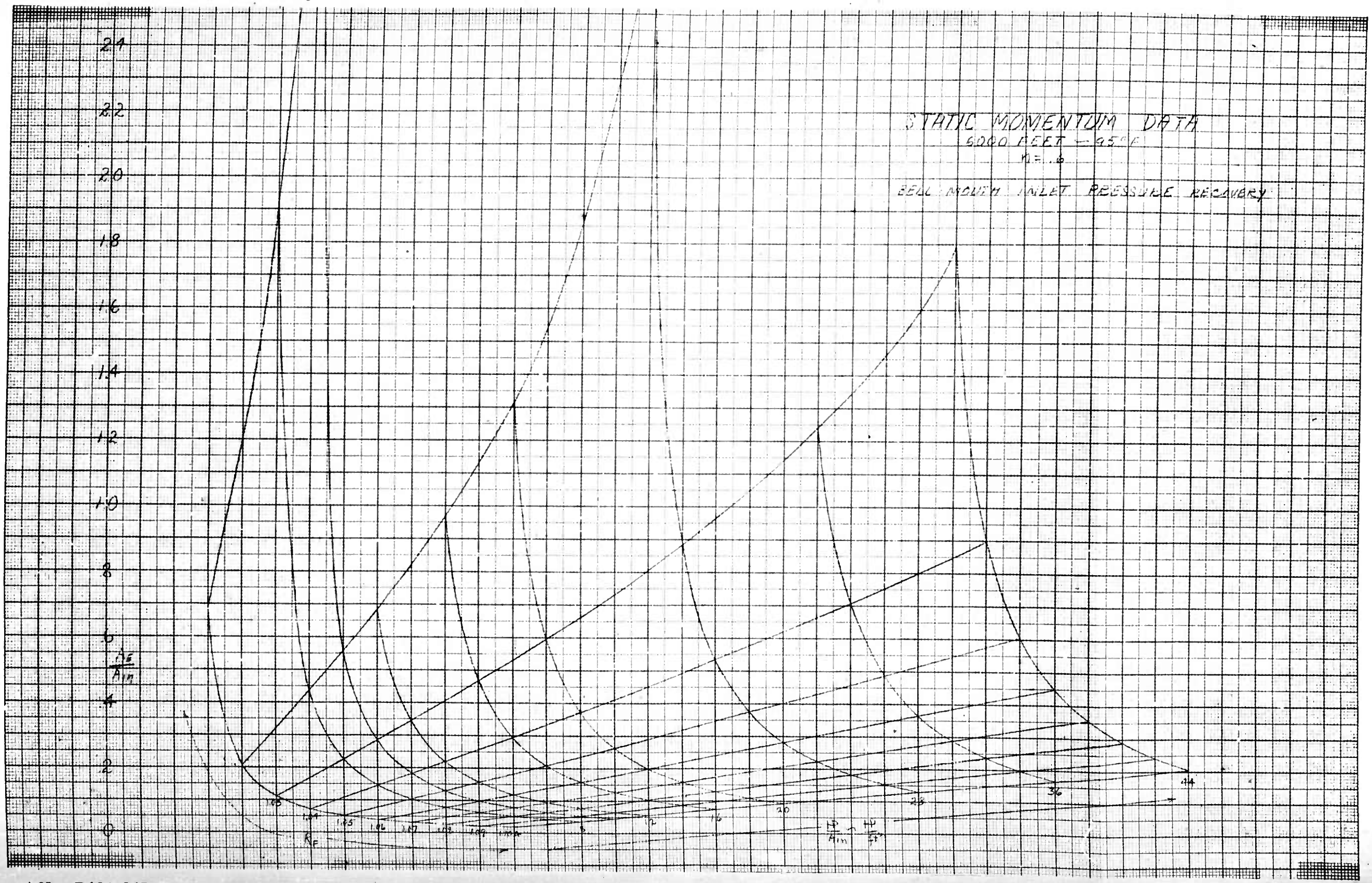

Figure A 10 cont

Figure A10 (Cont'd)

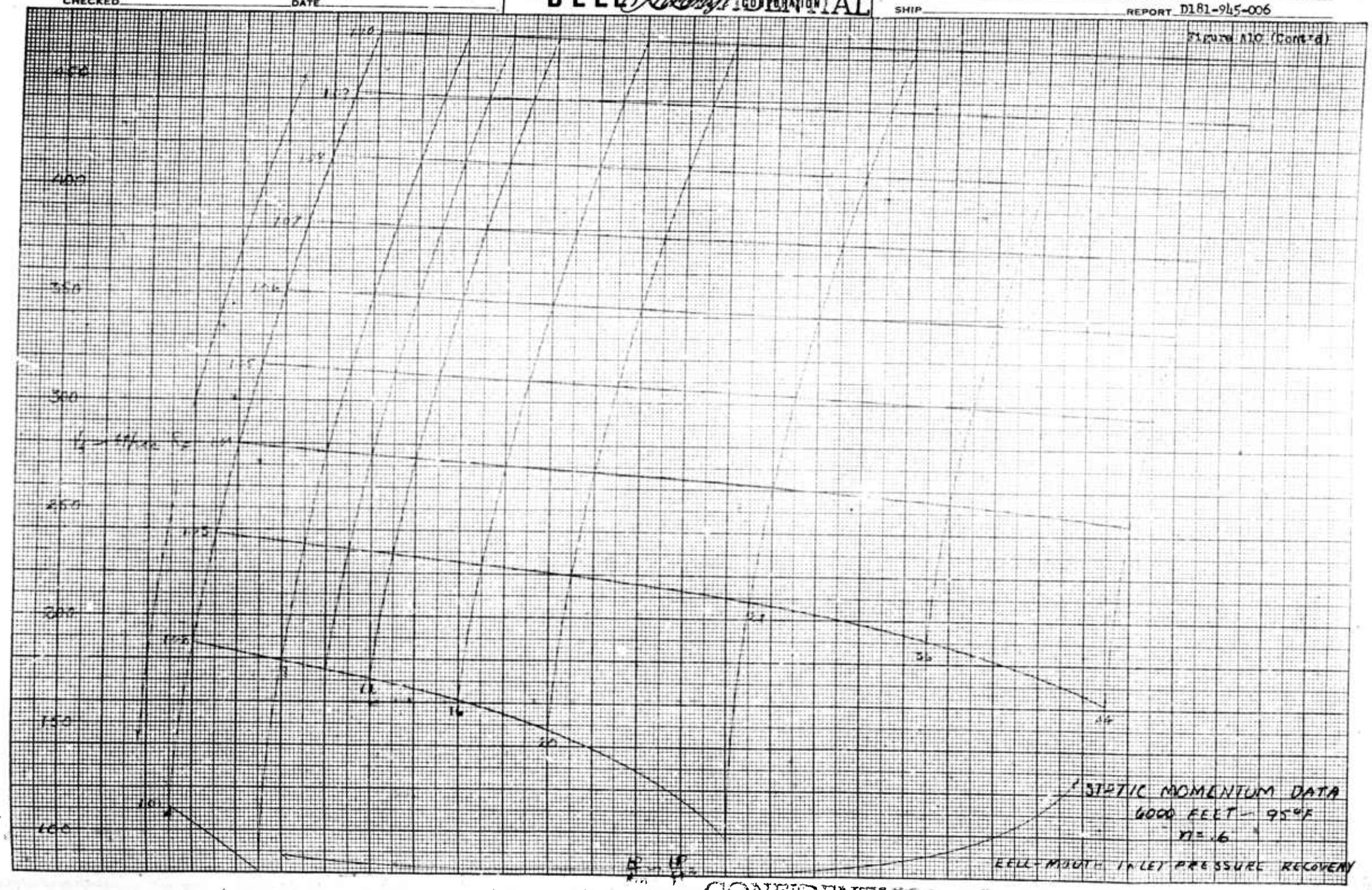

CONFIDENTIAL

Figure All

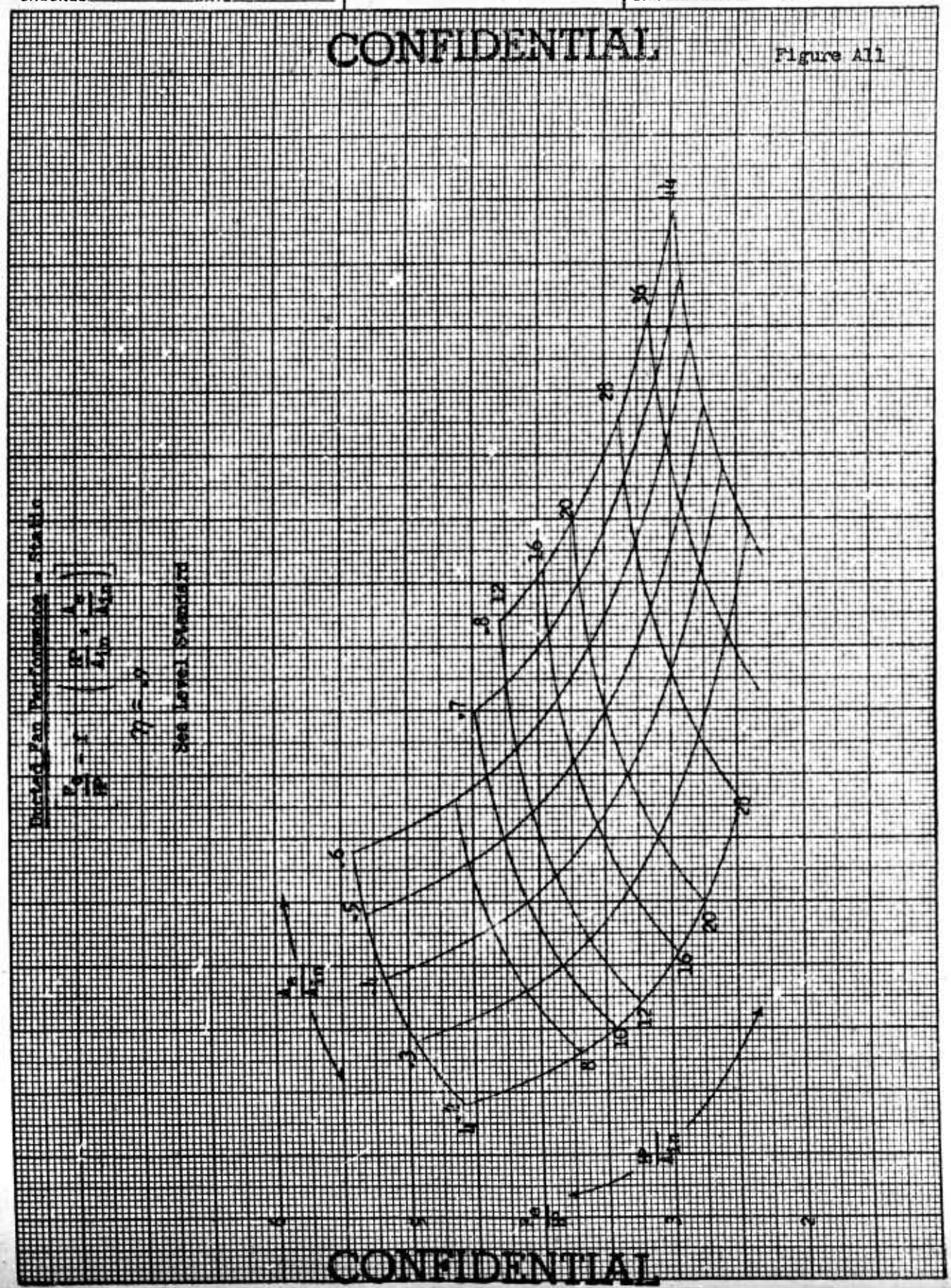

Figure A12

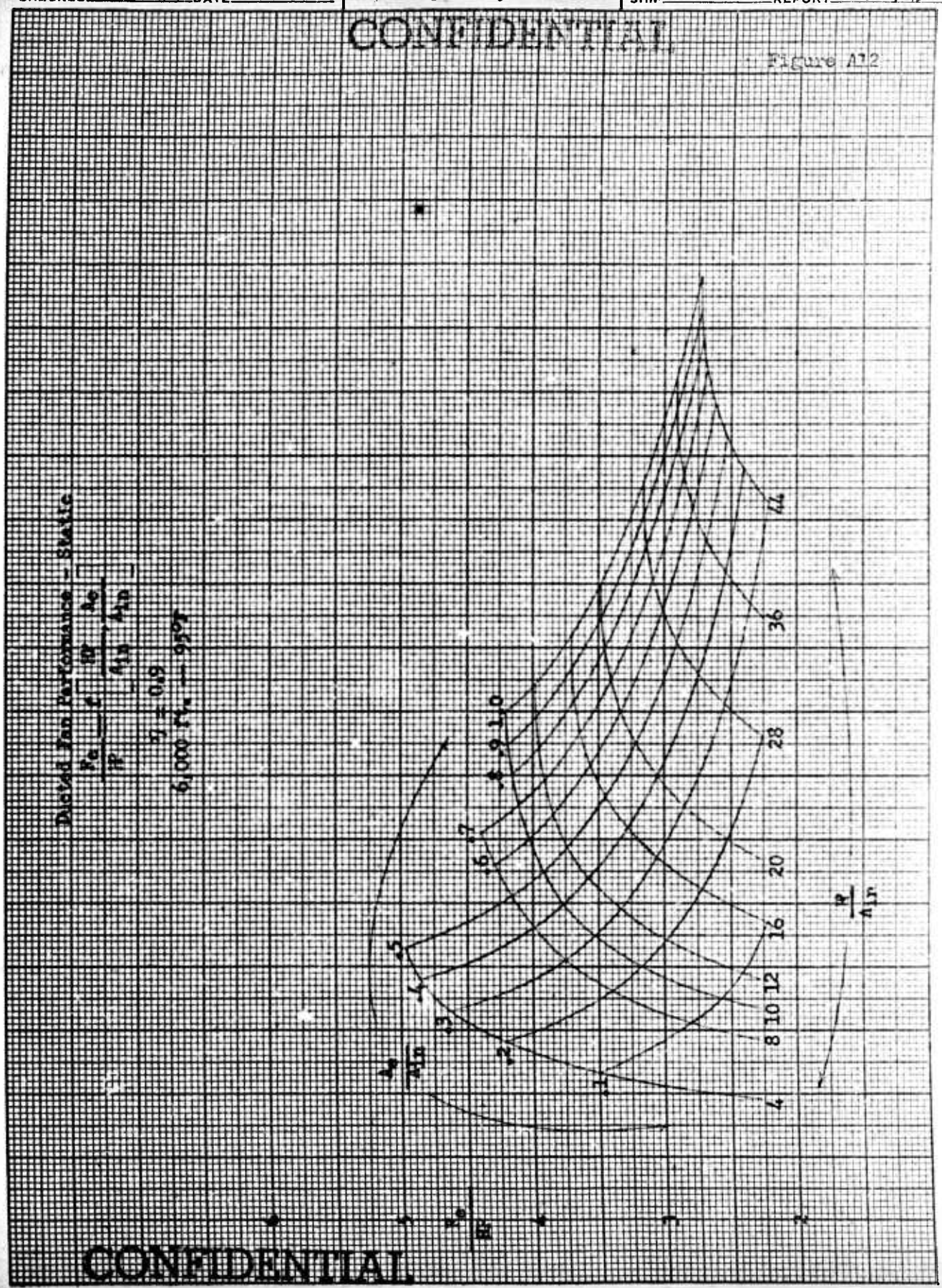

APPENDIX B

APPENDIX B

APPENDIX B (Continued)

Summary of In-Flight IBM Procedure

Input Values: a_o, T_o, ρ_o, P_o, HP/A_f, V_o, R_F, η

Constants: g = 32.2, R = 53.3, γ = 1.4, K = 10.95, k = .97

Step	Calculation	Equation
1.	M_o	V_o/a_o
2.	P_{t_o}/P_o	(1 - 3)
3.	T_{t_o}/T_o	(1 - 8)
4.	P_{t_o}	P_o ②
5.	T_{t_o}	T_o ③
6.	V_f	(1 - 40)
7.	M_f^2	(1 - 41)
8.	m/A_f	(1 - 42)
9.	V_e	(1 - 43)
10.	P_{t_e}/P_e	R_F k ②
11.	P_{t_f}/P_f	(1 - 3)
12.	V_e	(1 - 39)

Determine V_e satisfying steps ⑨ and ⑫ by iteration process.

13.	F/A_f	(1 - 44)
14.	F/HP	(1 - 45)

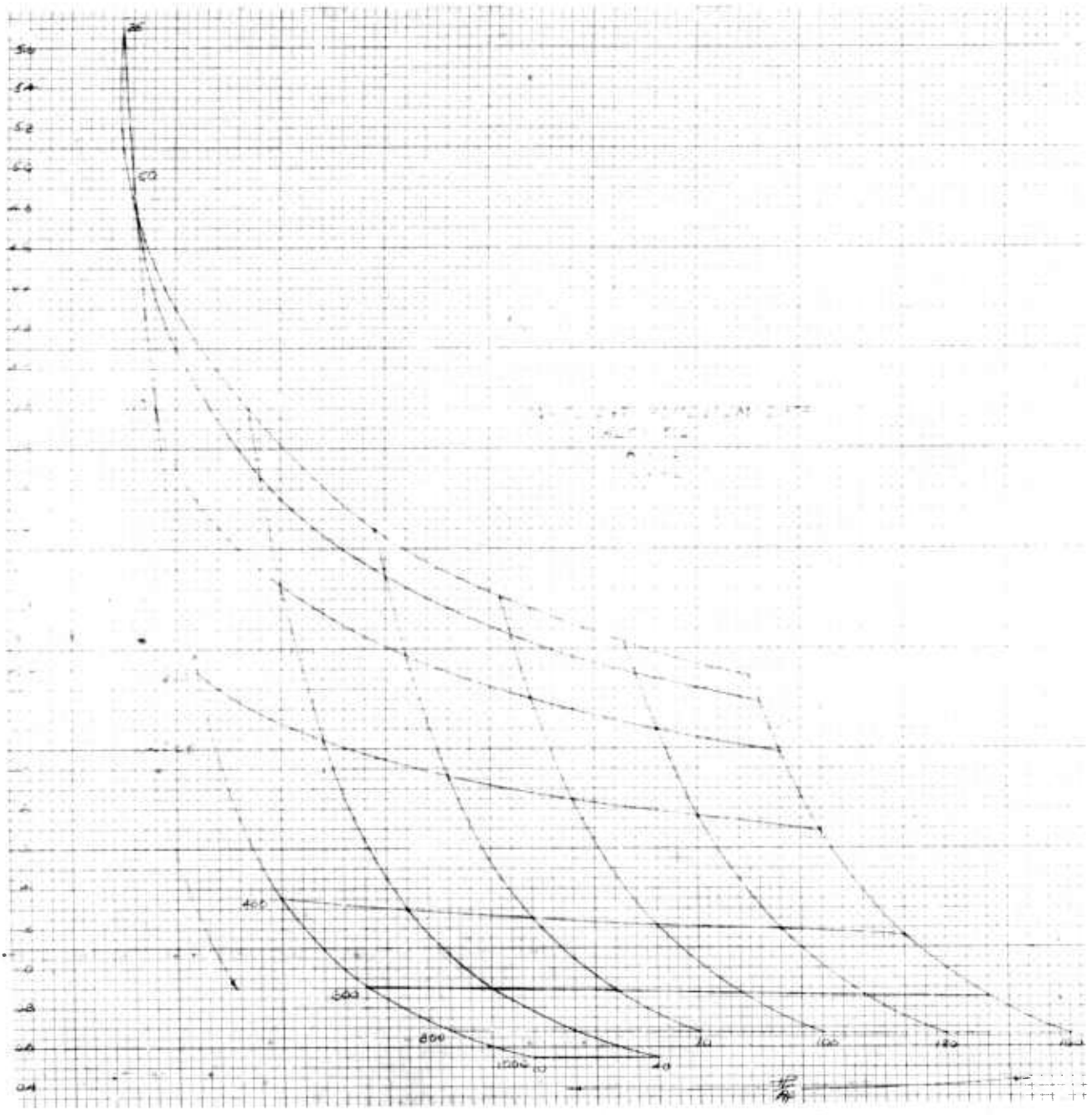

Figure B1

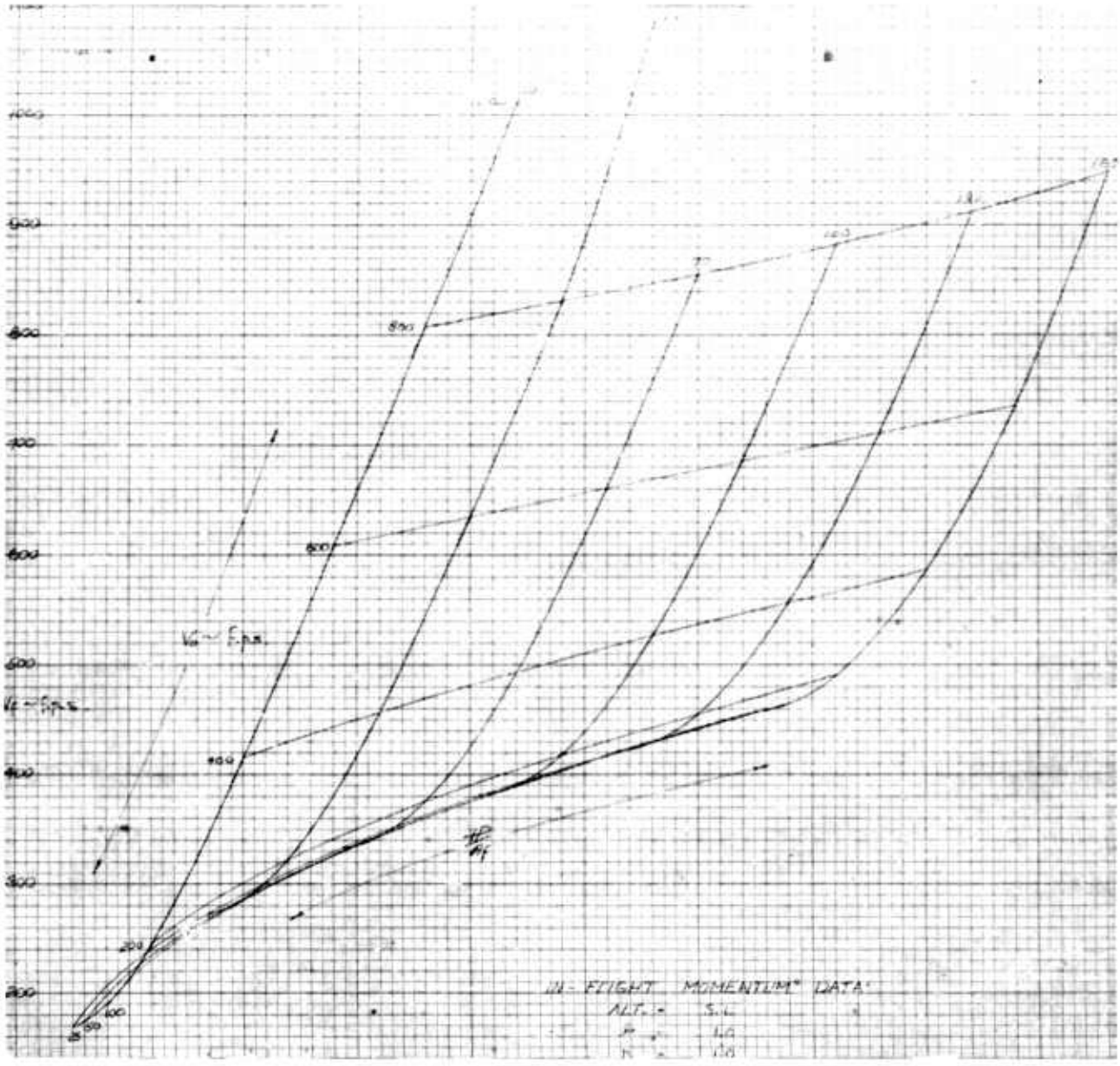

Report No. D181-945-006 Figure B1 cont

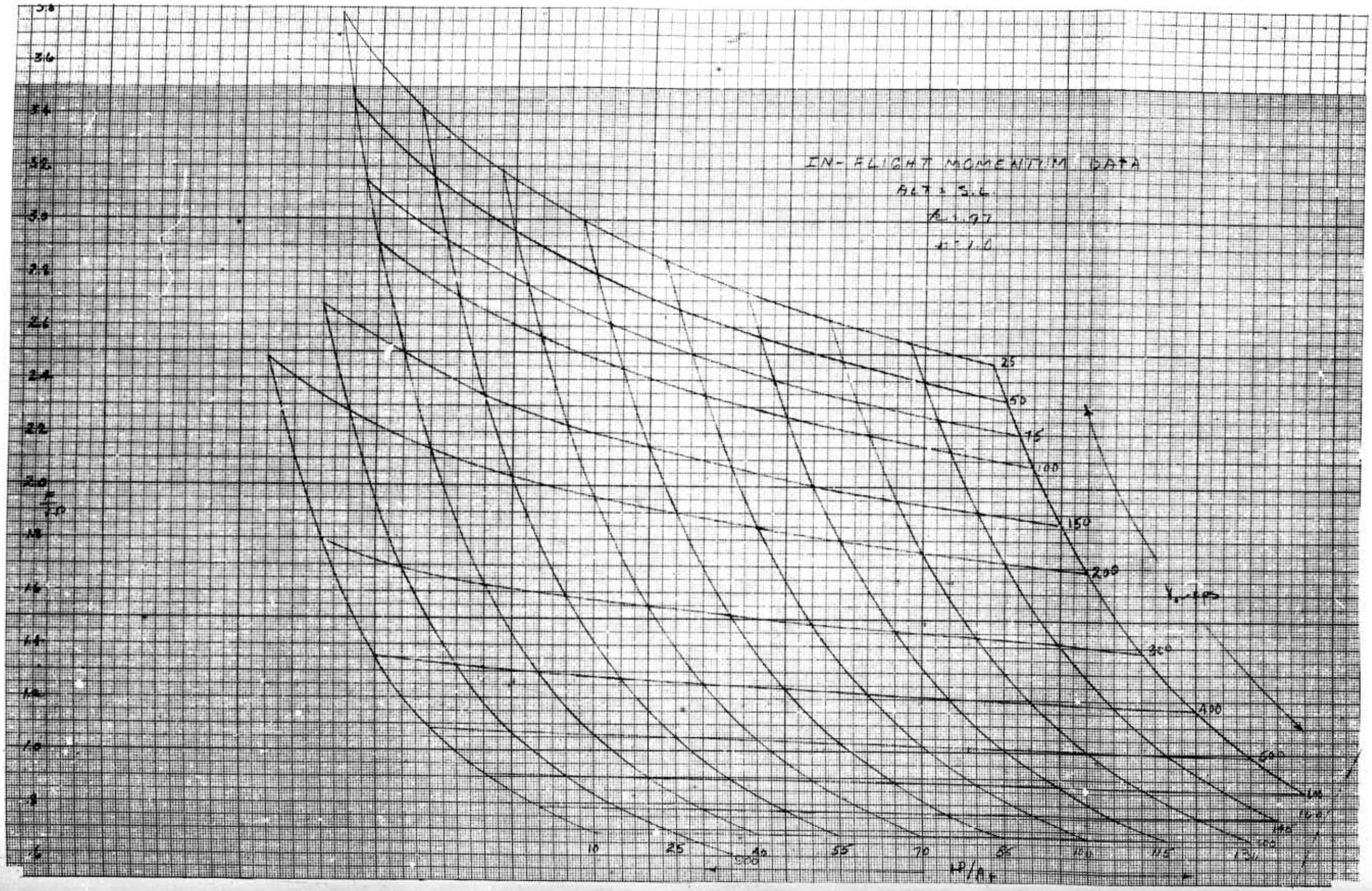
IN-FLIGHT MOMENTUM DATA
ALT = S.L.
M = .97
ΔT = 1.0
25
50
75
100
150
200
300
400
500
600
10
25
40
55
70
85
100
115
130
HP/A

Figure B2

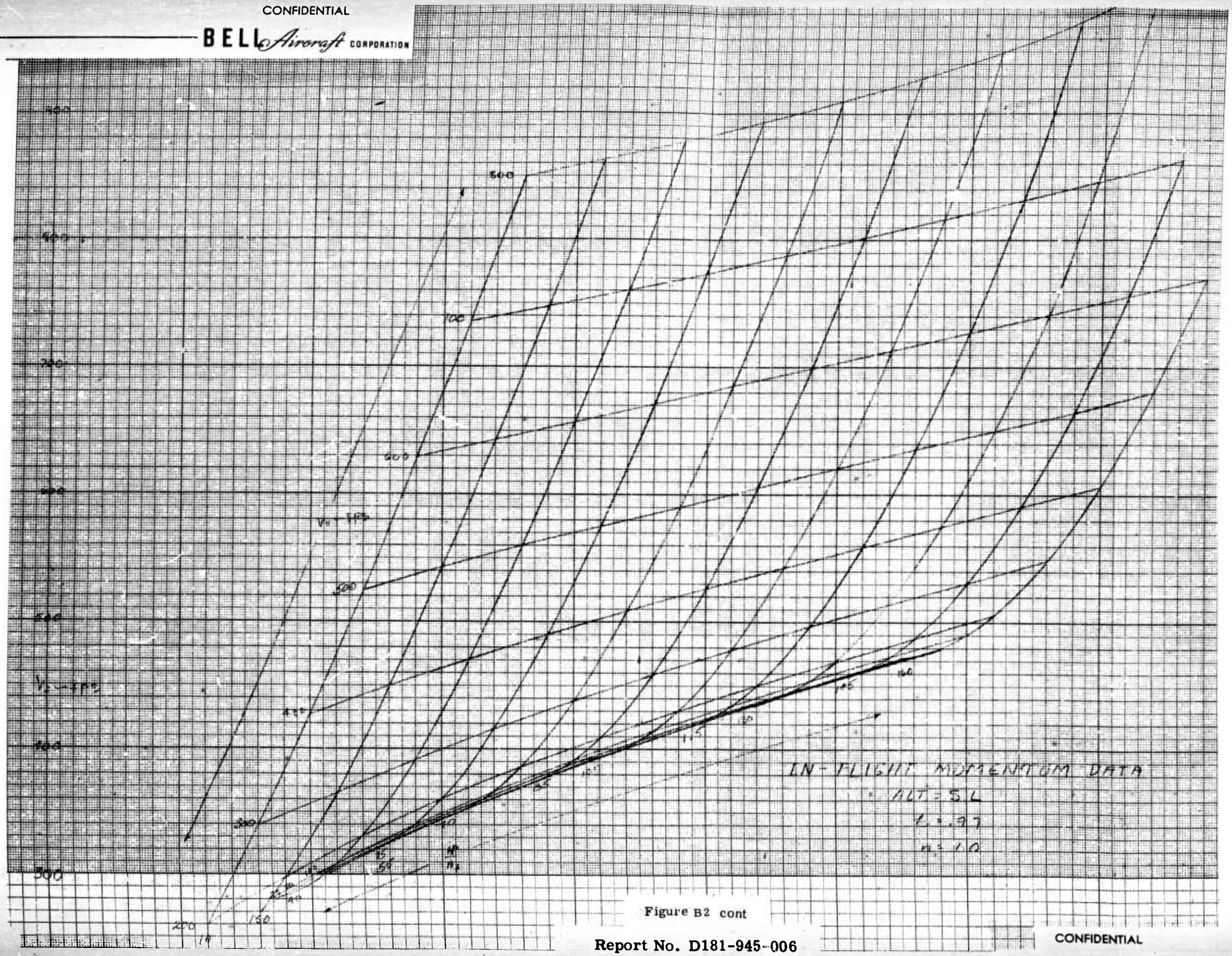

Figure B2 cont

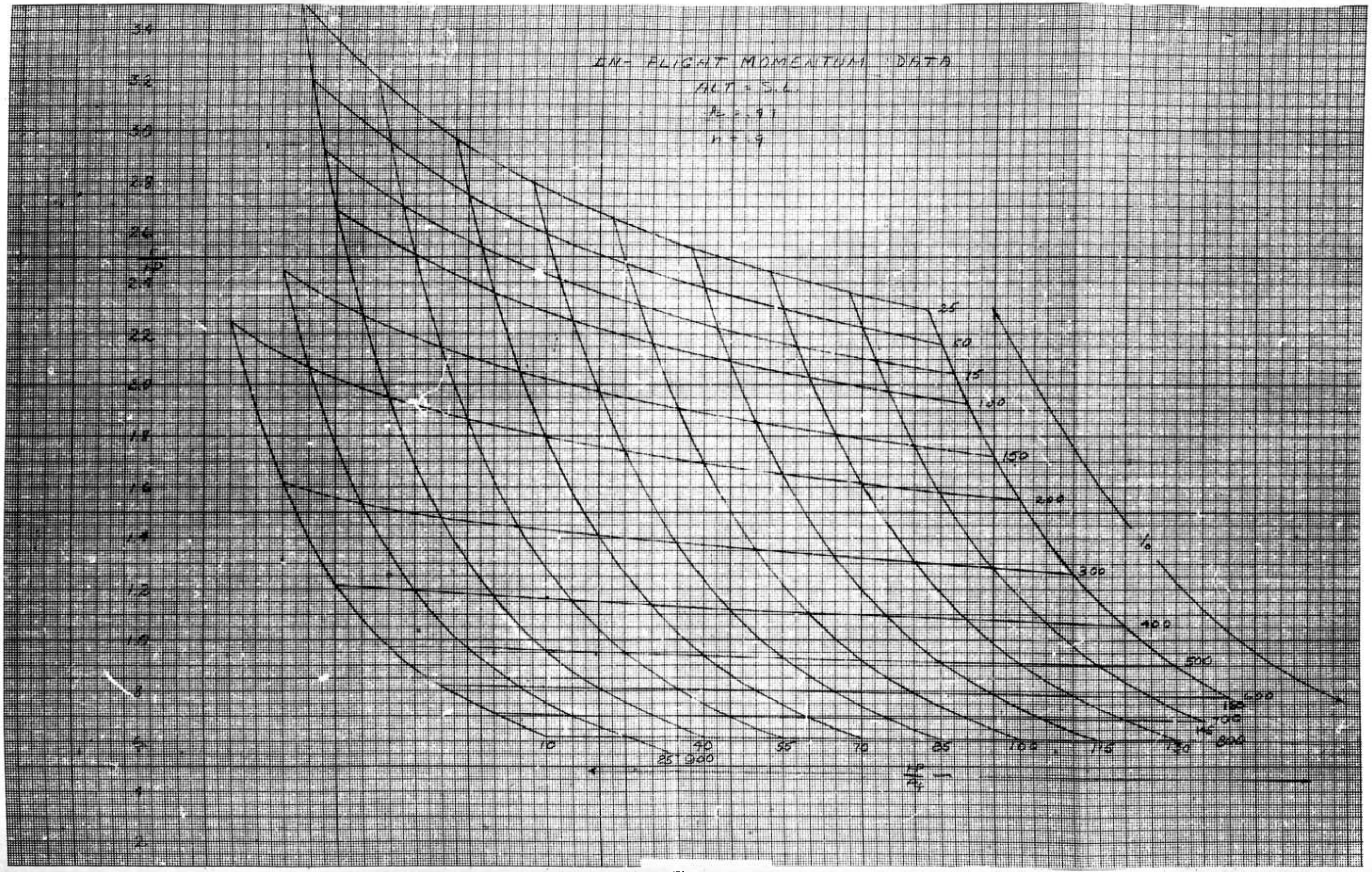
IN-FLIGHT MOMENTUM DATA
ALT = S.L.
R_c = .91
M = .9
3.4
3.2
3.0
2.8
2.6
$\frac{T_0}{T_{01}}$
2.4
2.2
2.0
1.8
1.6
1.4
1.2
1.0
.8
$\frac{P_2}{P_{01}}$
1.0
.2
25
50
75
100
150
200
300
400
500
600
700
800
900
10
25
40
55
70
85
100
115
130
145
$\frac{W\sqrt{\theta}}{\delta A_1}$

Figure B3

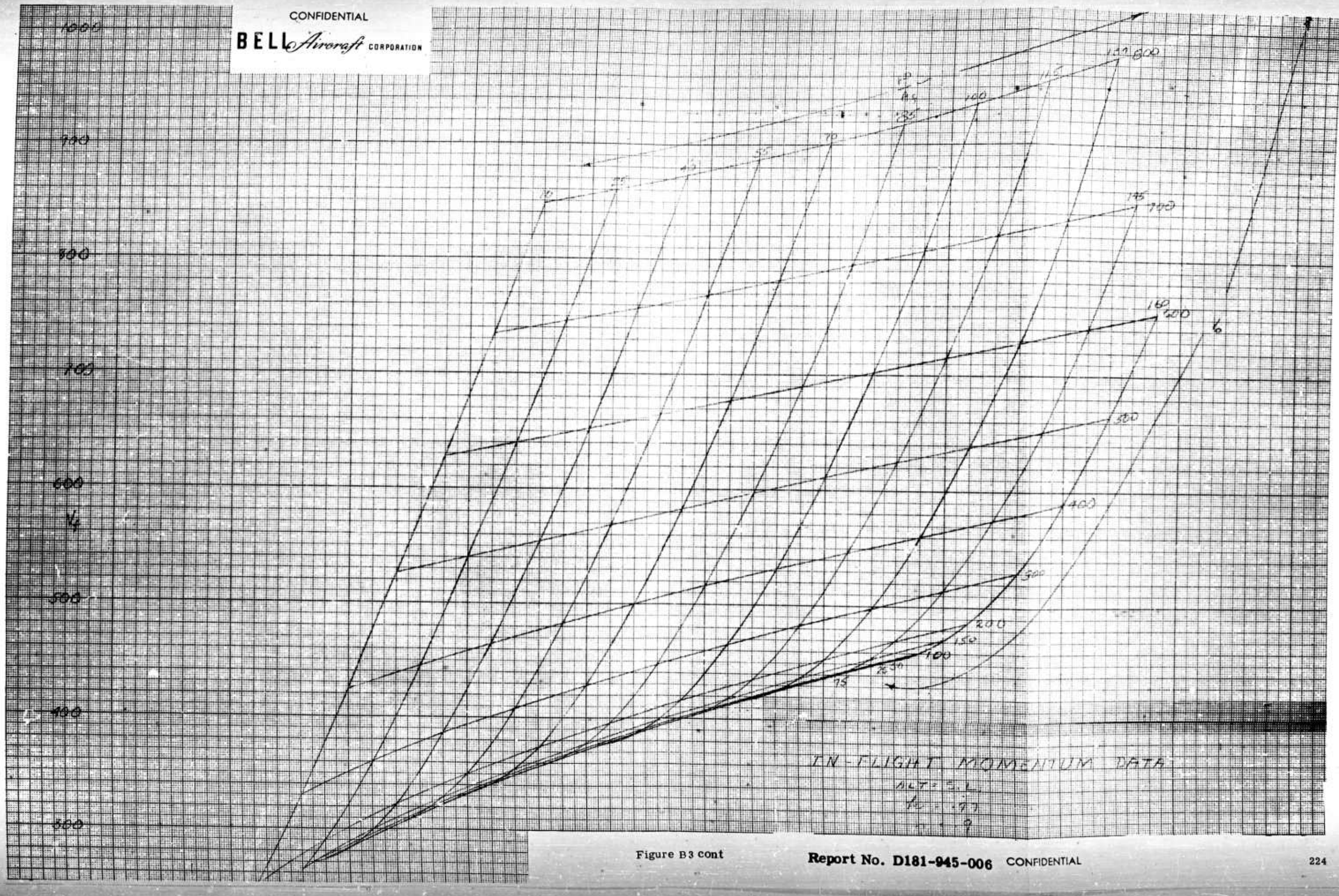

Figure B3 cont

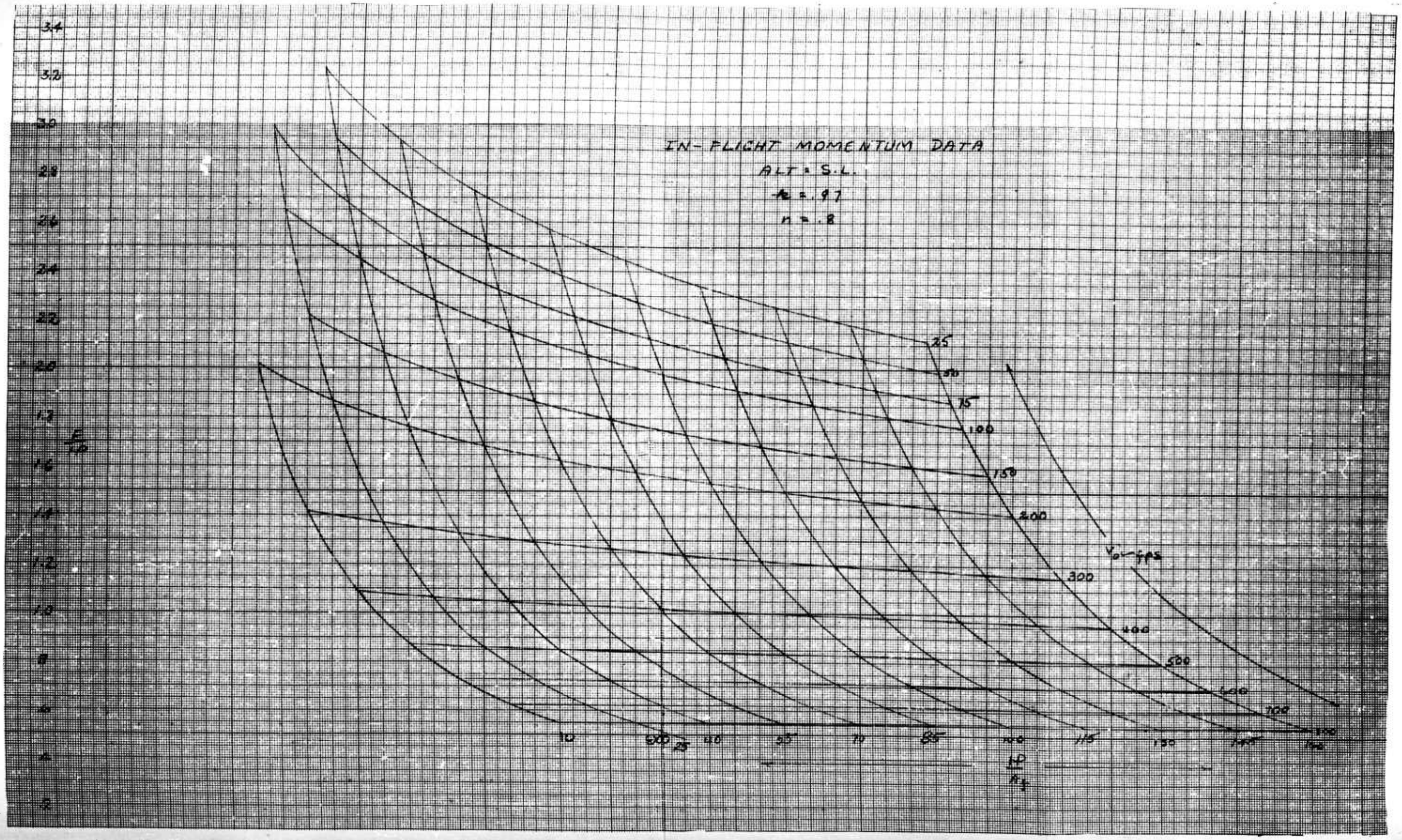
IN-FLIGHT MOMENTUM DATA
ALT = S.L.
M = .97
n = .8
3.4
3.2
3.0
2.8
2.6
2.4
2.2
2.0
1.8
1.6
1.4
1.2
1.0
.8
.6
.4
.2
0
$\frac{F}{A_0}$
25
50
75
100
150
200
V_0 - fps
300
400
500
600
700
800
10
20
25
40
55
70
85
100
115
150
200
250
$\frac{HP}{lb_s}$

Figure B4

BELL Aircraft CORPORATION

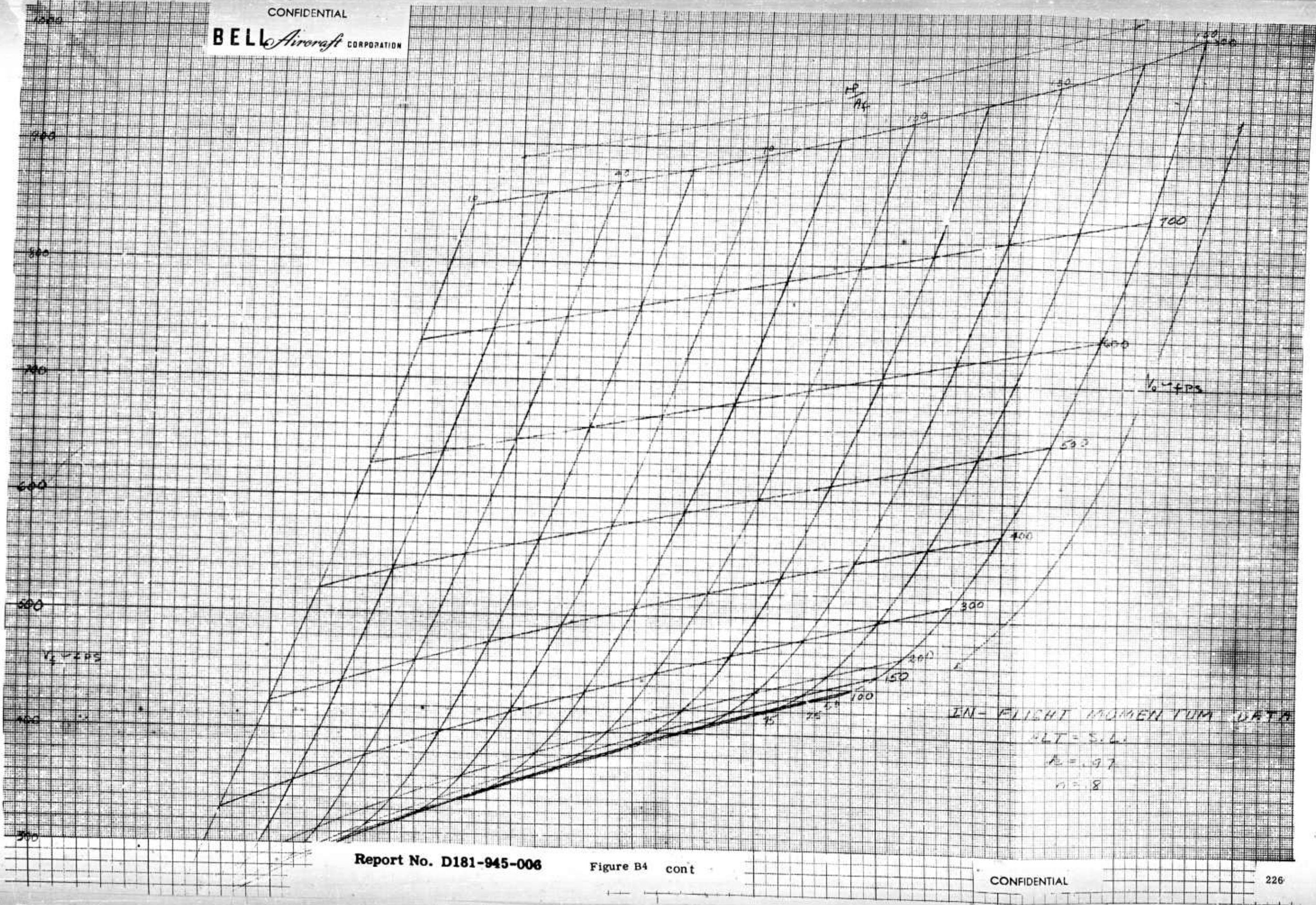

Report No. D181-945-006 Figure B4 cont

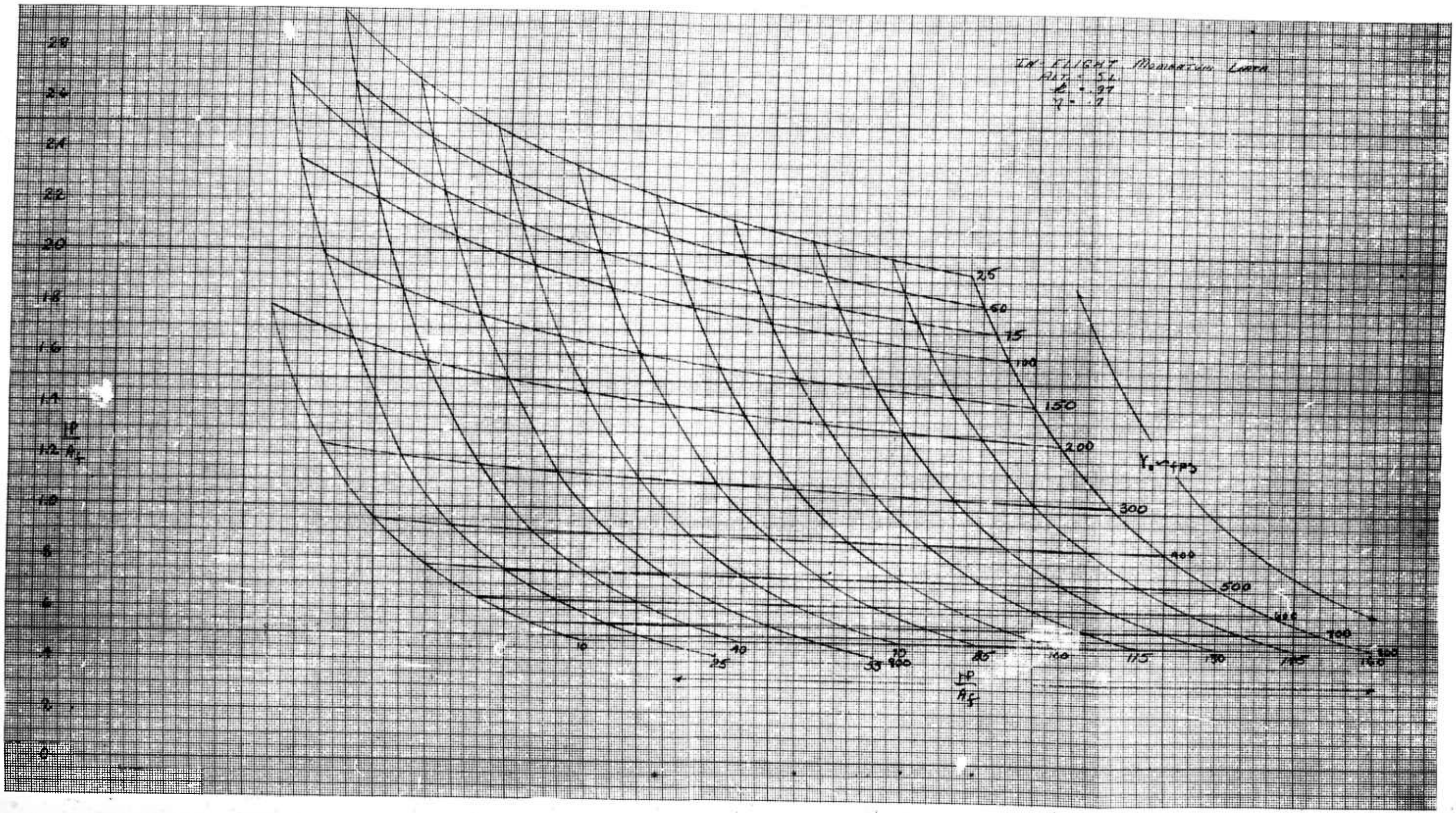

Report No. D181-945-006

Figure B5

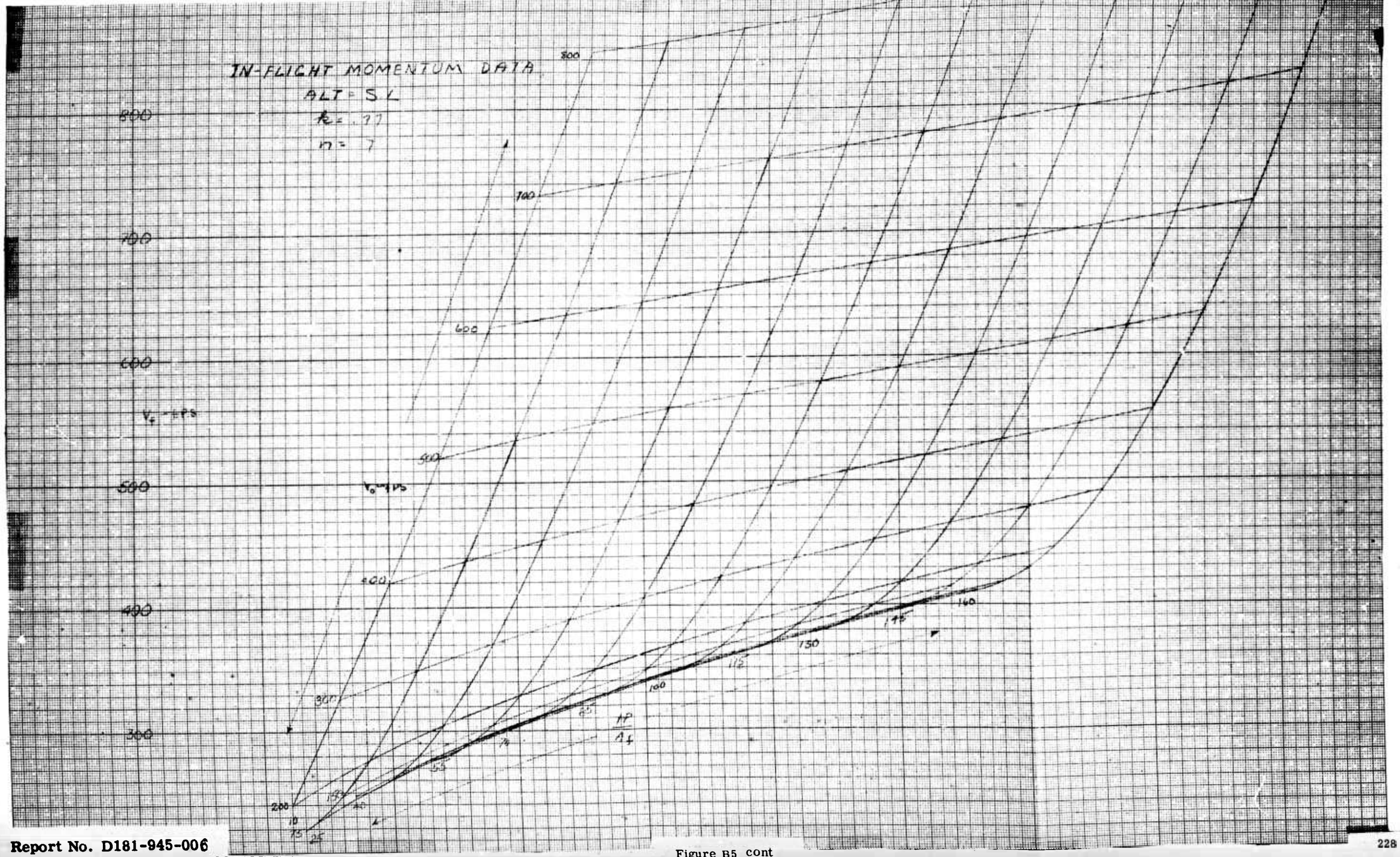

Figure B5 cont

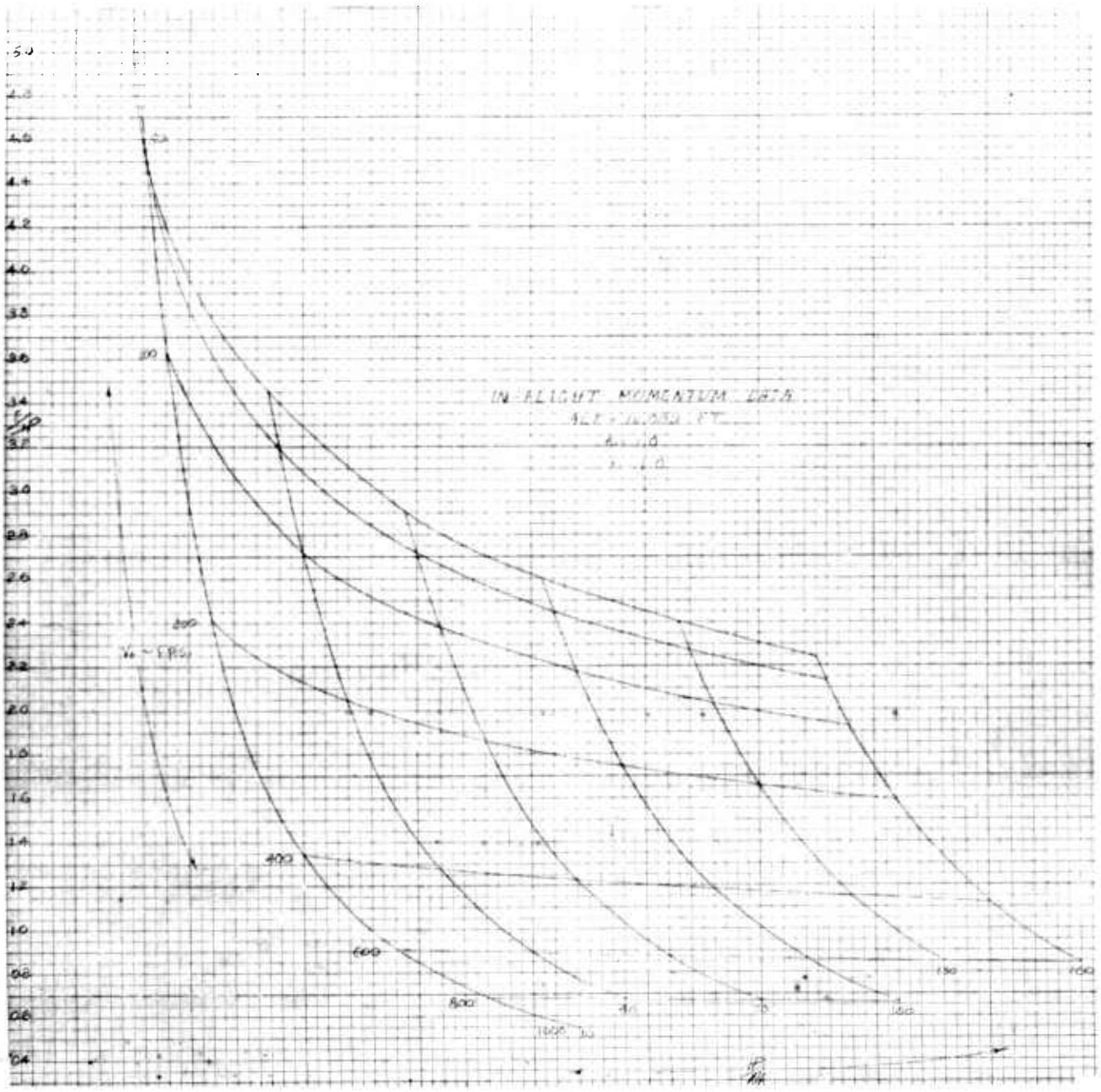

Report No. D181-945-006

Figure B6

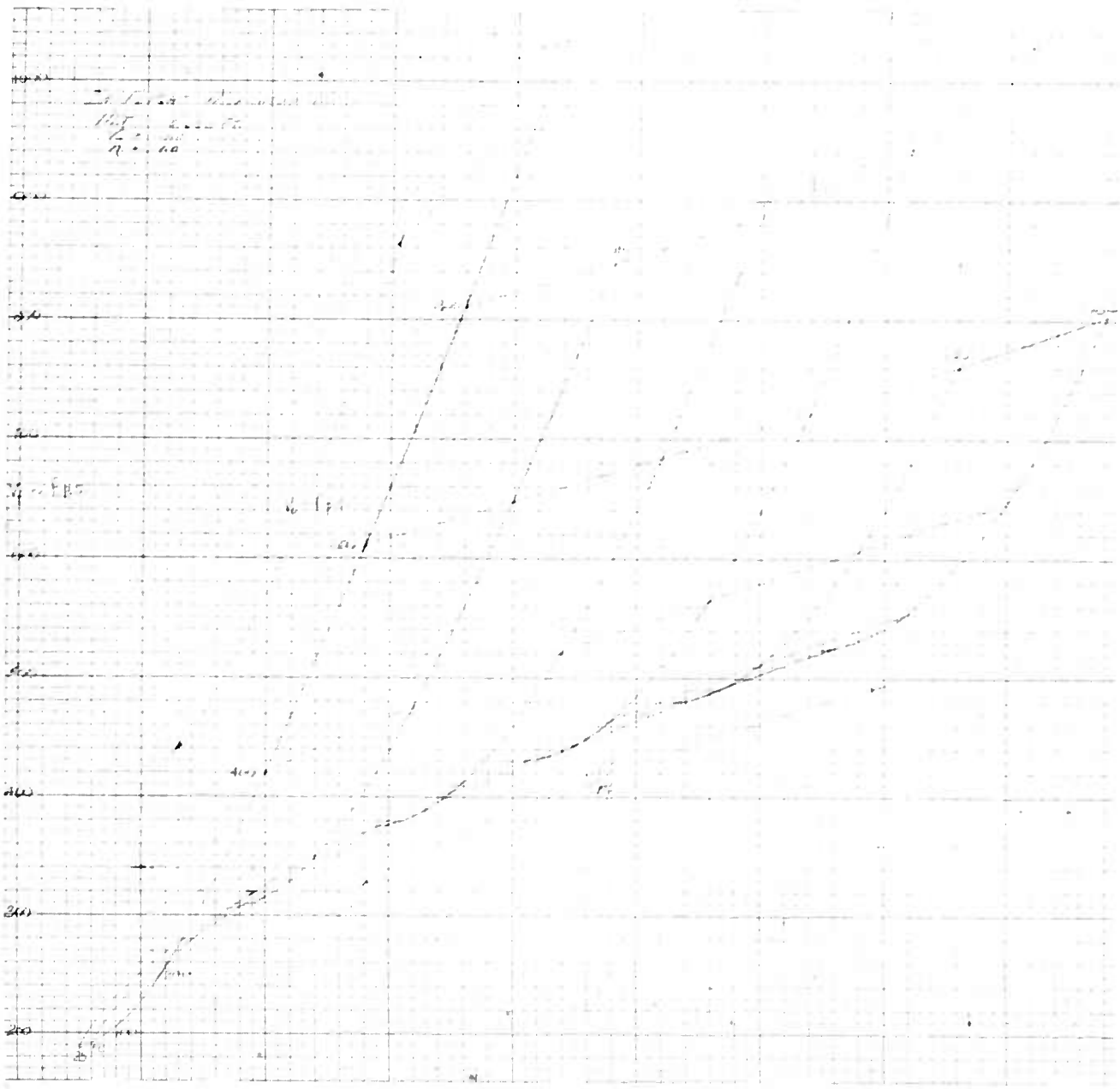

Report No. D181-945-006

Figure B6 cont

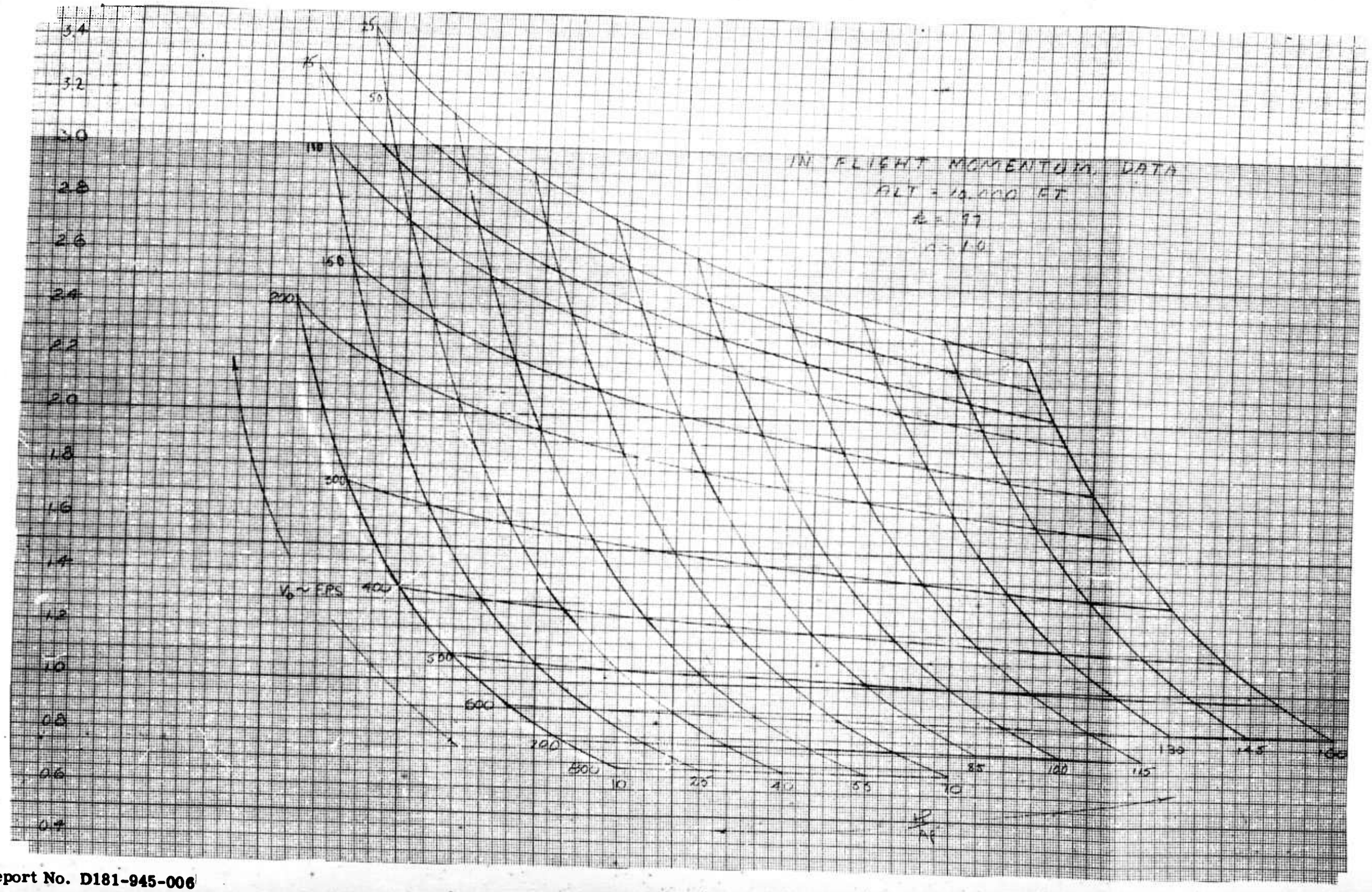
IN FLIGHT MOMENTUM DATA
ALT = 10,000 FT
L = 97
A = 10
3.4
3.2
3.0
2.8
2.6
2.4
2.2
2.0
1.8
1.6
1.4
1.2
1.0
0.8
0.6
0.4
V_0 ~ FPS
400
500
600
800
1000
150
200
250
300
25
50
100
85
100
115
130
145
160

Figure B7

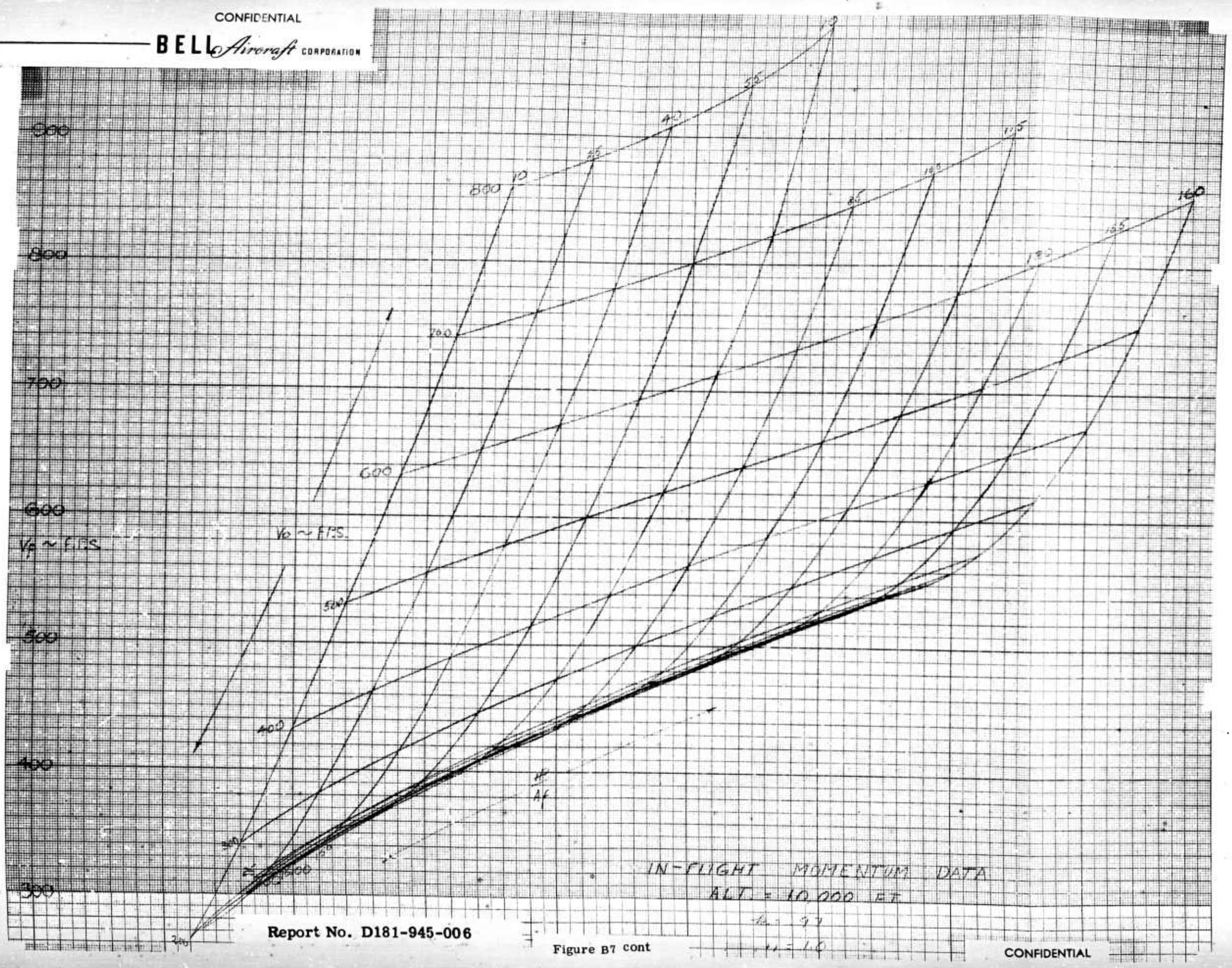

Figure B7 cont

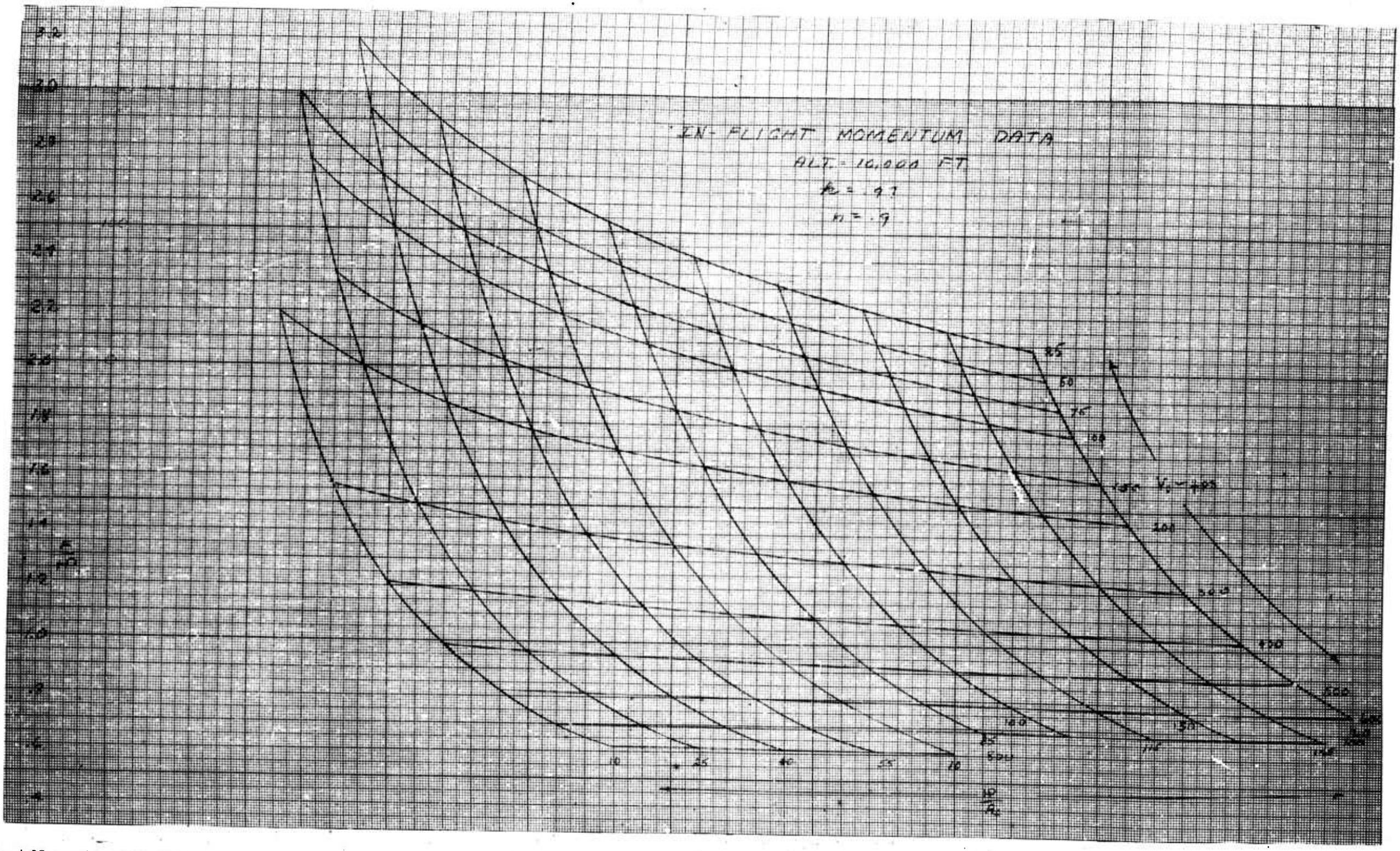

Report No. D181-945-006

Figure B8

BELL Aircraft CORPORATION

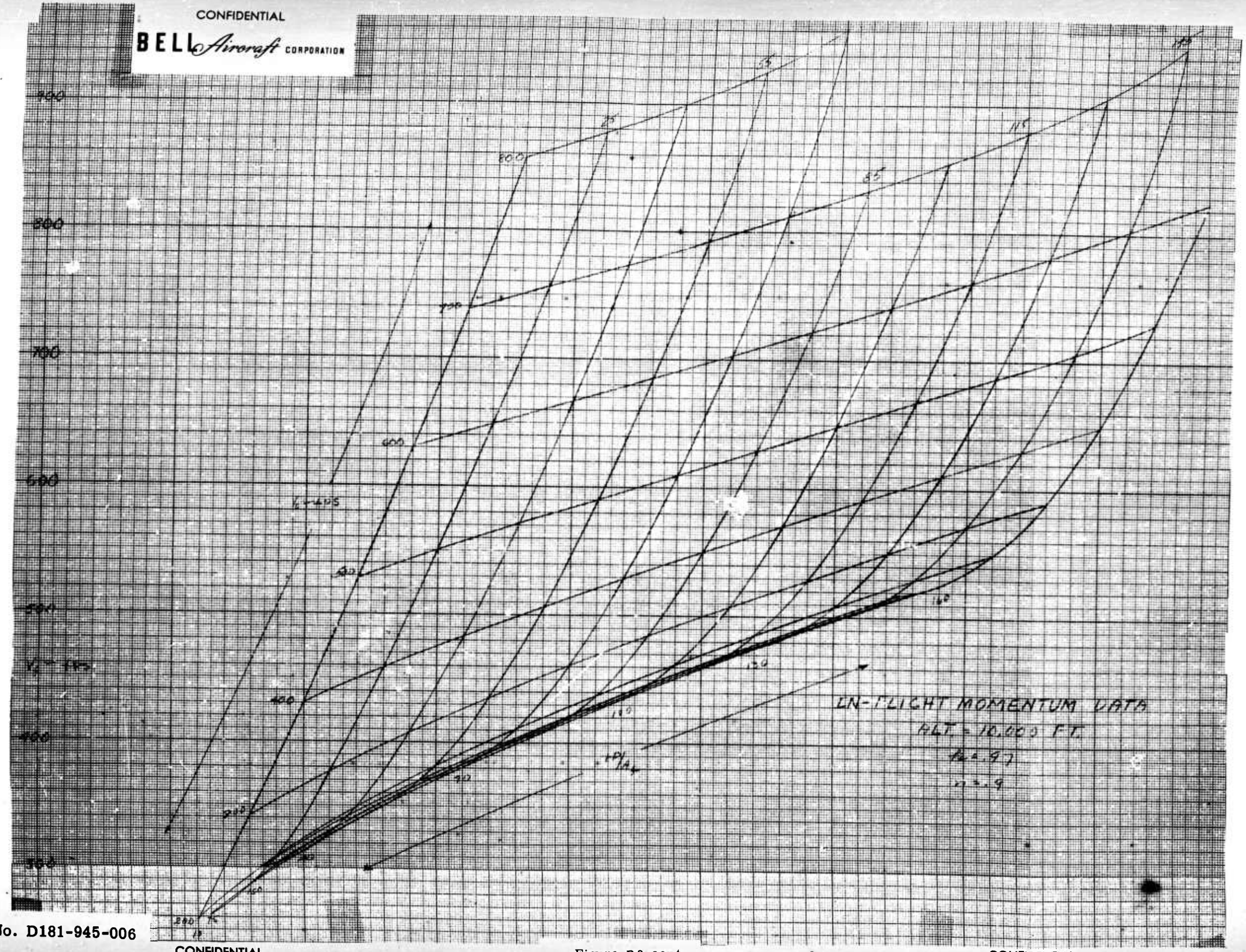

Figure B8 cont

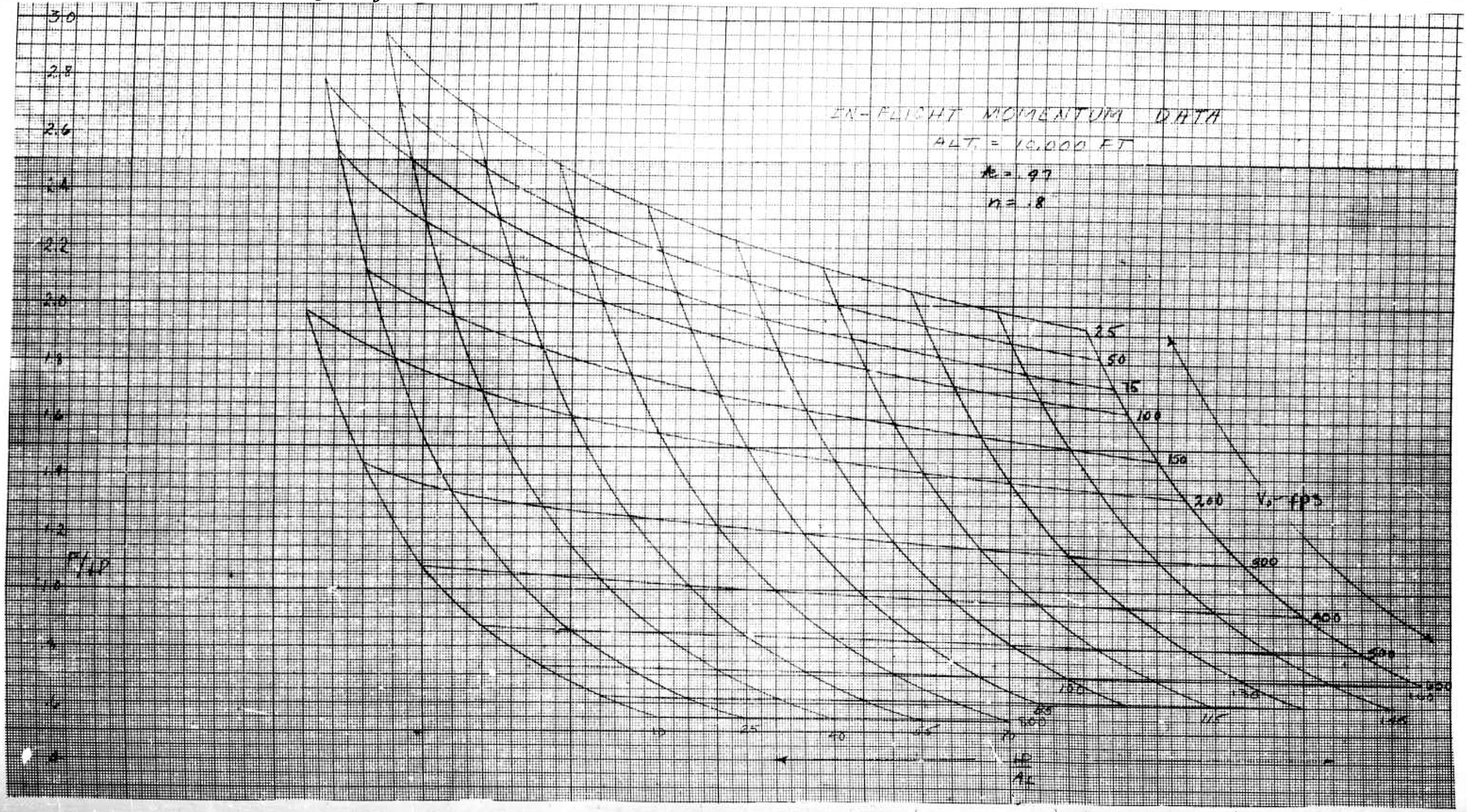
IN-FLIGHT MOMENTUM DATA
ALT. = 10,000 FT
η = .97
n = .8
F/LP
V_0 - FPS
25
50
75
100
150
200
300
400
500
600
LP/AL
10
25
40
55
70
85
100
115
130
145
3.0
2.8
2.6
2.4
2.2
2.0
1.8
1.6
1.4
1.2
1.0
.8
.6
.4

Figure B9

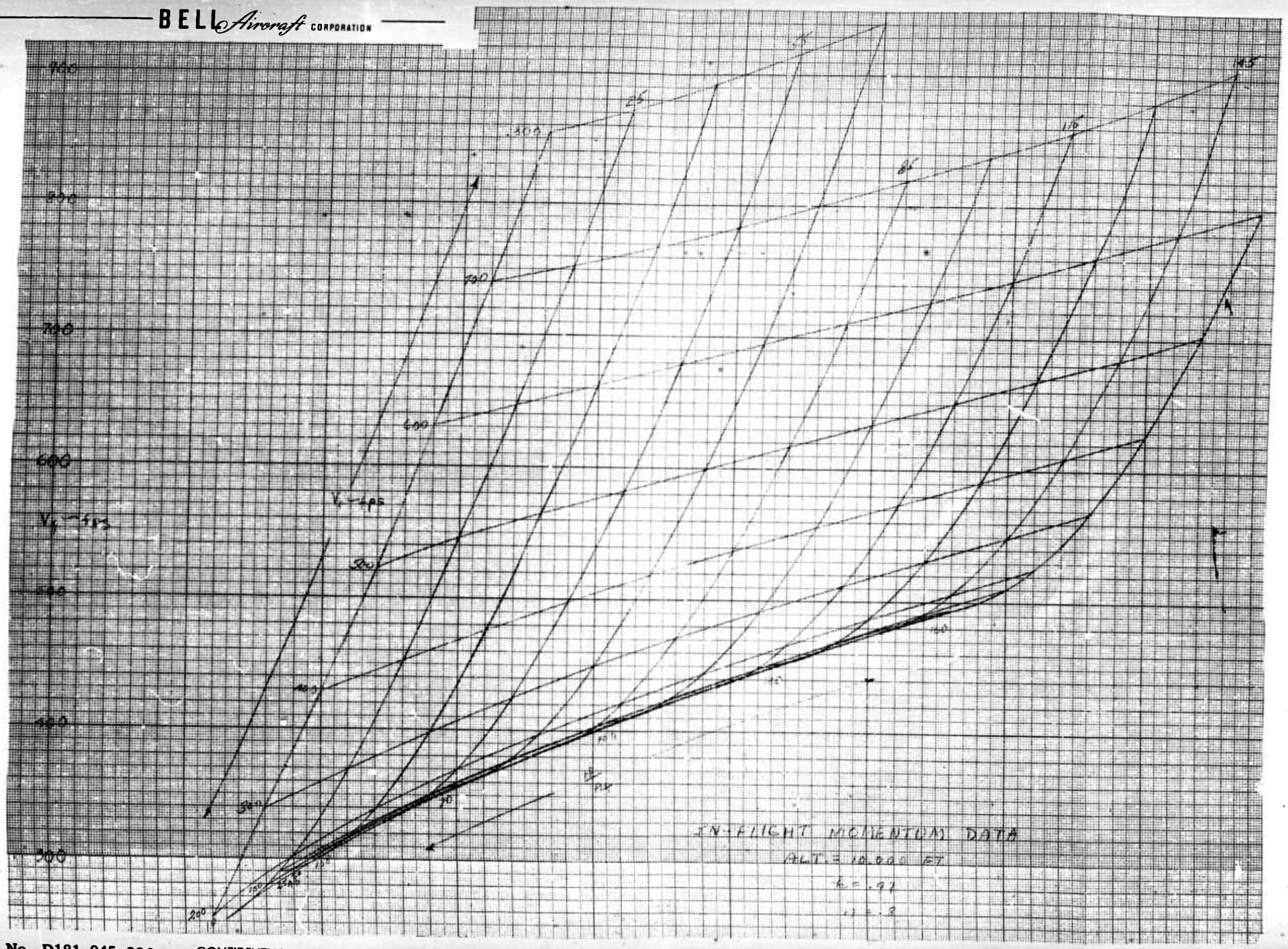

Figure B9 cont

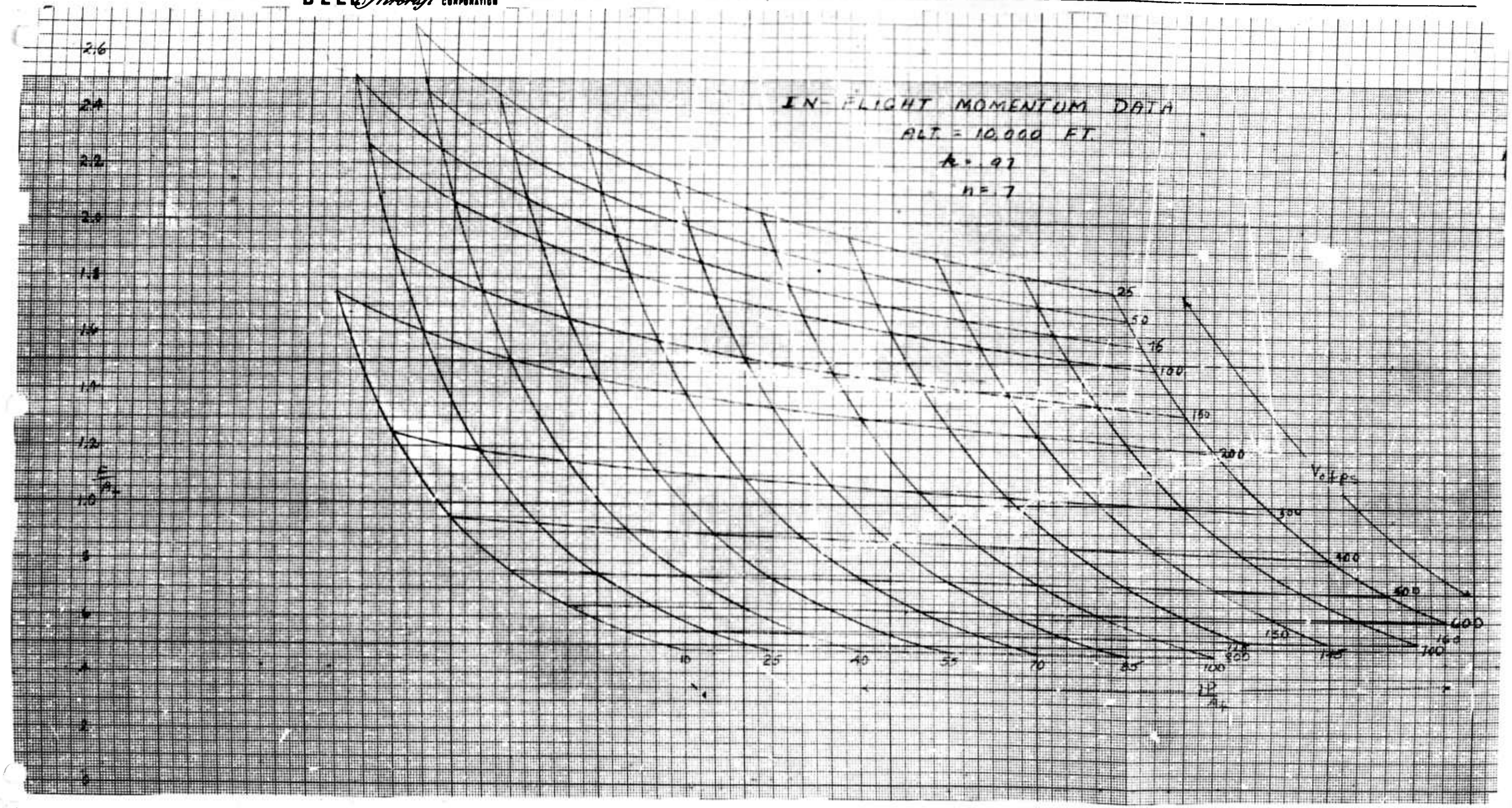
IN-FLIGHT MOMENTUM DATA
ALT. = 10,000 FT.
k = .97
n = 7
2.6
2.4
2.2
2.0
1.8
1.6
1.4
1.2
1.0
.8
.6
.4
.2
0
25
50
75
100
150
200
300
400
500
600
10
25
40
55
70
85
100
125
150
160
Volts

Figure B10

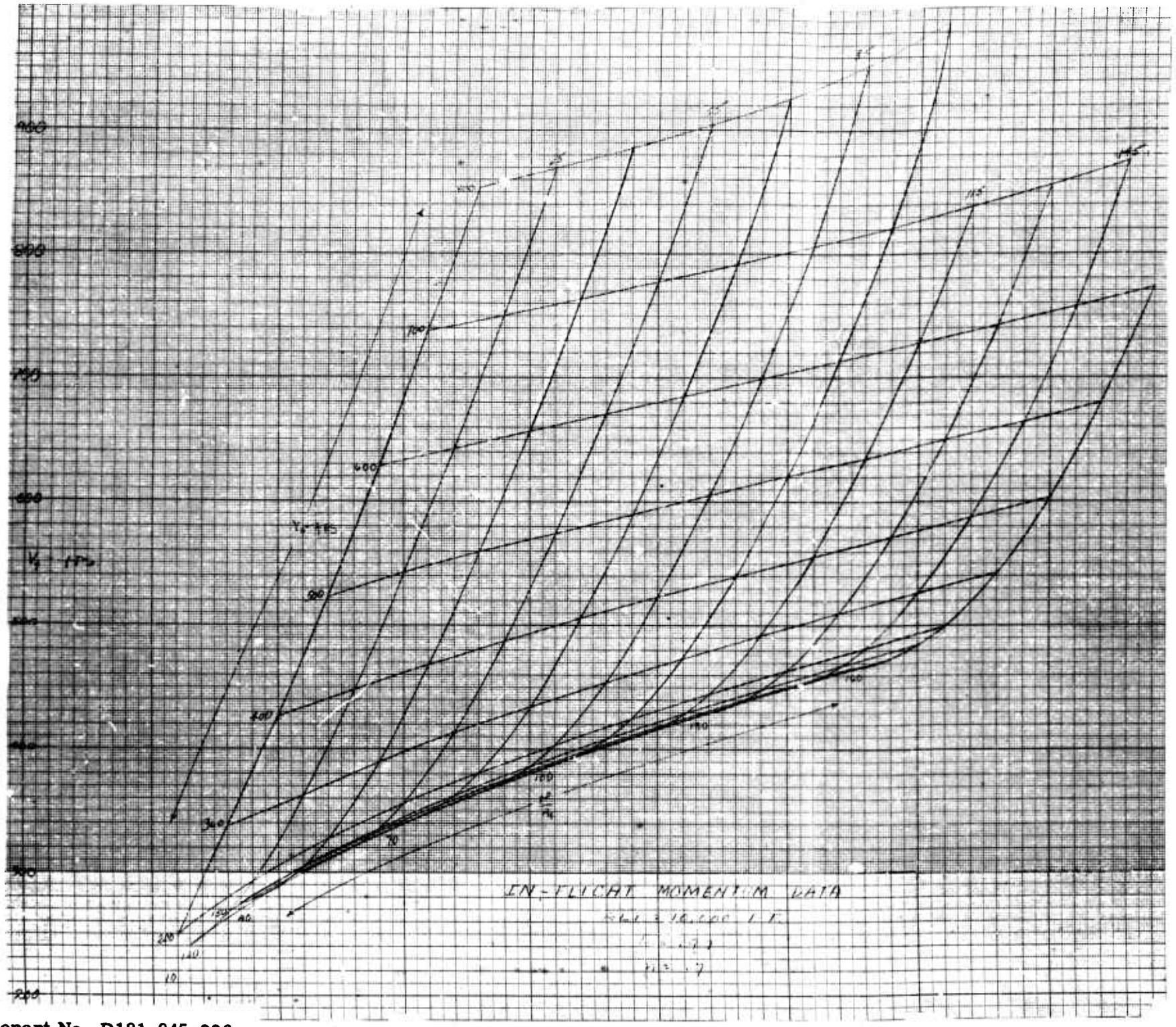

Figure B10 cont

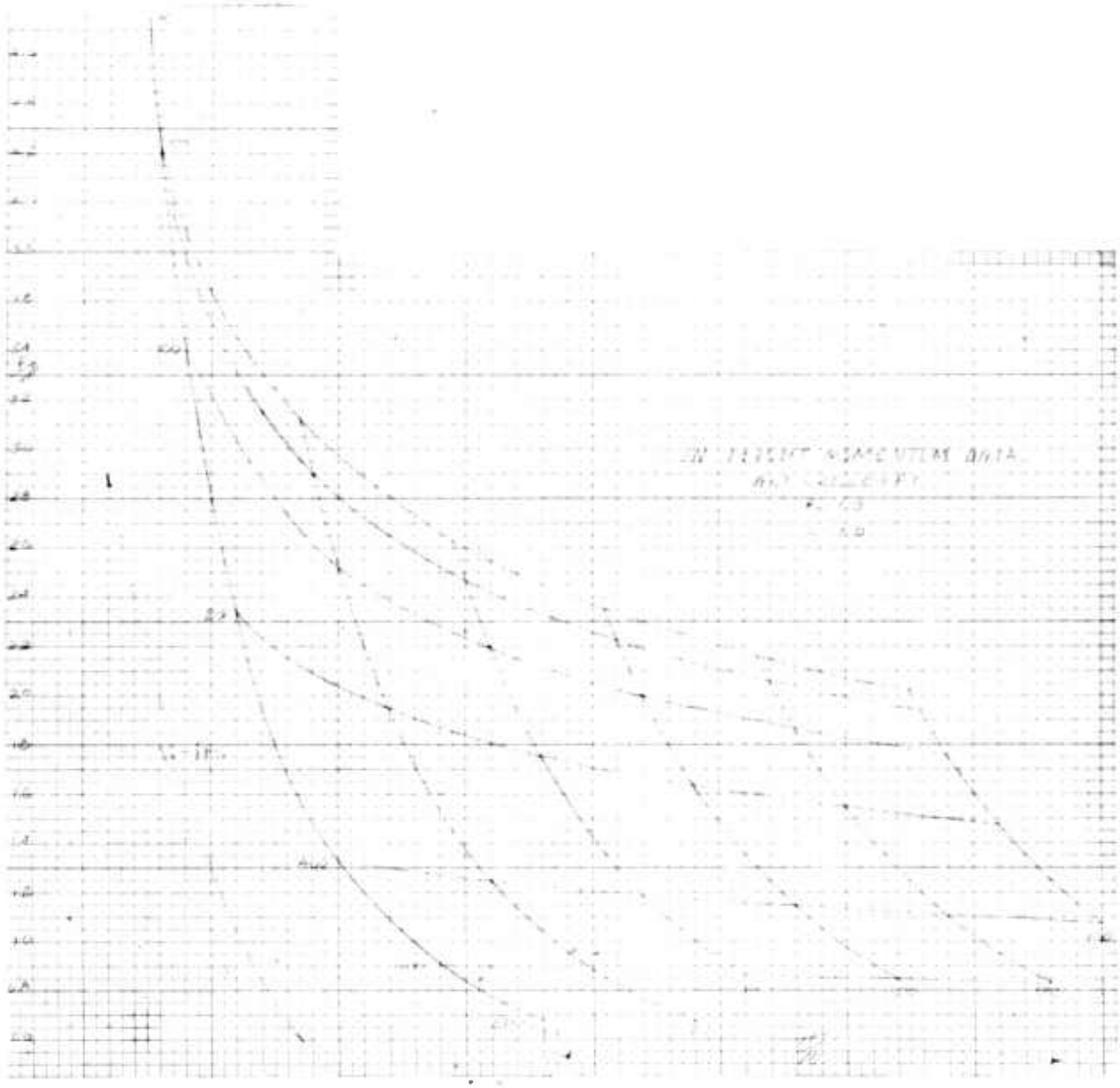

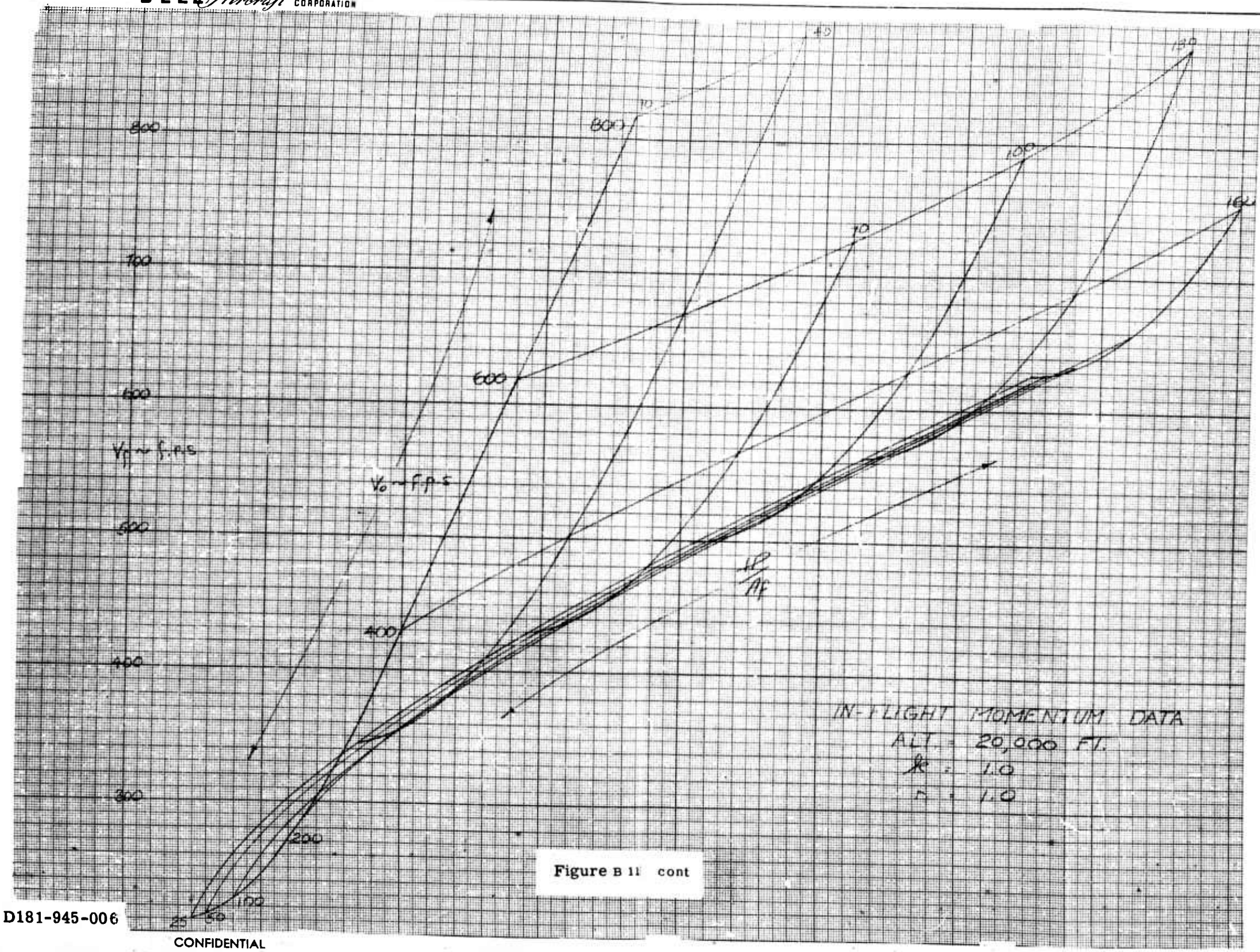

Figure B 11 cont

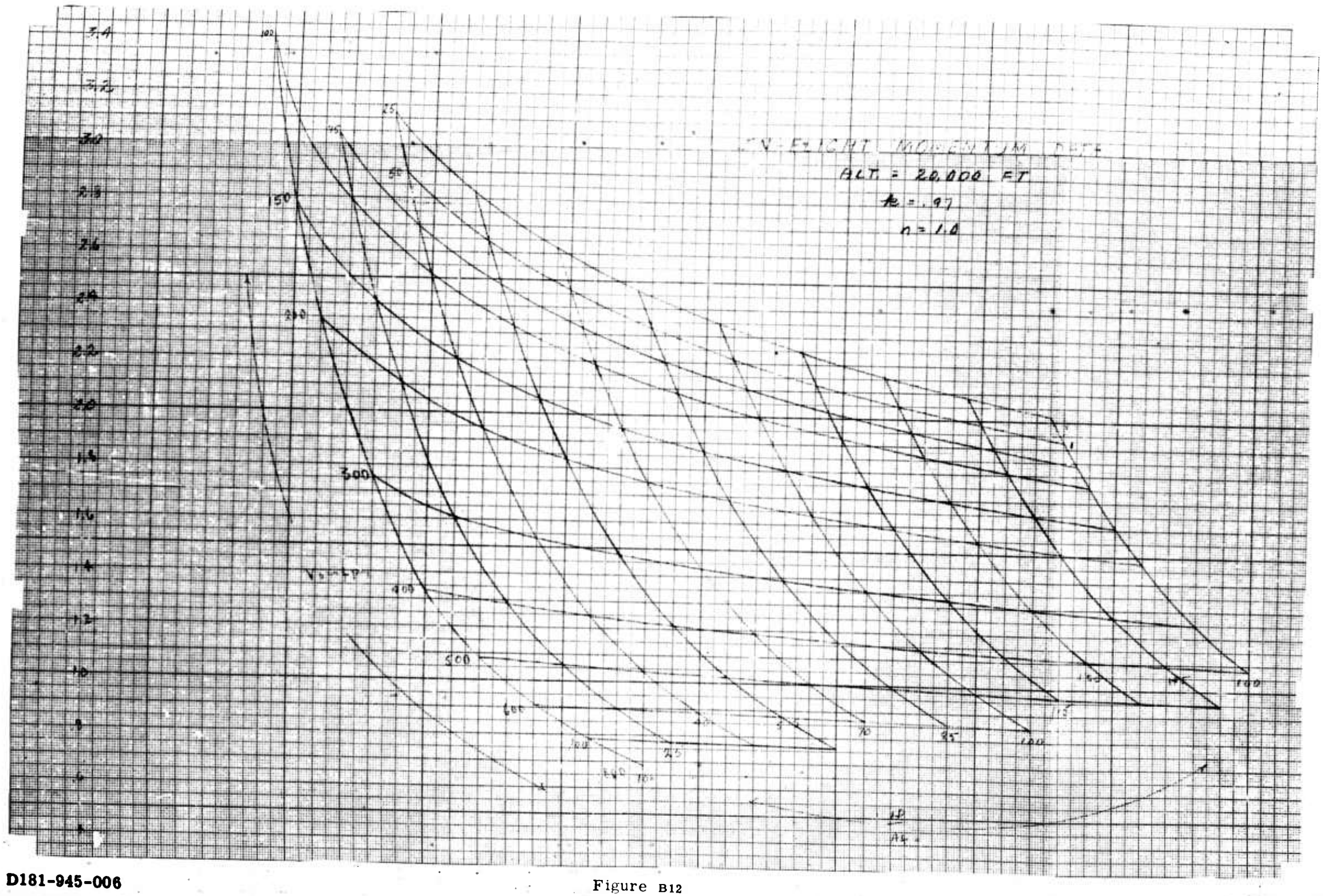
ALT = 20,000 FT
k = .97
n = 1.0
7.4
7.2
3.0
2.8
2.6
2.4
2.2
2.0
1.8
1.6
1.4
1.2
1.0
.8
.6
.4
102
95
85
80
150
300
400
500
600
700
800
140
120
100
75
45
15

Figure B12

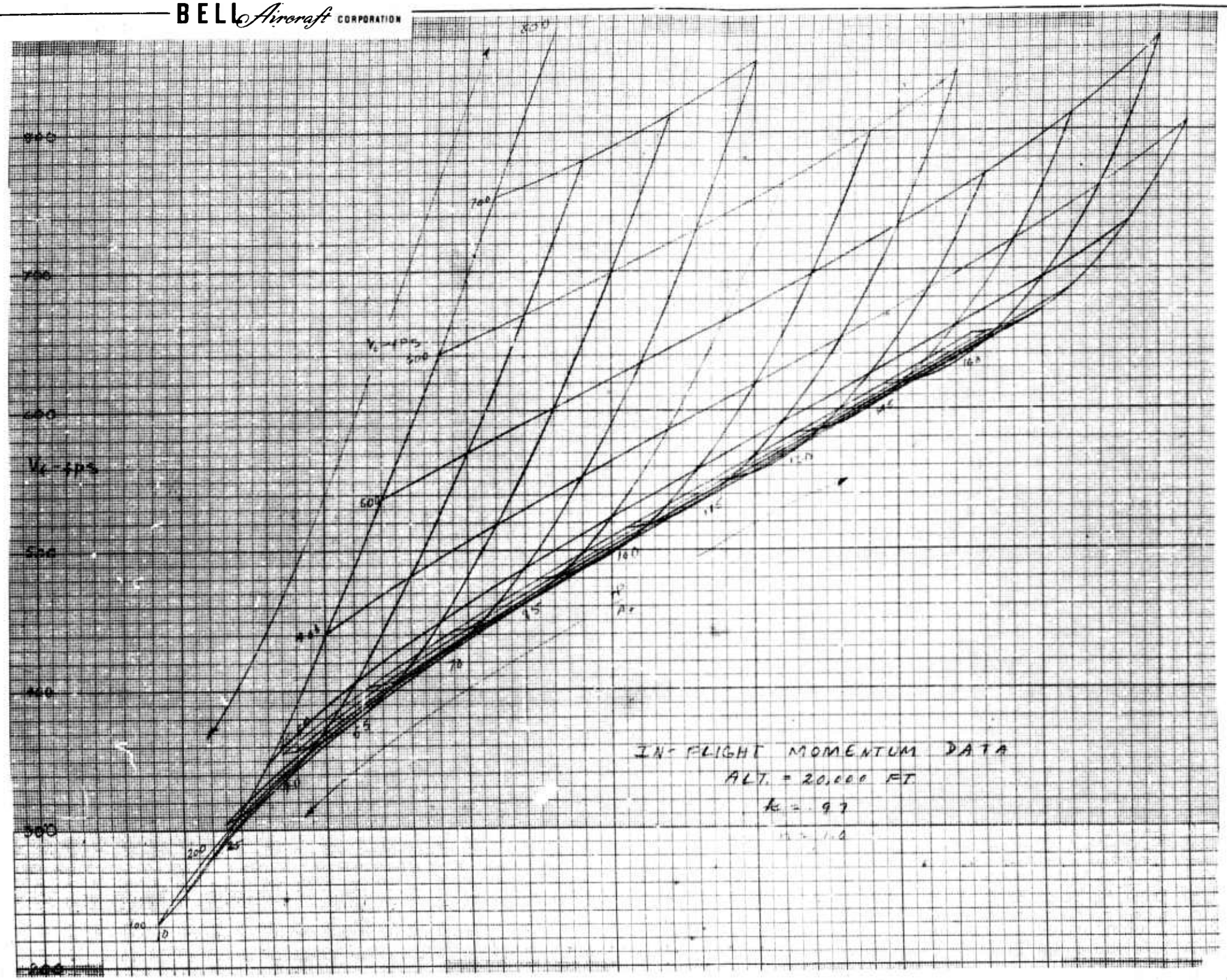
V_E - fps
IN-FLIGHT MOMENTUM DATA
ALT. = 20,000 FT
k = 97

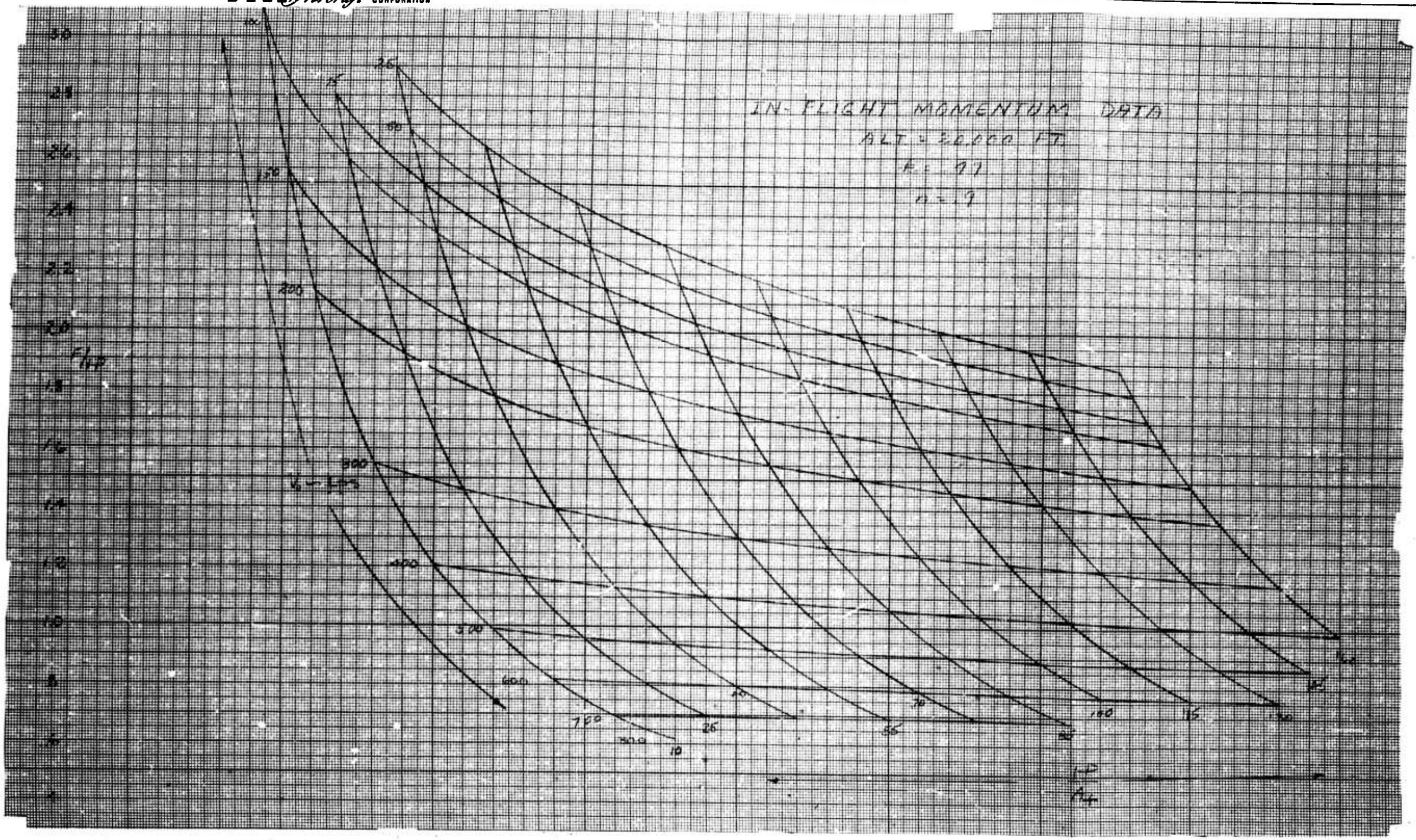
IN-FLIGHT MOMENTUM DATA
ALT = 20,000 FT.
K = .97
n = 1
Flight
W = 8000
400
300
600
700
500
10
20
30
40
50
60
80
100
120
140
160
180
200
220
240
260
280
300
320
340
360
380
400
420
440
460
480
500
520
540
560
580
600
620
640
660
680
700
720
740
760
780
800
820
840
860
880
900
920
940
960
980
1000

Figure B13

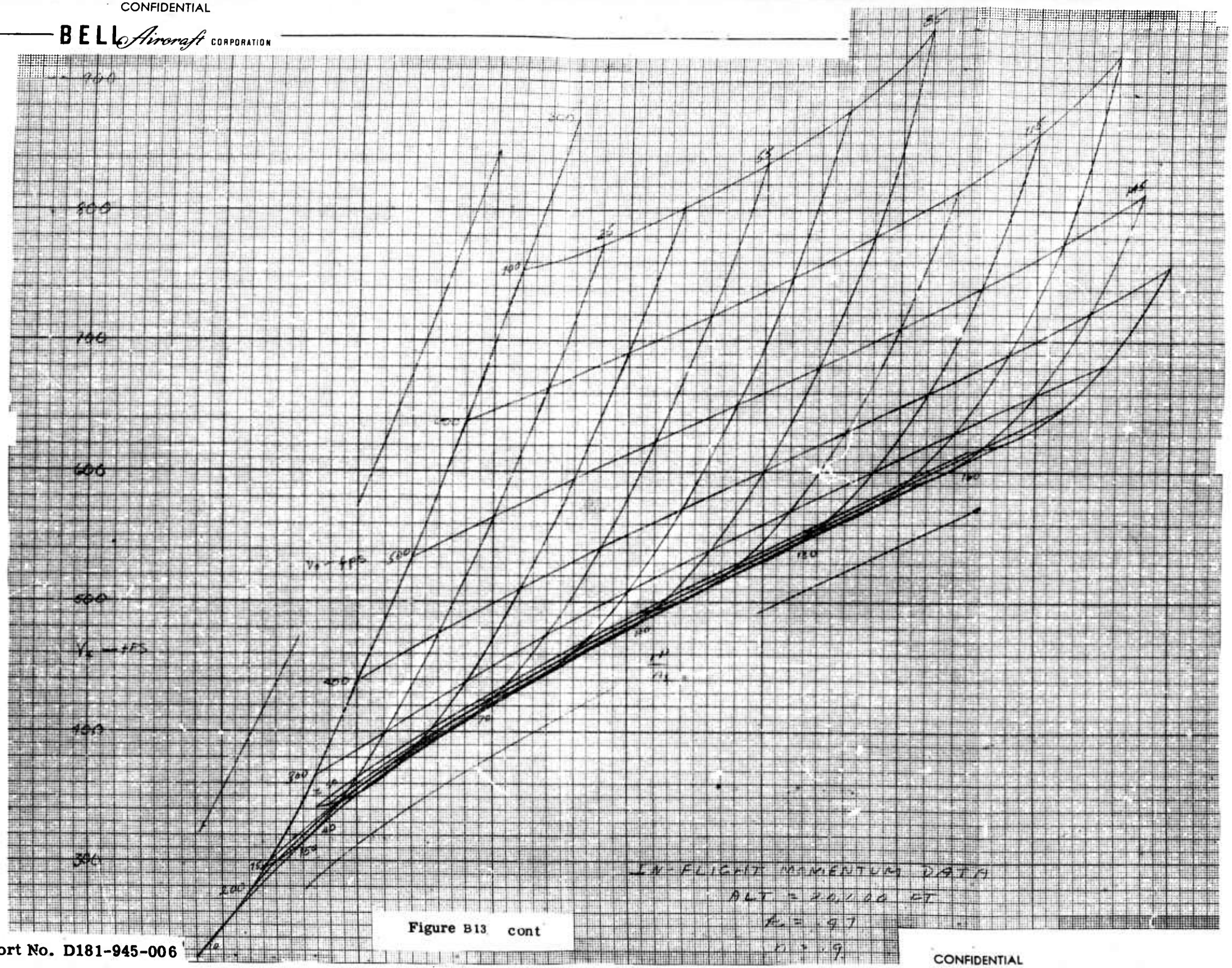

Figure B13 cont

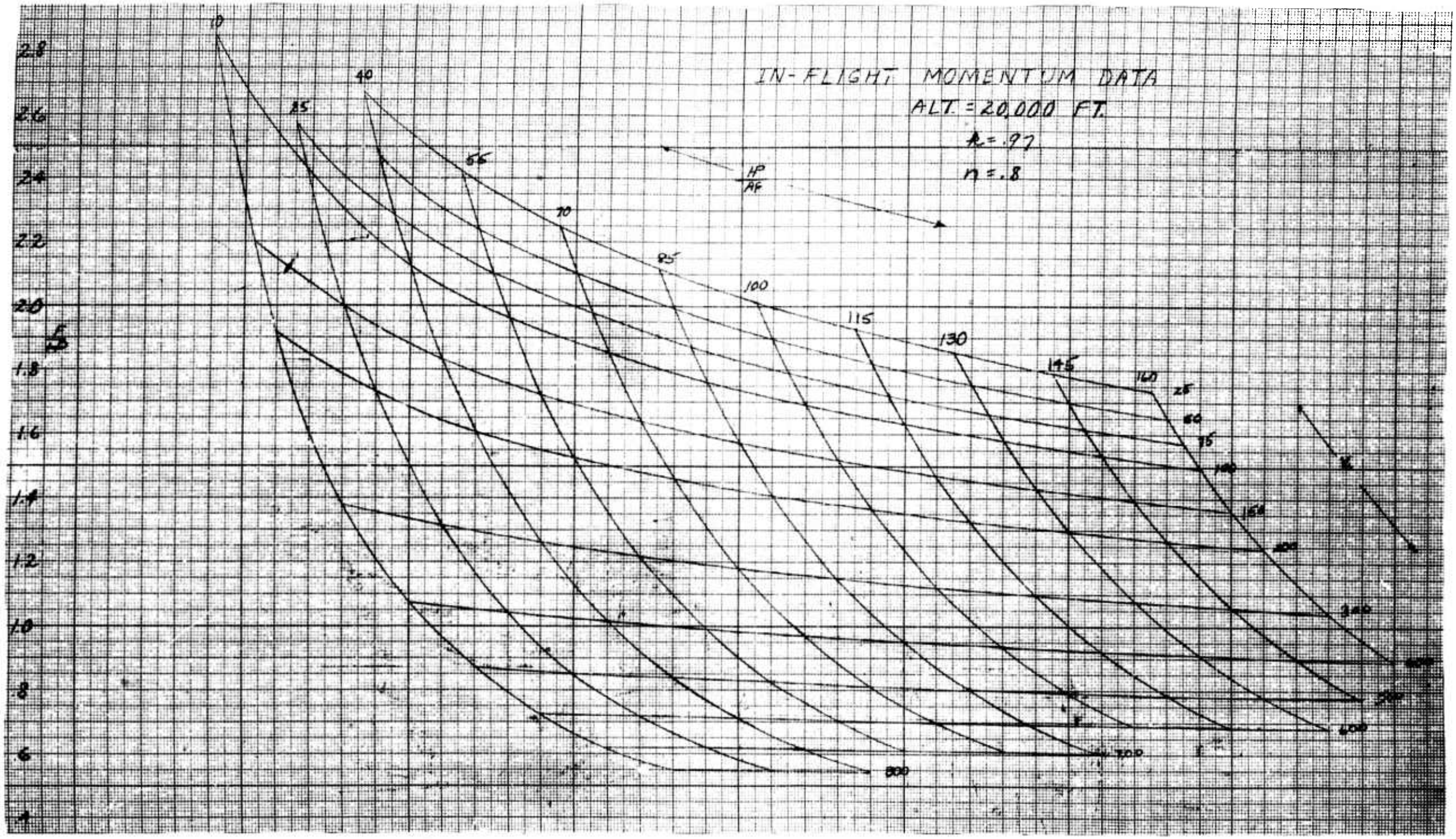

Report No. D181-945-006

Figure B|14

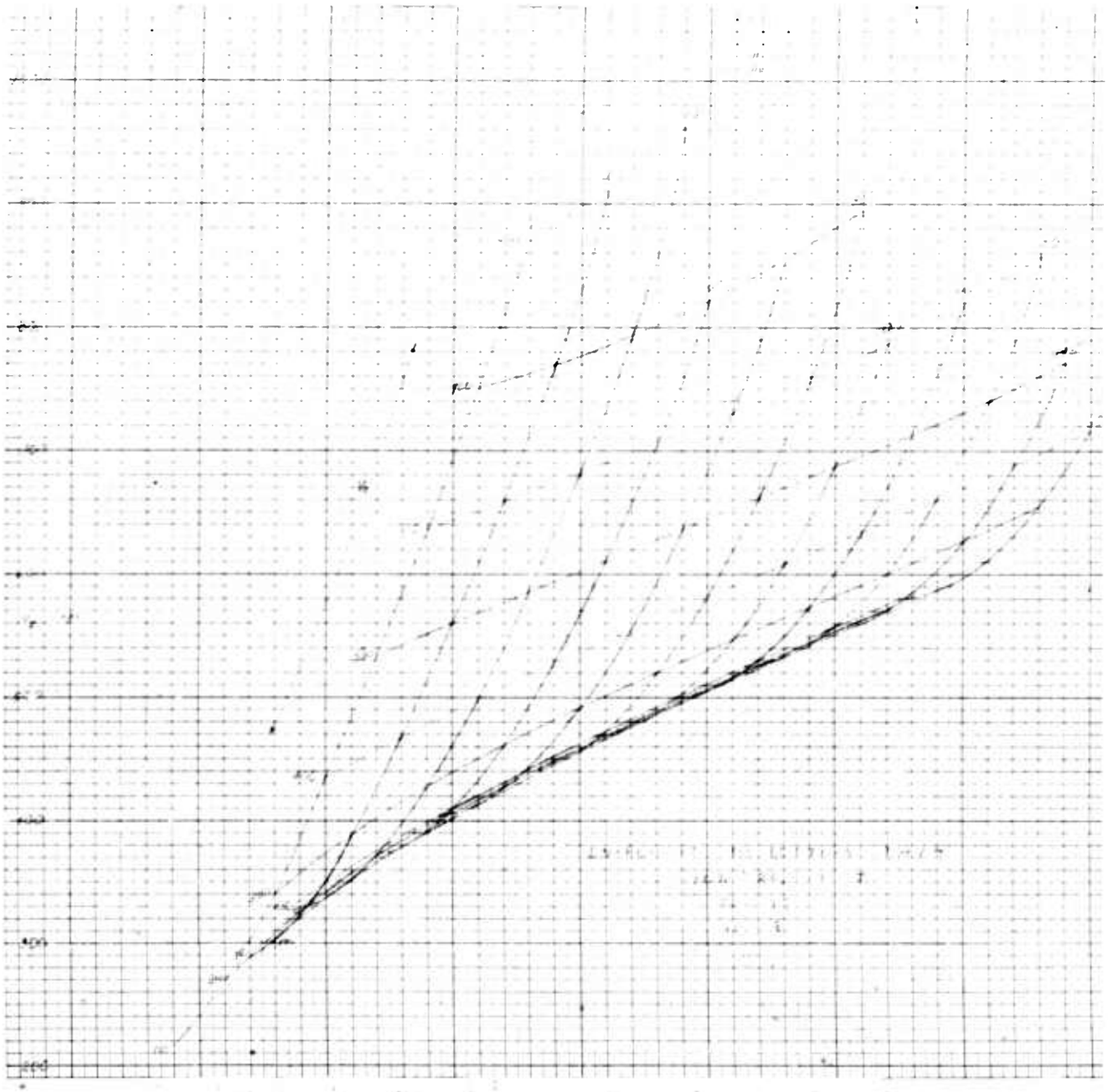

Figure B14 cont

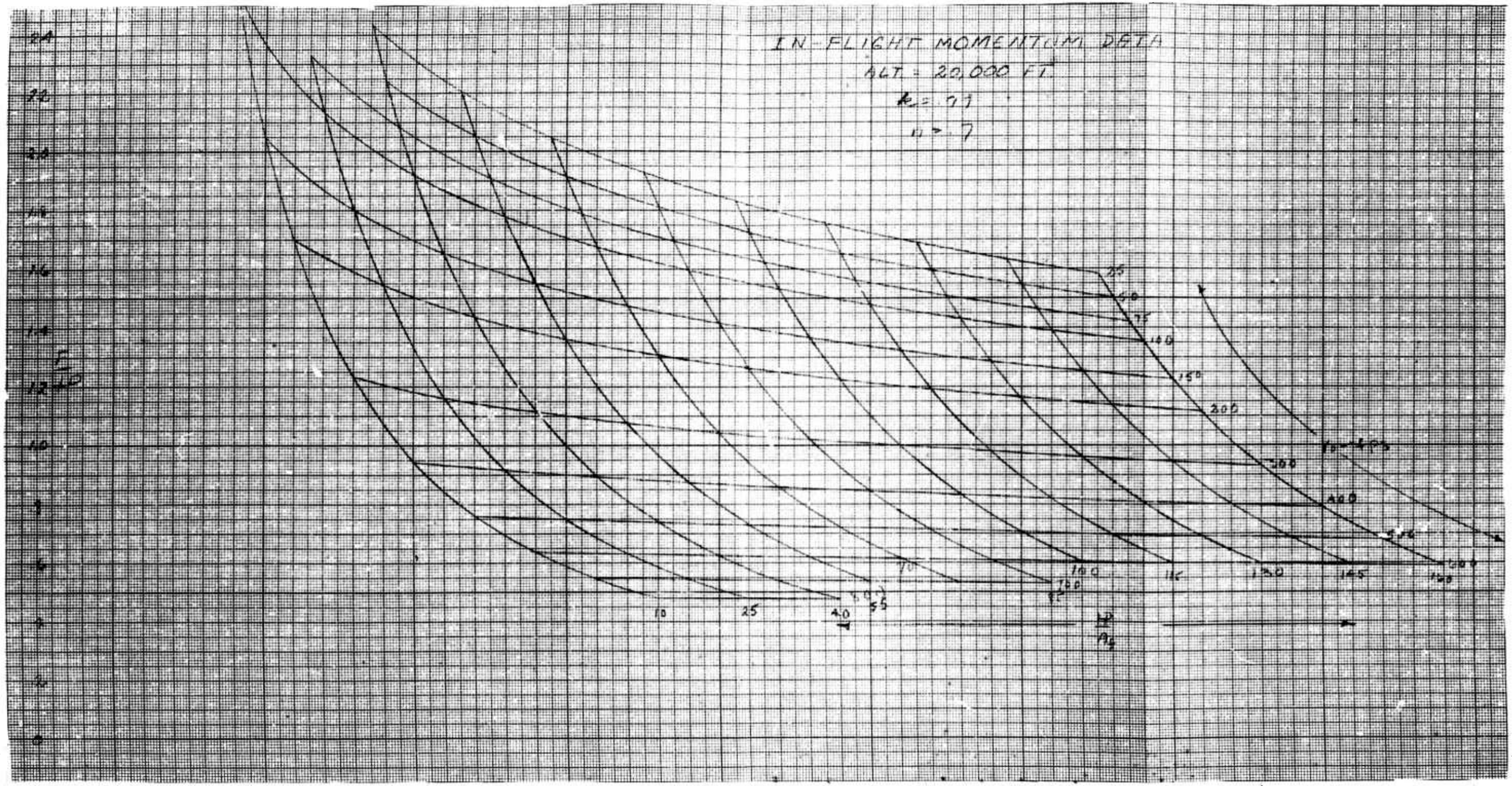
IN-FLIGHT MOMENTUM DATA
ALT. = 20,000 FT.
k = 77
n = 7
10
25
40
55
100
140
165
180
200
300
400
500
600
700
800
900
1000
1100
1200
1300
1400
1500
1600
1700
1800
1900
2000
2100
2200
2300
2400
2500
2600
2700
2800
2900
3000
3100
3200
3300
3400
3500
3600
3700
3800
3900
4000
4100
4200
4300
4400
4500
4600
4700
4800
4900
5000
5100
5200
5300
5400
5500
5600
5700
5800
5900
6000
6100
6200
6300
6400
6500
6600
6700
6800
6900
7000
7100
7200
7300
7400
7500
7600
7700
7800
7900
8000
8100
8200
8300
8400
8500
8600
8700
8800
8900
9000
9100
9200
9300
9400
9500
9600
9700
9800
9900
10000
10100
10200
10300
10400
10500
10600
10700
10800
10900
11000
11100
11200
11300
11400
11500
11600
11700
11800
11900
12000
12100
12200
12300
12400
12500
12600
12700
12800
12900
13000
13100
13200
13300
13400
13500
13600
13700
13800
13900
14000
14100
14200
14300
14400
14500
14600
14700
14800
14900
15000
15100
15200
15300
15400
15500
15600
15700
15800
15900
16000
16100
16200
16300
16400
16500
16600
16700
16800
16900
17000
17100
17200
17300
17400
17500
17600
17700
17800
17900
18000
18100
18200
18300
18400
18500
18600
18700
18800
18900
19000
19100
19200
19300
19400
19500
19600
19700
19800
19900
20000

Figure B15

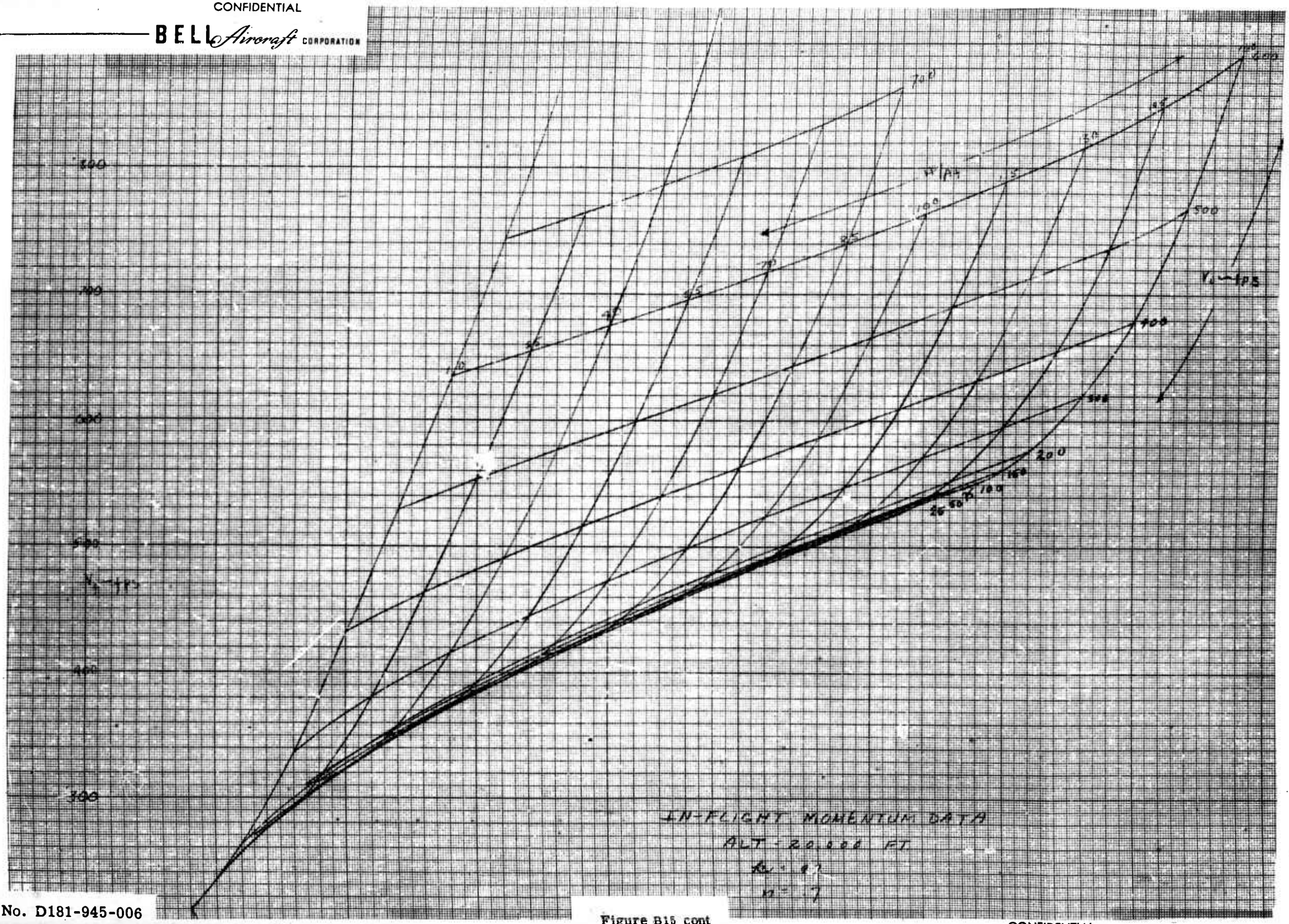

Figure B15 cont

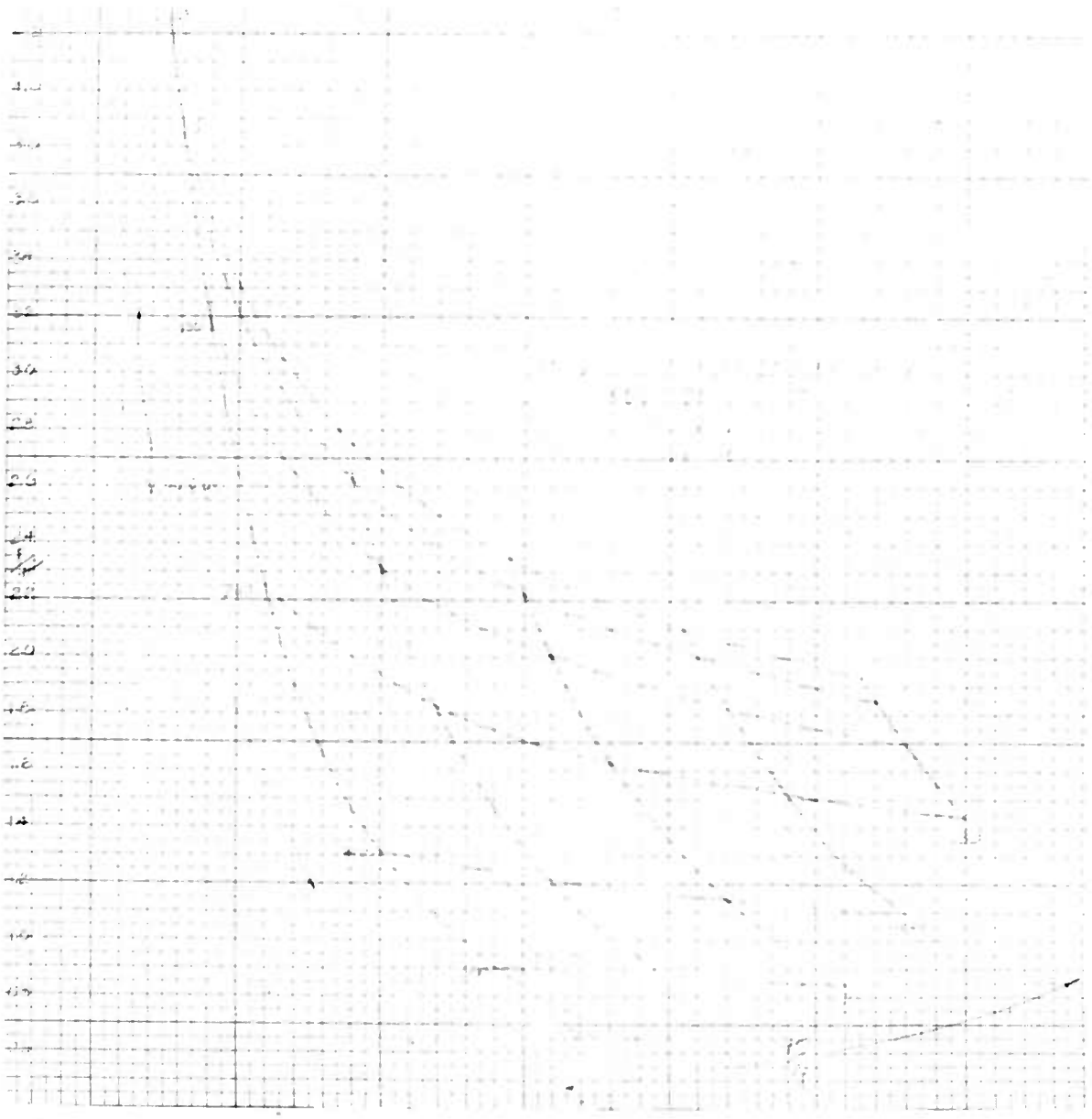

Report No. D181-945-006

Figure B16

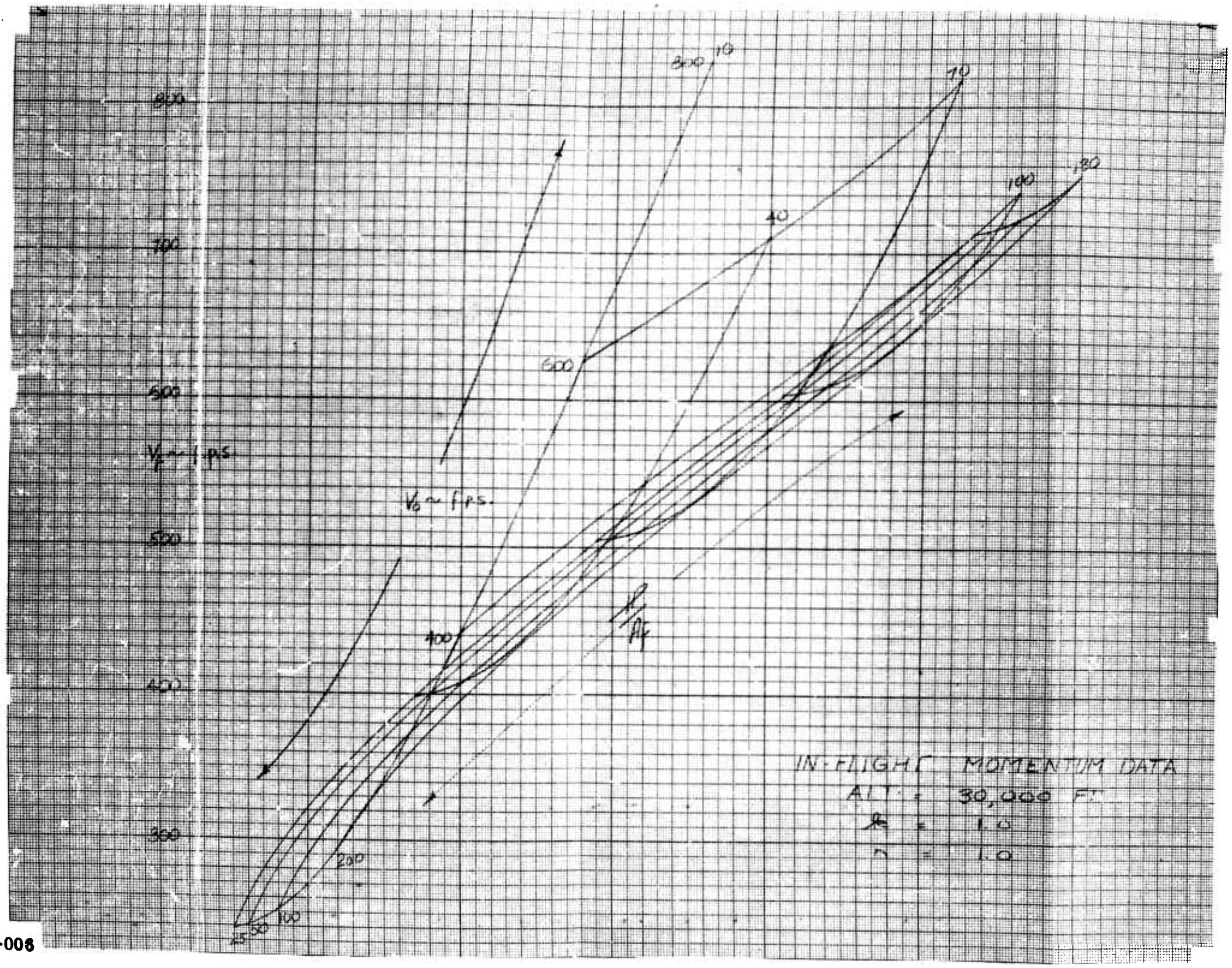

Figure B 16 cont

BELL Aircraft CORPORATION

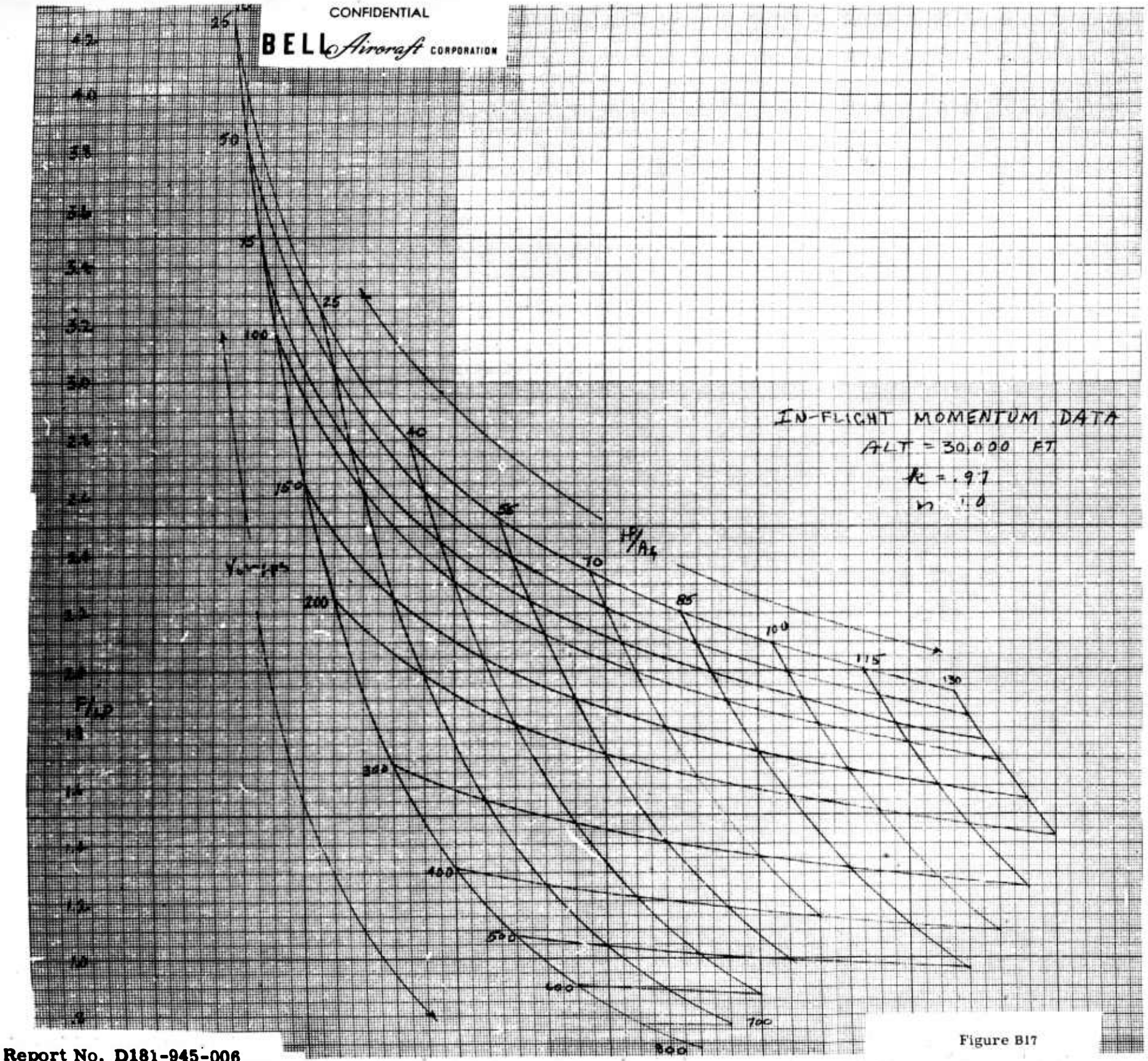

Figure B17

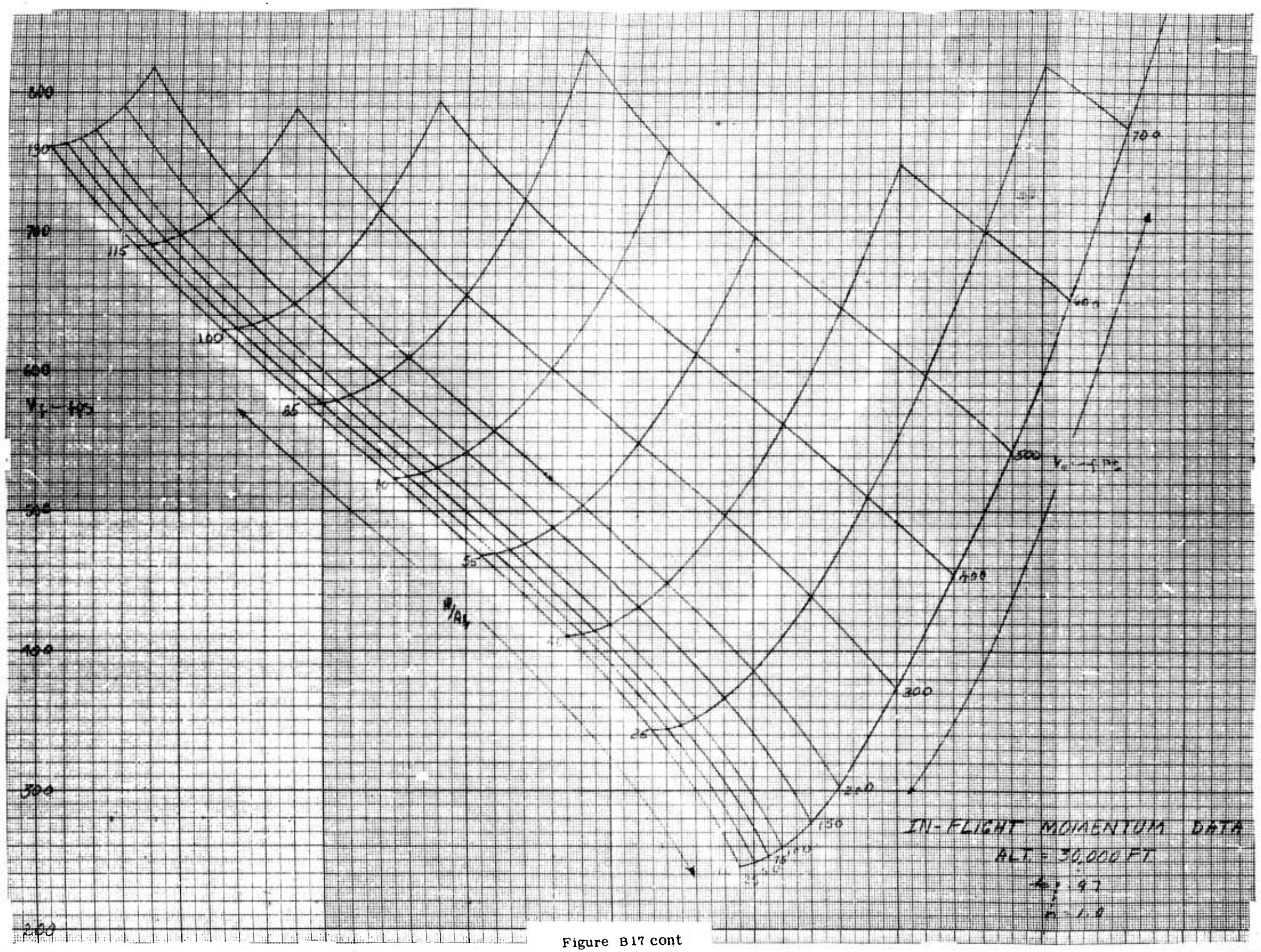

Figure B17 cont

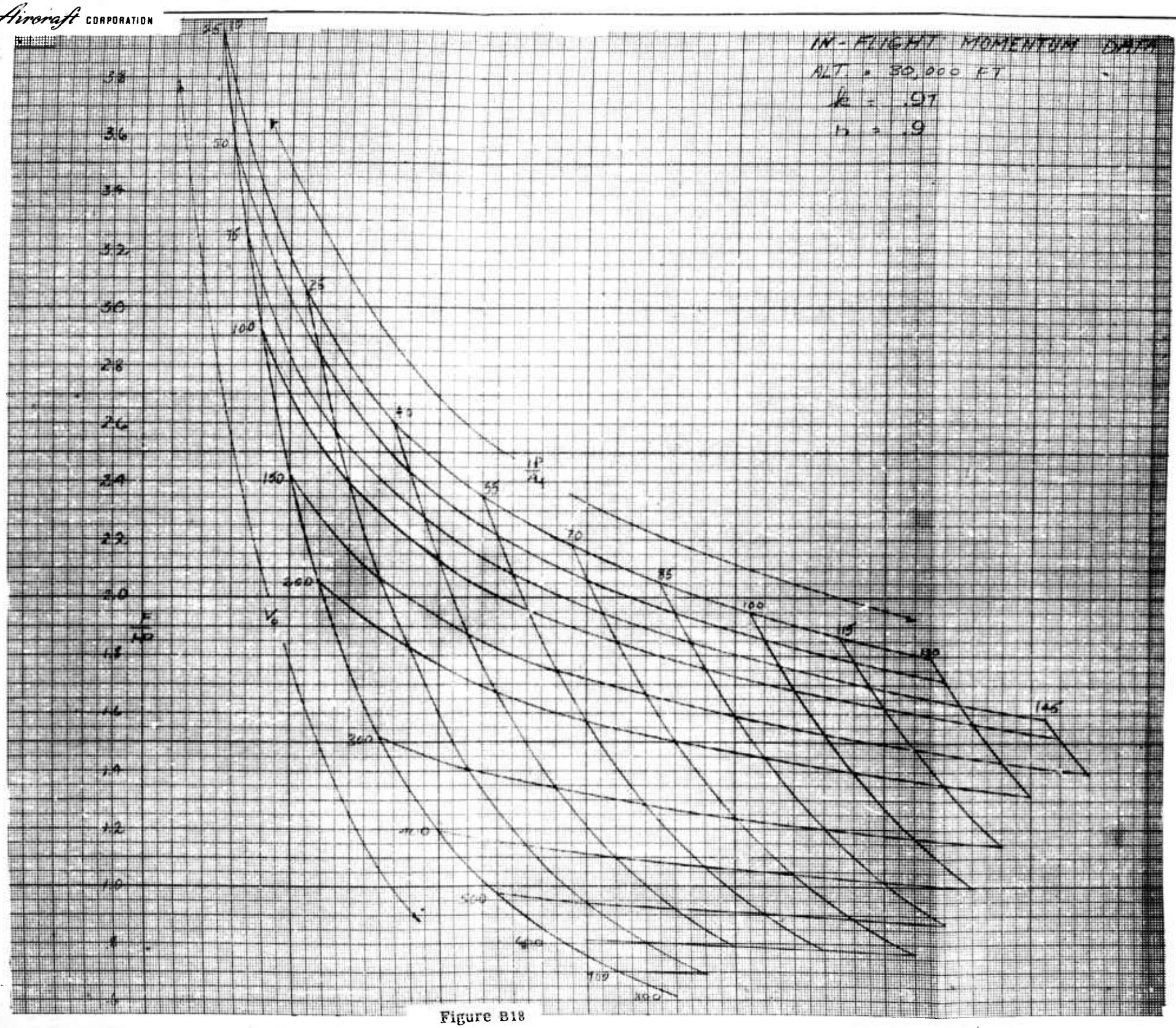
IN-FLIGHT MOMENTUM DRAG
ALT = 30,000 FT
k = .97
b = .9
F/HD
V/a
3.8
3.6
3.4
3.2
3.0
2.8
2.6
2.4
2.2
2.0
1.8
1.6
1.4
1.2
1.0
.8
.6
25
50
75
100
150
200
300
400
500
600
700
800
55
70
85
100
115
130
145

Figure B18

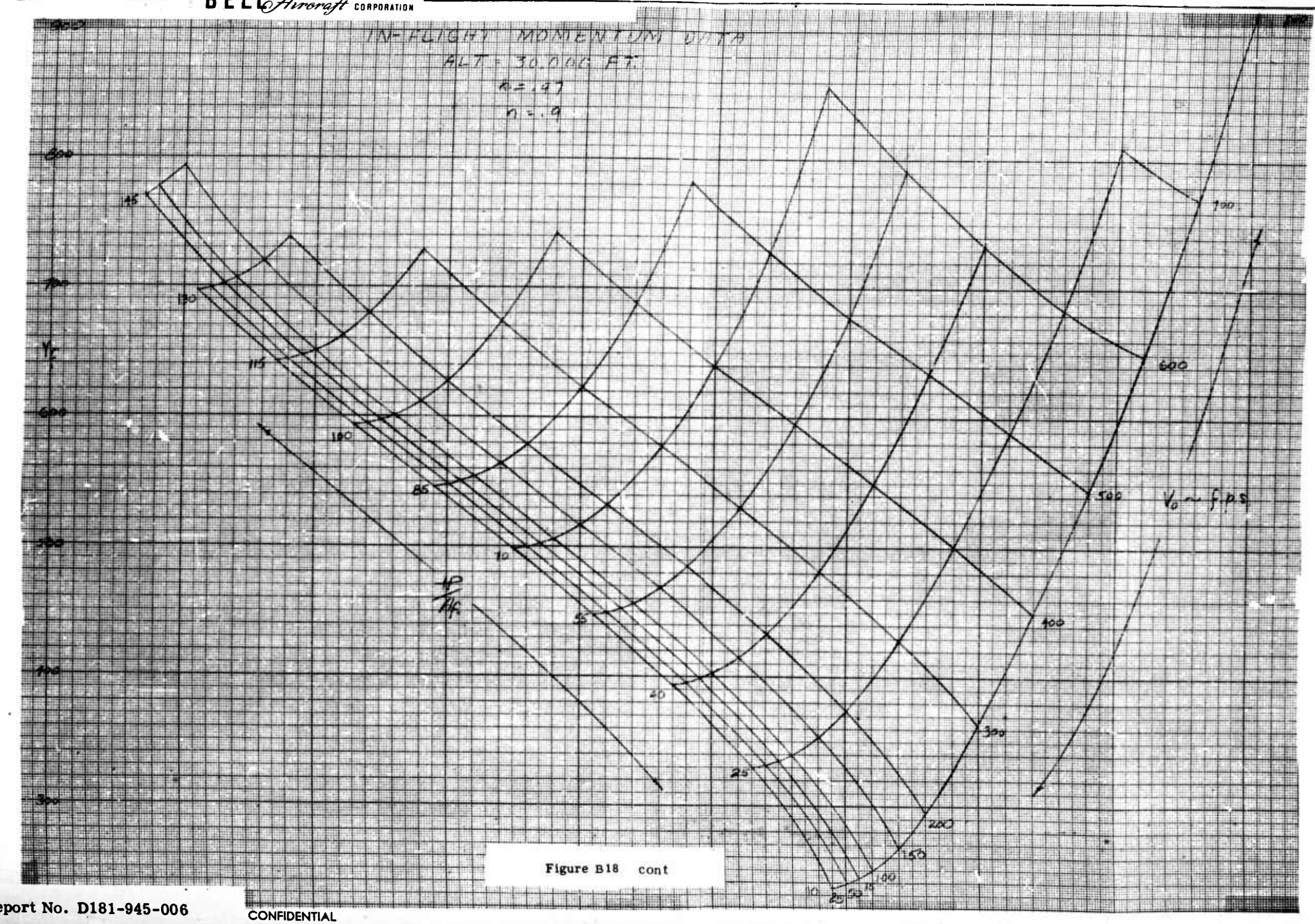

Figure B18 cont

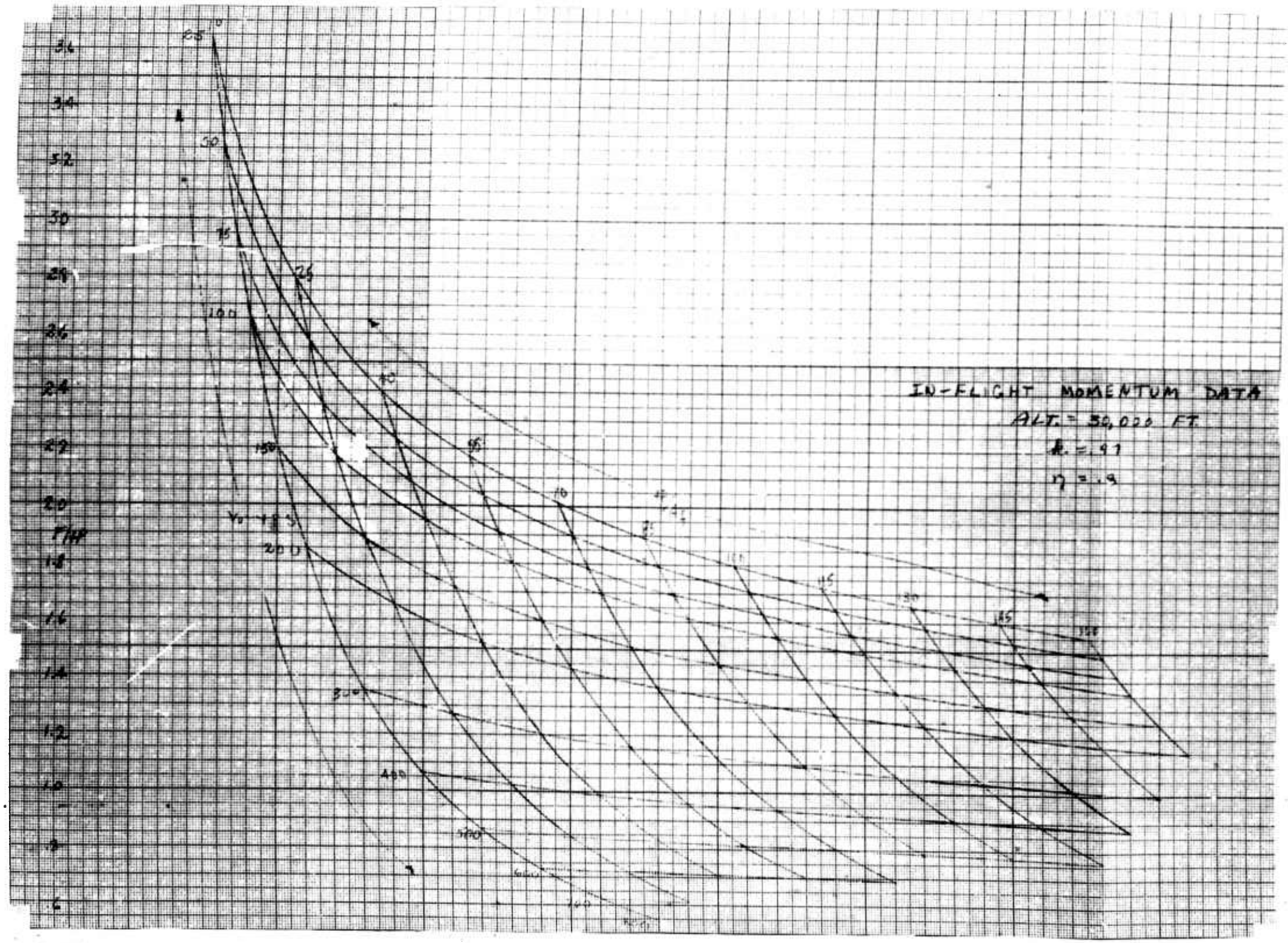

Figure B19

BELL Aircraft CORPORATION

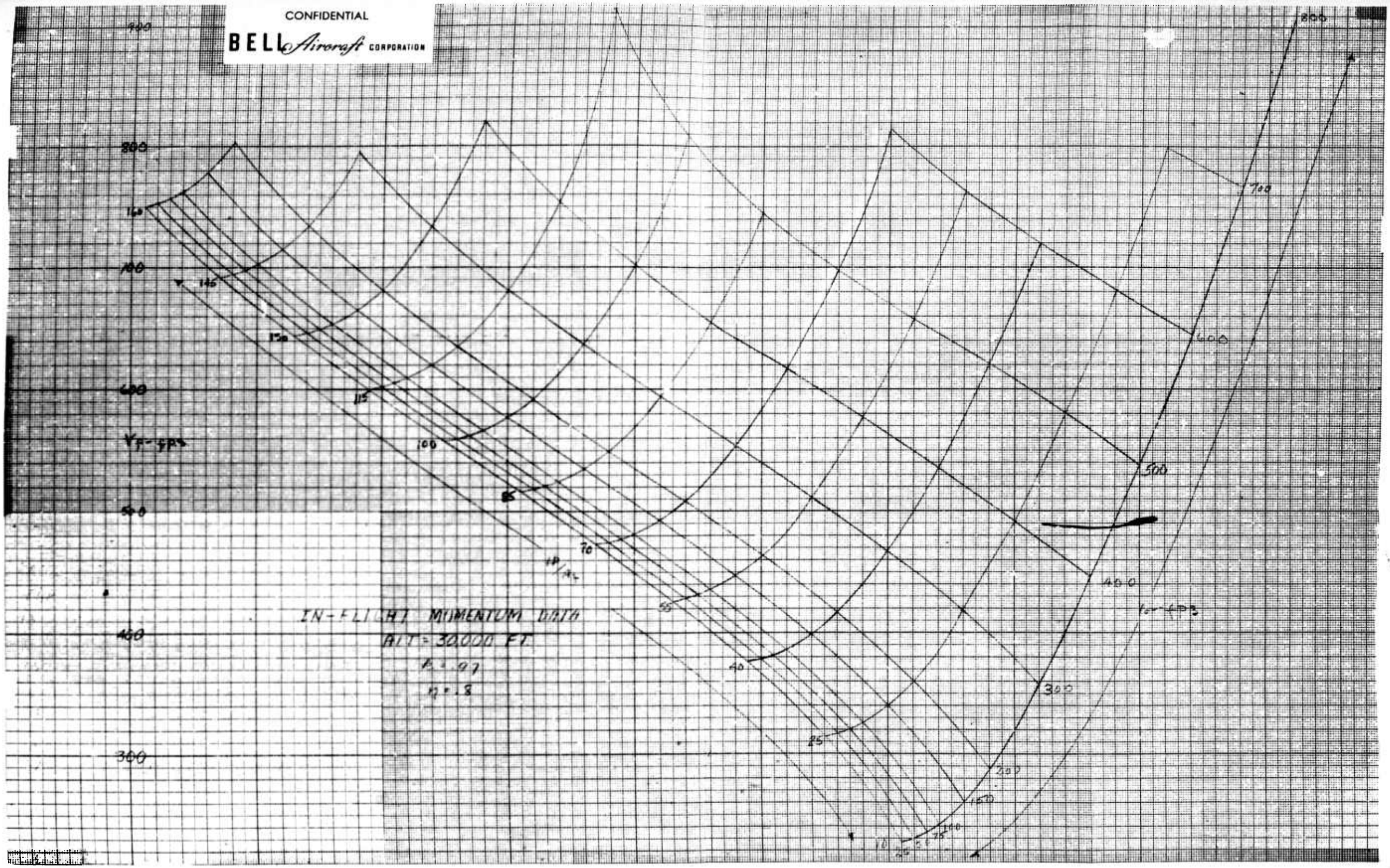

Figure B19 cont.

BELL Aircraft CORPORATION

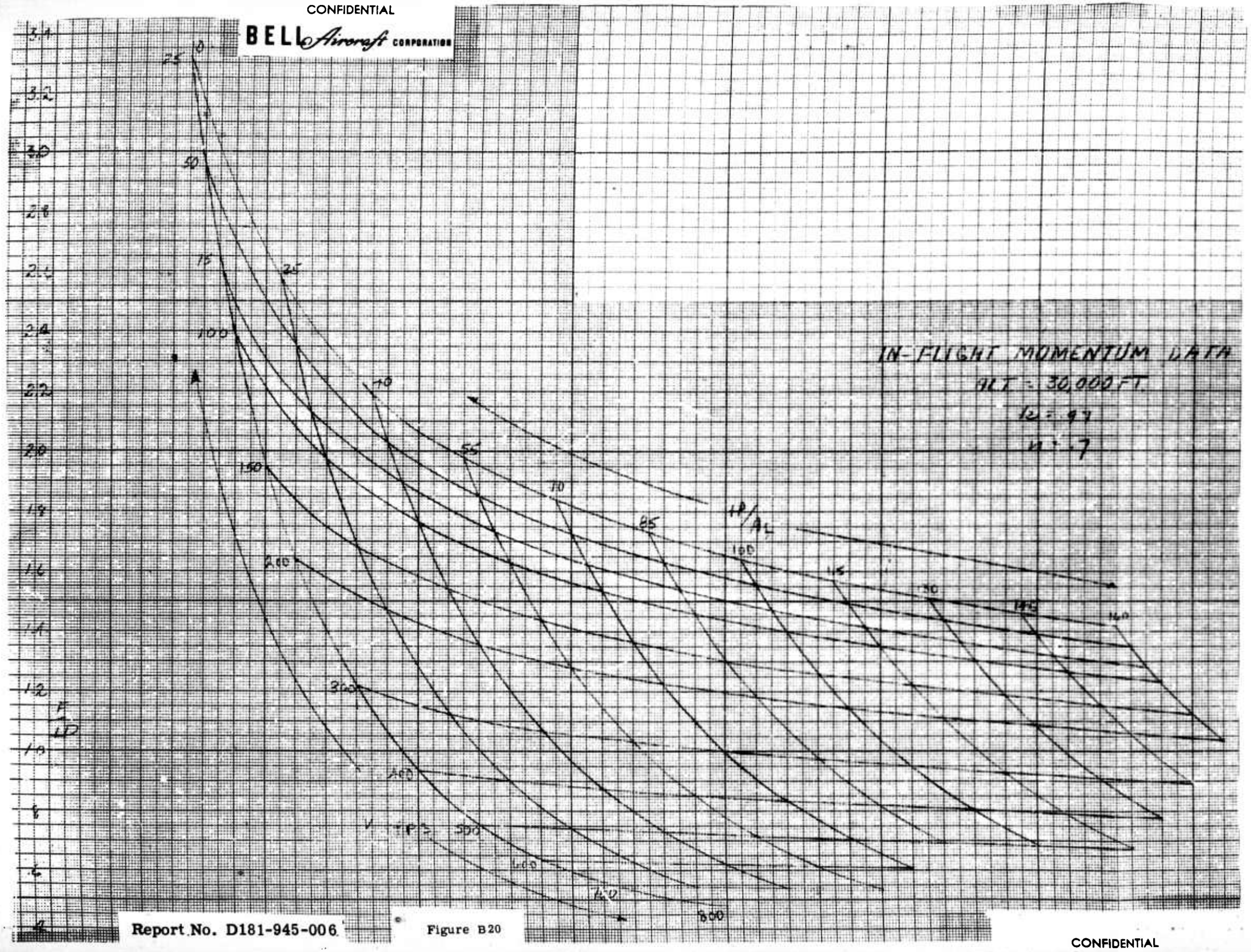

Report No. D181-945-006

Figure B20

BELL Aircraft CORPORATION

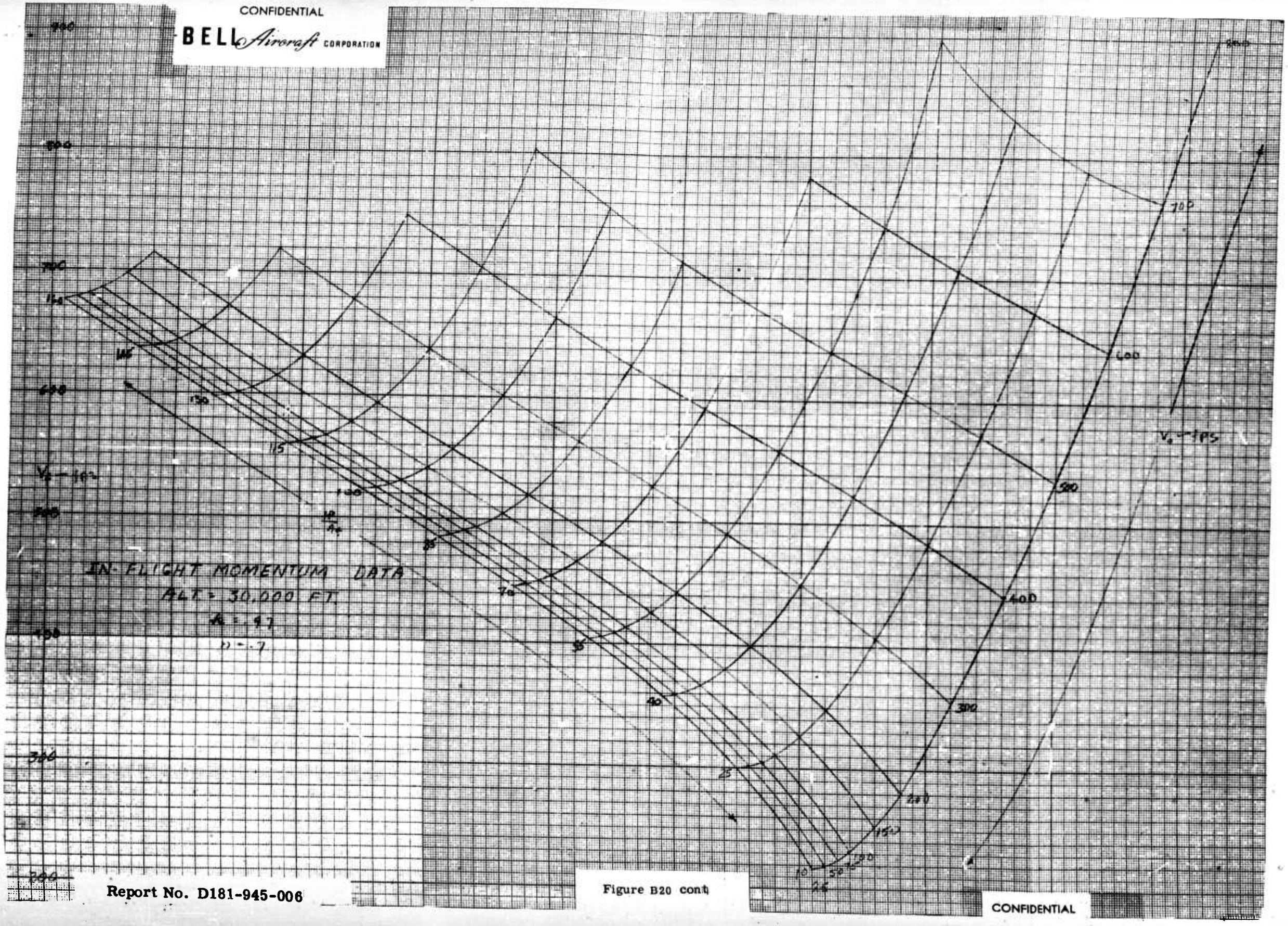

Figure B20 cont

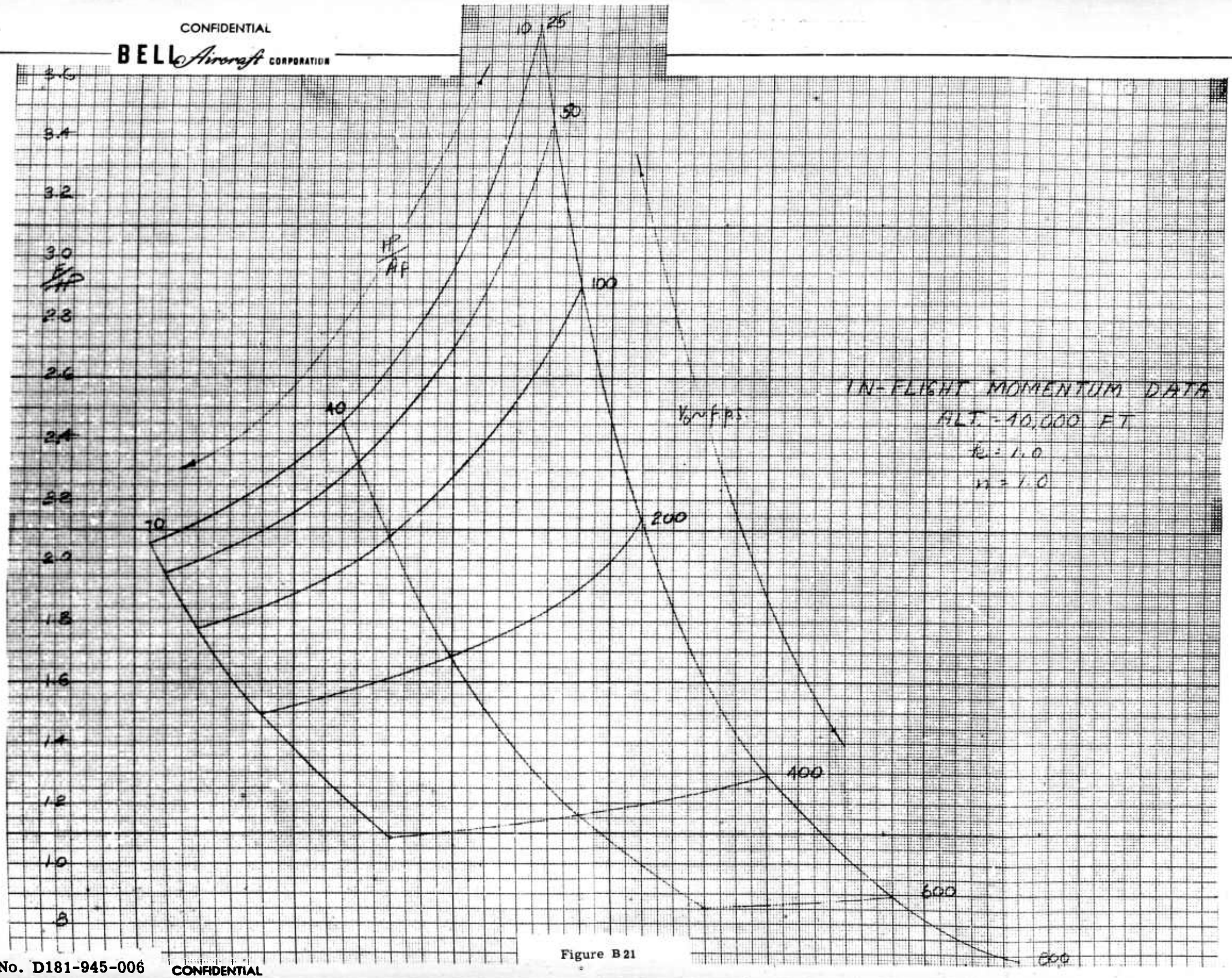
IN-FLIGHT MOMENTUM DATA
ALT. - 10,000 FT.
M = 1.0
M = 1.0
V_ENFPS
HP/AP
3.6
3.4
3.2
3.0
2.8
2.6
2.4
2.2
2.0
1.8
1.6
1.4
1.2
1.0
.8
1
10
25
50
100
200
400
600
800
10

Figure B 21

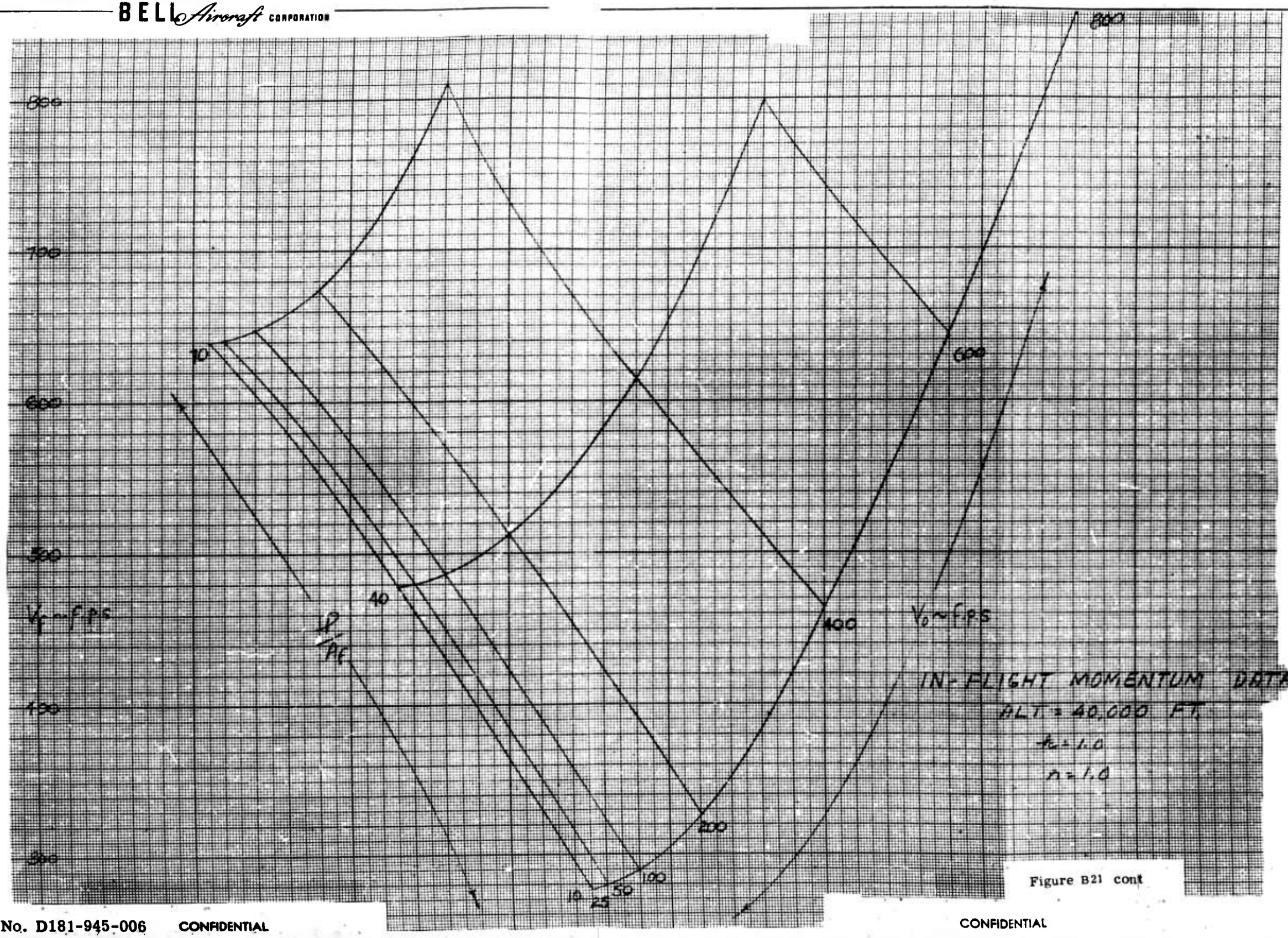

Figure B21 cont

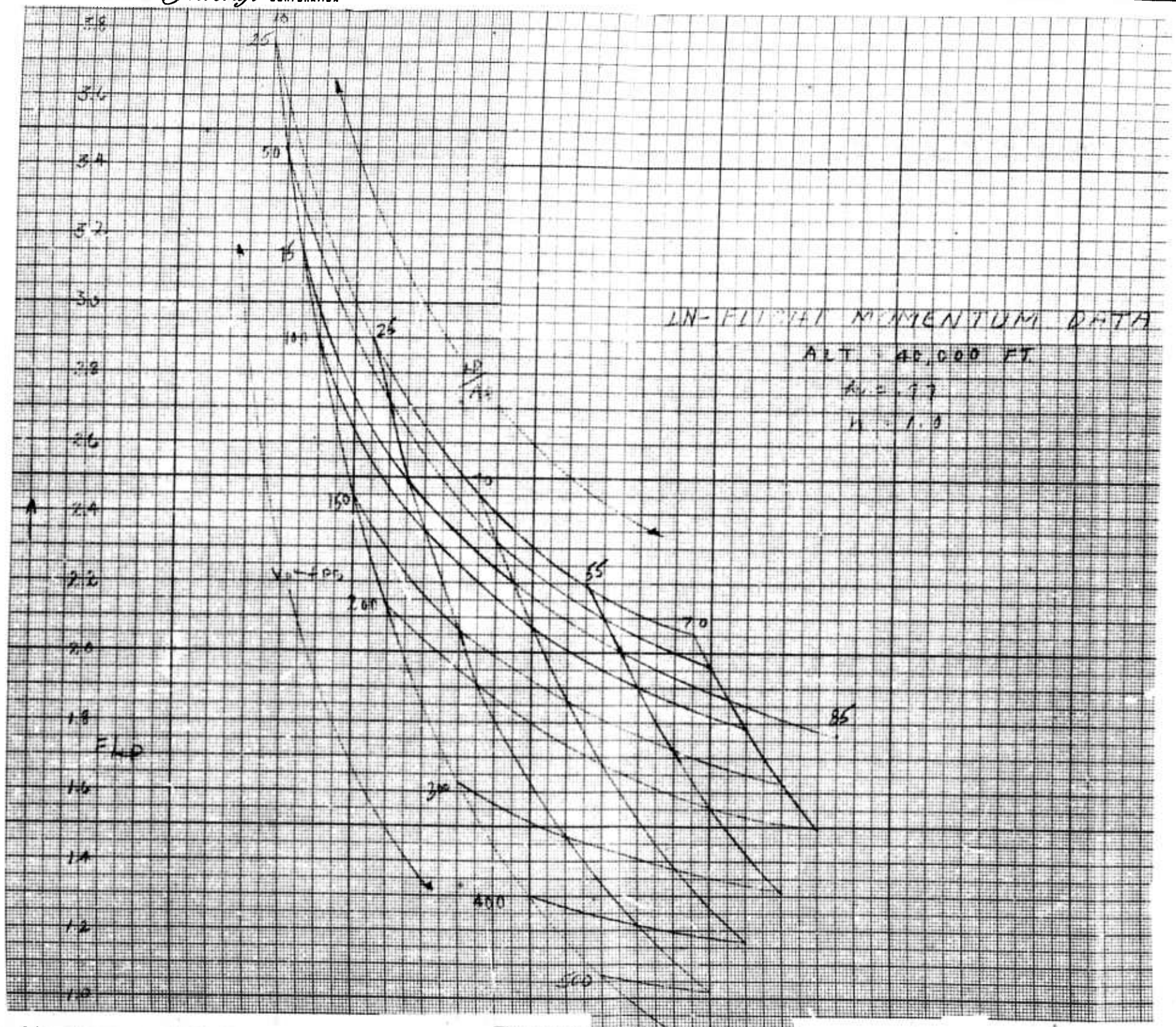

Figure B22

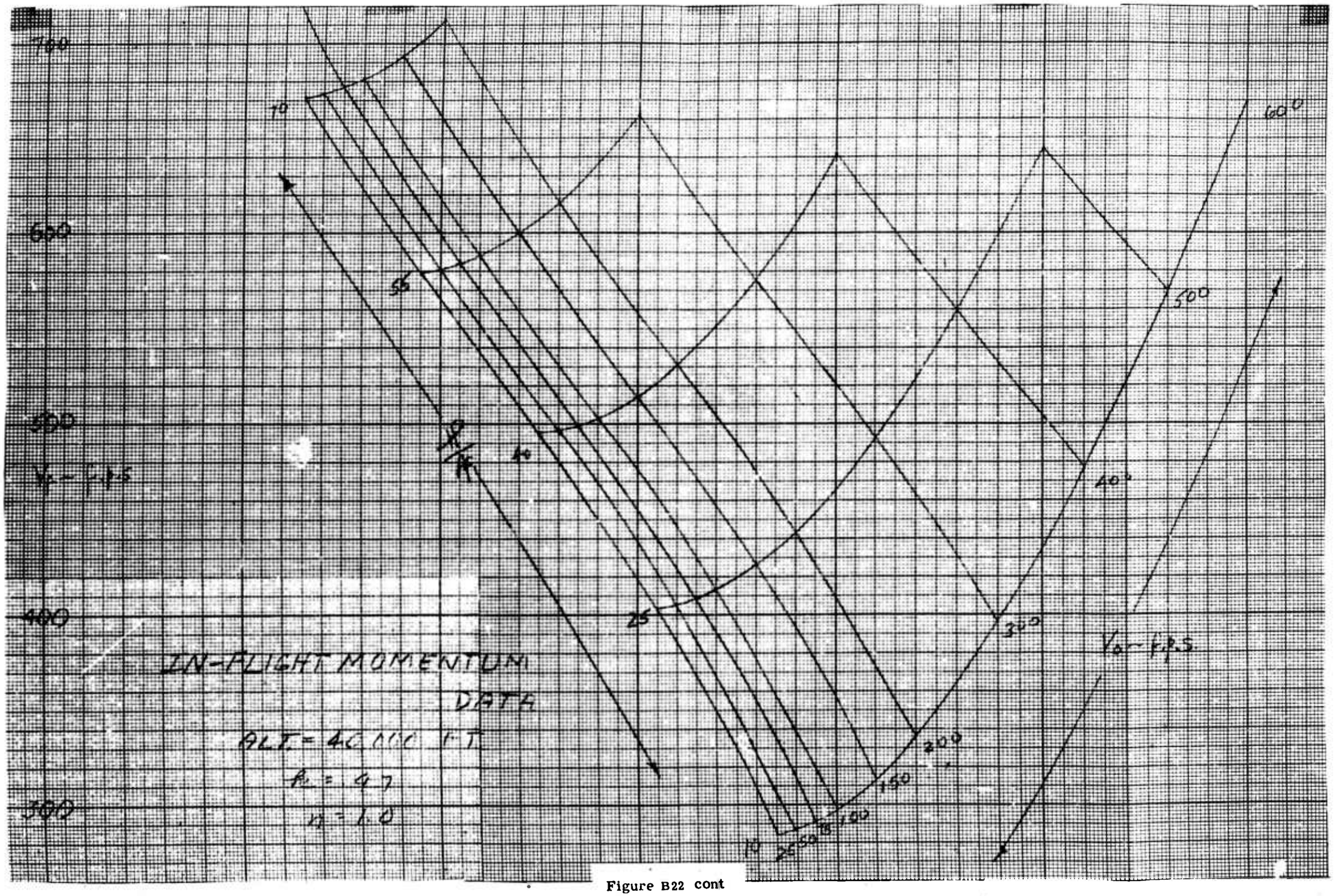

Figure B22 cont

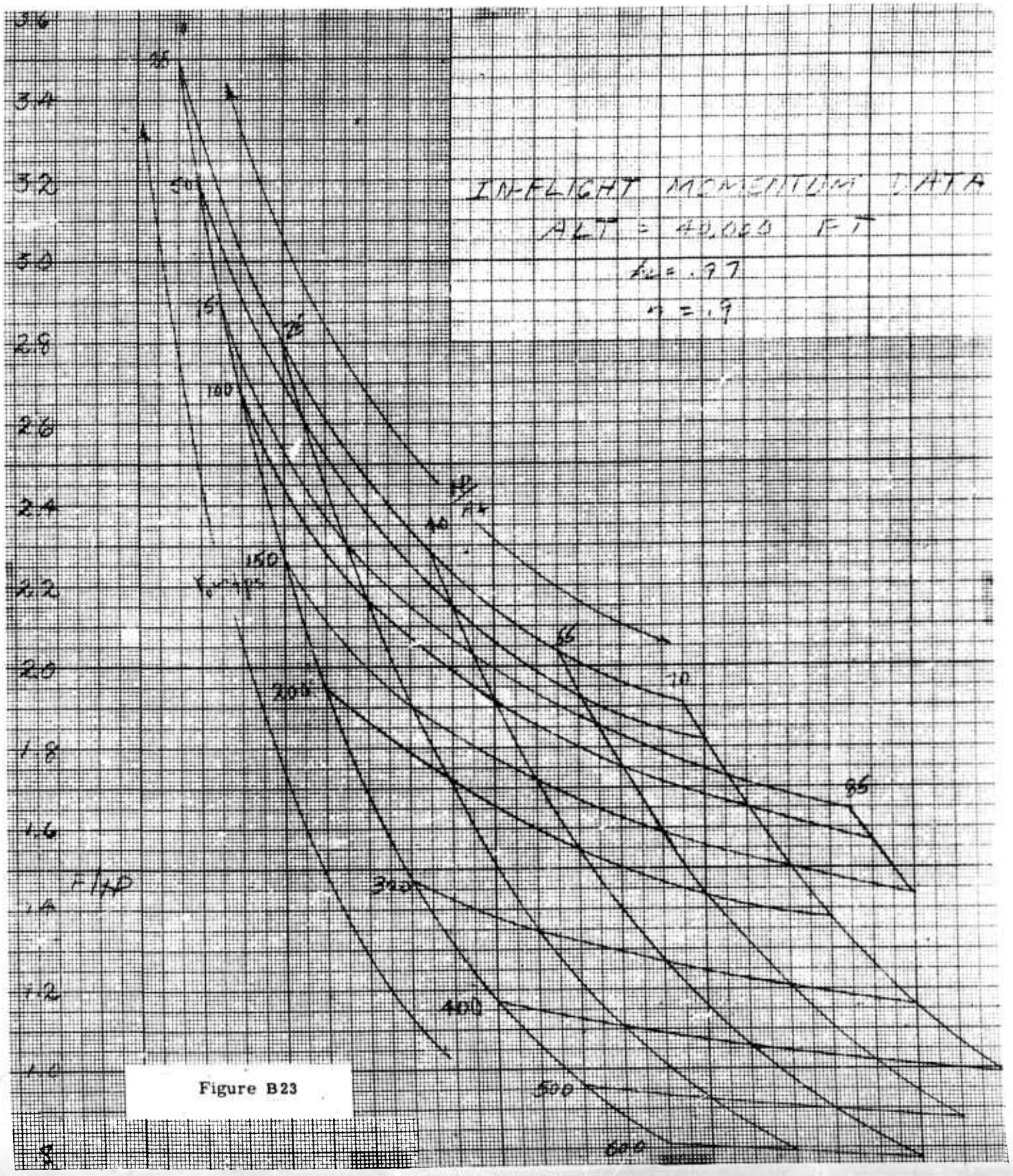
IN-FLIGHT MACH/ALTITUDE DATA
ALT = 40,000 FT
W = .97
n = 1.7
3.6
3.4
3.2
3.0
2.8
2.6
2.4
2.2
2.0
1.8
1.6
1.4
1.2
1.0
.8
95
90
85
80
75
70
65
60
55
50
45
40
35
30
25
20
15
10
5
100
150
200
300
400
500
600

Figure B23

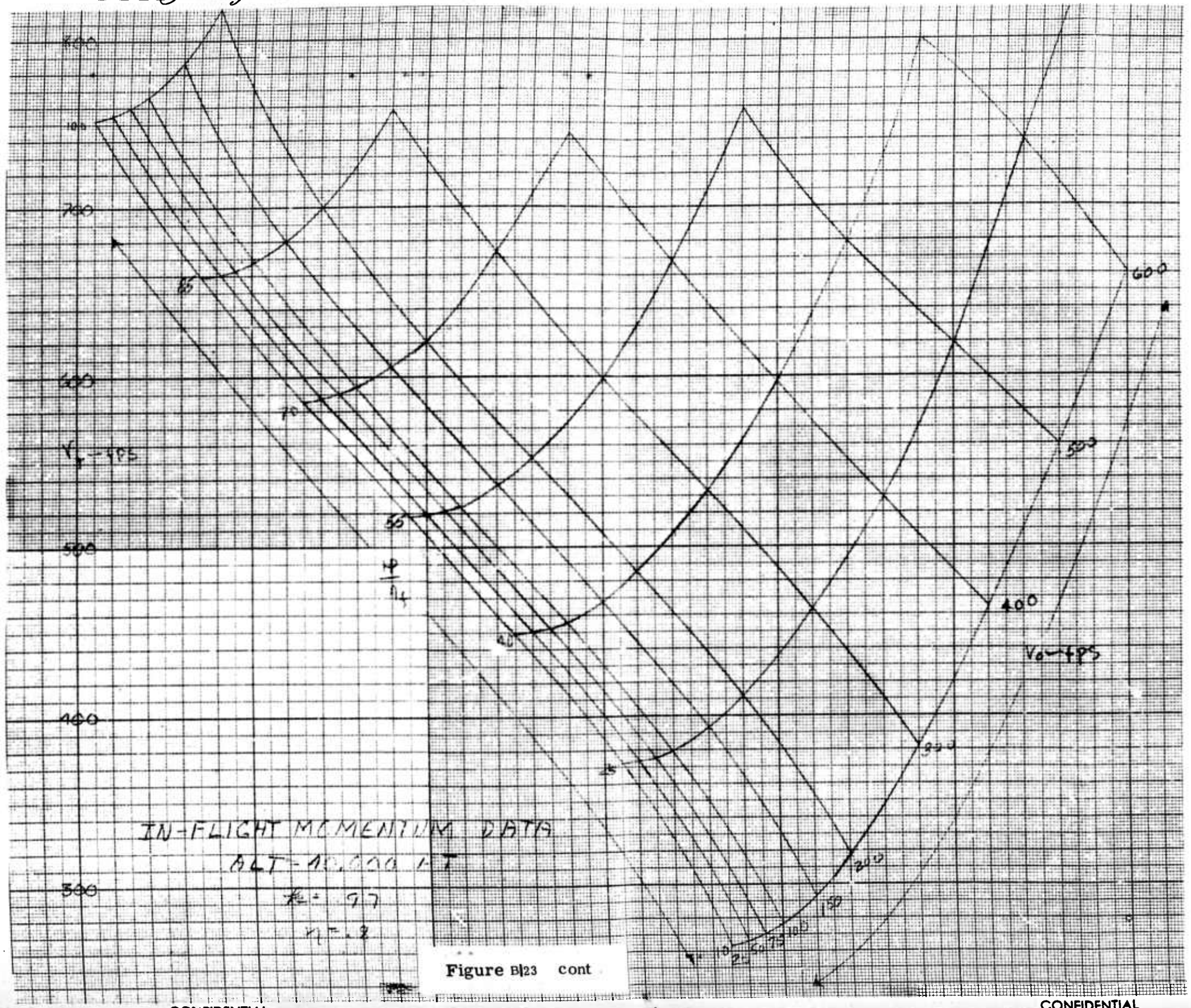

Figure B123 cont

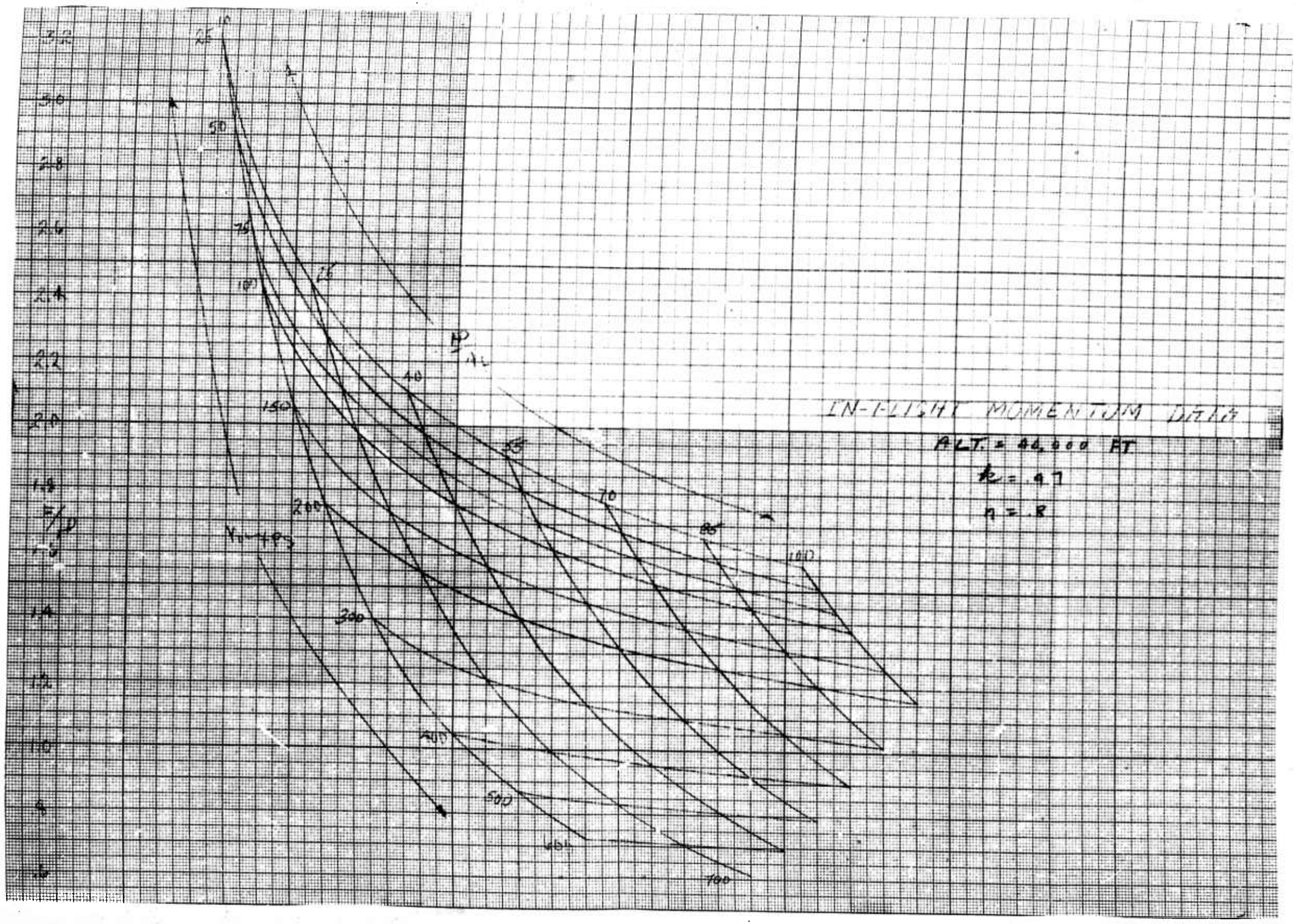
IN-FLIGHT MOMENTUM DATA
ALT. = 44,000 FT
k = .97
n = .8
M
V_T = 495
10
15
20
25
30
40
50
60
70
80
100
150
200
300
400
500
600
700
2.2
2.0
1.8
1.6
1.4
1.2
1.0
.8
.6

Figure B24

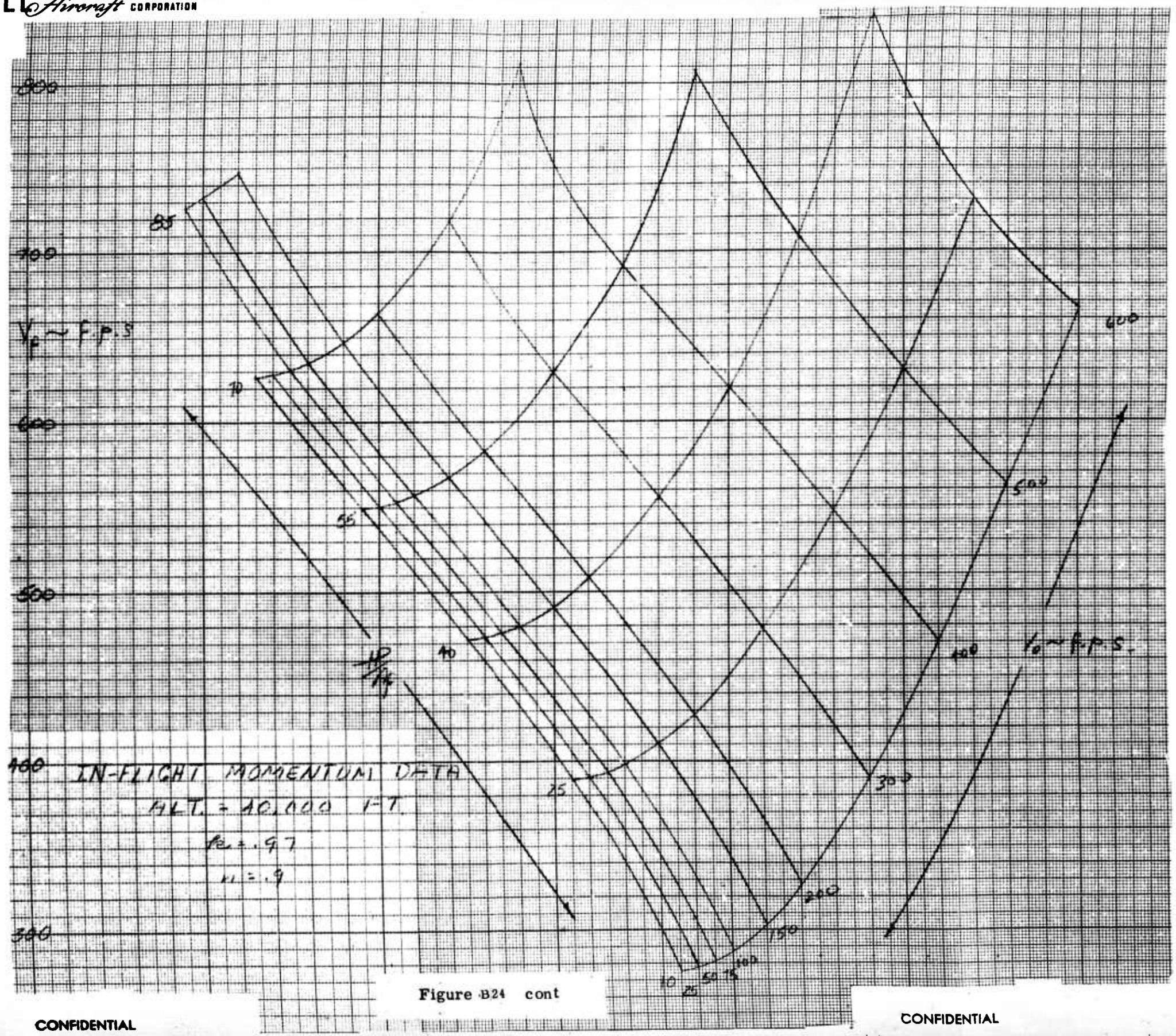

Figure B24 cont

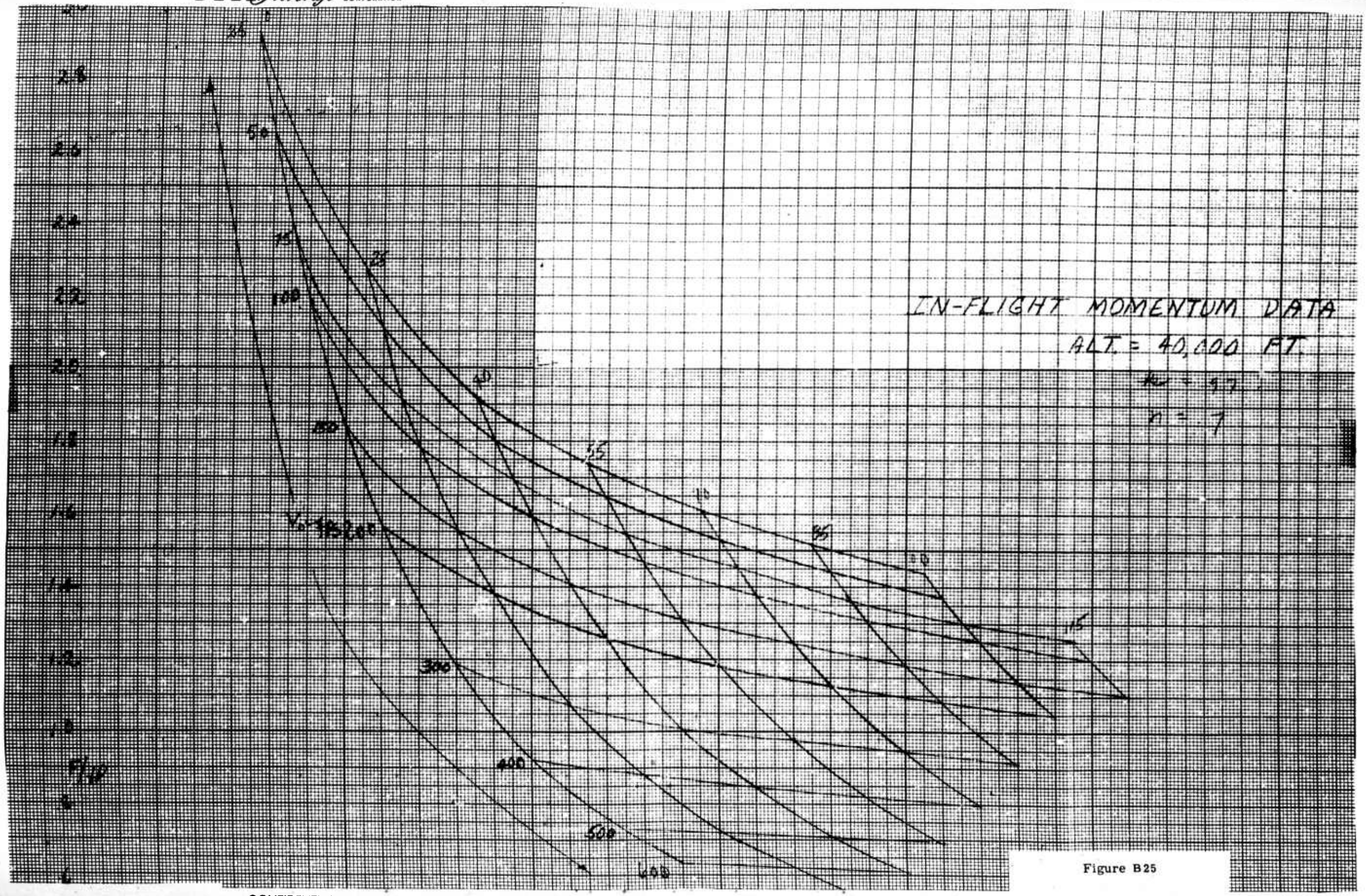
IN-FLIGHT MOMENTUM DATA
ALT. = 40,000 FT.
n = 1
2.8
2.6
2.4
2.2
2.0
1.8
1.6
1.4
1.2
1.0
.8
.6
.4
.2
0
Mo
Vo
300
400
500
600

Figure B25

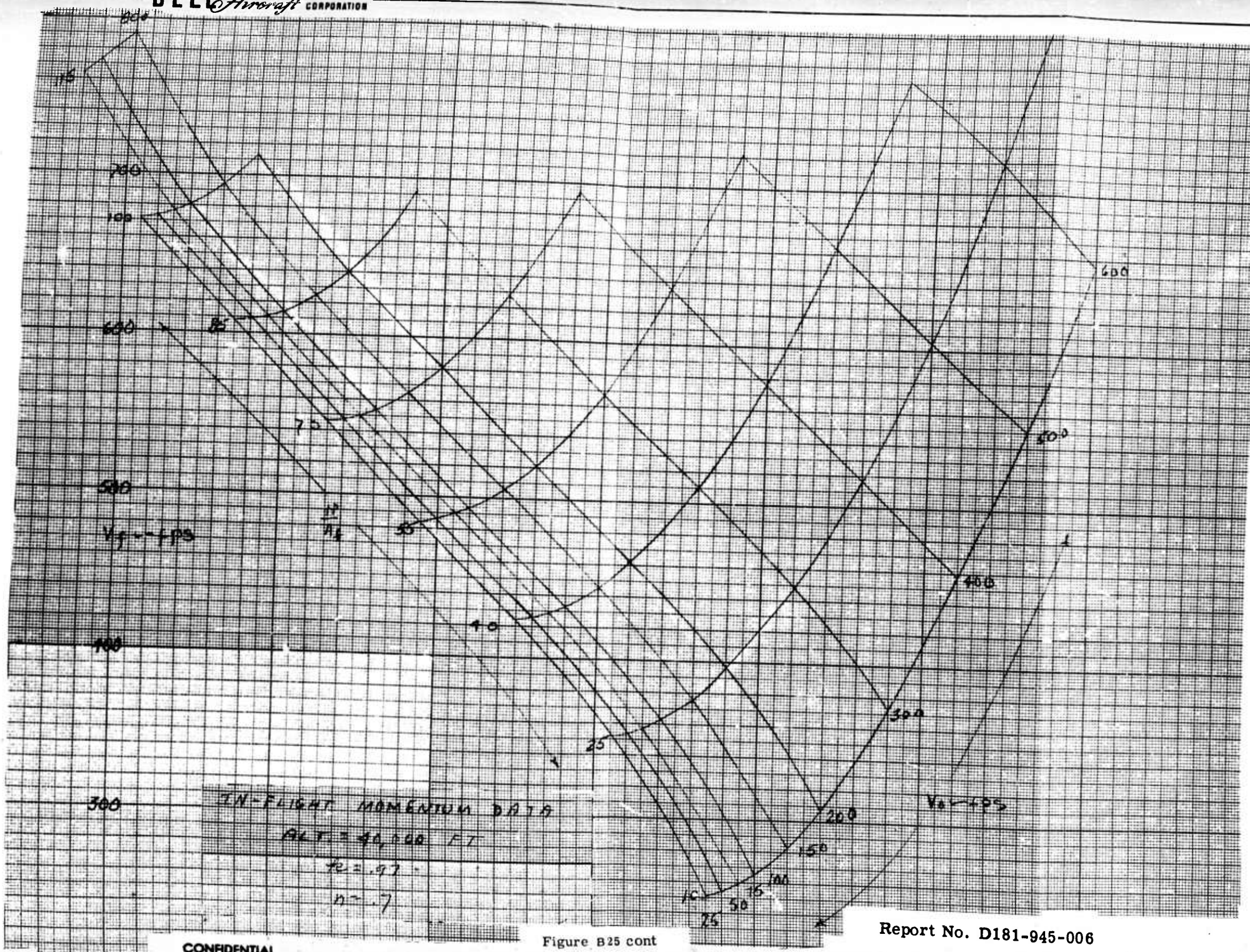

Figure B25 cont

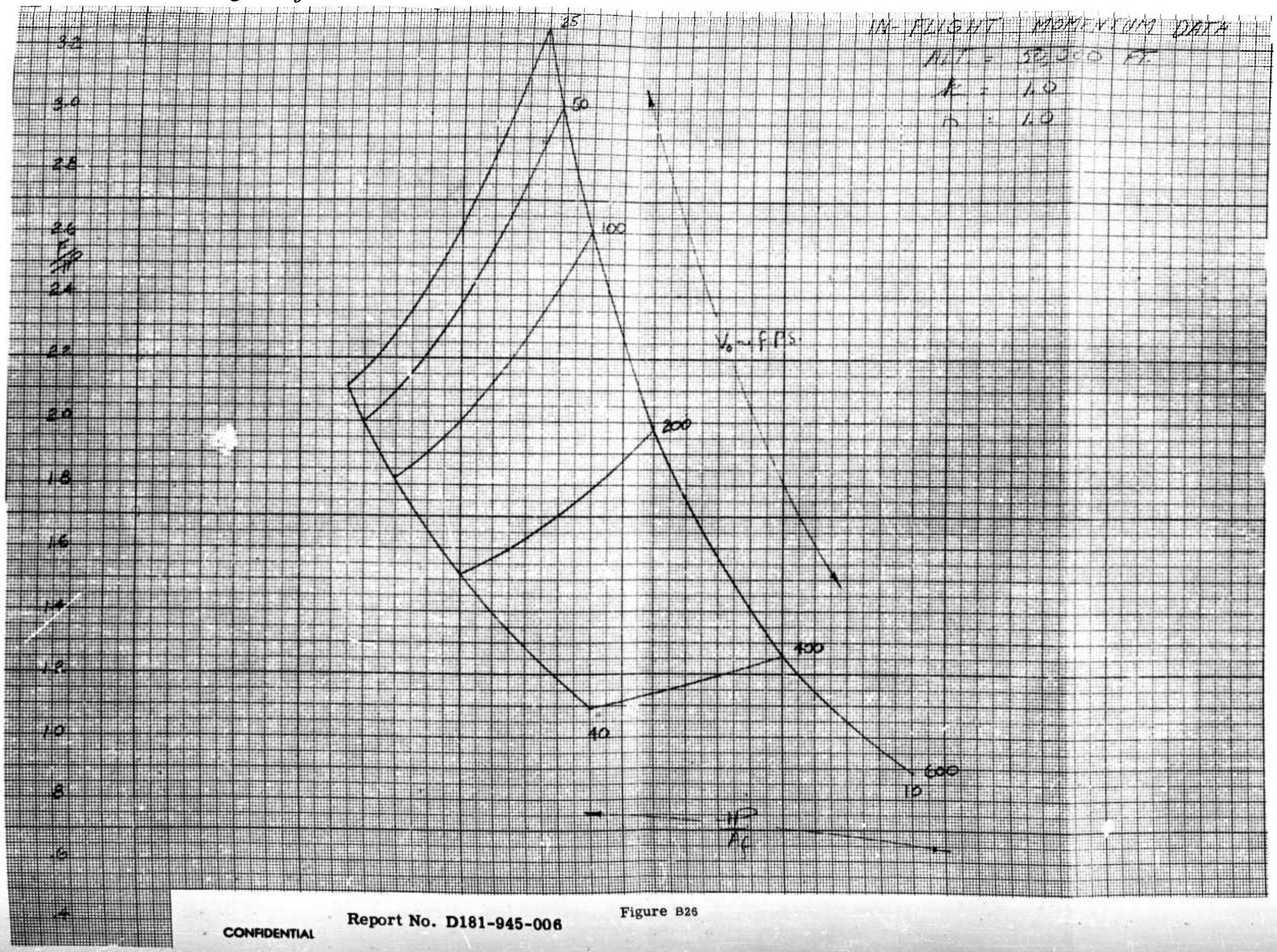
IN-FLIGHT PERFORMANCE DATA
ALT. = 50,000 FT.
K = 1.0
n = 1.0
V_o - FPS.
25
50
100
200
400
600
40
10
3.2
3.0
2.8
2.6
2.4
2.2
2.0
1.8
1.6
1.4
1.2
1.0
.8
.6
.4
$\frac{HP}{\Delta G}$

Figure B26

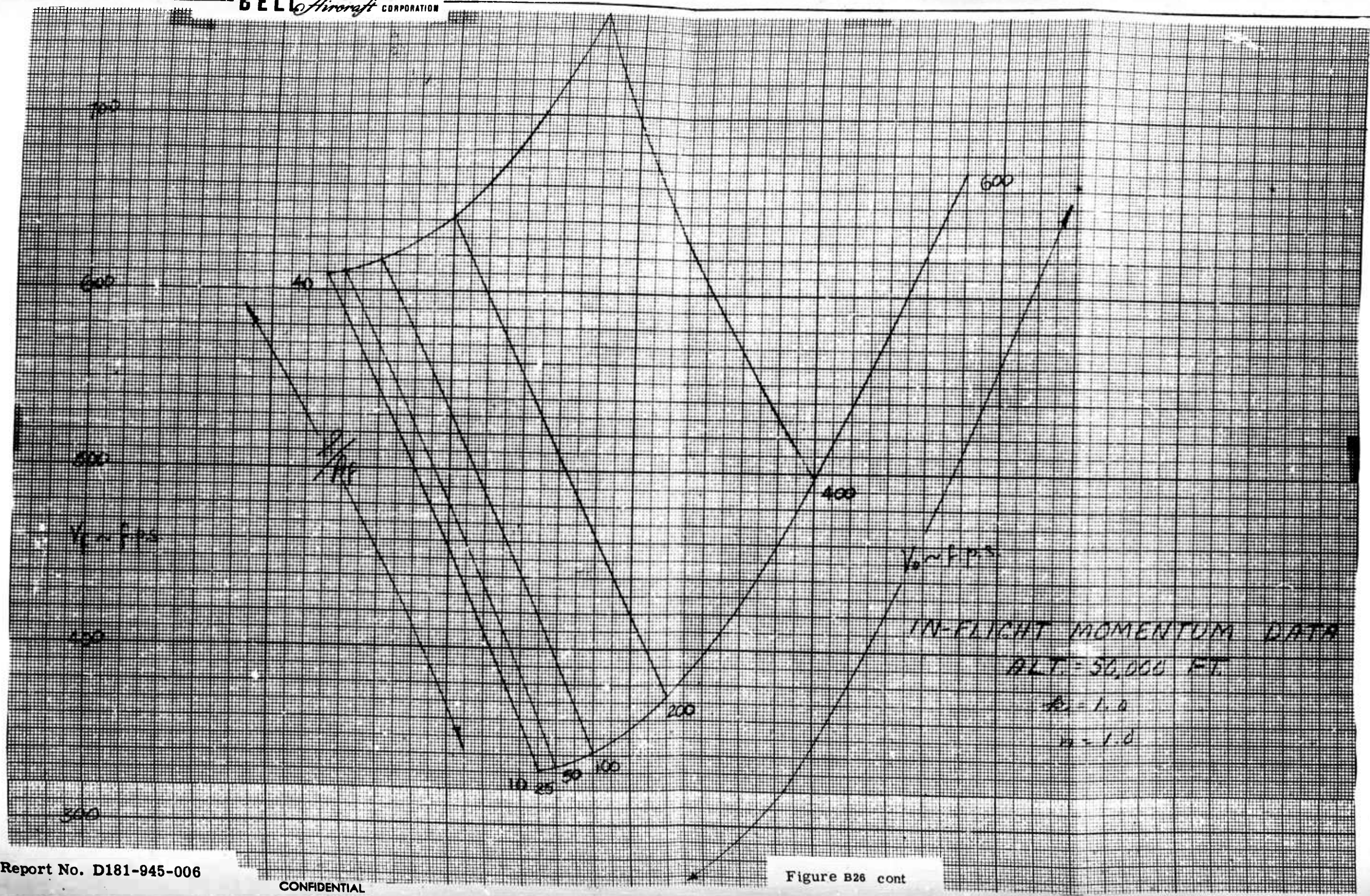

Figure B26 cont

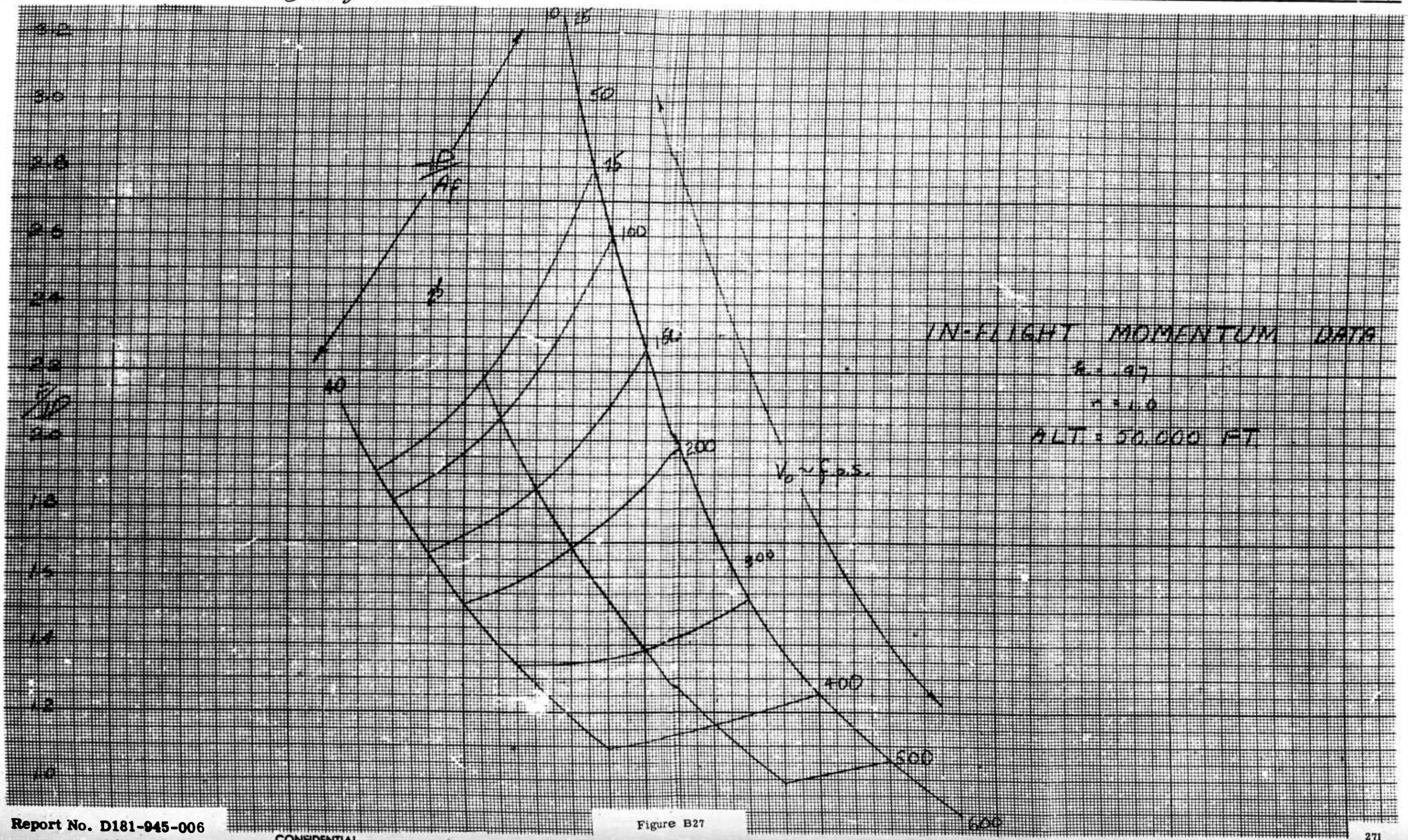
IN-FLIGHT MOMENTUM DATA
n = 1.0
ALT. = 50,000 FT.
V_o ~ f.p.s.
10
15
50
45
100
160
200
300
400
500
600
40
$\frac{D}{Ae}$
p

Figure B27

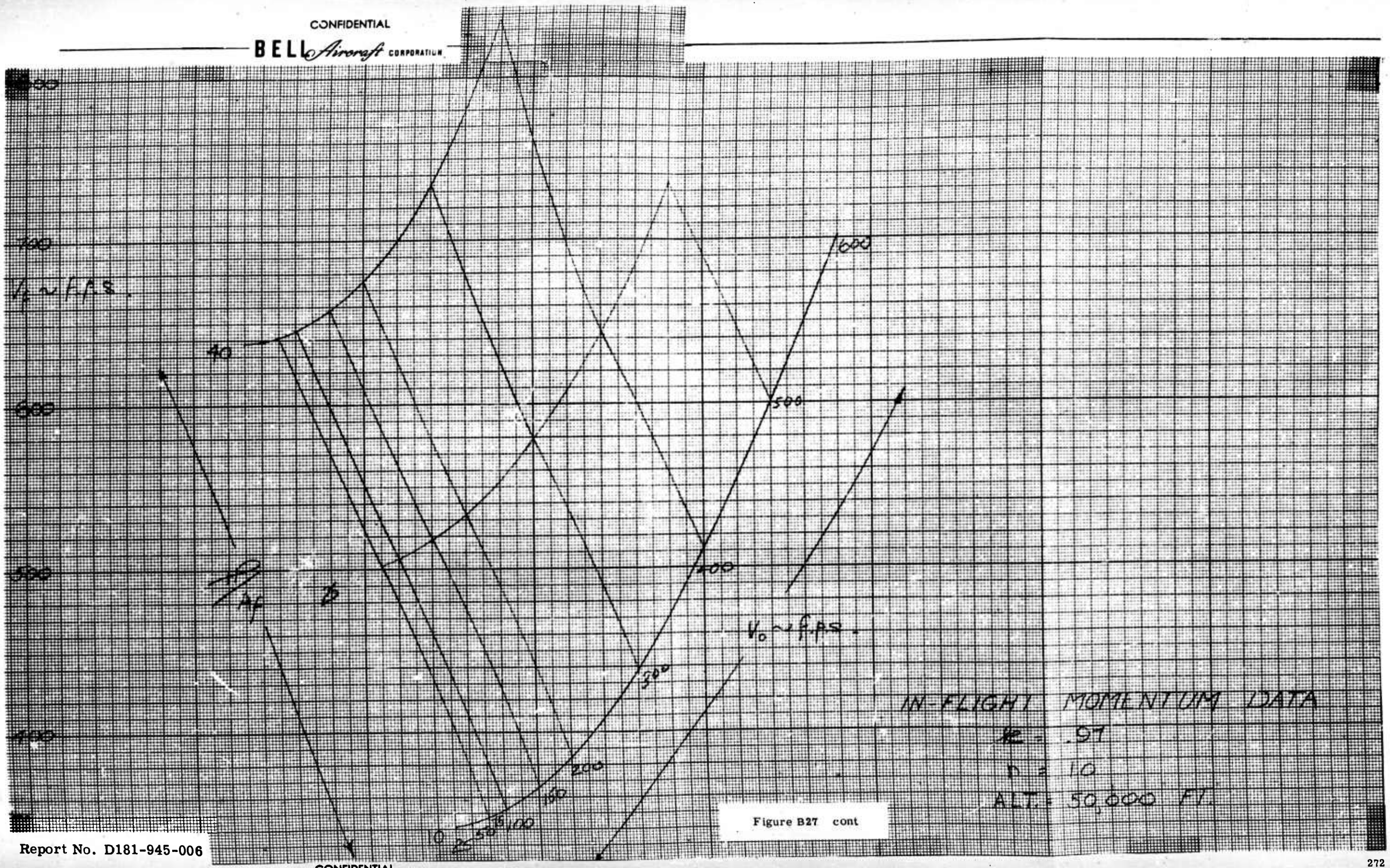

Figure B27 cont

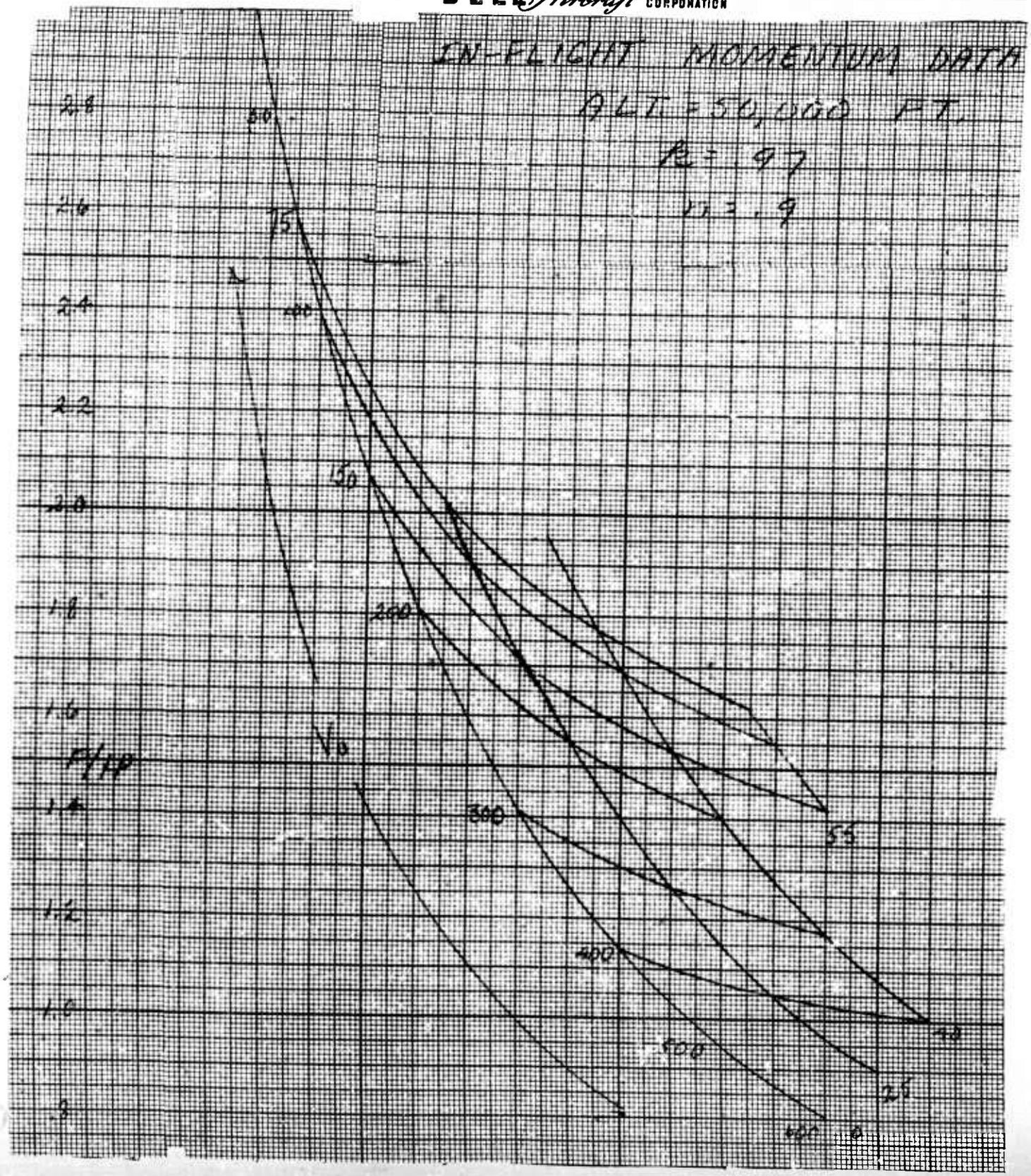

Report No. D181-945-006

Figure B 28

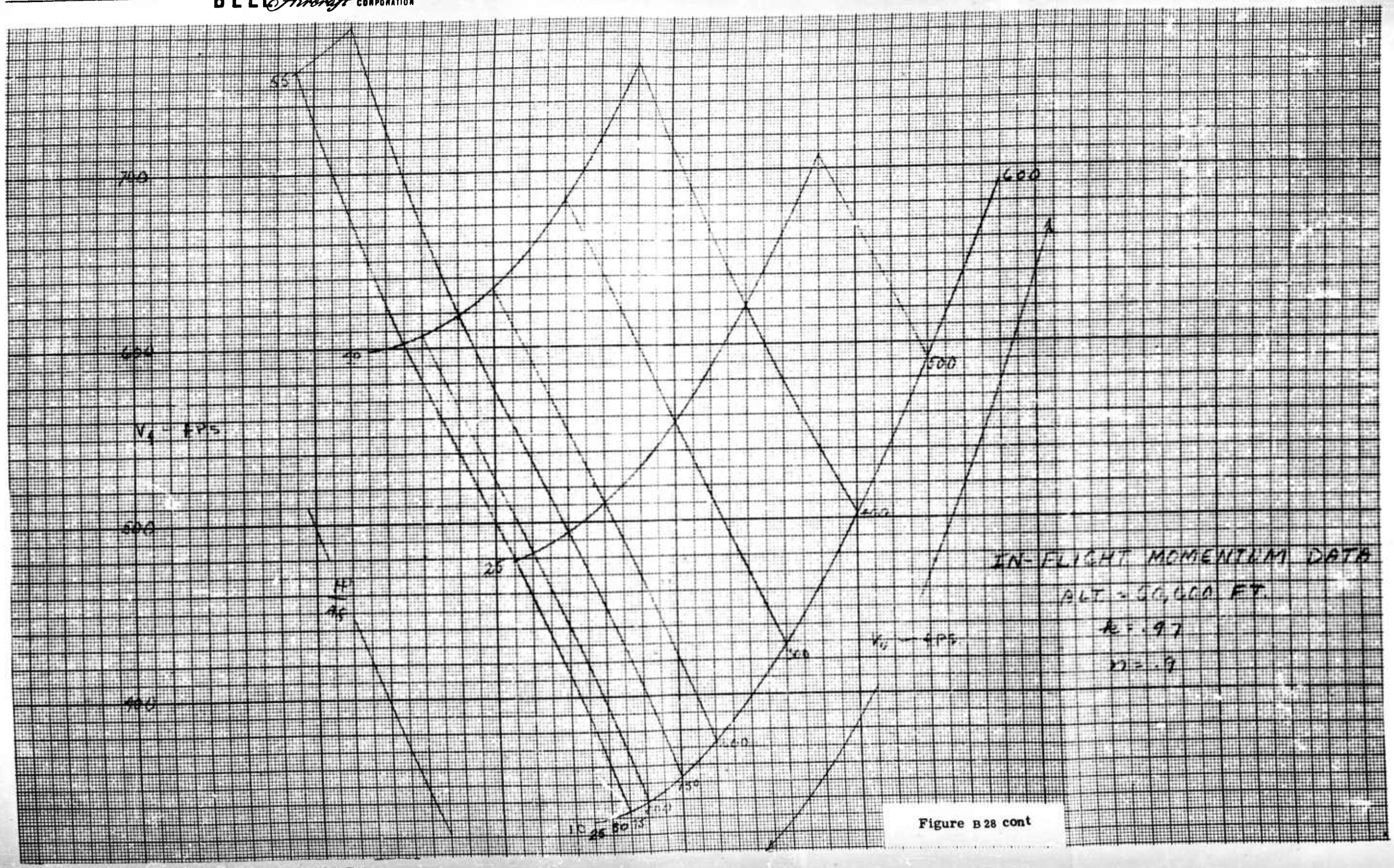

Figure B 28 cont

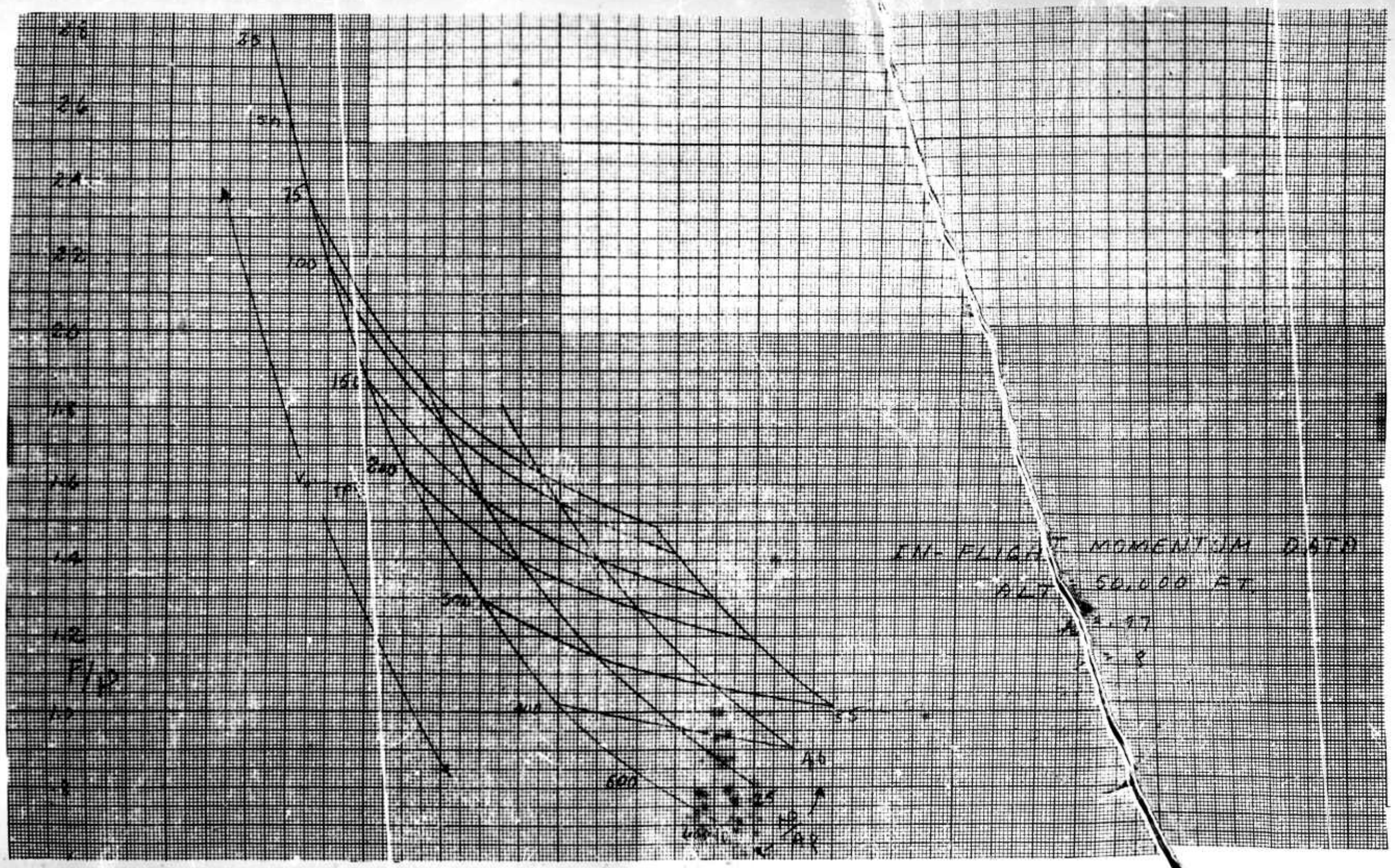
IN-FLIGHT MOMENTUM D.STD
ALT = 50,000 FT
M = .97
n = 3
35
25
100
840
600
F/P

Figure B29

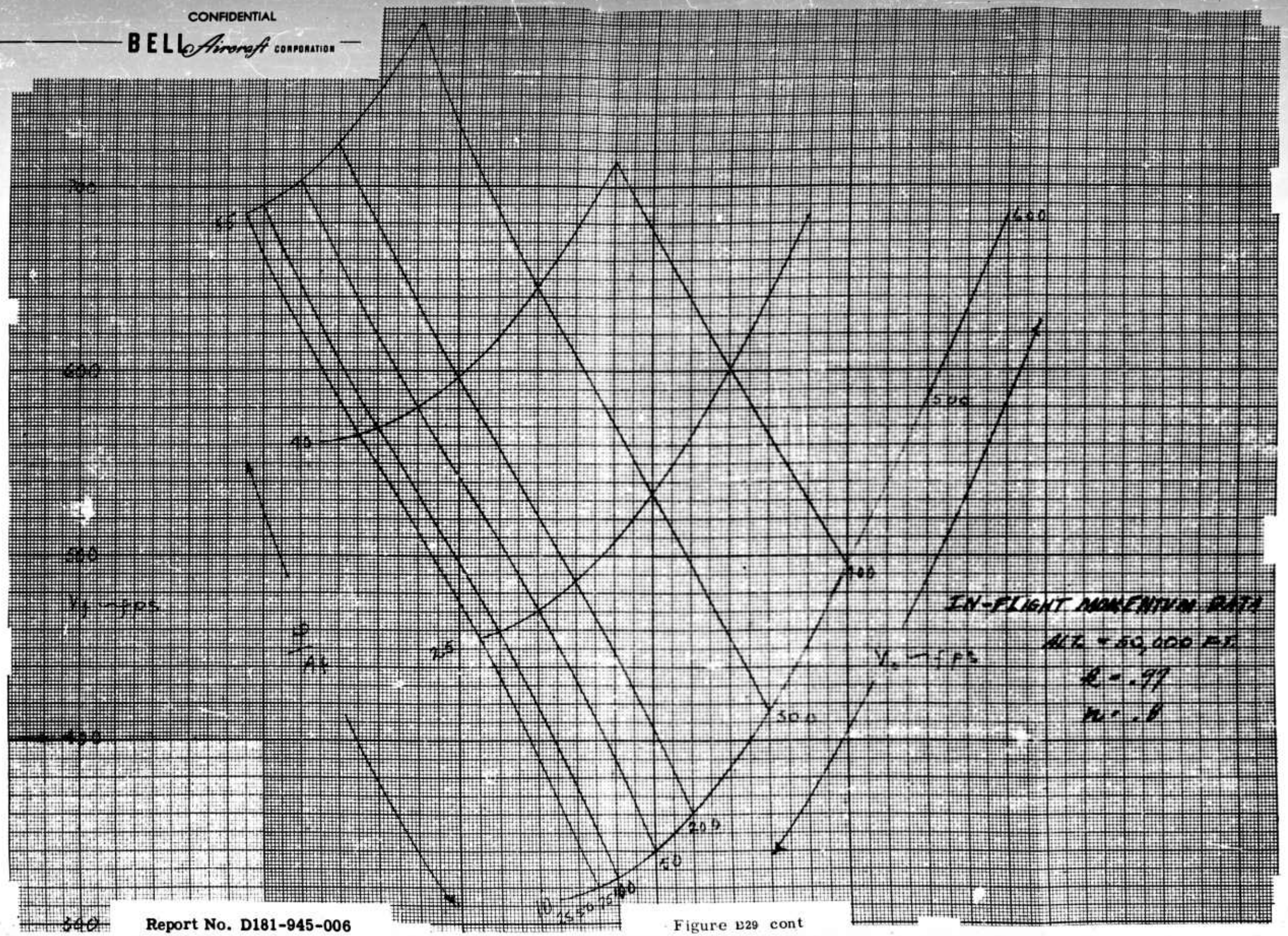

Figure D29 cont

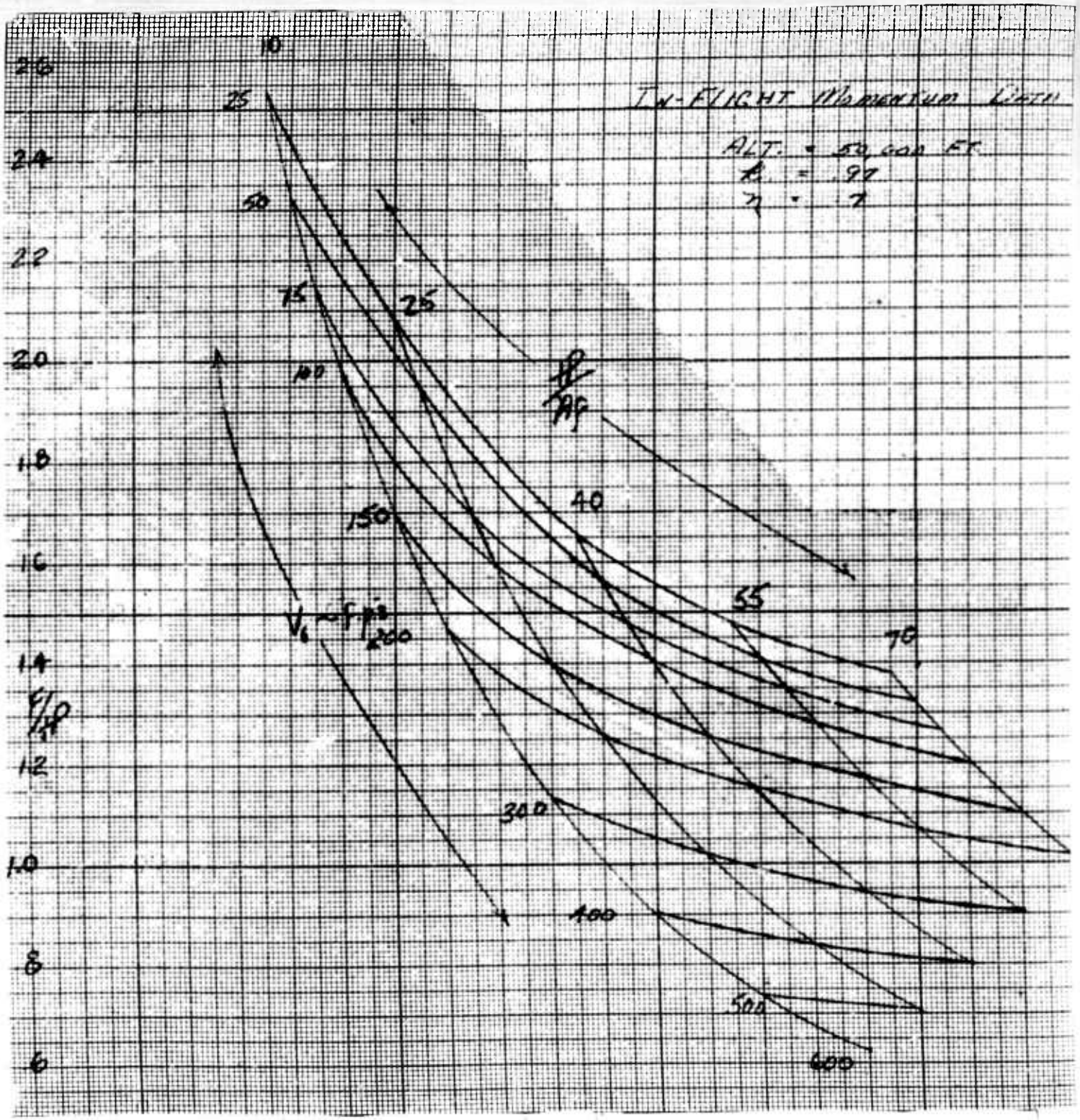

Report No. D181-945-006

Figure B30

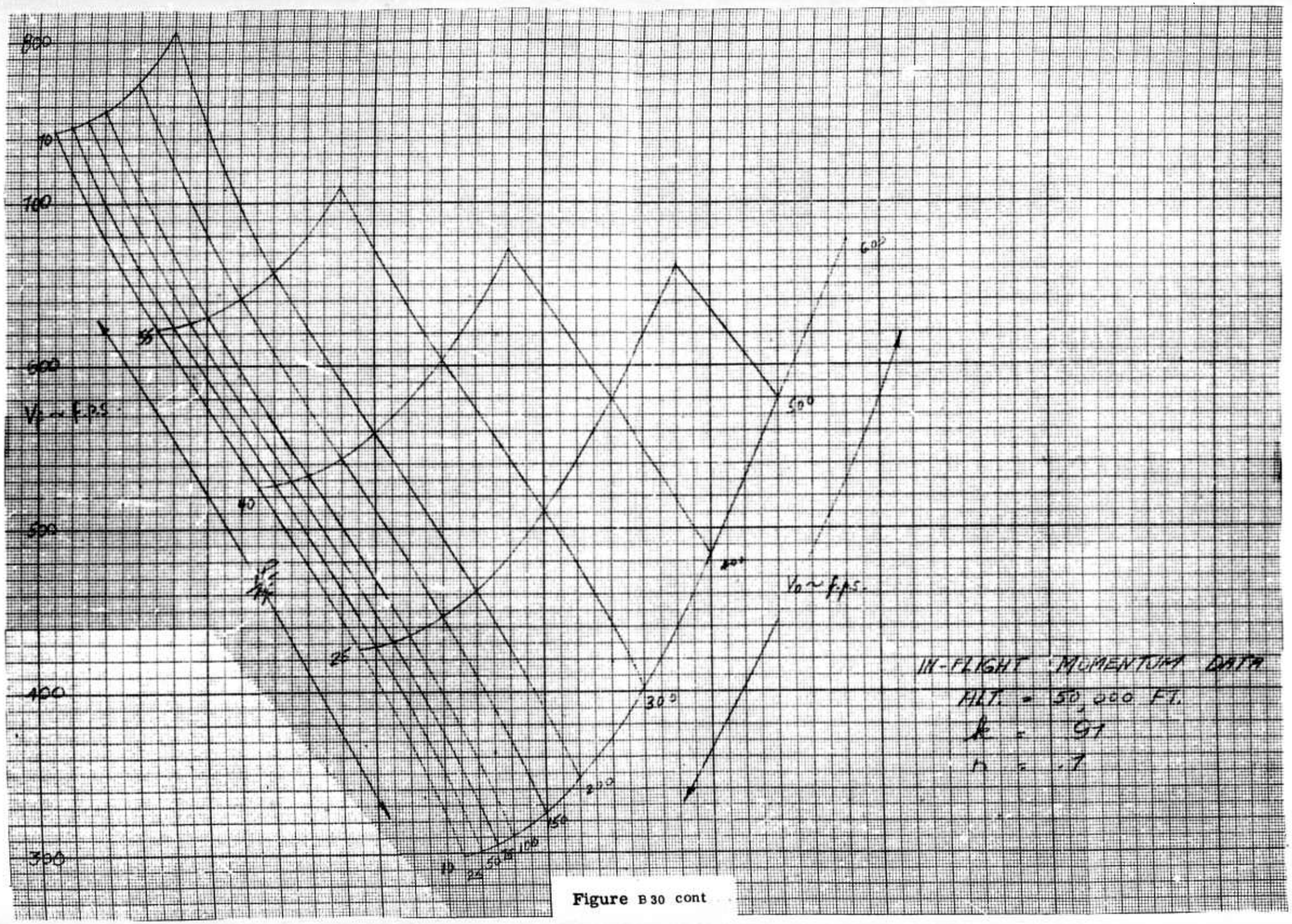

Figure B 30 cont

LOW SOLIDITY OFF-DESIGN CHARTS

(EXTRAPOLATED)

$R = \theta + 50(C_{l_0} - .4)$

REF. LEIGH
LEHMIN

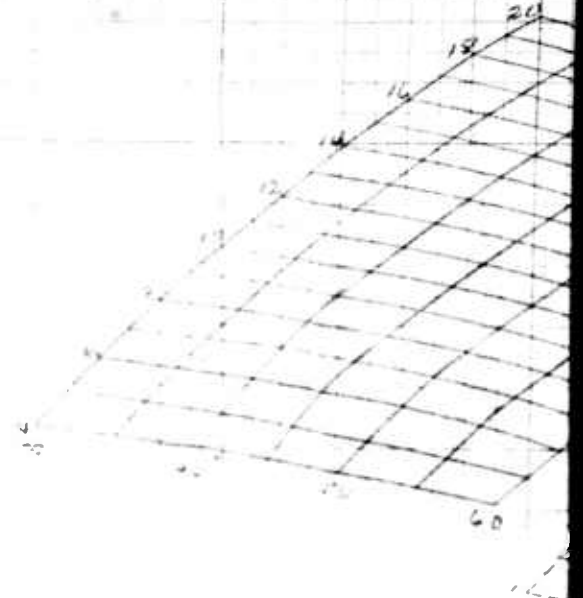

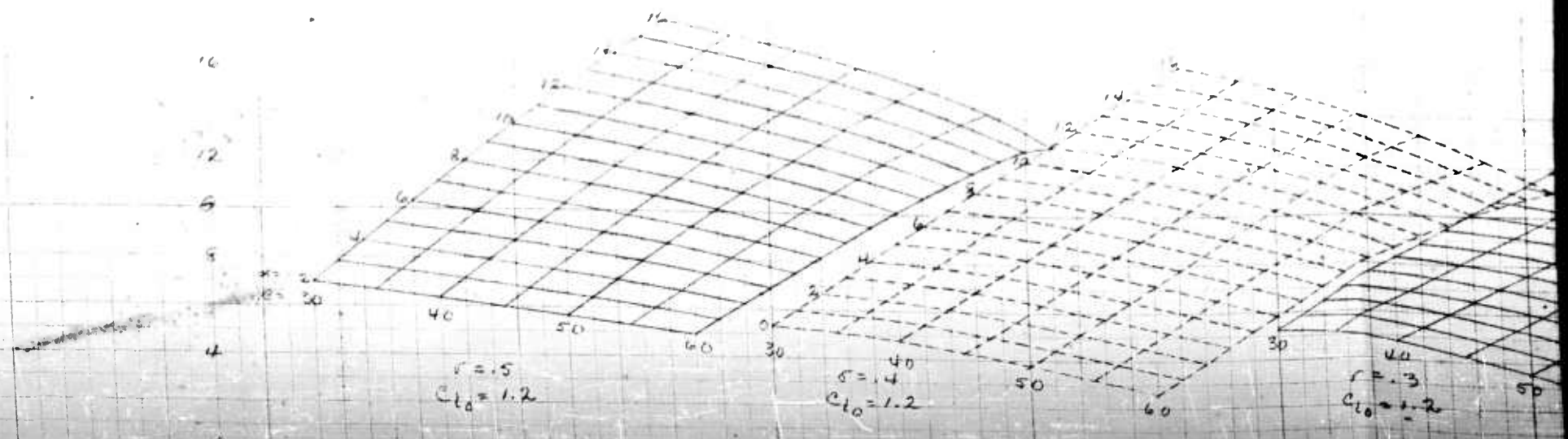

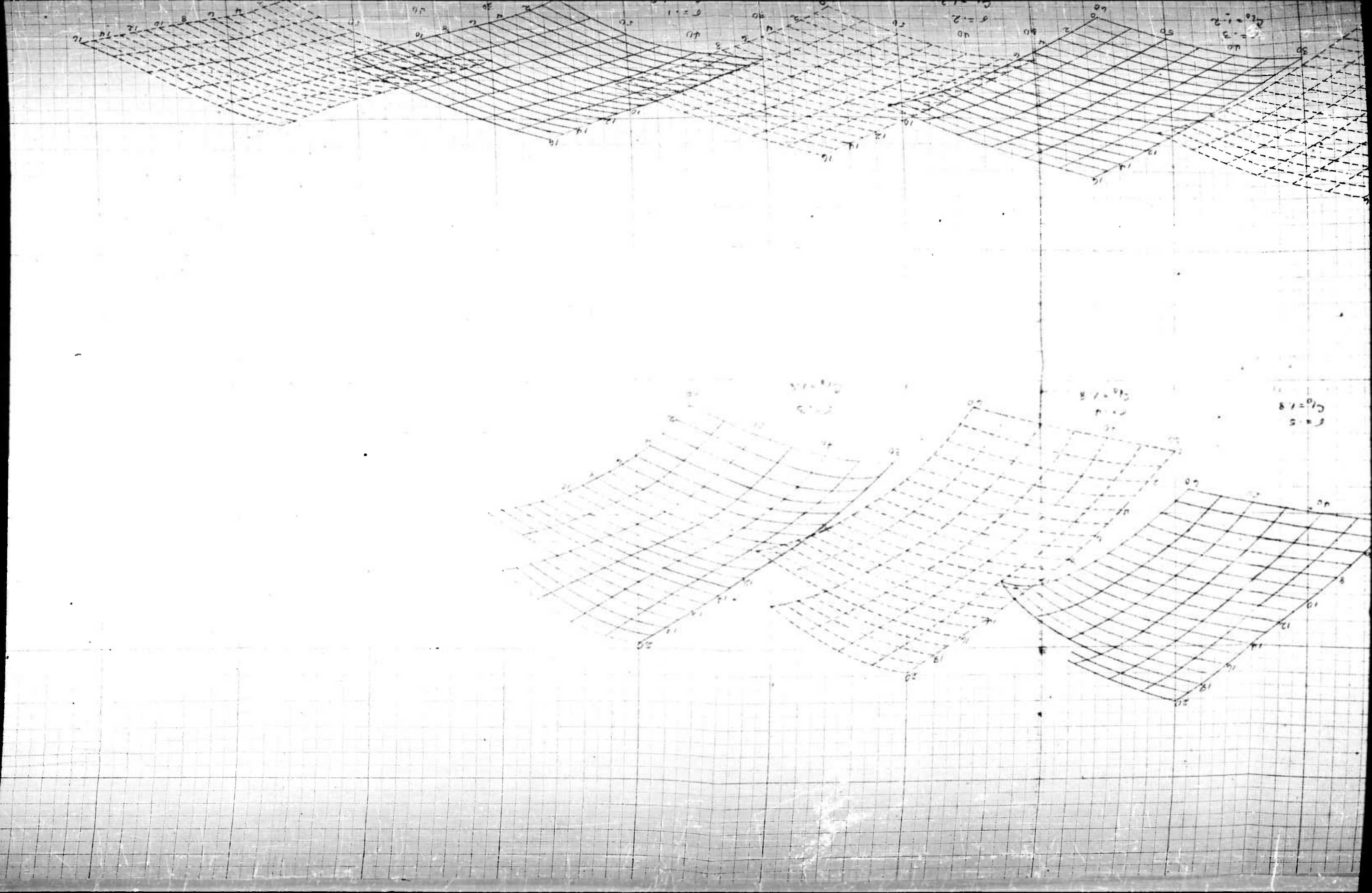

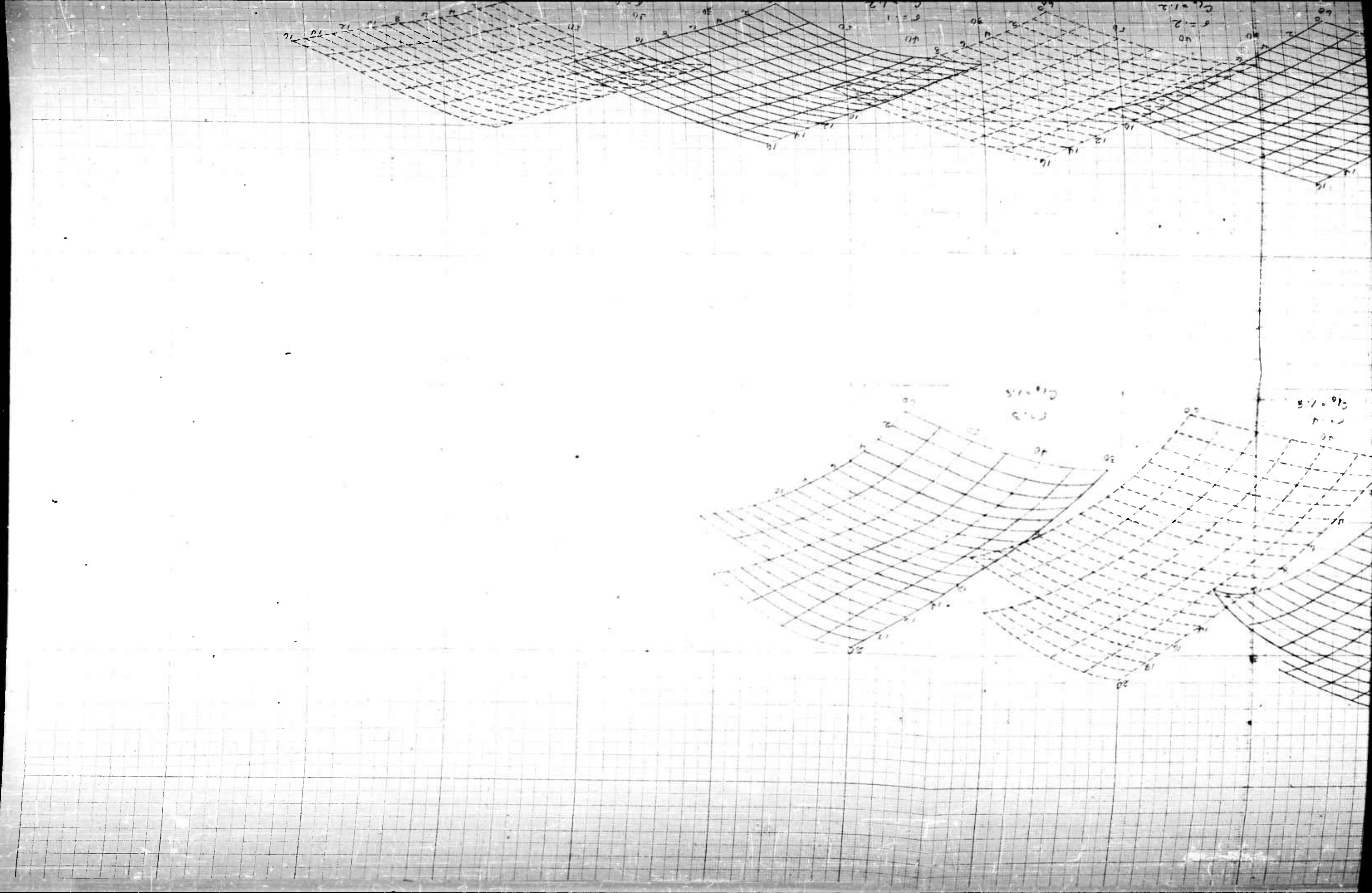

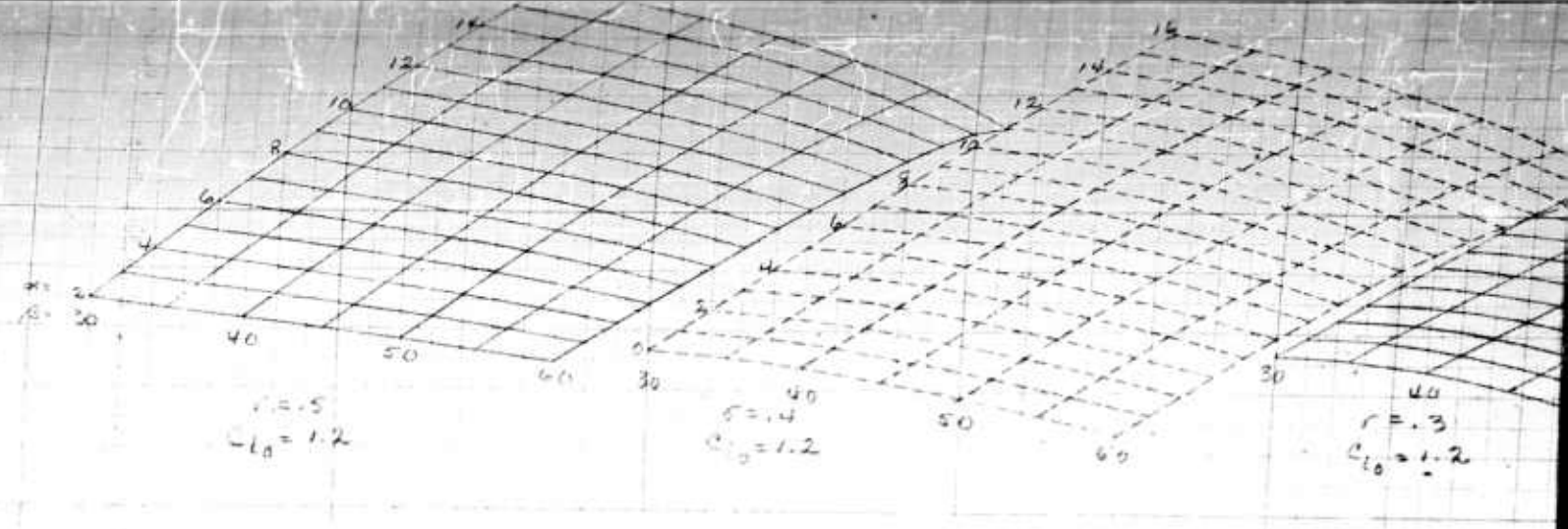

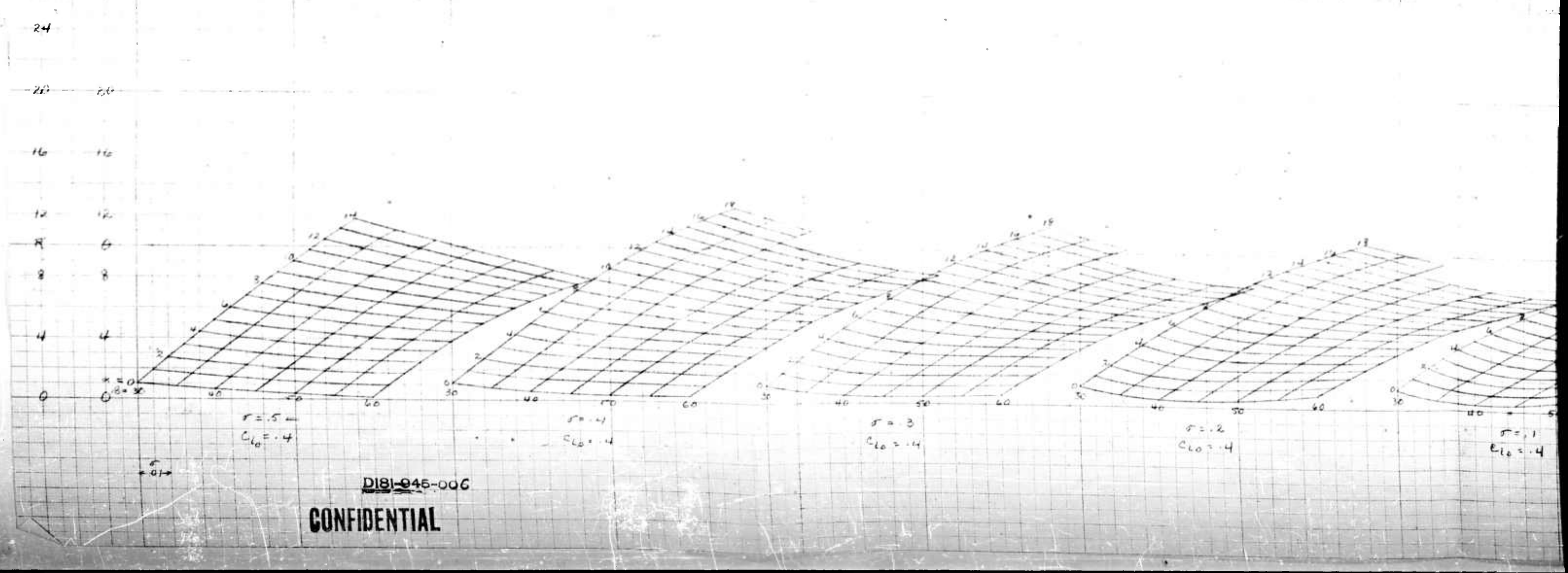

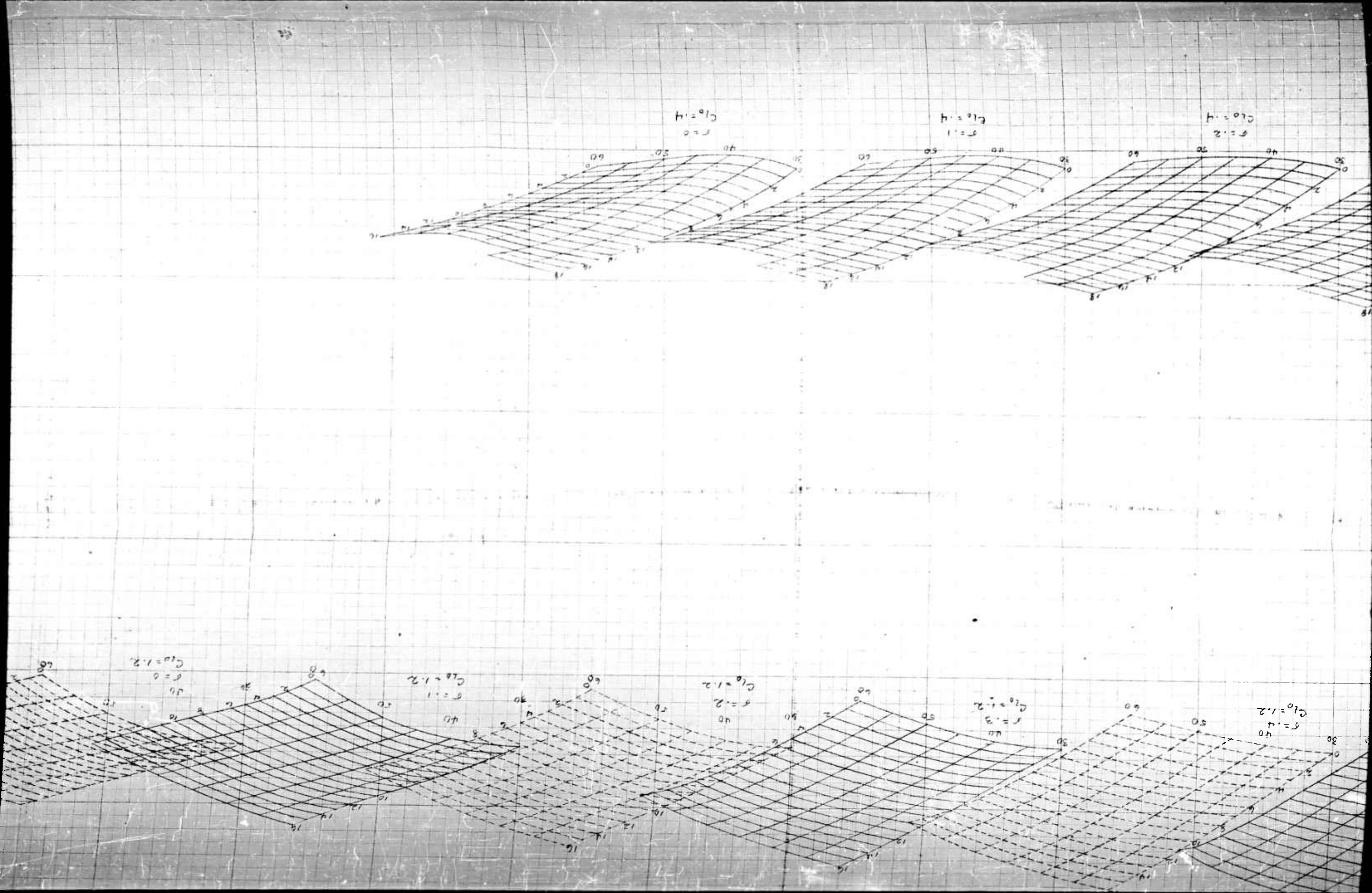
$\delta = 0$
$C_{l_0} = .4$
$\delta = .1$
$C_{l_0} = .4$
$\delta = .2$
$C_{l_0} = .4$
$\delta = 0$
$C_{l_0} = 1.2$
$\delta = .1$
$C_{l_0} = 1.2$
$\delta = .2$
$C_{l_0} = 1.2$
$\delta = .3$
$C_{l_0} = 1.2$
$\delta = .4$
$C_{l_0} = 1.2$